Miniaturized Drug Discovery Assays Targeting Macrophages in Fibrotic Diseases

Doctoral Thesis

for obtaining the academic degree

Doctor of Natural Sciences

(Dr. rer. nat.)

presented by

Sarah Groetzner

at the

Universität Konstanz

Faculty of Sciences

Department of Biology

in cooperation with

Boehringer Ingelheim Pharma GmbH & Co. KG

Konstanz, 2024

Date of oral examination: April 16th, 2024

First referee: Prof. Dr. Florian Gantner

Second referee: Prof. Dr. Thomas Brunner

Third referee: Prof. Dr. Daniel Legler

Contents

Acknowledgment

First, I want to sincerely thank Prof. Dr. Florian Gantner for giving me the possibility to write this interesting PhD Thesis at Boehringer Ingelheim Pharma GmbH & Co. KG, in cooperation with Prof. Dr. Thomas Brunner from the University of Konstanz. Thank you both for your time, your scientific support, and constructive discussions during the last years.

I also want to thank PD Dr. Ralf Heilker who provided personal and scientific support in all stages of this thesis and beyond. Thank you for always giving me the freedom to design and translate my research on my own. Your way of supervision made me become an independent scientist. Further, I want to thank Dr. Karim El Kasmi and Daniela Schlösser (lung repair and regeneration department) for scientific and technical assistance and fruitful discussions through the whole time of my PhD.

I want to thank all colleagues from the High-Throughput Biology group, headed by Dr. Amaury Fernandez. Every single group member contributed a little bit to the development of this work, and I want to especially thank Achim Lietz, Nadine Held, Michael Traub and Doris Goronski for their support. I would like to thank my former Master student Heiko Olbrich for his great work that pushed this thesis forward; supervising you was an easiness. A special thank you goes to Dr. Mozhgan Dehghan Harati being deeply involved in this experimental research. Moreover, I want to thank you for your support in every situation, either on a scientific or personal level. I found a friend in you and lab days became easier the moment you joined our group.

I also want to thank Dr. Johanna Brüggenthies and Julia Sauer for fruitful macrophage discussions and long coffee breaks or lunch dates together with Mozhgan.

A very big thank you goes to Dr. Teresa Bluhmki, my former supervisor who became my friend and life coach. You significantly contributed to my scientific education. I am sure that this thesis would not have been possible without your guidance and encouragement. Thank you for your patience, help and advice whenever I needed it.

Moreover, I would like to thank all former and current colleagues of the stem cell team at Trenzyme in Konstanz, especially Dr. Stefanie Traub, Dr. Tanja Waldmann and Dr. Christina Hänisch, for the scientific collaboration and support on the macrophage differentiation project.

I am extremely grateful to my friends and co-PhD students Natascha Piede and Janessa Hofeichner for encouraging phone calls or evenings with a lot of wine. With all my heart I thank my beloved gummi bears, and a special thank you goes to Franziska Stich for always being there for me in all stages of life.

I am grateful for my parents, siblings, grandparents, parents-in-law, and every single family member for always backing me up. Thank you for your motivating words and for your mental and financial support during the last ten years. I wouldn't have come this far without you.

With all my heart I want to thank my best friend, soulmate, partner in crime and beloved husband Patrick Groetzner. For your great patience, for your trust in me, for every single motivating word. For giving me confidence when I didn’t have any, for making me laugh, and for your endless love in all stages of this long journey. Thank you for always being there for me.

“Science, my lad, is made up of mistakes, but they are mistakes which it is useful to make, because they lead little by little to the truth."

Jules Verne

Summary

Macrophages have key regulatory functions in health and disease, such as fibrosis, and are therefore of high interest for drug discovery. Fibrosis is a result of chronic tissue damage leading to a deregulated wound healing process. Macrophages are involved in different phases of the fibrotic cascade and its onset is assumed to present a reaction to aberrant macrophage activation. Hence, there exists potential of modulating these cells for therapeutic benefits. In patients suffering from idiopathic pulmonary fibrosis (IPF), defective removal of apoptotic cells (efferocytosis) by macrophages was reported. Therefore, targeting macrophages and especially the modulation of their efferocytotic activity represents one strategy to diminish fibrotic processes in IPF. However, an impediment in drug discovery is the lack of physiologically relevant cellular *in vitro* models that can recapitulate the disease situation in patients. Most of the reported models lack relevant cells in sufficient quantity and thus, cannot be applied for screening campaigns. Hence, the aim of the presented work was to fill the gap of the unmet need for physiologically relevant *in vitro* drug discovery assays to target macrophage functions in fibrotic diseases.

To access large numbers of model cells, an upscaled protocol was established for differentiation of human induced pluripotent stem cells (iPSCs) into progenitor cells and subsequent maturation into functional macrophages. These iPSC-derived macrophages (IDMs) resembled monocyte-derived macrophages (MDMs) both with respect to phenotypical and functional characteristics.

To analyze macrophage functions in fibrotic diseases, a miniaturized high-content-imaging-based assay was established, enabling the analysis and quantification of both efferocytosis and phagocytosis for medium- to high-throughput applications. Utilizing IDMs and MDMs, the cells showed comparable pharmacology, as demonstrated by the analysis of Spleen tyrosine kinase (Syk) inhibitors, Dexamethasone, and a pro-fibrotic cocktail.

Besides reduced efferocytotic function of macrophages, an accumulation of senescent cells is reported for IPF patients. To analyze the potential link between these two conditions, a miniaturized co-culture set-up was established. Using differently induced senescent epithelial cells, the inhibitory effect of senescence signals on efferocytosis and phagocytosis was shown in this context. On the contrary, senolytic treatment of senescent epithelial cells triggered their apoptosis induction and resulted in increased efferocytotic activity. The insights gained from this study imply that senescent cells may be a potential cause of reduced efferocytotic activity. Hence, addressing senescent cells and their communication with macrophages could present a promising therapeutical approach.

In conclusion, the here established iPSC-derived macrophage model in combination with the miniaturized efferocytosis and phagocytosis assays can be implemented into large-scale screening campaigns and may open new routes to innovative therapeutic paths in the context of fibrosis and beyond.

Zusammenfassung

Makrophagen haben wichtige regulatorische Funktionen im gesunden Zustand und bei Erkrankungen, wie z.B. bei Fibrose, und sind daher für die Wirkstoffforschung von hohem Interesse. Fibrose ist das Ergebnis einer chronischen Gewebeschädigung, die zu einem deregulierten Wundheilungsprozess führt. Makrophagen sind in verschiedenen Phasen der fibrotischen Kaskade beteiligt, deren Induktion als Reaktion auf eine fehlgeleitete Makrophagenaktivierung vermutet wird. Die Modulation dieser Zellen könnte daher therapeutisch genutzt werden. Bei Patienten mit idiopathischer Lungenfibrose (IPF) wurde eine dysfunktionale Eliminierung apoptotischer Zellen (Efferozytose) durch Makrophagen festgestellt. Daher stellt das Targeting von Makrophagen und insbesondere die Modulation ihrer efferozytotischen Aktivität eine Strategie dar, um fibrotische Prozesse bei IPF zu reduzieren. Ein Hindernis in der Wirkstoffforschung ist jedoch das Fehlen physiologisch relevanter zellulärer *In-vitro*-Modelle, die die Krankheitssituation bei Patienten rekapitulieren können. Den meisten dieser Modelle fehlen relevante Zellen in ausreichender Menge und können daher nicht für Screening-Kampagnen verwendet werden. Das Ziel der vorgestellten Arbeit war es daher, diese Lücke zu schließen, die aufgrund des Mangels an physiologisch relevanten *In-vitro*-Assays besteht, um Makrophagenfunktionen bei fibrotischen Erkrankungen zu untersuchen.

Um eine große Anzahl von Modellzellen bereitzustellen, wurde ein hochskaliertes Protokoll zur Differenzierung von humanen induzierten pluripotenten Stammzellen (iPSCs) in Vorläuferzellen und anschließender Maturierung zu funktionellen Makrophagen entwickelt. Diese iPSC-abgeleiteten Makrophagen (IDMs) ähnelten Monozyten-abgeleiteten Makrophagen (MDMs) sowohl in Bezug auf phänotypische als auch funktionelle Eigenschaften.

Zur Analyse von Makrophagenfunktionen bei fibrotischen Erkrankungen wurde ein miniaturisierter High-Content-Imaging-basierter Assay etabliert, der die Analyse und Quantifizierung von Efferozytose und Phagozytose für Anwendungen mit mittlerem bis hohem Durchsatz ermöglicht. Unter Verwendung von IDMs und MDMs zeigten die Zellen eine vergleichbare Pharmakologie, wie die Analyse von Spleen Tyrosine Kinase (Syk)-Inhibitoren, Dexamethason und einem profibrotischen Cocktail zeigte.

Neben einer verminderten efferozytotischen Funktion der Makrophagen wird bei IPF-Patienten eine Akkumulation von seneszenten Zellen berichtet. Um den möglichen Zusammenhang zwischen diesen beiden Konditionen zu analysieren, wurde eine miniaturisierte Co-Kultur etabliert. Unter Verwendung unterschiedlich induzierter seneszenter

Epithelzellen wurde in diesem Zusammenhang die inhibitorische Wirkung von Seneszenzsignalen auf Efferozytose und Phagozytose gezeigt. Die senolytische Behandlung seneszenter Epithelzellen hingegen induzierte deren Apoptose und führte zu einer erhöhten efferozytotischen Aktivität. Die Erkenntnisse aus dieser Studie deuten darauf hin, dass seneszente Zellen eine potenzielle Ursache für eine reduzierte efferozytotische Aktivität sein könnten. Daher könnten seneszente Zellen und deren Kommunikation mit Makrophagen einen vielversprechenden therapeutischen Ansatz darstellen.

Zusammenfassend kann das etablierte iPSC-abgeleitete Makrophagenmodell in Kombination mit den miniaturisierten Efferozytose- und Phagozytose-Assays in umfangreiche Screening-Kampagnen implementiert werden und könnte somit innovative Therapien im Kontext der Fibrose und darüber hinaus ermöglichen.

List of abbreviations

CAN	Acetonitrile
AGM	Aorta-gonads-mesonephros
Alpha	Amplified luminescent proximity homogeneous assay
ATP	Adenosine triphosphate
AT	Alveolar type
AGC	Automatic gain control
BAL	Bronchoalveolar lavage
Bcl-2	B-cell lymphoma 2
BH3	Bcl-2 homology domain 3
BM-DC	Bone marrow-derived dendritic cell
BMDM	Bone marrow-derived macrophage
BMP-4	Bone morphogenetic protein 4
BSA	Bovine serum albumin
CARD9	Caspase recruitment domain-containing protein 9
CCL	CC-chemokine ligand
CD	Cluster of differentiation
CDK	Cyclin-dependent kinase
ChiPSC	Cellartis human iPSC
CXCL	Chemokines C-X-C motif ligand
DAMP	Danger-associated molecular pattern
DIA	Data-independent acquisition
DMSO	Dimethyl Sulfoxide
DNA	Deoxyribonucleic acid
DoD	Day of differentiation
D-PBS	Dulbecco's Phosphate buffered saline
d-zymosan	Depleted zymosan
ECM	Extracellular matrix
E. coli	*Escherichia coli*
EDTA	Ethylenediaminetetraacetic acid
EMT	Epithelial-to-mesenchymal transition
FBS	Fetal bovine serum
FGF	Fibroblast growth factor
FMO	Fluorescence minus one
FLT-3L	Fms-related tyrosine kinase 3 ligand

GAPDH	Glyceraldehyde-3-phosphate dehydrogenase
GAS6	Growth-arrest-specific gene-6
HABA	4'-hydroxyazobenzene-2-carboxylic acid
HEPES	4-(2-hydroxyethyl)-1-piperazineethanesulfonic acid
HIFBS	Heat-inactivated fetal bovine serum
hiPSC	Human induced pluripotent stem cell
HSC	Hematopoietic stem cell
iAlveoli	Immortalized Human Alveolar Cell Type I
IC_{50}	Maximal inhibitory concentration
IDM	iPSC-derived macrophage
IFN-γ	Interferon-gamma
IL	Interleukin
ILD	Interstitial lung diseases
IPF	Idiopathic pulmonary fibrosis
IQR	Interquartile range
KDR	Kinase insert domain receptor
KO	Knockout
LANCE	Lanthanide chelate excite
LMNB1	Lamin B1
Lin-28	Homolog A LIN28A
LPS	Lipopolysaccharide
LysoPC	Lysophosphatidylcholine
MAD	Median absolute deviation
M-CSF	Macrophage colony-stimulating factor
MDM	Monocyte-derived macrophage
MKI67	Marker Of Proliferation Ki-67
MFG-E8	Milk fat globule EGF factor 8
MFI	Mean fluorescence intensity
MMP	Matrix metalloproteinase
MPC	Macrophage progenitor
mRNA	Messenger ribonucleic acid
m/z	Mass-to-charge ratio
NANOG	Nanog Homeobox
NEAA	Non-essential amino acids
OCT4	Octamer-binding transcription factor 4
PBMC	Peripheral blood mononuclear cell

Pen/Strep	Penicillin-Streptomycin
PFA	Paraformaldehyde solution
PODXL	Podocalyxin-like
POLR2A	RNA polymerase II subunit A
PS	Phosphatidylserine
QPCT	Glutaminyl-peptide cyclotransferase
qRT-PCR	Quantitative reverse transcription polymerase chain reaction
Rho	Ras homologue
RZ’	Robust Z'
SA	Senescence-associated
SAEC	Small airway epithelial cell
SASP	Senescence-associated secretory phenotype
SCAP	Senescent cell anti-apoptotic pathway
SCF	Stem cell factor
SD	Standard deviation
SDC	Sodium deoxycholate
SEM	Standard error of the mean
S/N	Signal-to-noise
SOX2	Sex-determining region Y (SRY)-Box Transcription Factor 2
StemFit Basic04 CT	StemFit Basic04 Complete Type
Syk	Spleen tyrosine kinase
S1P	Sphingosine-1-phosphate
TFA	Trifluoroacetic acid
TGFβ	Transforming growth factor beta
TIM	T cell immunoglobulin mucin receptor
TNF	Tumor necrosis factor
TPO	Thrombopoietin
UTP	Uridine triphosphate
UV	Ultraviolet
VEGF-A	Vascular endothelial growth factor A
WT	Wildtype

1. Introduction

1.1 Macrophages in health and disease

Macrophages are crucial players of host immunity and key regulators in different phases of homeostasis throughout the different tissues of the body[1]. Virtually all tissues are populated by long-lived self-maintaining populations of tissue-resident macrophages. A large portion of these adult macrophages is derived from progenitors during embryogenesis, populating developing tissues before birth. Embryonic hematopoiesis occurs in independent waves and consists of two main phases[2,3]. Primitive hematopoiesis takes places in the yolk sac and results in myelo-erythroid development that gives rise to primitive macrophages and populates the embryo once the blood circulation is established. The consecutive definitive hematopoiesis occurs in the aorta-gonads-mesonephros (AGM) region and produces hematopoietic stem cells (HSCs)[2–4]. Precursors derived from both the yolk sac and AGM region populate the fetal liver, becoming the primary hematopoietic spot during embryogenesis. These fetal liver-derived precursors invade then other hematopoietic organs (e.g., bone marrow and spleen) via the blood circulation, which ultimately host HSCs[2–4]. During hematopoiesis in the fetal liver, monocytes are generated that populate embryonic tissues and differentiate into macrophages at this site. Thereby, they reduce the population of yolk sac-derived macrophages, depending on the tissue. Accordingly, the proportions of progenitors derived from either yolk sac or fetal liver vary between different tissues[3]. To some extent, tissue-resident macrophages are additionally derived from blood monocytes. During adult hematopoiesis, monocytes develop in the bone marrow and give rise to monocyte-derived macrophage populations after recruitment from the peripheral blood to the injured tissue[1].

Both tissue-resident and monocyte-derived macrophages are involved in core homeostatic functions. Besides the protective roles, macrophages may also be involved in pathological processes[2,3]. The functional role of macrophages in a variety of different mechanisms is linked to their capacity to rapidly react and adapt to transitions in their local environment, which is referred to as plasticity[2]. Both tissue signals and the communication with other tissue-resident cell types provoke changes in their functional phenotypes, resulting in heterogeneous macrophage subsets[1,5,6]. The two extremes of polarization *in vitro* represent the classically activated macrophage (referred to as M1 and caused by Interferon-γ (IFN-gamma) and/or lipopolysaccharide (LPS) treatment) and the alternatively activated macrophage (referred to as M2 and caused by Interleukin-4 (IL-4)/ Interleukin-13 (IL-13) treatment)[6]. With an intermediate spectrum of phenotypically different macrophage subpopulations, this leads to

macrophages participating in diverse apparently antagonistic functional processes[1,5,7]. The binary M1/M2 concept may help to assign a respective macrophage function in the fibrotic cascade. In this context, M1-programmed macrophages release pro-fibrotic molecules, resulting in local fibroblast activation which triggers their differentiation into myofibroblasts. In the subsequent resolution phase, macrophages appear to adopt an M2-phenotype in order to execute remodeling functions. Hence, the same cells that orchestrate the early inflammatory phase may also be involved in consecutive tissue repair processes[8]. Consequently, macrophages can act as drivers and regulators of diseases, as shown for the development of organ fibrosis: In response to continuously exposed tissue-derived injury factors in a chronic setting, macrophages are hindered from exhibiting a physiological repair and homeostatic program. Instead, they adopt an aberrant activation phenotype that prevents a physiological tissue repair[7,9]. Hence, there exists potential of modulating this cell type for therapeutic benefits.

A main function of macrophages is their phagocytic activity, which is essential for both host defense against pathogens and homeostatic functions, such as the clearance of apoptotic cells, a process termed efferocytosis[10]. The removal of apoptotic cells exhibits distinct morphological features and special downstream signaling in comparison to classical phagocytosis of microbes[11]. In fact, efferocytosis requires its own mechanisms for sensing, identification, and subsequent removal of apoptotic cells[12]. Per day, the typical healthy human adult shows a turnover rate of more than 10^{11} cells, and apoptotic cells display elementary alterations that discriminates them from viable cells[12,13]. Macrophages are attracted and located to apoptotic cells via ‘find-me-signals’ released by the dying cells as a result of effector Caspase activation (i.e., Caspases 3 and 7; Fig. 1 a). These communication signals include adenosine triphosphate (ATP) and uridine triphosphate (UTP), chemokine C-X3-C motif ligand 1 (CX3CL1), sphingosine-1-phosphate (S1P), and lysophosphatidylcholine (LysoPC)[13]. During the apoptotic program, phosphatidylserine (PS) in the cellular membrane redistributes from the inner to the outer leaflet as a consequence of Caspase activity. This exposure of PS acts as the primary ‘eat-me-signal’ for macrophages and is detected by specific cell-surface receptors, such as stabilins, integrins, T cell immunoglobulin mucin receptors (TIMs), and TAMs (Fig. 1 b). These receptors either bind directly to the apoptotic cell or via bridging molecules, such as Growth-arrest-specific gene-6 (GAS6), protein S or Milk fat globule EGF factor 8 (MFG-E8). In addition, some surface proteins act as ‘don't-eat-me’ signals and mediate an inhibition of efferocytosis, such as CD47, CD24 and CD31[11,13–15]. Building of an efferocytic synapse between PS and efferocytosis-associated receptors culminates in the activation of the Ras homologue (Rho) family of small GTPases, coordinating cytoskeletal rearrangement. Mediating actin polymerization is required for the formation of the efferosome

(membrane-bound compartments containing the efferocytosed cell), which stretches around and envelopes the apoptotic cell for subsequent internalization[11,13]. Efferosomes become progressively acidic after internalization, and ultimately fuse with lysosomes, containing enzymes needed for degradation of the engulfed cell into its cellular building blocks[16]. Consequently, efferocytosis presents an anti-inflammatory mechanism by preventing the release of potentially toxic intracellular contents before the onset of membrane permeability. In addition, the efferocytotic program results in a suppression of innate immune responses and promotes resolution by stimulating macrophage secretion of anti-inflammatory and immunosuppressive mediators, such as transforming growth factor beta (TGFβ)[11,16]. Hence, under physiological conditions, efferocytosis is crucial for both tissue homeostasis and resolution of inflammation, and uncleared apoptotic cells are scarce due to efficient and rapid removal in healthy individuals[12,16]. In contrast, defective efferocytosis can lead to the accumulation of apoptotic cells. Uncleared cellular corpses may undergo secondary necrosis, release danger-associated molecular patterns (DAMPs), driving inflammatory responses[11,16]. In fact, defective efferocytosis along with the accumulation of apoptotic cells was reported in association with several chronic inflammatory and fibrotic diseases[17–19].

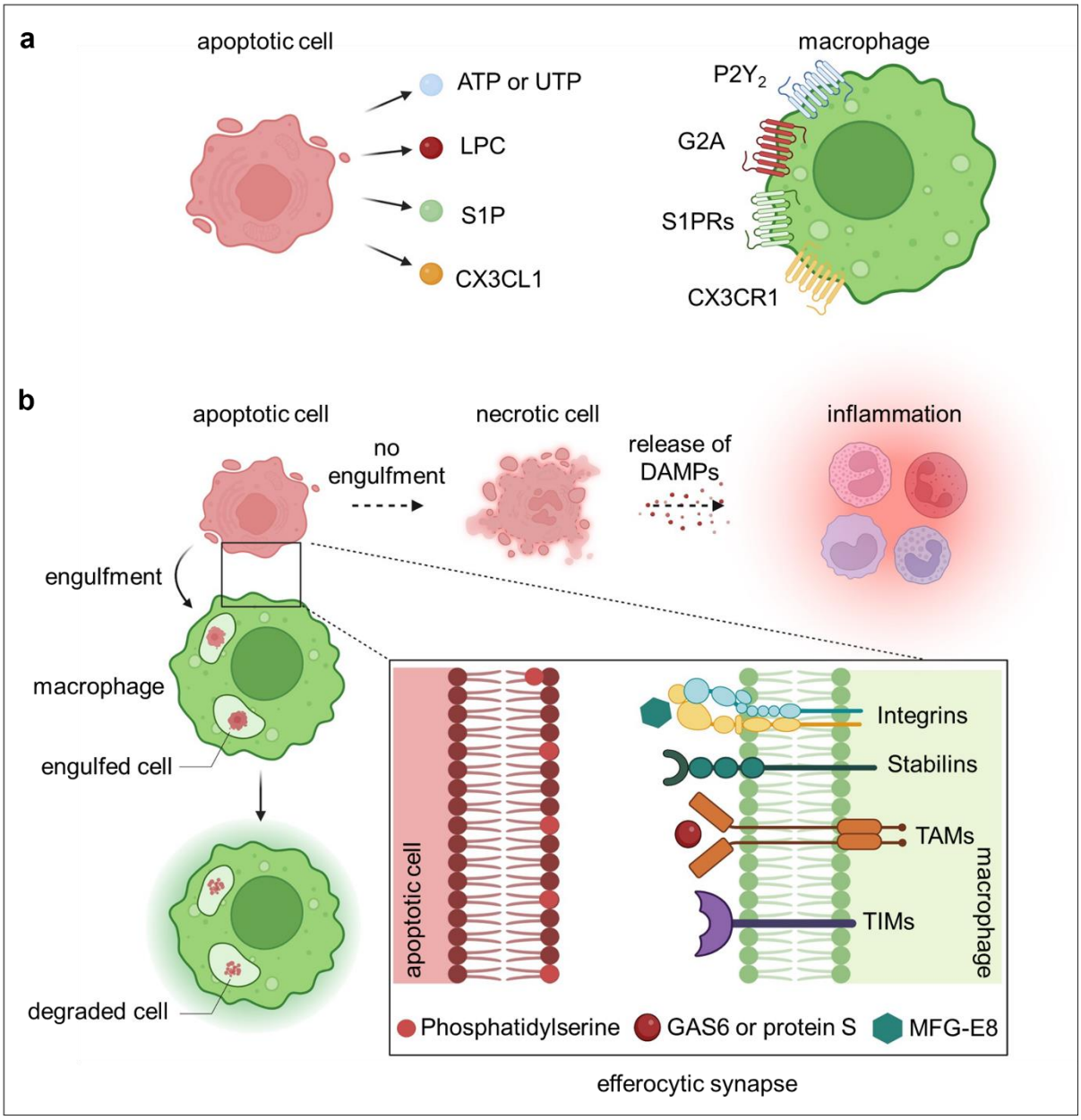

Figure 1. Efferocytosis as an anti-inflammatory mechanism. (a) 'Find-me-signaling' by apoptotic cells recruits macrophages by the release of chemokines (chemokine C-X-C motif ligand 1 (CXCL1)), lipids (sphingosine 1-phosphate (S1P)), lysophosphatidylcholine (LPC) and nucleotides (ATP, UTP). These 'find-me-signals' are recognized by specific macrophage cell surface receptors. **(b)** 'Eat-me-signaling' and the generation of the efferocytic synapse after localization of the apoptotic cell. Phosphatidylserine is the major 'eat-me-signal' being externalized in the outer leaflet of apoptotic cells being recognized by different efferocytotic receptors. These receptors either bind directly to the apoptotic cell (by stabilins and T cell immunoglobulin mucin receptors (TIMs)) or bind via bridging molecules, such as GAS6, protein S or MFG-E8 (by TAMs and integrins). After engulfment, the apoptotic cell is degraded by the formation of the phagolysosome. Non-engulfed apoptotic cells become necrotic, release danger-associated molecular patterns (DAMPs), thereby promoting inflammatory processes. Modified from Doran et. al, 2020.

1.2 Fibrotic diseases

Fibrosis can affect nearly every tissue of the body and is a leading cause of mortality, being accountable for up to 45 % of all deaths in the industrialized world[20]. In fibrotic pathogenesis, this reparative wound healing process is deregulated, leading to an excessive accumulation of extracellular matrix (ECM) components in and around a damaged or inflamed tissue, which culminates in architectural remodeling. Under physiological conditions, the formation of fibrotic tissue is an essential phase of tissue repair, and fibrosis and tissue repair are fundamentally intertwined mechanisms. Upon injury, local tissue-resident fibroblasts are activated, and produce and secrete both inflammatory factors and ECM molecules[20,21]. In addition, fibroblasts enhance their contractility[20]. Ultimately, these processes result in the initiation of the wound healing reaction. In case of either a minor or non-recurrent injury, the response acts efficiently and leads to a transient remodeling process. In contrast, severe or persistent damage generates a continuous accumulation of excess ECM components and hence, permanent scarring. Fibrosis is a pathological feature of many chronic inflammatory or autoimmune diseases, such as rheumatoid arthritis, Crohn's disease, and scleroderma. Aberrant tissue architecture may lead to dysfunctional organs and ultimately death, as seen in patients suffering from idiopathic pulmonary fibrosis (IPF)[20,21].

1.2.1 Idiopathic pulmonary fibrosis

Idiopathic pulmonary fibrosis (IPF) is the most common type among interstitial lung diseases (ILD) with unknown etiology and affects worldwide approximately 5 million people[22]. The disease is anatomically defined by chronic progressive pulmonary fibrosis within the lung epithelium, involving alveolar epithelial cells, local fibroblasts, and immune cells, such as macrophages. This process significantly impairs the physical lung function, and disrupted gas exchange ultimately leads to respiratory failure. Shortness of breath, chronic dry cough and finger clubbing represent classical, but unspecific disease symptoms[23,24]. IPF affects mostly older people, and the time-point at presentation averages around the age of 65 years. Approximately 50 % of the patients die with a survival rate of 3-5 years after diagnosis, and current treatment options are highly limited. With only two available approved anti-fibrotic pharmaceuticals, IPF remains an inevitably lethal disease, since nintedanib (Ofev®) and pirfenidone (Esbriet®) only drag the deterioration of the lung function[25,26]. Accordingly, elucidating the disease mechanisms along with identifying novel therapeutical targets is of pivotal importance.

1.2.2 Architecture of the human lung

Although the exact reasons and mechanisms leading to IPF onset are still unknown, chronic injury of the alveolar epithelium is considered to present a key factor triggering fibrosis[26]. Accordingly, the lung epithelium plays a major role in IPF research models. The primary function of the lung is gas exchange, supplying the organism with oxygen. This process is accomplished by a complex cellular architecture, consisting of a variety of different cell types (Fig. 2). The trachea directs inhaled air through its tubular branches, which divide into shrinking bronchioles. The latter end in air sac clusters, called alveoli, which are responsible for the gas exchange[27–29]. The pulmonary epithelium shows a distinct cellular population patterning along the proximal-to-distal axis. The distal alveolar compartment shapes the blood-air barrier. This epithelial monolayer is built up of a mix of alveolar type I (AT I) and type II (AT II) cells and is additionally populated by fibroblasts and alveolar macrophages[27,30–32]. Large AT I cells cover approximately 95 % of the alveolus, mediating the gas exchange. AT II cells protect alveolar structures by producing surfactant, and in addition serve as precursors for AT I cells. Accordingly, AT II cells are actively participating in regenerative processes and thus, maintain alveolar tissue homeostasis[29]. The healthy lung hosts distinct macrophage populations being capable of self-renewal. Alveolar macrophages populate the airways, controlling the immunological homeostasis in the alveolar space. Interstitial macrophages reside in the tissue and likewise exert immunoregulatory functions[8,26,28]. Emerging signals upon injury or inflammation recruit monocytes into the lung, which differentiate into macrophages and support tissue-resident macrophage pools in repair processes[8,26]. In contrast, the more proximal airways are lined by a pseudostratified epithelium, being composed of basal, ciliated, and secretory cells. Basal cells present a self-renewing population, they act as precursors for both ciliated and secretory cell types and are fundamental for the epithelial recovery upon tissue damage[32]. This cell type is located directly on the basement membrane of the airway epithelium and segregates it from the stroma, which is composed of an ECM and a cellular compartment with fibroblasts, co-existing with smooth muscle cells, immune cells, and endothelial cells[27,32]. Hence, a manifold of different cell types shapes the respiratory microenvironment to ensure proper gas exchange and to maintain lung tissue homeostasis. However, a variety of agents may have harmful effects, destructing the respiratory architecture, which is highly affected in IPF and other interstitial lung diseases[26].

1.2.3 Pathobiological processes contributing to the development of Idiopathic pulmonary fibrosis

Pathobiological processes of IPF are mediated by complex interactions between a variety of different cell types and signaling pathways (Fig. 2). After decades of research to elucidate the underlying pathobiology, some risk factors and environmental exposures appear to be the primary causes triggering the pathogenic cascade. These factors include smoking, chronic viral infections, and gastroesophageal reflux in tandem with genetic dispositions and age-related susceptibilities[23,25,26]. In the context of these risk factors, local perpetuated microinjury of the alveolar epithelium may lead to maladaptive epithelial repair processes along with abnormal epithelial cell activation, apoptosis, and senescence[26,33]. The dysregulated epithelial cells are among the known key players of the disease by secreting harmful molecules and thus, actively propagating the pro-fibrotic niche[34]. Additionally, the epithelial cells recruit and interact with mesenchymal, endothelial, and immune cells, such as macrophages. This crosstalk results in the activation of ECM-producing fibroblasts and myofibroblasts, boosting the pro-fibrotic milieu by secreting a plethora of pro-fibrotic activators[26,34,35]. Among these, TGFβ is the key mediator in fibrotic conditions and its signaling pathway is markedly upregulated in aberrant epithelial cells[26,34]. It mediates epithelial cell apoptosis and epithelial-to-mesenchymal transition (EMT), further production of pro-fibrotic factors, myofibroblast activation and senescence induction[26,34,36]. Under physiological conditions, tissue repair usually resolves with apoptosis induction in the activated myofibroblasts. However, in a fibrotic setting, pro-fibrotic mediators and myofibroblasts persist in the tissue, leading into a vicious circle[26,35]. The excessive amassing of ECM components ultimately culminates in a remodeled architecture of the lung interstitium and disrupts the gas exchange[37].

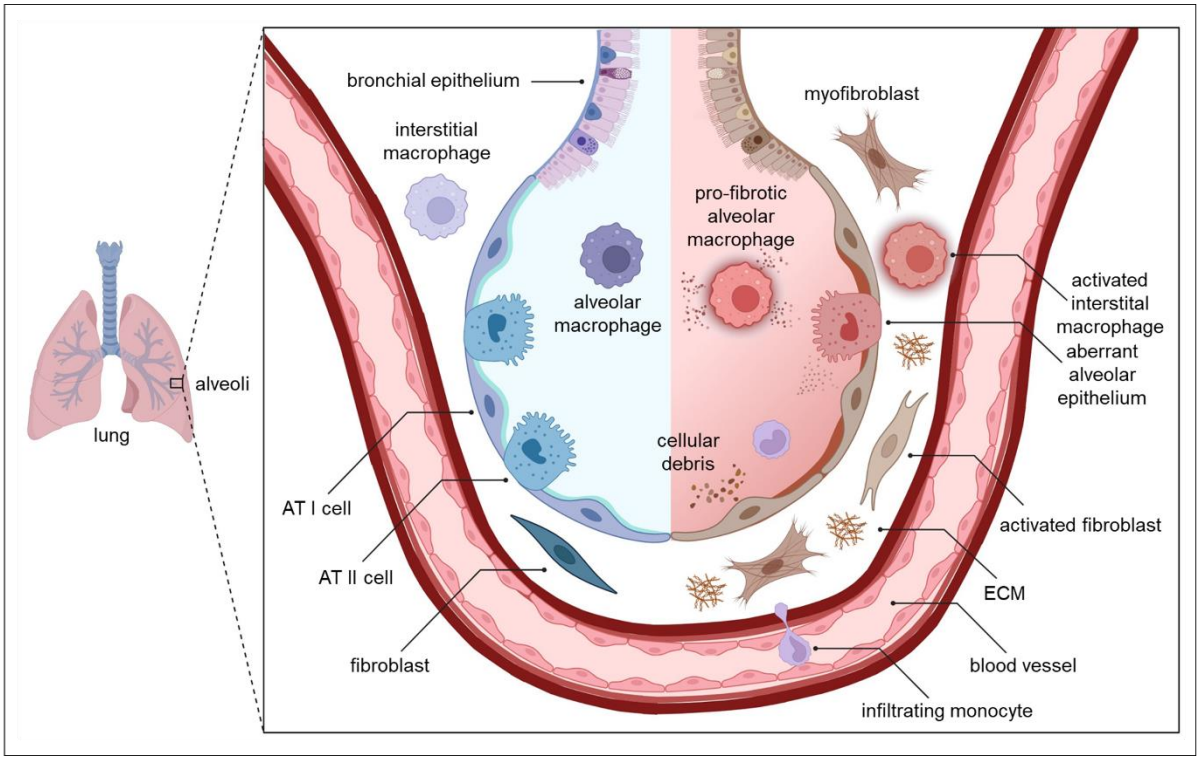

Figure 2. The alveolar microenvironment in a homeostatic condition (left) and in a fibrotic setting (right). The trachea leads the air through the bronchi, which divide into smaller bronchioles, being lined by a pseudostratified bronchial epithelium, ending in alveoli. The alveolar microenvironment in the distal airways is primarily built up of alveolar epithelial cells type 1 (AT I), alveolar epithelial cells type 2 (AT II), fibroblasts and tissue-resident macrophages residing both in the interstitium and in the alveolus. Gas exchange is mediated by large, squamous AT I cells, while AT II cells produce surfactant for the protection of alveolar structures and serve as progenitors for AT I cells. In a fibrotic setting observed in IPF, the alveolar epithelium is aberrantly activated. The epithelial cells secrete harmful molecules, and recruit and interact with mesenchymal and immune cells, whereby pro-fibrotic macrophage subsets populate the fibrotic niche. The crosstalk of aberrant epithelial cells with the mentioned cell types culminates in the activation of ECM-producing fibroblasts and myofibroblasts, leading to alveolar remodeling and fibrotic changes of the parenchyma, which ultimately restricts the gas exchange.

Although the pathobiological cascade of IPF is directed by aberrant epithelial-mesenchymal crosstalk, the resulting activated immune system may also orchestrate fibrotic processes[35]. Macrophages represent the most abundant innate immune cell type in the distal lung tissue and exhibit a unique role with being involved in all phases of the wound healing process[1,38]. Accordingly, these cells play a substantial role in the fibrotic setting and macrophage-mediated processes have extensively been studied[19,39]. Macrophages behave remarkably plastic, being capable of adopting both disease-driving and -resolving phenotypes depending on local environmental factors[1]. Previously, macrophages were categorized into binary subtypes, the classically activated M1 and alternatively activated M2 macrophages[5]. The corresponding concept implied that M1 macrophages act in an anti-fibrotic manner, while M2 macrophages exhibit pro-fibrotic functions[8]. However, more recent studies suggest that the M1 and M2 phenotypes are only two extremes of a reversible continuous polarization, oversimplifying the functional heterogeneity of the highly plastic macrophages[5,6]. Nevertheless, the binary concept may help to assign a respective macrophage function in the fibrotic cascade. With

respect to this classification, increased amounts of M1-biased cells mediate both epithelial apoptosis and reparative failure. In contrast, excessive M2 macrophages drive deregulated wound healing responses[7]. Though, local factors may influence the respective macrophage subtype. M1-phenotypic macrophages may switch to M2 macrophages involving signals derived from efferocytosis, for instance[8]. Accordingly, the same cells controlling early inflammatory responses may be involved in the following tissue repair processes. However, there is increasing evidence that pro-fibrotic macrophage subsets dominate the fibrotic niche in IPF settings. This population stimulates fibroblast proliferation and activation by the production of TGFβ1 and soluble factors. Moreover, macrophages play a role in ECM remodeling through secretion of matrix metalloproteinases (MMPs) and their involvement in collagen synthesis[1,7,26]. These macrophages are also associated with the production of CC-chemokine ligand 18 (CCL18)[26,40]. This chemokine is upregulated in serum and bronchoalveolar lavage (BAL) fluid of IPF patients, and mortality correlates with the CCL18 levels. *In vitro*, CCL18 leads to fibroblast activation and recruiting of T-lymphocytes, preserving a positive feedback circuit with fibroblasts to boost their collagen synthesis[26]. Thus, a persistent activation or recruitment of pro-fibrotic macrophages may contribute to fibrosis.

Macrophages also modulate fibrosis through efferocytosis of apoptotic cells. The removal attenuates inflammation via downregulation of inflammatory factor generation and simultaneously through the production of anti-inflammatory mediators. However, these include growth factors such as TGFβ1, thereby promoting tissue repair[19,26]. In this case, the macrophages act in a pro-fibrotic manner. On the other hand, efferocytosis of apoptotic myofibroblasts, for instance, may curb the production of pro-fibrotic mediators and ECM components by eliminating the responsible cells. Accordingly, efferocytosis is able to modulate both the onset and resolution of fibrosis through a variety of mechanisms[41]. Increased amounts of apoptotic cells were detected in BAL fluid of IPF patients, arising either as a result of cellular damage or impaired efferocytotic activity[19]. In fact, defective efferocytosis has been reported for multiple chronic respiratory diseases, including IPF[11]. This directly drives the disease pathogenesis by enhancing inflammatory processes and impeding repair mechanisms[11]. Therefore, targeting macrophages and especially the modulation of their efferocytotic activity represents one strategy to diminish fibrotic processes in IPF. Recently it was shown, that macrophage-mediated efferocytosis was negatively regulated by senescent cells, being highly abundant in lungs of IPF patients[39,42]. Importantly, experimental mouse models have shown that removal of these senescent cells mitigated pulmonary fibrosis and additionally recovered the lung function. Moreover, senotherapy in a clinical study with IPF patients revealed an improvement of their physical function. These data indicate that cellular senescence could be a mechanism which regulates pathophysiological processes of IPF and

may drive defective macrophage efferocytosis[42,43]. Hence, targeting senescent cells represents a promising therapeutic approach in the context of IPF.

1.3 Cellular senescence in health and disease

Cellular senescence is a common feature during aging**.** However, it appears to be a significant mechanism during the pathogenesis of age-related chronic lung diseases, including IPF. In this state of cell cycle arrest, the cells undergo phenotypical changes, which may be disease-driving. Due to shortened telomeres after repeated cell division cycles, cells enter a quiescent state as a result of replicative senescence. Deoxyribonucleic acid (DNA) damage-response pathways are induced, activating p53. Cellular stress may also activate the senescence program and culminates in the activation of the cyclin-dependent kinase inhibitor p16INK4 (p16). Both p53 and p16 activate the cyclin-dependent kinase inhibitor p21CIP1 (p21), inhibiting cyclin-dependent kinase-2/4 (CDK2/4) and ultimately leading to cell cycle arrest[44]. Different stimuli are known to induce a senescent phenotype *in vitro*. A replicative senescent state can be activated via serial passaging. Hereby, multiple cell divisions result in exhausted proliferation potential, triggered by telomere shortening in non-transformed cells[45]. Additionally, various anti-cancer drugs were reported to activate a senescent state. This is achieved either by inducing DNA damage, for instance by the use of the topoisomerase II inhibitor etoposide or by CDK inhibitors, such as palbociclib[45,46]. In bronchial epithelial cells, TGFβ was also shown to trigger senescence[47].

In the senescent state, the cells activate senescent cell anti-apoptotic pathways (SCAPs), resulting in apoptosis resistance. *In vitro*, senescent cells exhibit irregular structures with enlarged and flattened cell shapes and accumulate dysfunctional lysosomes with increased activity of senescence-associated (SA)-β-galactosidase[45,48]. These cells remain metabolically active and adopt a senescence-associated secretory phenotype (SASP), through which they may influence adjacent cells. They secrete a broad spectrum of proteins associated with age-related diseases, such as the proinflammatory cytokines Tumor necrosis factor alpha (TNFα), Interleukin 1 beta (IL-1β) and Interleukin 6 (IL-6), the chemokines C-X-C motif ligand 1 (CXCL1) and CC-chemokine ligand (CCL2), growth factors like TGFβ, and different MMPs. Thereby, the SASP may cause structural alterations, along with tissue devastation, and fibrosis. The composition of released SASP-associated factors may differ between cell types and could contribute to the low-grade inflammation observed in various chronic lung diseases[44]. Accumulating senescent cells may result in dysfunctional repair, defective immunological pathways, as well as chronic, low-grade pulmonary inflammation, which further promotes senescent processes.

Senescence has been shown to aggravate IPF, and a minority of IPF patients exhibit mutation-associated reduced telomere lengths. In the prominent bleomycin mouse model, the administration of the DNA-damaging compound bleomycin recapitulates many disease-associated characteristics in the mice that are also observed in humans IPF patients. Alveolar, bronchial, and mesenchymal cells are involved in the development of IPF and all of them show increased SA-β-galactosidase activity. Moreover, the cells exhibit upregulated p16 and p21 levels and *in vitro* studies revealed TGFβ to participate as a key factor in the p53-independent p21 activation. Senescent bronchial cells also release IL-1β, which is suggested to promote myofibroblast differentiation along with elevated ECM production[49]. Furthermore, the SASP analysis of *in vitro* generated senescent fibroblasts revealed a pro-fibrotic secretome, containing for instance TGFβ[24]. Importantly, the p16 levels and abundance of several SASP factors apparently correlate with IPF severity[24]. Accordingly, accumulating evidence indicates cellular senescence as a disease-driving mechanism in the development of lung fibrosis. To maintain tissue integrity, the amount of senescent cells must carefully be monitored in order to restrict their potential negative effect. For instance, the functionality of macrophages may be affected, mediated by phenotypic changes induced by senescent cells[50]. A known mechanism through which both apoptotic and senescent cells communicate with macrophages is via their 'eat-me-signals'. However, senescent cells appear to upregulate the 'don't-eat-me-signal' CD47 on their cell surface, thereby diminishing the phagocytotic activity of macrophages[50].

Since senescent cells are currently considered to play pivotal roles in the pathobiological processes of IPF, their pharmacological targeting offers a promising strategy for the therapy of lung fibrosis. Senotherapeutics aim to eliminate senescent cells and are composed of senomorphics and senolytics. Senomorphics are small molecule drugs suppressing SASP pathways without eliminating the senescent cells. In contrast, senolytics represent small molecules being able to selectively eliminate senescent cells through induction of apoptosis. The latter drugs target the upregulated SCAPs, encompassing e.g., the B-cell lymphoma 2 (Bcl-2) family. Bcl-2 proteins are for instance activated by the Bcl-2 homology domain 3 (BH3) mimetic ABT263 (navitoclax), thereby inducing the apoptotic program. With respect to IPF, the potential benefits of senotherapeutic drugs were already reported for the bleomycin mouse model. The co-administration of the tyrosine kinase inhibitor Dasatinib and natural compound Quercetin ameliorated both pulmonary functions and physical health of the mice[24]. Moreover, this combination resulted in improved physical functions of IPF patients, as shown in a senolytics phase I study[43,51]. Consequently, senotherapeutics represent a promising approach for the treatment of lung fibrosis.

1.4 Cellular models to study the macrophage-epithelial crosstalk

Pathobiological processes of IPF are regulated by a complex interaction between multiple different cell types[26]. Recently, the contribution of macrophage-mediated processes has extensively been studied[19,39]. Hence, co-cultures between macrophages and epithelial cells, the key players in IPF development, are of interest to increase the physiological relevance of the observations.

In vitro studies on macrophages traditionally were limited by the availability of suitable model cells. Tissue-resident macrophages represent the most relevant biological model. However, these cells are scarce in both humans and in animal systems, and isolation processes affect their cellular activity. Available immortalized cell lines (e.g., THP-1 cells) allow for experimental reproducibility and provide cells in large quantity but cannot recapitulate the complexities of *in vivo* macrophages. Moreover, these cells only represent monocyte-like cells that may be differentiated into macrophages. Primary macrophages can be generated by *in vitro* differentiation from either isolated bone marrow or blood monocytes. Although these cells are easily accessible, this presents a low-yield and time-consuming approach, and the cells exhibit donor-to-donor variations. Recent approaches to generate macrophages rely on the technology of human induced pluripotent stem cells (hiPSCs), overcoming the impediments of existing macrophage models. HiPSCs are easily available and may be genetically manipulated. To produce macrophages, iPSCs are kept in conditions that drive a stepwise differentiation via embryonic hematopoiesis recapitulating pathways. Accordingly, iPSC-derived macrophages (IDMs) are currently considered to reflect tissue-resident macrophages better than other existing cell models. Moreover, the associated protocols are scalable and standardizable, and may supply research approaches with consistent, virtually unlimited amounts of macrophages.

Recently developed human cellular models with respect to lung epithelial cells are also based on hiPSCs[52]. Additionally, cancer or immortalized cell lines are in frequent use to model the IPF phenotype, such as A549 cells. These cells are derived from a human alveolar cell carcinoma and are considered of being representative of AT II cells, although A549 do not exhibit all specific alveolar characteristics[53]. In contrast, primary AT II cell cultures are regarded as the most useful *in vitro* model, but their use is limited by tissue availability[54]. Another prominent model is predicated on primary human small airway epithelial cells (SAECs), which are derived from the distal part of the human lung and thus, do not correspond to the alveolar epithelium, where the disease is assumed to emerge[33,53]. Culturing macrophages together with epithelial cells improves the recapitulation of the *in vivo* situation

compared to studying each cell type isolated, thus increasing the physiological relevance, and improving pre-clinical models.

1.5 Aims and objectives of this thesis

Macrophages are currently considered to play a substantial role in the pathophysiological development of fibrotic diseases, such as IPF. In fact, increased amounts of apoptotic cells were detected in the BAL fluid derived from IPF patients, paired with the observation of defective efferocytosis[19]. This results in amplified inflammatory processes and restricted repair processes, further promoting the disease progression[11]. Moreover, cellular senescence could be a mechanism which regulates pathophysiological processes of IPF. Senescent cells are highly abundant in lungs of IPF patients and could be responsible for defective macrophage efferocytosis[42,43]. More precisely, a recent study revealed that macrophage-mediated efferocytosis was negatively regulated by senescent cells[39]. Hence, macrophage targeting and particularly the modulation of their efferocytotic activity represents a fibrosis-moderating approach. However, *in vitro* studies on macrophages are limited by both the availability of appropriate model cells and physiological relevant assays suited for drug discovery applications. To date, the medical treatment options to target IPF are limited, and consequently, there is an unmet need for miniaturized and high-throughput capable assays to investigate macrophage functions in disease contexts. The main aims of this thesis were to establish robust miniaturized drug discovery assays targeting macrophages in fibrotic diseases and to apply these assay formats to investigate the role of macrophages in fibrotic pathogenesis.

Thus, the first objective of this work was to establish a robust and scalable stepwise differentiation protocol to derive macrophages from human iPSCs, including cell banking of intermediate cells and subsequent in-depth characterization with comparison to monocyte-derived macrophages. The second objective of this study consisted of the application of this platform to the development of miniaturized drug discovery assays for high-throughput applications. Using macrophages derived from iPSCs and monocytes, the development of both a miniaturized high-content-imaging-based efferocytosis and phagocytosis assay was intended. Based on this, the third objective was to establish and miniaturize co-cultures between macrophages and senescent epithelial cells to mimic the fibrotic setting. By this co-culture, the link between senescence signals derived from epithelial cells and the macrophage's efferocytosis activity was analyzed.

The investigations in this work are expected to help building up a platform, based on macrophages derived from human iPSCs and primary blood cells, to advance both target and therapeutic compound screening in drug development in the field of fibrotic diseases.

2. Results

2.1 Upscaled process for the differentiation of human iPSCs towards derived macrophages

Adapting previously published protocols[55,56], an upscaled differentiation process from hiPSCs to macrophages was established which provided sufficient numbers of IDMs to enable medium- to high-throughput applications. This protocol allowed for the efficient generation of functional macrophages achieved through the stepwise and directed *in vitro* differentiation of hiPSCs, including a cell banking step at an intermediate stage.

2.1.1 Quality controls of human iPSC lines

Initially, a quality control of human iPSC lines was performed to confirm genome integrity. Molecular karyotyping of Cellartis hiPSC (ChiPSC) lines ChiPSC7, ChiPSC12, ChiPSC18 and ChiPSC22 was carried out at LIFE & BRAIN GmbH, whereby no serious chromosomal aberrations were detected (supplementary Fig. S1-S4).

2.1.2 Transfer to colony-like growth and pluripotency analysis

Previously published protocols for the differentiation of hiPSCs into macrophages had been based upon hiPSC lines that were expanded under the more cumbersome colony growth conditions[55–60]. However, this protocol applied several monolayer growth-adapted ChiPSC lines, and in consequence, a new step was inserted into the protocol after ChiPSC amplification to transfer the previously monolayer-expanded cells towards colony culture. The hiPSC line 201B7 grows by default in colonies and was used in parallel as a reference cell line. The switch from monolayer to colony-like growth for the ChiPSC lines was achieved through the replacement of medium and coating solution being regularly used for the 201B7 line. This resulted in a colony morphology of the ChiPSC lines similar to that of the line 201B7 (Fig. 3, Fig. S5). To provide more flexibility to the upscaling process, a freeze-thaw step was established to generate “ready-to-use” frozen aliquots from the previously expanded and then colony growth-adapted ChiPSCs.

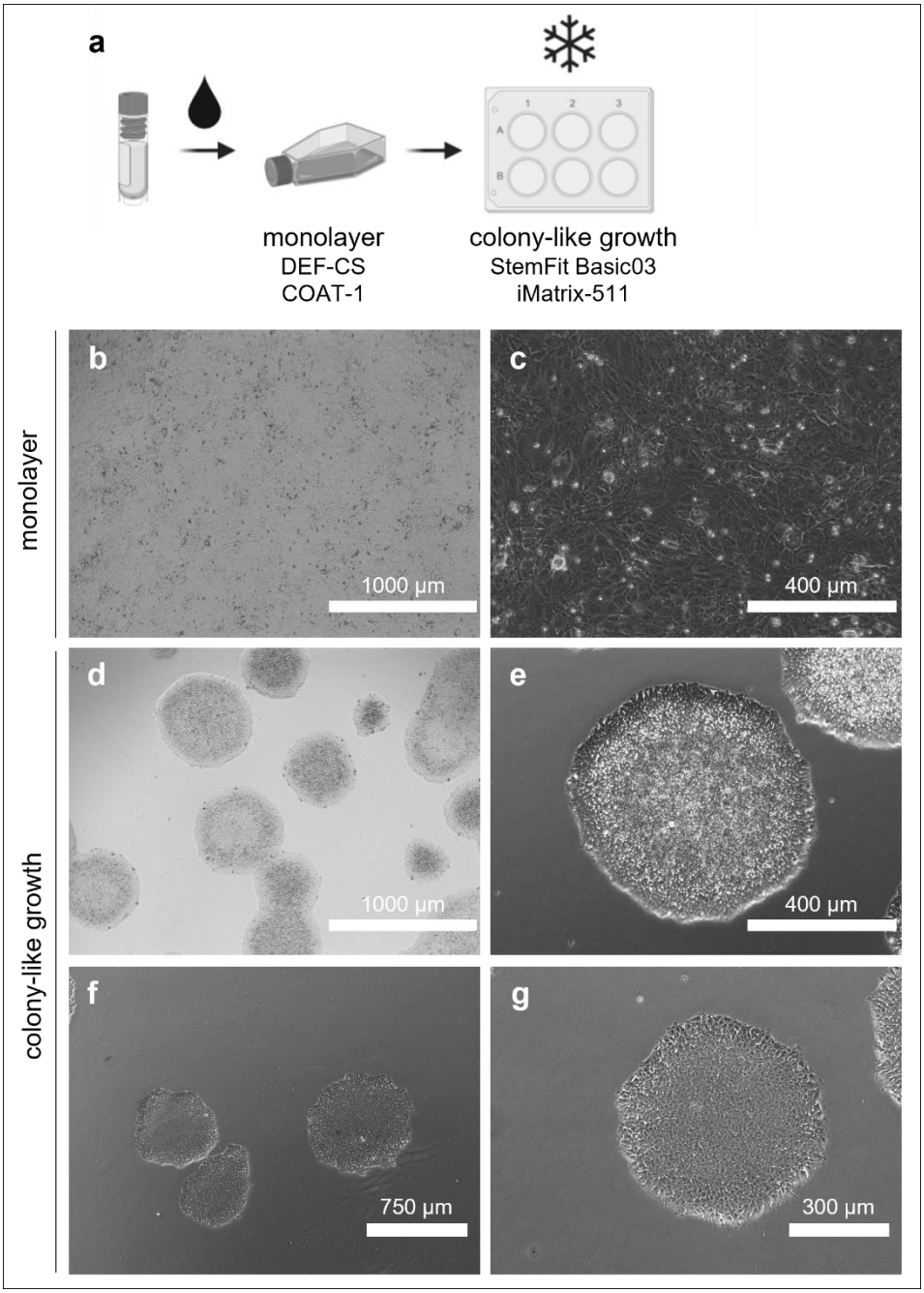

Figure 3. Culture system transfer of ChiPSC12 from monolayer to colony growth. (a) Transfer scheme of ChiPSC lines. After a pre-culture as a monolayer, the cells were transferred to colony growth. After one week, the cells growing in colonies were cryopreserved. **(b+c)** Monolayer growth of ChiPSC12 by culture in DEF-CS/COAT-1. **(d+e)** ChiPSC12 after transfer in a culture system with StemFit Basic03/ iMatrix-511 showing colony growth. **(f+g)** hiPSC line 201B7 growing by default in the colony format using StemFit Basic03/ iMatrix-511.

To confirm the pluripotent state of the ChiPSC lines after transfer, a PluriTest and Scorecard analysis of the lines ChiPSC7, ChiPSC12, ChiPSC18, ChiPSC22 and additionally 201B7 were carried out at Thermo Fisher Scientific. All tested hiPSC lines growing in the colony format passed the PluriTest analysis, comparing them with an hiPSC control line and a non-hiPSC line (Fig. 4 a and Table 1).

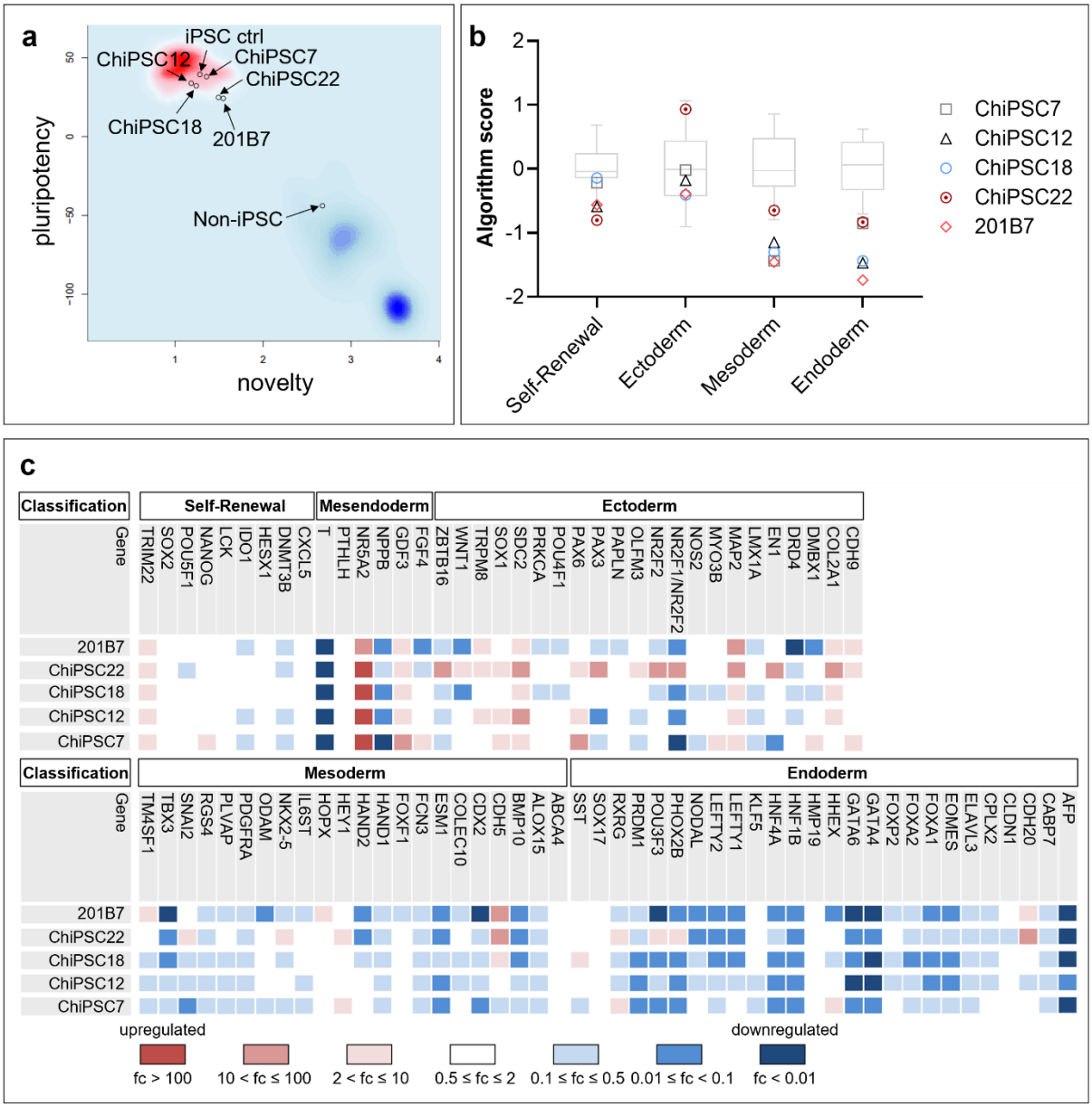

Figure 4. Pluripotency evaluation and differentiation potential of employed hiPSC lines. (a) Pluripotency and novelty x/y scatter plot showing the comparison of the five employed hiPSC lines to non-hiPSC cells and a hiPSC control. The red and blue background hint to the empirical distribution of the pluripotent (red) and non-pluripotent (blue) samples in the reference data set. The samples refer to cells, which were transferred to colony-growth (N = 1). **(b)** Scorecard RT-PCR analysis of the five employed hiPSC lines showing the algorithm scores for up- or downregulation of the pluripotency (self-renewal), ectoderm, mesoderm, and endoderm markers relative to the reference set of nine undifferentiated pluripotent stem cell lines. The range for the undifferentiated reference data set is indicated by the grey box plot (N = 1). **(c)** Scorecard RT-PCR analysis of the five employed hiPSC lines showing the gene expression patterns of markers for pluripotency (self-renewal), mesendoderm, ectoderm, mesoderm, and endoderm. Colors correlate to the fold change (fc) in expression of the indicated gene relative to the undifferentiated reference data set (N = 1).

Table 1. PluriTest results for different tested human iPSC lines. ChiPSC lines were transferred to colony growth prior to the analysis. Positive pluripotency values refer to a strongly expressed model-based pluripotency signature. The pluripotency score (PluriCor) indicates the strength of pluripotency expression, and the novelty score (NovelCor) shows the model fit.

Sample ID	PluriTest Result	PluriCor	NovelCor
ChiPSC7	Pass	37.947	1.35787
ChiPSC12	Pass	33.786	1.1836
ChiPSC18	Pass	32.174	1.241
ChiPSC22	Pass	24.779	1.49389
201B7	Pass	24.195	1.54871
iPSC ctrl	Pass	39.339	1.28215
Non-iPSC	Fail	-43.937	2.67515

The Scorecard algorithm scores for up- or downregulation of self-renewal (pluripotency), ectoderm, mesoderm and endoderm markers were compared to a reference set of nine undifferentiated pluripotent stem cell lines. The calculated scores were predominantly in the range of the undifferentiated reference data set (Fig. 4 b and c). 201B7, ChiPSC7, ChiPSC12 and ChiPSC18 showed Scorecard values which correspond to a full pluripotency, whereby the expression level of the mesoderm and endoderm markers was even below that in the Scorecard reference data set. An exception was line ChiPSC22, which exhibited both a strong downregulation of self-renewal genes and a strong upregulation of ectoderm markers. To analyze the effect of the culture system transfer from monolayer to colony growth side by side with respect to the pluripotency state, the hiPSC lines were characterized on the messenger ribonucleic acid (mRNA) and protein level for the expression of pluripotency markers (Fig. 5, Fig. S6, Fig. S7). Both on protein and mRNA level, the cells lines expressed classical pluripotency markers, such as sex-determining region Y (SRY)-Box Transcription Factor 2 (SOX2), octamer-binding transcription factor 4 (OCT4) and Nanog Homeobox (NANOG) for both cell culture conditions. The transfer to colony growth conditions including the subsequent cell banking step had no negative impact on the protein levels of the investigated pluripotency markers, while a slight decrease in the Podocalyxin-like (*PODXL)* gene expression on the mRNA level was observed after transfer for ChiPSC12. Hereby, the lines ChiPSC22 and 201B7 displayed the weakest pluripotency marker abundance on the protein level in comparison to the other tested lines. In summary, all tested ChiPSC lines were successfully adapted to colony growth, whereby no serious effect was observed with respect to the pluripotency state.

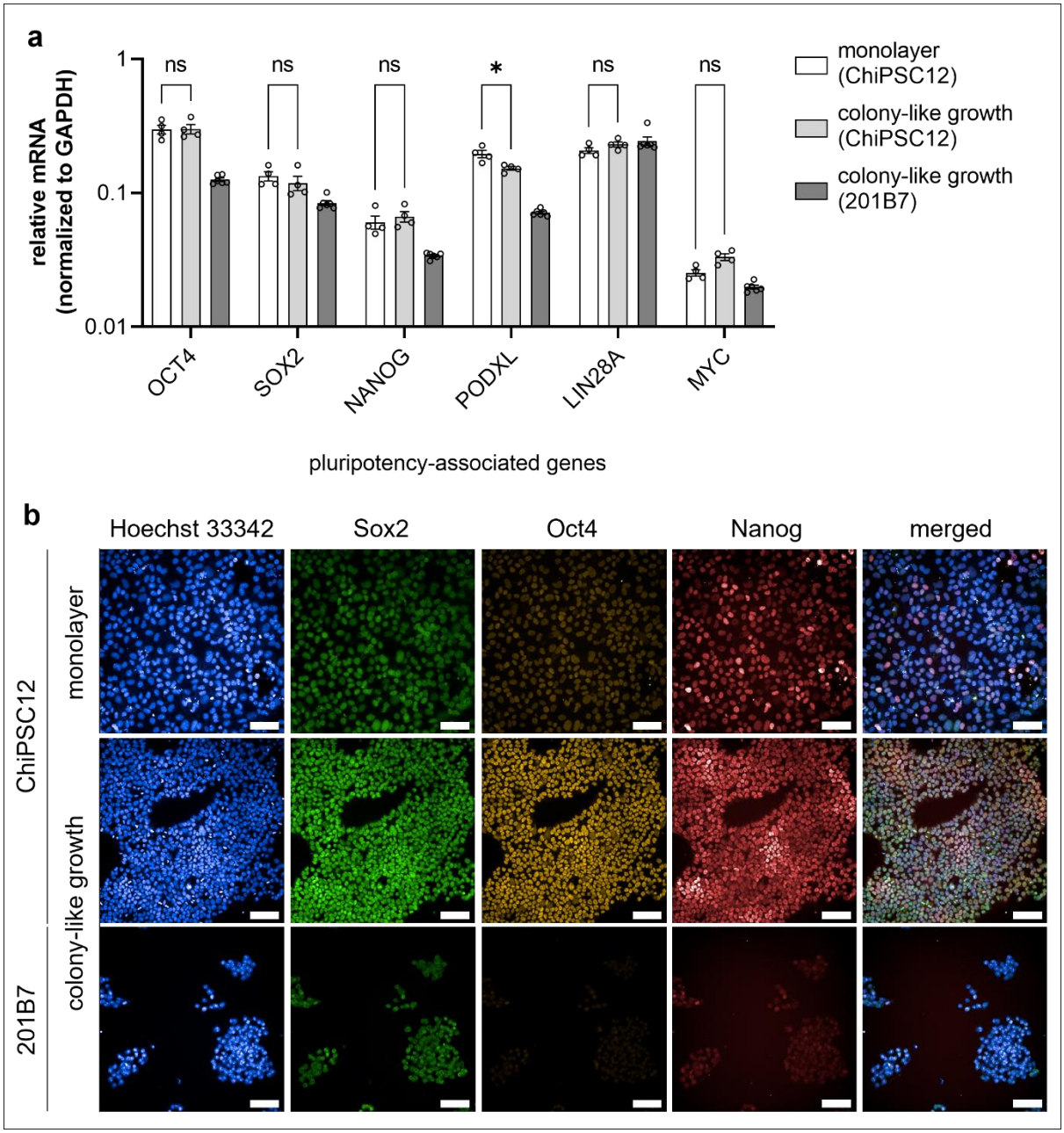

Figure 5. Pluripotency analysis of hiPSC lines 12 and 201B7. (a) Verification of pluripotency by RT-PCR. ChiPSC12 was cultured either in DEF-CS and COAT-1 coated plates (monolayer growth) or was transferred and cultured in StemFit03 medium and iMatrix-511 coated plates (colony-like growth) before cryopreservation. Line 201B7 was cultured in StemFit Basic03 medium and iMatrix-511 coated plates (colony-like growth). Data are representative for ChiPSC12 (N = 3; 201B7: N = 1) and show the mean ± SEM (n = 4-6); two-way ANOVA: ns = not significant, *p<0.05. **(b)** Immunolabeling for classical pluripotency markers (N = 3 (ChiPSC12), N = 1 (201B7); n = 6-8). Scale bar = 50 µm. All parameters were set globally across the images and therefore relative intensity can be quantitatively compared.

2.1.3 Differentiation towards human iPSC-derived macrophages

To derive human macrophages from iPSCs, a directed differentiation protocol was established as shown in Fig. 6 a. After a pre-culture of the previously colony growth- adapted ChiPSC lines for regeneration after thawing, the cells were seeded for colony expansion and subsequent differentiation induction. Starting at day of differentiation (DoD) 0 with pluripotent cells (Fig. 6 b), the cells were pushed towards mesoderm differentiation (DoD2; Fig. 6 c). The development of hemogenic endothelium and subsequently the generation of hematopoietic progenitor cells was forced until DoD13 (Fig. 6 d). From DoD14 on (Fig. 6 e), floating macrophage progenitor cells (MPCs) were harvested weekly for up to four times. Progenitors were frozen and after thawing, the cells were seeded for final macrophage maturation (DoD21; Fig. 6 f and g). The whole differentiation process was carried out with all five above described ChiPSC lines, and the IDMs derived from the lines 201B7, ChiPSC7, ChiPSC12, ChiPSC18 and ChiPSC22 were referred to as IDM#B7, IDM#7, IDM#12, IDM#18, and IDM#22, respectively.

A representative upscaled and optimized differentiation protocol starting with 1800 hiPSCs resulted in 3×10^7 macrophage progenitors from multiple harvests (see Table 2), which were cryopreserved. During the final maturation step towards macrophages, the cells still proliferated to some extent, increasing the final cell yield of IDMs three- to four-fold, which resulted in a macrophage cell count of $9 \times 10^7 – 1.2 \times 10^8$ produced from a single T-175 flask (see Table 2). In total, this number of IDMs translates into up to 24,000 data points in the 384-microplate or into up to 120,000 data points in the 1536-microplate format for the below established efferocytosis assay. Thus, the production of MPCs with eleven T-175 flasks would cover the scope of a primary screening campaign in the 1536-well format with one million data points.

Table 2. Cumulative cell count of progenitors (MPCs) and derived macrophages (IDMs) differentiated in a T-175 flask and resulting producible data points in different microplate formats. *With 5000 cells per well, ** with 1000 cells per well.

Initially seeded cells	**Cumulatively produced cells**		**Microplates (data points)**	
hiPSCs	MPCs	IDMs	384-well*	1536-well**
1800	3×10^7	$9 \times 10^7 – 1.2 \times 10^8$	18,000 – 24,000	90,000 – 120,000

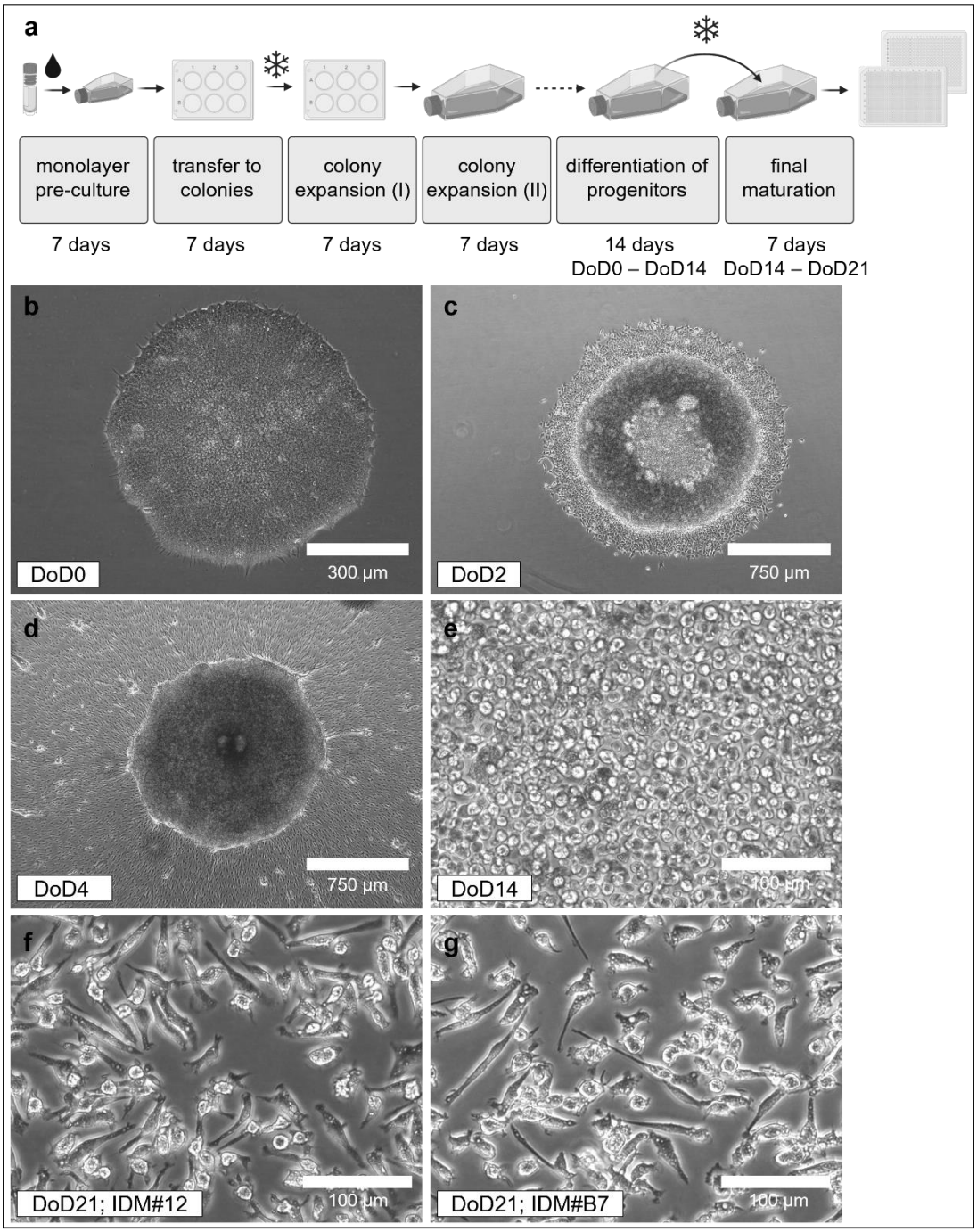

Figure 6. Upscaled protocol produces functionally active iPSC-derived macrophages utilizable for medium- to high-throughput applications. (a) Schematic of the stepwise differentiation including cell banking steps. Only ChiPSC12 was transferred from monolayer to colony-growth prior to differentiation induction, including a cell banking step. After a pre-culture for colony expansion (I) after thawing in 6-well plates, the cells were seeded for expansion of the colonies (II) and subsequent differentiation induction in T-175 flasks. 14 days after differentiation induction, progenitors were harvested weekly for up to four times. Progenitors were frozen and after thawing, the cells were seeded for final macrophage maturation. Fully matured macrophages were seeded in assay plates (384-well or 1536-well format). **(b-e)** Morphological changes during differentiation to iPSC-derived macrophage progenitors. Representative bright field images of the morphology from an undifferentiated colony at DoD0 (day of differentiation; b) and developing progenitors during the differentiation at DoD2 (c), DoD4 (d) and at DoD14 (e) using ChiPSC12. Between DoD4 and DoD14, the colony morphology only changes slightly, and accordingly, a representative image from DoD4 was selected. **(f+g)** Representative bright field images of iPSC-derived macrophages at day DoD21 (7 days after seeding the macrophage progenitors with M-CSF) for IDM#12 (f) and IDM#B7 (g).

2.1.3.1 Protocol optimizations and adaptations for high-throughput applications

To improve and adapt this protocol for high-throughput applications, several modifications were tested out. Using ChiPSC12, the impact of different stem cell media and varying concentrations of two proteins in the media was analyzed with respect to the differentiation outcome. Additionally, the cryopreservation of macrophage progenitors was tested.

The selection of stem cell media may have a great impact on the differentiation outcome. Accordingly, three different StemFit media were tested with respect to progenitor yield and marker expression levels in the IDMs. The usage of StemFit Basic02 and StemFit Basic03 needed the manual addition of fibroblast growth factor 2 (FGF-2), a crucial regulator of pluripotency[61]. In contrast, StemFit Basic04 Complete Type (StemFit Basic04 CT) already contained FGF-2. While StemFit Basic02 and StemFit Basic03 exhibited comparable morphologies of both progenitors and derived macrophages, StemFit Basic04 CT resulted in heterogeneous populations with respect to cellular shape and size (Fig. 7 a-f). Flow cytometry analysis of produced IDM#12 for the macrophage markers CD14, CD45, CD163 and CD206[62–64] revealed likewise a heterogeneous macrophage population produced with StemFit Basic04 CT and indicated a proportion of non-leukocytic cells of approximately 25 % based on the CD45 expression (Fig. 7 g). For the other two tested media, this proportion was below 2.4 %. Furthermore, the macrophage progenitor yield was significantly reduced with StemFit Basic04 CT (Table 3) and only two harvests in total were possible. With the usage of StemFit Basic03, the highest progenitor yield was obtained, and derived macrophages showed a solid phenotype. On this account, StemFit Basic03 was used for all consecutive differentiation approaches.

Table 3. Macrophage progenitor yield using three different media during maintenance and expansion phase prior to differentiation induction in ChiPSC12. Shown is the yield per 6-well plate.

StemFit medium	1st harvest	2nd harvest	3rd harvest	4th harvest	cumulative
Basic02	4×10^6	4×10^6	7×10^6	8×10^6	2.3×10^7
Basic03	2×10^6	6×10^6	1×10^7	8×10^6	2.6×10^7
Basic04 CT	3×10^6	7×10^5	not possible	not possible	3.7×10^6

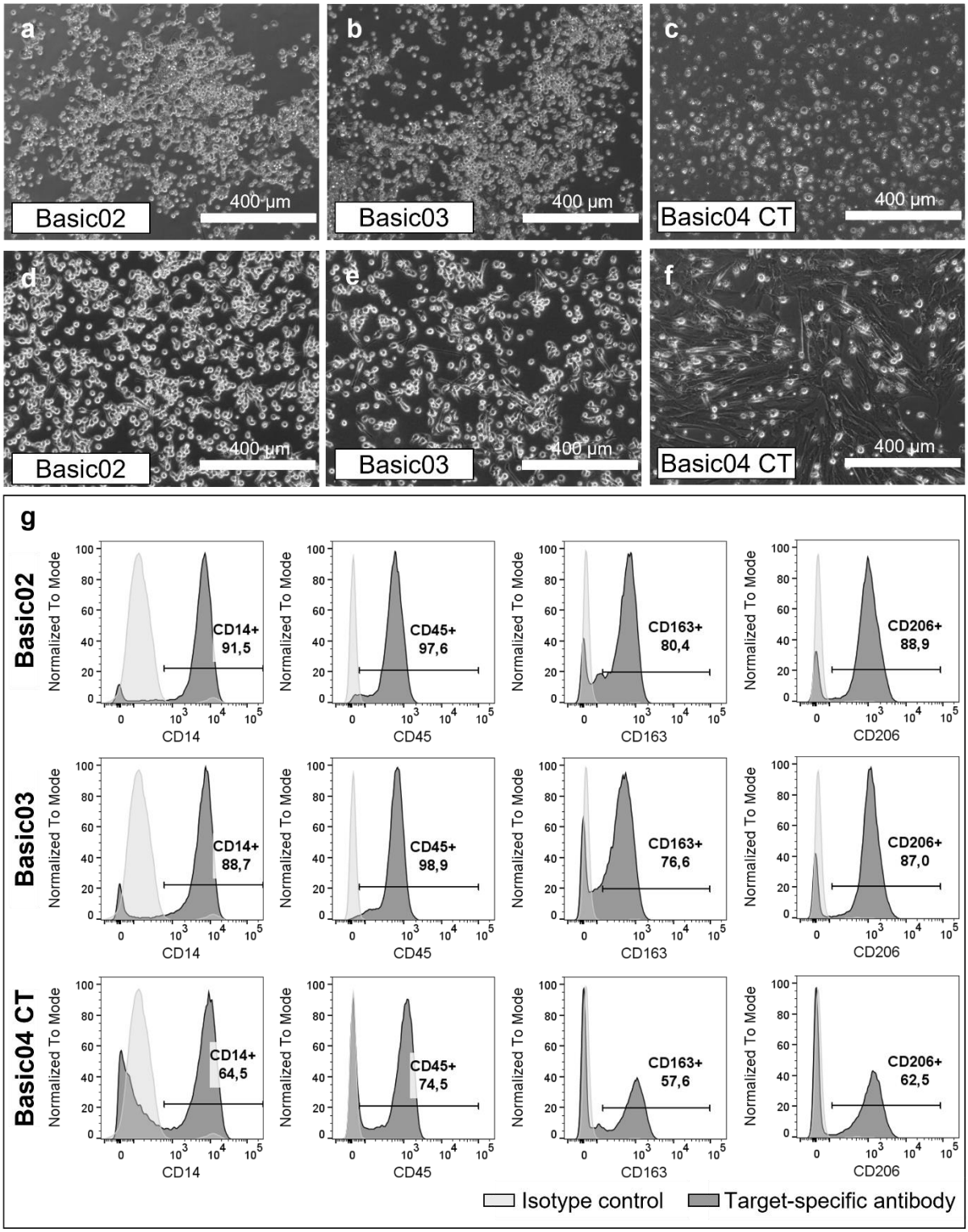

Figure 7. Optimization of maintenance and expansion medium. ChiPSC12 was maintained and expanded prior to differentiation induction using three different stem cell media. **(a-f)** Morphology of macrophage progenitors (a-c) and IDMs (d-f; N = 1). **(g)** Flow cytometry analysis of produced IDM#12 for the macrophage markers CD14, CD45, CD163 and CD206 (in %; N = 1). Gating is based on 1 % isotype control.

To further increase the yield of macrophage progenitors, different concentrations of Vascular endothelial growth factor A (VEGF-A) between DoD4 and DoD7 were tested, since this factor is needed for expansion and differentiation of hematopoietic precursor cells, which are characterized by CD34 expression[61]. As shown in Fig. 8 a and Table 4, the titration of VEGF-A had no effect on the percentage of CD34 positive progenitor cells at DoD7. However, the mean fluorescence intensity (MFI) was approximately 65 % higher when using the lowest VEGF-A concentration compared to the highest applied concentration.

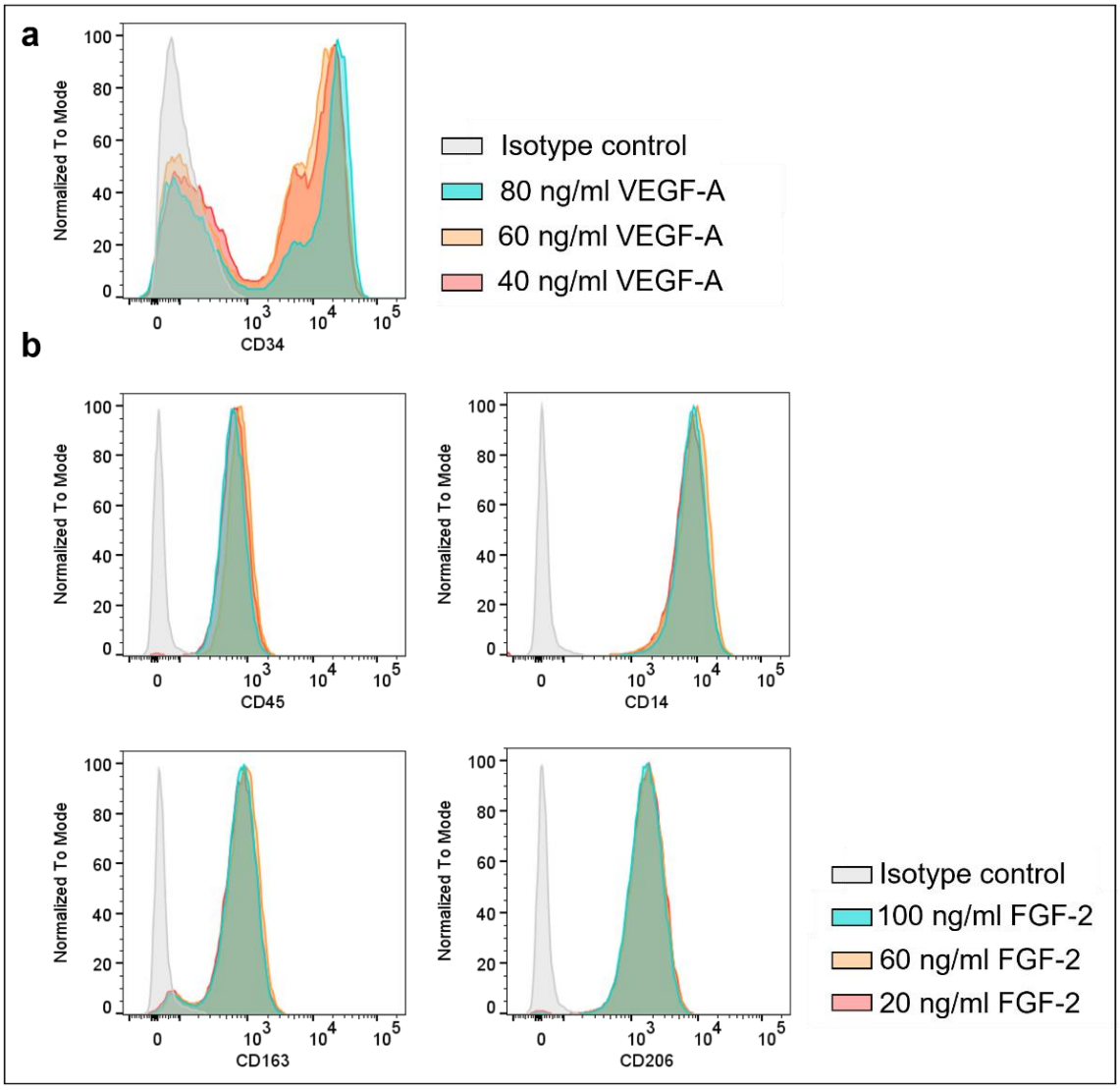

Figure 8. Optimization of differentiation protocol. (a) Flow cytometry analysis of progenitors at DoD7 for the marker CD34 (in %) to assess the effect of different VEGF-A concentrations between DoD4 and DoD7 (N = 1). **(b)** Flow cytometry analysis of IDM#12 for the macrophage markers CD14, CD45, CD163 and CD206 (in %) to analyze the effect of different FGF-2 concentrations prior to differentiation induction and during the maintenance phase (N = 2). Gating is based on 1 % isotype control.

Table 4. Percentages and mean fluorescence intensity (MFI) of CD34 positive cells for different applied VEGF-A concentrations between DoD4 and DoD7 in ChiPSC12.

VEGF-A concentration	$CD34^+$ cells	MFI
40 ng/ml	62 %	19928
60 ng/ml	63 %	12562
80 ng/ml	60 %	12907

FGF-2 primarily functions in maintaining pluripotency but is also involved in differentiation pathways[61]. Hence, the correct balance of the protein in the stem cell medium is of pivotal importance, to maintain a pluripotent state and reduce potential spontaneous differentiations. Accordingly, the effect of different FGF-2 concentrations in the iPSC expansion phase prior to differentiation induction was analyzed with respect to the differentiation outcome. A flow cytometry analysis with IDMs for the macrophage markers CD14, CD45, CD163 and CD206 was performed and revealed no impact on marker expression (Fig. 8 b and Table 5). For this reason, a FGF-2 concentration of 100 ng/ml and a VEGF-A concentration of 40 ng/ml between DoD4 and DoD7 was used for all consecutive differentiation approaches.

Table 5. Percentages of IDM#12 cells positive for the macrophage markers CD45, CD14, CD163 and CD206 for different applied FGF-2 concentrations prior to differentiation induction.

FGF-2 concentration	$CD45^+$ cells	$CD14^+$ cells	$CD163^+$ cells	$CD206^+$ cells
20 ng/ml	99.5 %	99.4 %	93.2 %	99.3 %
60 ng/ml	99.9 %	99.9 %	94.2 %	99.7 %
100 ng/ml	99.9 %	99.9 %	94.2 %	99.6 %

To enable the establishment of large stocks of IDM progenitors that can be used for a screening or drug candidate profiling with accordingly diminished lead times, freezing of progenitors was tested. Progenitor cells from multiple harvests were cryopreserved after each harvest round and later on served as starting points for the final phase of macrophage differentiation. Upon thawing, the MPCs showed high recovery rates (> 90 % viability). To analyze the impact of macrophage progenitor cryopreservation on macrophage marker expression, a flow cytometry analysis was performed, comparing IDMs derived from non-cryopreserved or cryopreserved progenitors (Fig. 9). Both tested IDM lines showed an increased expression of all analyzed macrophage markers when they were derived from cryopreserved progenitors.

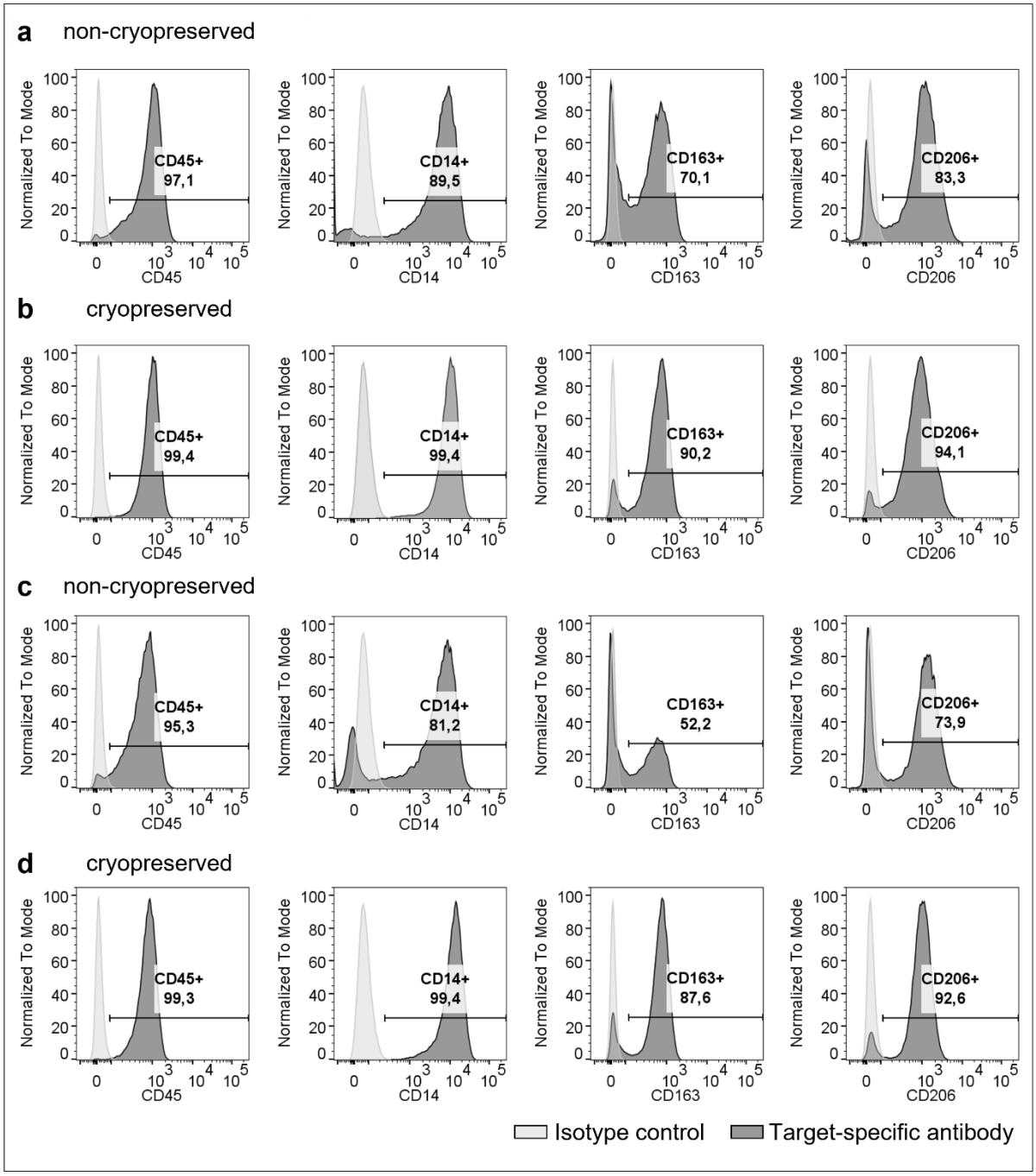

Figure 9. Impact of macrophage progenitor cryopreservation on macrophage marker expression. Flow cytometry analysis of IDM#12 (a+b) and IDM#B7 (c+d) derived from non-cryopreserved (a+c) or cryopreserved (b+d) progenitors for macrophage markers CD45, CD14, CD163 and CD206 (in %; N = 1). Gating is based on 1 % isotype control.

2.1.3.2 Kinetic marker measurement of progenitor cells in different stages of differentiation

To retrace the different stages during the differentiation process applying the optimized protocol, a flow cytometry analysis of progenitors was performed between DoD2 and DoD14 for ChiPSC12 (Fig. 10 a-d) and 201B7 (Fig. 10 e-h). During mesoderm differentiation (DoD2; Fig. 10 a and e) and hemogenic endothelial induction (DoD4; Fig. 10 b and f), Kinase insert domain receptor (KDR; mesodermal marker[61]) expression was maintained and was downregulated after this timepoint (DoD7; Fig. 10 c and g). From this stage on, cells were positive for CD34, an early hematopoietic marker[61]. Leukocytic cells, shown by CD45 expression[63], were produced slowly from DoD7 on until DoD14 (Fig. 10 d and h). Myeloid cells detected by CD14 expression[62] arose from DoD14 on (Fig. 10 d and h). ChiPSC12 and 201B7 cells demonstrated a similar marker pattern over the analyzed time course. However, both lines showed slight differences for the respective marker expression levels.

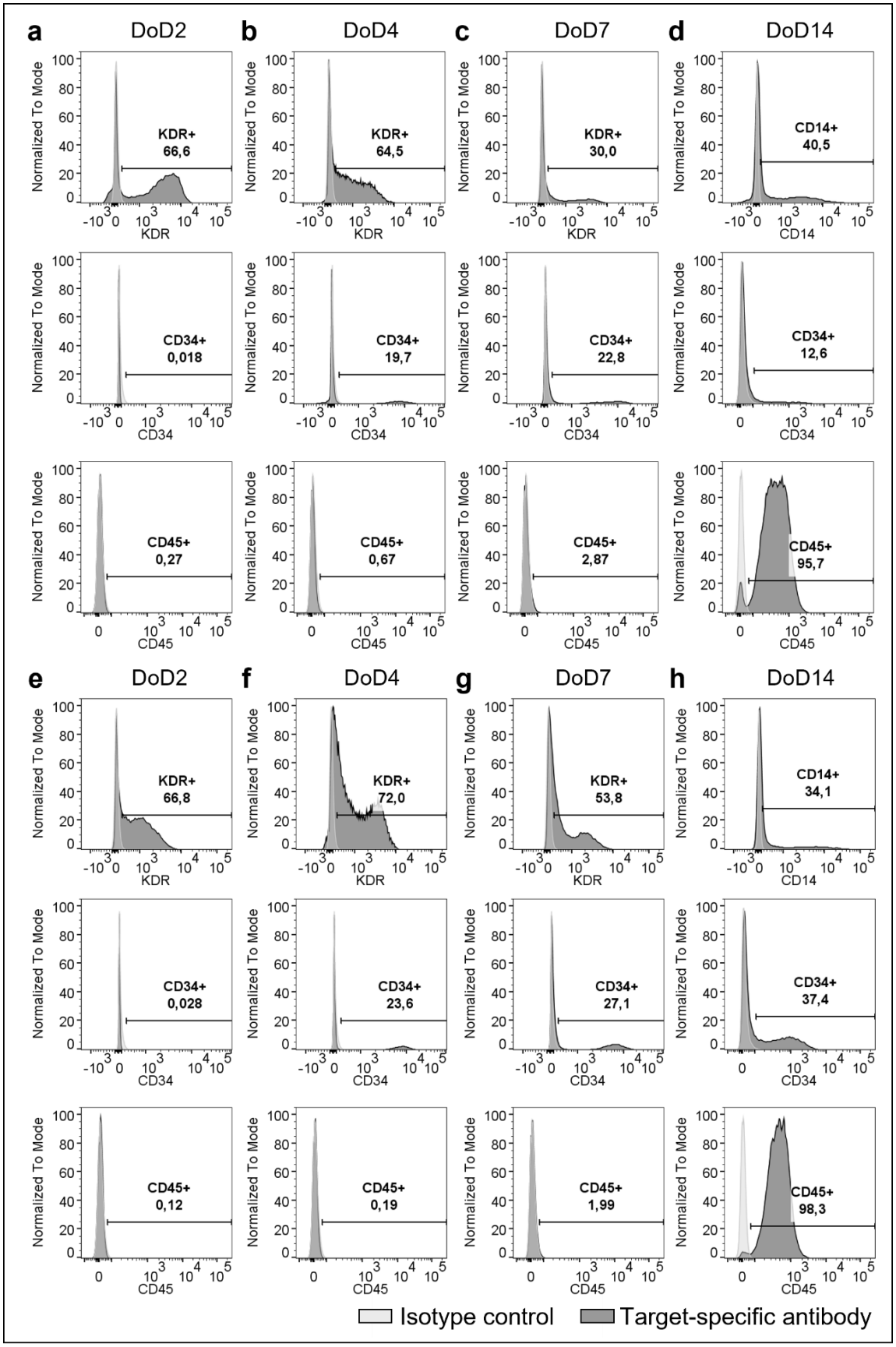

Figure 10. Changes in marker expression during the differentiation to macrophage progenitors. Flow cytometry analysis of progenitors derived from ChiPSC12 (a-d) or 201B7 (e-h) for KDR, CD34, CD14 and CD45 (in %) at DoD2 (a+e), DoD4 (b+f), DoD7 (c+g) and DoD14 (d+h; N = 1). Gating is based on 1 % isotype control.

2.1.3.3 Detailed comparison of iPSC-derived macrophages to monocyte-derived macrophages

Applying the optimized protocol, macrophages were differentiated using cryopreserved progenitors and analyzed in comparison to monocyte-derived macrophages. All produced IDMs derived from five different hiPSC lines in total displayed similar morphologies compared to MDMs using brightfield microscopy (Fig. 11 a-c and Fig. S8 d-f). However, cells of ChiPSC line 7 behaved differently during the progenitor differentiation process. The cells showed a distinct differentiation rate in comparison to all other tested lines (data not shown) and were therefore excluded for subsequent analyses or differentiation approaches. IDM#12, IDM#18, IDM#22 and IDM#B7 displayed a strong expression of the leukocytic lineage surface marker CD45[63] (> 96 % positive cells for all macrophage types) and were highly positive for the myeloid marker CD14[62] (> 92 % for all macrophage types; Fig. 11 d-f, Fig. S8 g and h). The macrophage markers CD163 and CD206[64] were expressed at a moderate to high level on IDMs (> 65 % for CD163, > 75 % for CD206) and MDMs (> 83 % for CD163, > 91 % for CD206). IDM#12 and IDM#B7 displayed the highest expression levels in comparison to the other tested lines (CD45: > 99 %; CD14: > 95 %; CD163: > 87 % and CD206: > 96 % positive cells). To validate their functional activity with respect to phagocytosis, IDMs were incubated with pHrodo-labeled *Escherichia coli* (*E. coli)* bioparticle conjugates. All tested IDM types revealed a similar phagocytotic activity as MDMs (Fig. 11 g-i and Fig. S8 i and j). Since IDMs derived from lines ChiPSC12 and 201B7 were functionally active and exhibited the strongest macrophage marker expression levels, all subsequent approaches were performed using these two lines in parallel.

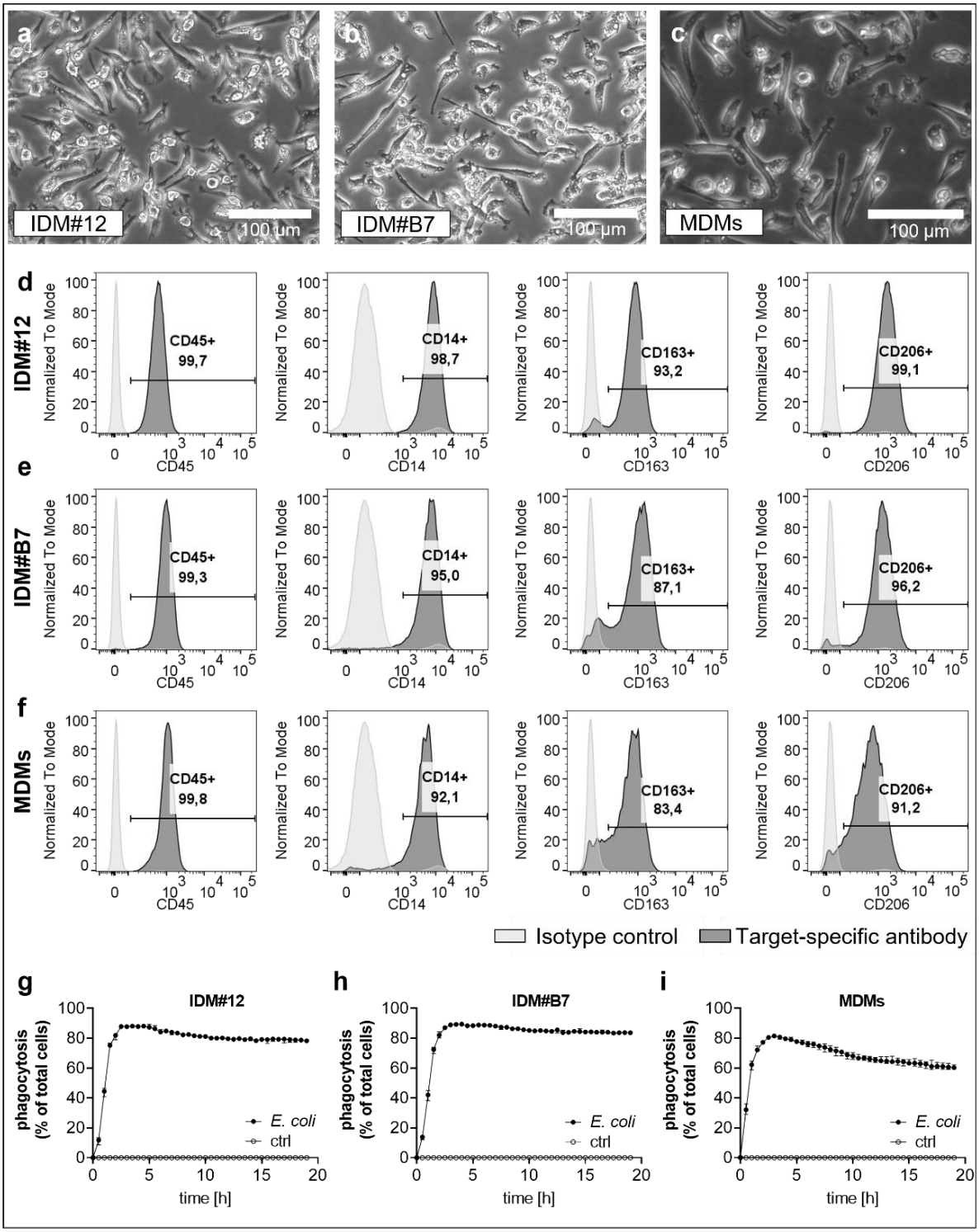

Figure 11. Comparison of iPSC-derived macrophages with monocyte-derived macrophages. (a-c) Representative brightfield images of IDM#12 (a), IDM#B7 (b) and MDMs (c). **(d-f)** Representative macrophage marker expression levels of CD45, CD14, CD163 and CD206 of IDM#12 (d), IDM#B7 (e) and MDMs (f; in %; IDM#12: N = 5; IDM#B7: N = 3; MDMs: N = 2). Gating is based on 1 % isotype control. **(g-i)** Representative phagocytotic activity of IDM#12 (g), IDM#B7 (h) and MDMs (i) treated with pHrodo-labeled *E. coli* bioparticles (median ± IQR; n = 7 (IDM#12), n = 14 (IDM#B7, MDMs); some error bars are not visible). Assay was measured in the Opera Phenix HTS System in a kinetic mode (IDM#12: N = 3; IDM#B7: N = 3; MDMs: N = 4).

A primary functional characteristic of macrophages is their plasticity to diverse stimuli and the subsequent polarization into different cellular phenotypes[2]. Accordingly, changes in the cellular proteome responses in differentially polarized macrophages were analyzed by a quantitative proteomics study (Fig. 12). To compare IDMs derived from lines ChiPSC12 and 201B7 with MDMs derived from different donors, cells were polarized for 24 hours either with LPS to induce a pro-inflammatory state or with an IL-4/IL-13 cocktail to drive the cells towards an anti-inflammatory, pro-homeostatic condition. A naïve condition was induced by treatment with the vehicle control. IDMs and MDMs responded collectively in a similar manner. However, individual proteins were differentially expressed (Fig. 12 a+b). Principal component analysis (PCA) showed that the LPS condition separated from the other two conditions (Fig. 12 c). The naïve state was close to the anti-inflammatory state for both macrophage cell types. Moreover, a separation between IDMs and MDMs was found on the component 2 (source effect).

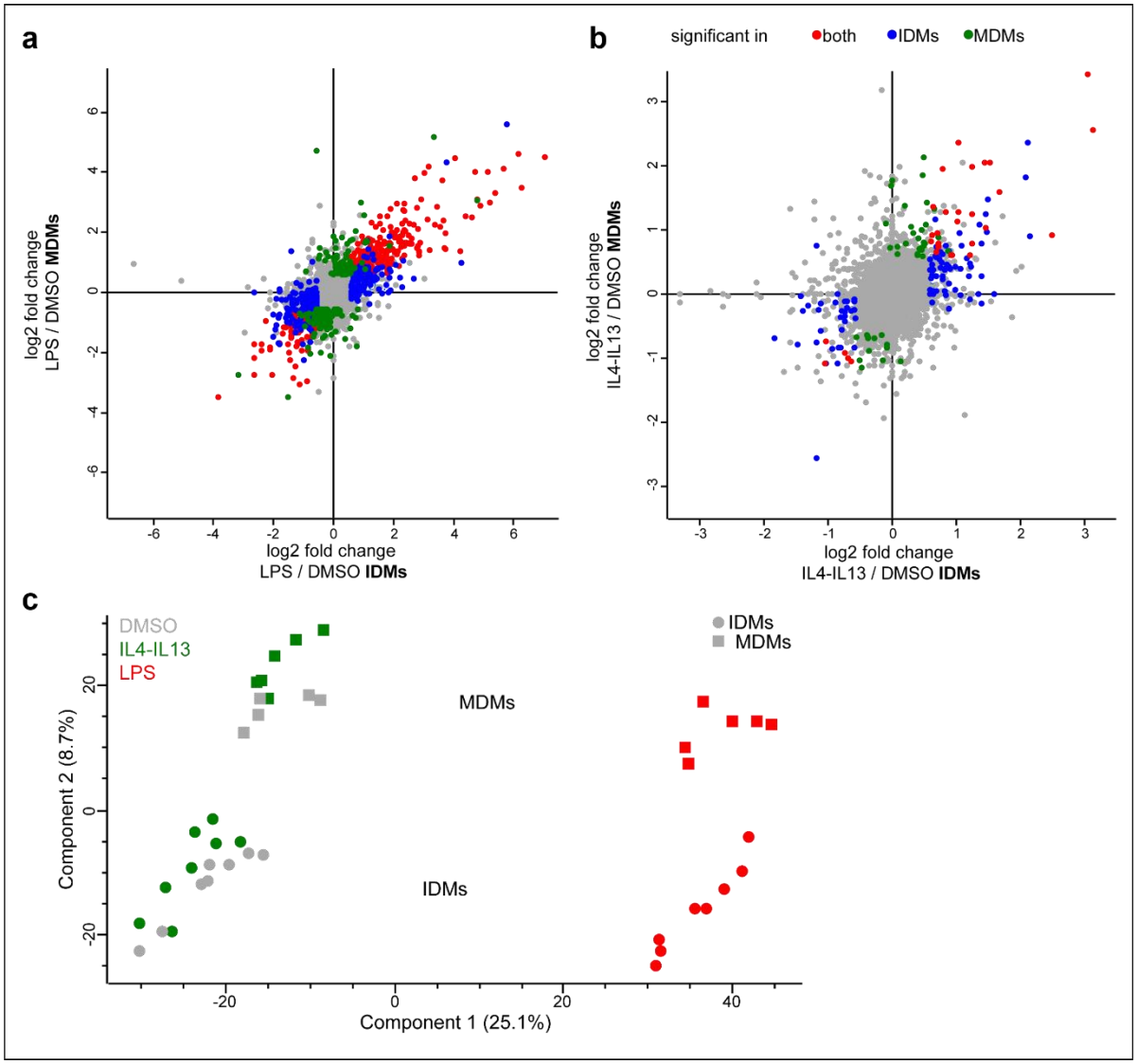

Figure 12. Proteomic changes in iPSC- and monocyte-derived macrophages upon LPS or IL-4/IL-13 stimulation. Macrophages were treated for 24 h with either LPS, IL-4/IL-13 or vehicle control. **(a+b)** Scatter plot shows the correlation (Pearson correlation coefficient 0.68) of log2 fold changes from IDMs (derived from ChiPSC12 and 201B7) and MDMs comparing the protein intensities of LPS- (a) or IL-4/IL-13-treated (b) to DMSO-treated cells, respectively. Proteins are displayed in color when significantly deregulated (fold change ≥1.5, Benjamini-Hochberg adjusted p-value <0.05) in both cell types (red), in IDMs only (blue) and MDMs only (green). **(c)** Principal component analysis (PCA) plot of proteomic data obtained from treatment of IDMs and MDMs with either LPS, IL-4/IL-13 or vehicle control (IDMs: N = 1, n = 4; MDMs: N = 3, n = 2).

To test whether the generated IDMs were able to release mediators in response to a specific stimulation, the cells were stimulated with depleted zymosan, simulating a pathogen infection (Fig. 13). Similar to MDMs, the IDMs showed a significant and at least 145-fold increase of TNFα levels.

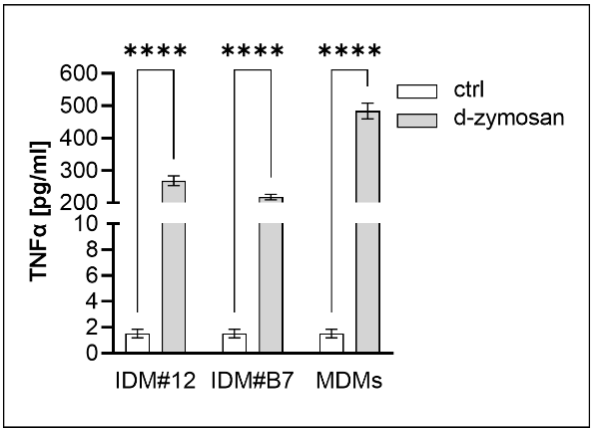

Figure 13. Functional analysis of iPSC-derived macrophages in response to Dectin-1 stimulation. IDMs and MDMs were treated with depleted zymosan (d-zymosan) and analyzed for TNFα on protein level (mean ± SEM; n = 4; N = 1 (IDMs), N = 2 (MDMs). Two-way ANOVA: ****p < 0.0001.

In summary, the here established upscaled high-yield protocol produced freezable macrophage progenitors suitable for high-throughput applications. The derived macrophages were functionally active and shared typical features with primary monocyte-derived macrophages, such as morphology, macrophage marker expression, mediator release and phagocytotic activity.

2.2 Development of a miniaturized high-content imaging-based efferocytosis assay

One focus of this work was to analyze a pivotal function of macrophages: the efferocytotic removal of apoptotic cells. Efferocytosis as a target mechanism for new e.g., anti-fibrotic or anti-cancer drugs may have a great impact on future treatment options. To enable higher throughput applications, a high-content-imaging-based efferocytosis assay in the 384-well and 1536-well microplate format with an endpoint measurement after 5 hours was established using the Opera Phenix High-Content Reader in this study.

2.2.1 Efferocytosis of irradiated Raji prey cells by iPSC-derived or monocyte-derived macrophages

To maintain tissue homeostasis, macrophages must distinguish between live and dying cells, which is regulated by 'eat-me-signals' presented on the surface of apoptotic cells being a pre-requisite for subsequent engulfment[11]. To ensure a reproducible apoptosis induction of the employed Raji suspension prey cells, a UV-C light chamber was used, which granted a uniform illumination and a constant distance between the UV lamps and the cell layer. The size of the chamber provided enough space for the simultaneous irradiation of ten 14 cm-diameter dishes containing Raji cells, which constitutes a sufficient number of prey cells for 32 or 42 microplates of the 384-well or 1536-well format, respectively. To investigate the apoptotic state of the Raji prey cells after UV irradiation, two key indicators of apoptosis were monitored over time: Caspase 3/7 activation and externalization of the 'eat-me-signal' Phosphatidylserine (PS), as shown by Annexin V binding[11,65] (Fig. 14 a and b). As shown in Fig. 14 b, at five hours after UV pulse irradiation (corresponding timepoint to the efferocytosis assay endpoint), 83 % of the cells were positive for Caspase 3/7 and 79 % were positive for Annexin V binding, whereas only a smaller fraction of the non-irradiated control cells was positive for Caspase 3/7 (22 %) or Annexin V binding (21 %). In parallel to the Raji cell line, other potential prey cells were tested and analyzed for apoptosis induction (Fig. S9). However, the Raji cells showed the most reproducible apoptosis induction and had the advantage of being suspension cells, simplifying the prey cell preparation. On this account, the Raji cell line was selected to serve as prey cell type in the presented assay set-up.

To monitor the efferocytotic engulfment of an irradiated Raji cell by a macrophage, the Raji cell was surface-labeled with the pH-sensitive pHrodo dye. The assay principle is envisioned as follows: during efferocytosis, the Raji cell is transferred from the approximately neutral pH of the extracellular medium into the acidic macrophage efferosome. The respective pH change leads to an increased pHrodo fluorescence intensity (Fig. 14 c and d). Indeed, a high number

of efferocytotic events was observed microscopically when UV-irradiated pHrodo-labeled Raji cells had been co-incubated with IDMs over a time course of 24 hours (Fig. 14 f-i). To verify the authenticity of the observed efferocytotic process, confocal stack measurements were carried out. Vertical sections across macrophages reconstructed from the confocal scan demonstrated that the pHrodo signal indeed originated from an intracellular compartment within macrophages (Fig. 14 e).

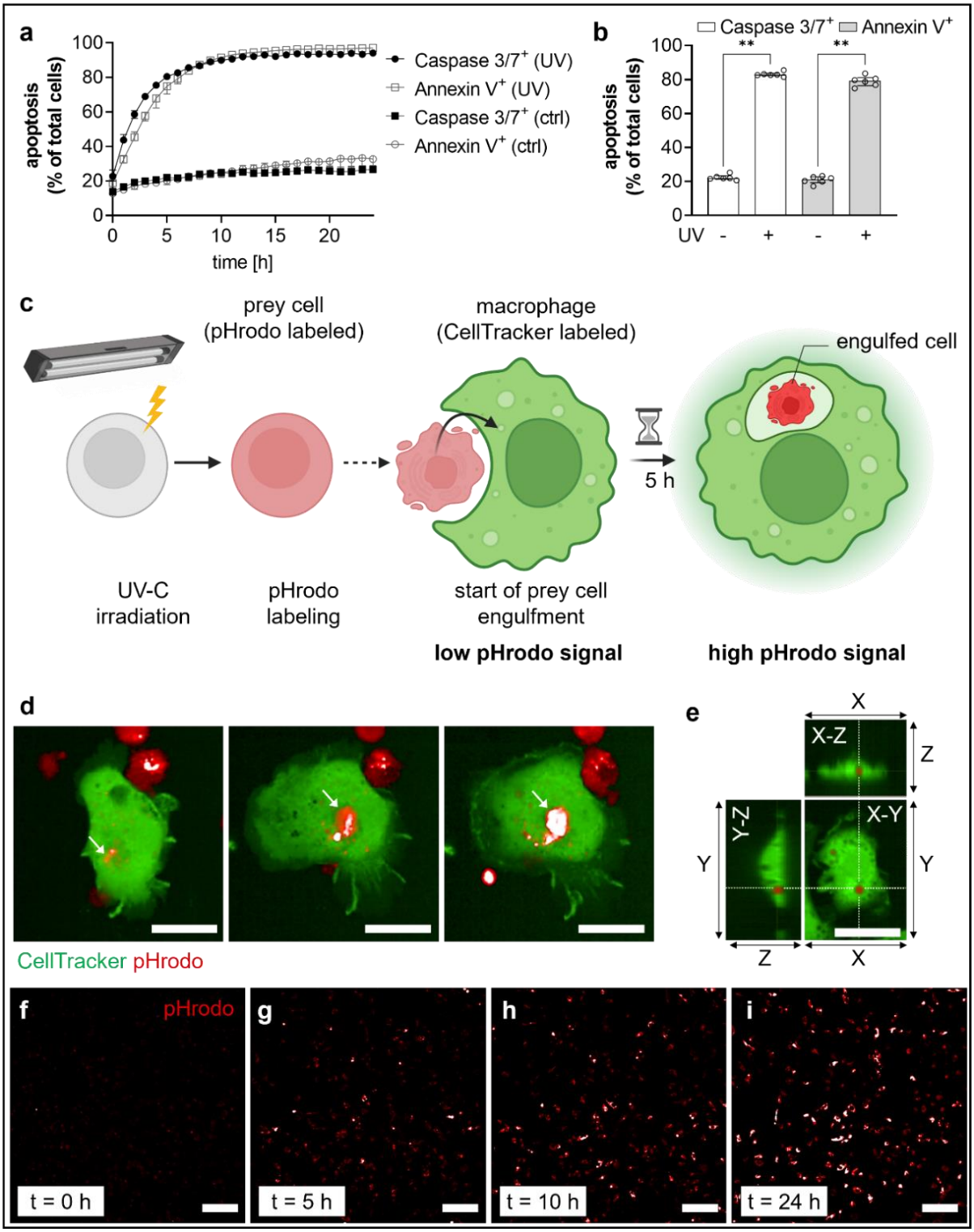

Figure 14. Irradiated Raji cells suit as prey cells for both iPSC-derived and monocyte-derived macrophages. **(a+b)** Activity of Caspase 3/7 and exposure of Phosphatidylserine shown by Annexin V binding in irradiated (UV) and non-irradiated control Raji prey cells over a time course of 24 hours (a) or at t = 5 h after treatment (corresponds to efferocytosis assay endpoint; b). Data points are representative (N = 4) and show the median ± IQR (n = 6); Kruskal-Wallis-test: **p < 0.01. **(c)** Efferocytosis assay principle. Macrophages were labeled with a fluorescent CellTracker green dye and treated with pHrodo-labeled irradiated prey cells exhibiting a low pHrodo signal. Efferocytosis was quantified by an increase in pHrodo fluorescence within the macrophages as a result of prey cell engulfment and subsequent efferosomal acidification. **(d)** Close-up showing the uptake of a prey cell by a macrophage quantified by a pHrodo fluorescence increase. **(e)** Confocal image (XYZ by stack measurement) of

Figure legend continues on the next page

IDM#12 cells (green) and engulfed prey cells visualized by the pHrodo signal (red). The lateral view was reconstructed based upon a section of the confocal scan. Scale bar = 20 µm, magnification = 63X. **(f-i)** Confocal images taken directly after prey cell addition (t = 0 h; f), after 5 hours (g), 10 hours (h) and 24 hours (i) showing efferocytosing IDM#12 cells by the bright red areas. All parameters were set globally across the images and therefore relative intensity can be quantitatively compared. Scale bar = 100 µm, Magnification = 20X.

2.2.2 Development of an image-based efferocytosis co-localization algorithm

To enable a quantification of the efferocytotic activity rate, a co-localization-based image analysis algorithm was established. For the development of this algorithm, macrophages pre-treated with 1 µM cytochalasin D were compared with vehicle-treated macrophages. Cytochalasines largely inhibit efferocytosis by restricting macrophage mobility and prey cell engulfment due to inhibition of actin polymerization[66]. Image analysis was performed using the Columbus software from Perkin Elmer. A detailed description of the analysis algorithm based on sequential building blocks is provided in the methods section. Briefly, in the first step, macrophages were detected based on their CellTracker green signal (Fig. 15 a) and defined as “whole cell” regions. Next, engulfed prey cells were detected as so-called “spots” based on the acidic pH-enhanced pHrodo signal (Fig. 15 b). The search for such spots was restricted to the pre-defined “whole cell” regions eliminating false-positive spots outside the macrophages and leaving only “inside spots” corresponding to bona fide engulfed prey cells. That way, the residual pHrodo fluorescence from non-eaten prey cells was excluded. Subsequently, the mean intensity properties of the spots were calculated based on the pHrodo signal. In the last step, the percentage of macrophages was calculated that displayed at least one efferocytosis event, i.e., that contained at least one “inside spot”. In this context, only these “inside spots” were taken into consideration that surpassed a minimum spot area and that exceeded a pre-defined threshold of fluorescence intensity (Fig. 15 c).

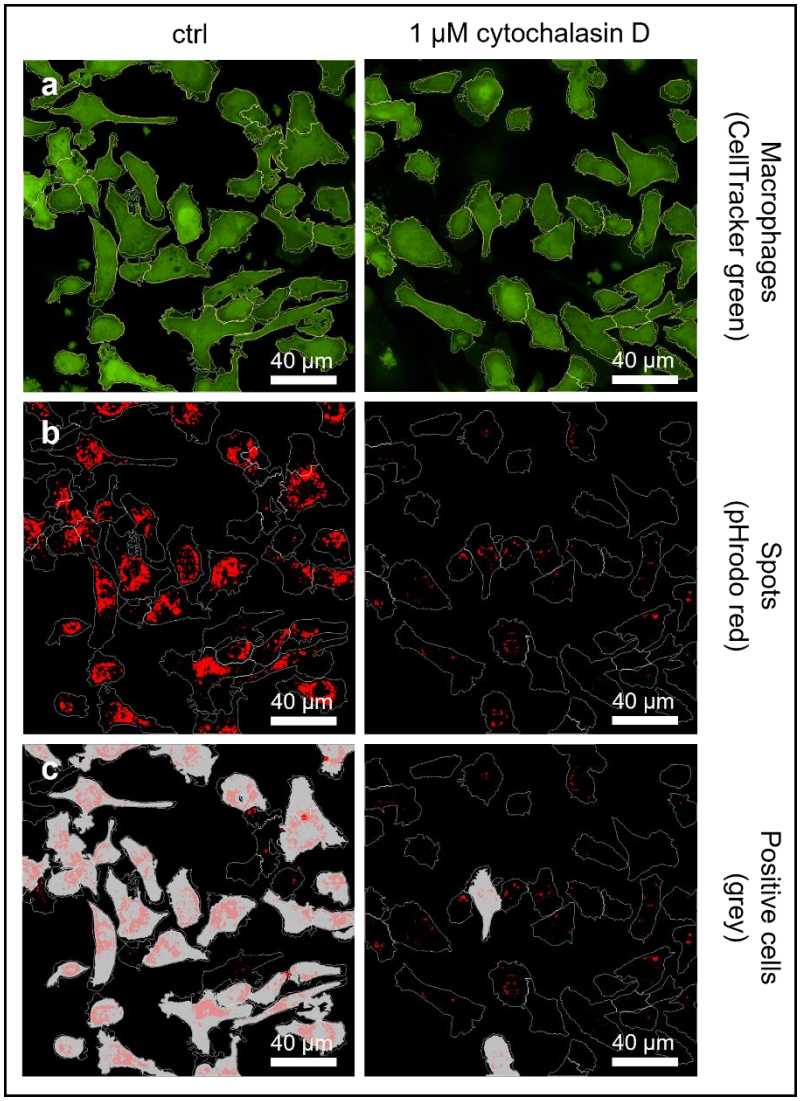

Figure 15. Image-based efferocytosis analysis algorithm detects spots exclusively in macrophages. The analysis algorithm was developed based on pretreated IDMs or MDMs with 1 µM cytochalasin D (efferocytosis inhibitor) or vehicle control prior to Raji prey cell addition. Plate was measured 5 hours after prey cell addition in the Opera Phenix HTS System and shows example images of IDM#12. All parameters were set globally across images between conditions and therefore the relative intensity can be quantitatively compared.

(a) Macrophages were detected based on their CellTracker green signal and a surrounding region was added around the detected cells. Yellow border = cell, white border = cell and surrounding region (whole cell). **(b)** Spots were detected exclusively within defined whole cells from (a) and the intensity properties of the spots were calculated based on the pHrodo signal. White border = whole cell, red spots = detected efferocytosis events. **(c)** Cells were selected based on their total spot intensity calculated in (b) using a defined threshold. White border = whole cell, red spots = detected efferocytosis events, grey = selected macrophages being positive for efferocytosis.

2.2.3 Basal efferocytotic activity of iPSC- and monocyte-derived macrophages

To achieve a higher throughput for the presented assay set-up, real time kinetics cannot be used. However, to select an appropriate timepoint at which to measure the efferocytotic activity, the assay was run in a kinetic mode using the live-cell chamber of the Opera Phenix with irradiated and control prey cells (Fig. 16). Spontaneous apoptosis likewise occurs among non-irradiated cells (compare Fig. 14 a and b). Accordingly, a certain number of efferocytosis events was also observed for the non-irradiated prey cells. This basal uptake of non-irradiated Raji cells by MDMs and IDM#B7 was similar after 5 hours (around 37 %), while IDM#12 exhibited a slightly lower basal activity with approximately 29 % (Fig. 16 c-f). However, for every analyzed macrophage type, a significantly higher percentage of efferocytosis events was detectable when the macrophages were provided with irradiated prey cells. This was also shown for IDMs derived from ChiPSC lines 18 and 22 (Fig. S10). Based on the live cell kinetic

data from several MDM donors and IDMs derived from four different lines in total, the incubation time of the macrophages with the prey cells was fixed at 5 hours.

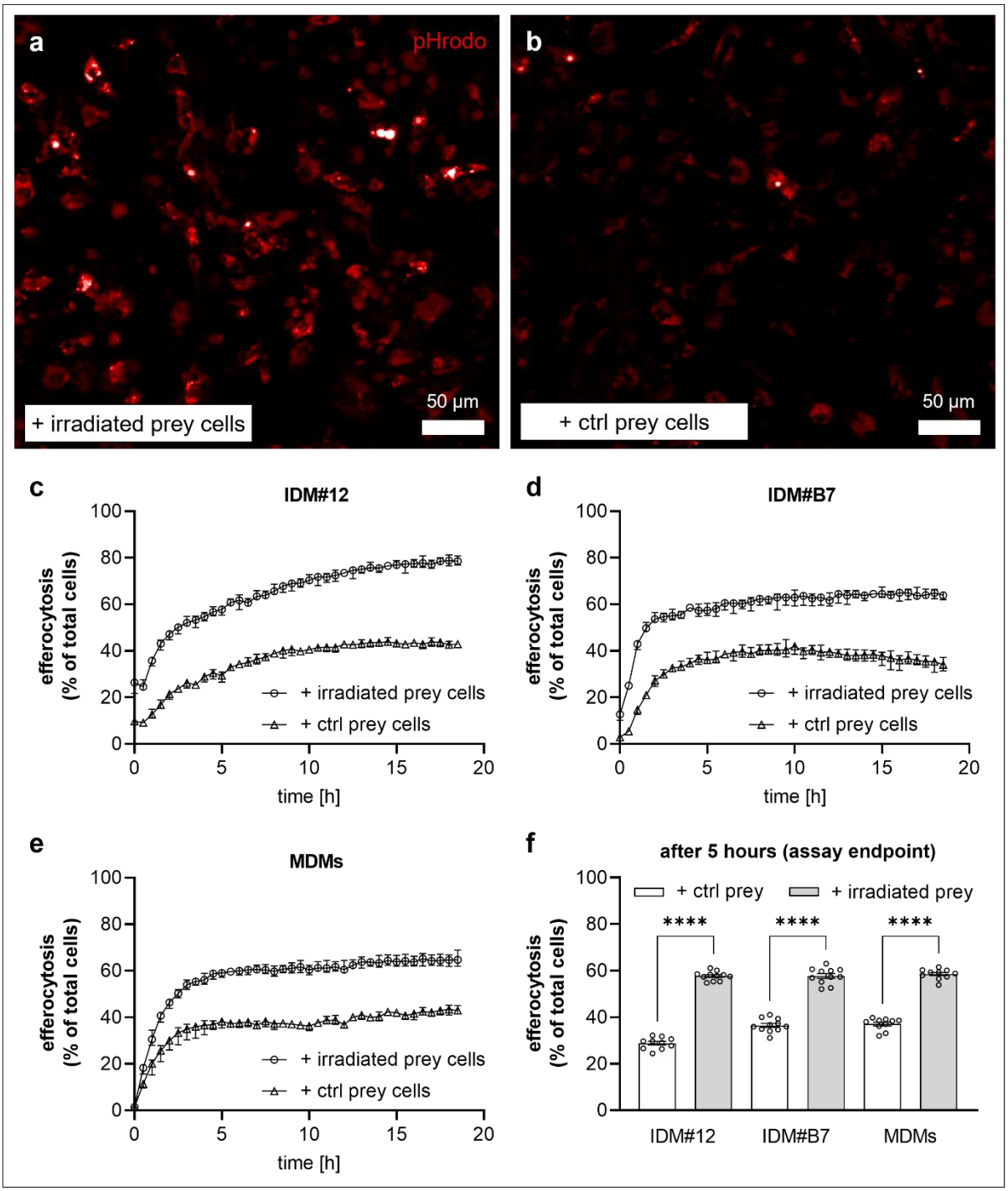

Figure 16. Irradiated Raji cells serve as prey cells for both iPSC-derived and monocyte-derived macrophages. (a+b) Confocal images taken 5 h after irradiated (a) or ctrl (b) prey cell addition showing efferocytosing IDM#12 by the bright red areas (pHrodo signal). All parameters were set globally across the images and therefore relative intensity can be quantitatively compared. **(c-f)** Representative efferocytosis data (N = 2) using IDMs derived from two different hiPSC lines incubated with irradiated or ctrl Raji cells as prey. Assay was conducted as kinetics (shown in c-e; median ± IQR; n = 11 (IDMs) or n = 10 (MDMs)) and extracted data for the time point 5 hours after prey cell addition are shown in f (mean ± SEM; n = 11 (IDMs) or n = 10 (MDMs)); one-way ANOVA: ****p<0.0001.

2.2.4 Quantification of the pharmacological cytochalasin D effect by the high-content-imaging-based efferocytosis assay

To assess whether the established efferocytosis assay delivered a sufficient signal window, MDMs and IDMs were pre-treated with 1 µM cytochalasin D or vehicle prior to prey cell addition. Efferocytosis events were detected and quantified based on the process described above, revealing a significant and an at least four-fold decrease of efferocytosis positive cells after cytochalasin D treatment (Fig. 17 a-c). To determine whether the assay format allowed for concentration-response experiments, macrophages were pre-treated with different concentrations of cytochalasin D. As shown in Fig. 17 d, the analysis algorithm revealed comparable IC_{50} values of 330 nM (IDM#12), 380 nM (IDM#B7), and 390 nM (MDMs; donor #1) between the different macrophage types (Table 6). Likewise, different MDM donors displayed similar IC_{50} values of 280 nM (donor #2) and 340 nM (donor #3; supplementary Fig. S11 a and Table S1).

Table 6. Statistical details of concentration-dependent stimulation experiments with cytochalasin D in iPSC- and monocyte-derived macrophages. Data are based on non-linear fits (log(inhibitor) vs. response - Variable slope (four parameters)). *CI = confidence interval.

Cytochalasin D Best-fit values	**IDM#12**	**IDM#B7**	**MDMs, donor #1**
Bottom [%]	4	7	8
Top [%]	73	53	61
IC_{50} [nM], (95 % CI*)	330 (310; 350)	380 (330; 440)	390 (360; 420)

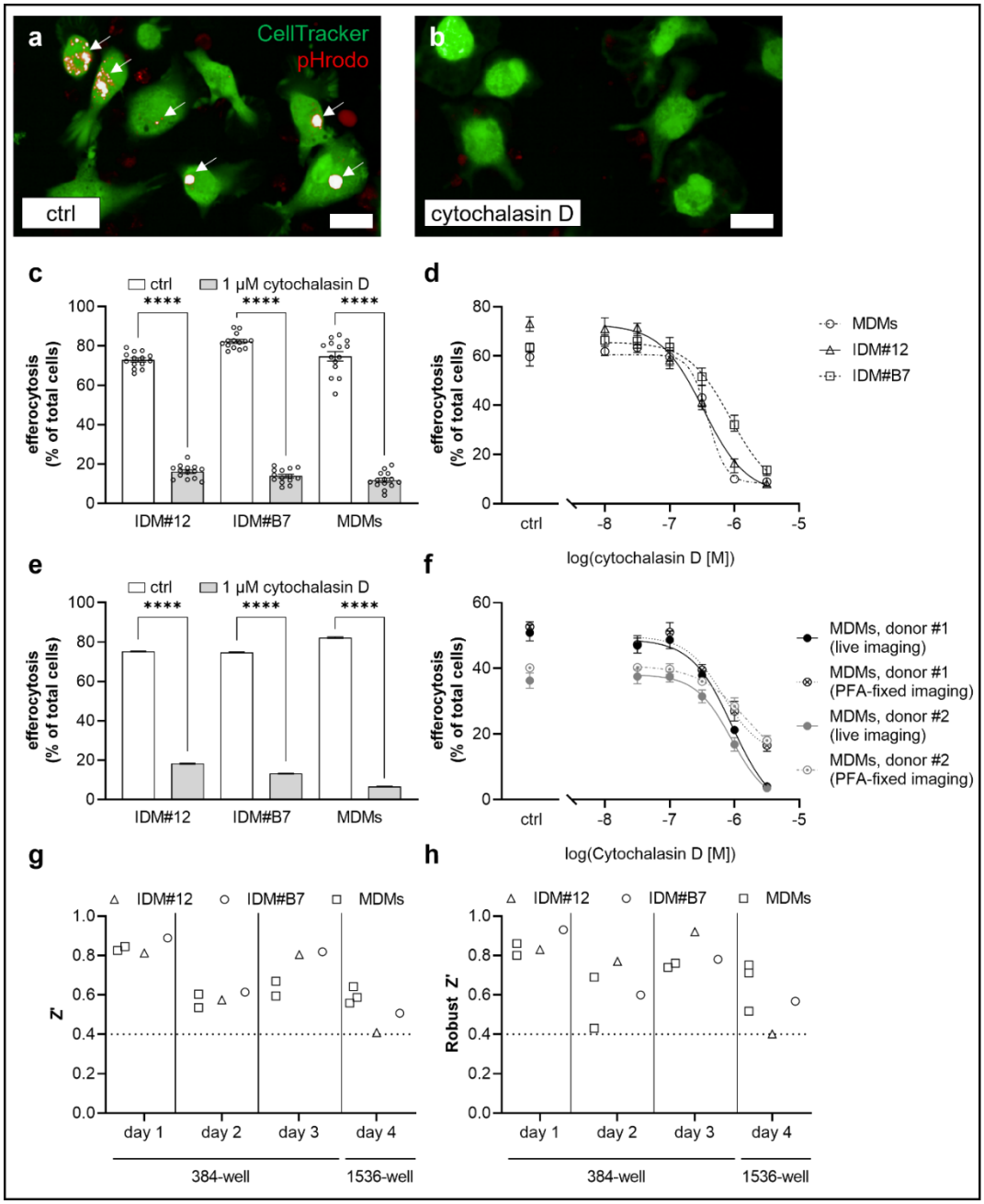

Figure 17. High-content-imaging-based efferocytosis assay quantifies the pharmacological effect of cytochalasin D with comparable IC_{50} values between iPSC- and monocyte-derived macrophages. Macrophages were pre-treated with cytochalasin D (efferocytosis inhibitor) or vehicle control prior to Raji prey cell addition. Plate was measured 5 hours after prey cell addition in the Opera Phenix HTS System and data are based on the developed analysis algorithm. **(a+b)** Close-up of macrophages treated with cytochalasin D (b) or ctrl (a) and co-cultured with irradiated prey cells. All parameters were set globally across images between conditions and therefore the relative intensity can be quantitatively compared. Scale bar = 20 µm. **(c)** Quantification of efferocytosis modulation. Data points are representative (IDM#12: N = 4; IDM#B7: N = 5; MDMs: N = 15) and show mean ± SEM (n = 14), one-way ANOVA: ****p<0.0001. **(d)** Concentration-dependent efferocytosis reduction. Data points are representative (IDMs: N = 4; MDMs: N = 9) and show the median ± IQR (n = 14; some error bars are not visible). **(e)** Quantification of efferocytosis modulation in the miniaturized 1536-well microplate format. Data points are representative (IDM#12: N = 4; IDM#B7: N = 3; MDMs: N = 7) and show mean ± SEM (n ≥ 308); one-way ANOVA: ****p<0.0001. **(f)** Concentration-dependent reduction of efferocytosis, assessed by a paraformaldehyde (PFA)-fixed assay variant in comparison to live imaging. Data points show the mean ± SEM (n = 4; some error bars are not visible; N = 1). **(g+h)** Robustness of the assay in a 384-well (day 1-3) or 1536-well (day 4) microplate. Z‘ (g) and robust Z‘ (h) values were calculated from independent experiments (day 1-4).

To determine the robustness of the established assay and the analysis algorithm, the mean and standard deviation and the median and median absolute deviation values were calculated for the treatment with 1 µM cytochalasin D or vehicle to calculate the Z' and robust Z', respectively[67,68]. In independent experiments with MDMs derived from different donors and several IDM preparations derived from the two different hiPSC lines, the observed Z' and RZ' values were in an acceptable range for different experimental occasions (Fig. 17 g and h). To increase the throughput for the established efferocytosis assay, a miniaturized version of it using 1536-well microplates with the same settings was established. Similar to the efferocytosis assay conducted in the 384-well format, the cytochalasin D treatment led to a significant and at least four-fold decrease of efferocytosis positive cells (Fig. 17 e) and the calculated Z' and RZ' values were likewise in an acceptable range (Fig. 17 g and h). To further adapt this assay for high-throughput applications, a PFA-fixed assay variant in comparison to live imaging was tested. As shown in Fig. 17 f, a concentration-dependent reduction of efferocytosis was possible in the fixed assay variant. However, the resulting IC_{50} values from the fixed assay variant (donor #1: 670 nM; donor #2: 1.57 µM) differed from the values resulting from the live cell imaging (donor #1: 920 nM; donor #2: 900 nM), and the signal window was reduced. For this reason, all subsequent experiments were performed with the previously established live cell imaging assay variant.

The here presented assay was established to enable applications which need a higher throughput. In contrast, the IncuCyte imaging platform presents a commonly applied microscopy-based approach to quantify efferocytosis by pHrodo labeling of prey cells with low- to medium-throughput[69] (Fig. S12 a and b). In comparison to an IncuCyte-based efferocytosis assay, the here established assay was shown to better distinguish between true efferocytotic events and background signal (Fig. S12 c-e). A concentration-dependent efferocytosis inhibition by cytochalasin D was demonstrated by the IncuCyte system (Fig. S12 f), though showing a higher data variance and different resulting IC_{50} values compared to the high-content-imaging based assay (Fig. S12 g).

2.2.5 Modulation of macrophage-mediated efferocytosis by Spleen tyrosine kinase (Syk) inhibitors

Syk is a kinase de-regulated in patients suffering from IPF[70]. Previous studies showed, that Syk inhibition prevented both bleomycin-induced fibrosis and inflammation in the skin and in the lung[71,72]. To assess the assay performance in the above developed set-up, and to test whether efferocytosis is a Syk-mediated process, three previously characterized Syk inhibitors were analyzed with regard to their ability to modulate the efferocytotic activity of macrophages. ER 27319 maleate (Fig. 18 a) is an acridone-related compound and effectively inhibits the tyrosine phosphorylation of Syk and consequently its activation[73]. GSK 143 (Fig. 18 b) acts as a direct inhibitor of the Syk kinase activity[74]. Piceatannol (Fig. 18 c) is a natural stilbene and a resveratrol analog, possessing potential anti-inflammatory, anti-cancer, and antioxidant properties[75]. Like GSK 143, piceatannol is a direct inhibitor of the Syk kinase activity[76]. All three tested Syk inhibitors inhibited efferocytosis in a concentration-dependent manner. In addition, the IC_{50} values for all three cell types were virtually identical with respect to the individual inhibitors (Table 7).

Table 7. Statistical details of concentration-dependent stimulation experiments with different Syk inhibitors in iPSC- and monocyte-derived macrophages. Data are based on non-linear fits (log(inhibitor) vs. response - Variable slope (four parameters)). *CI = confidence interval.

Syk inhibitor **(Best-fit values)**	**Macrophage type**		
ER 27319 maleate	**IDM#12**	**IDM#B7**	**MDMs**
Bottom [%], (95% CI)*	2 (1; 3)	4 (3; 5)	4 (3; 4)
Top [%]	73 (73; 74)	79 (79; 80)	73 (73; 74)
IC_{50} [µM]	1.5 (1.4; 1.6)	2.1 (2.0; 2.1)	2.0 (1.9; 2.3)
GSK 143	**IDM#12**	**IDM#B7**	**MDMs**
Bottom [%], (95% CI)*	16	24	3 (1; 4)
Top [%]	78	69	77 (76; 78)
IC_{50} [µM]	3.3 (3.3; 3.4)	4.6 (4.3; 5.0)	3.2 (3.1; 3.4)
Piceatannol	**IDM#12**	**IDM#B7**	**MDMs**
Bottom [%], (95% CI)*	25 (24; 27)	34 (32; 36)	36 (35; 37)
Top [%]	77 (77; 78)	71 (70; 72)	75 (74; 75)
IC_{50} [µM]	15 (14; 16)	20 (17; 22)	20 (18; 22)

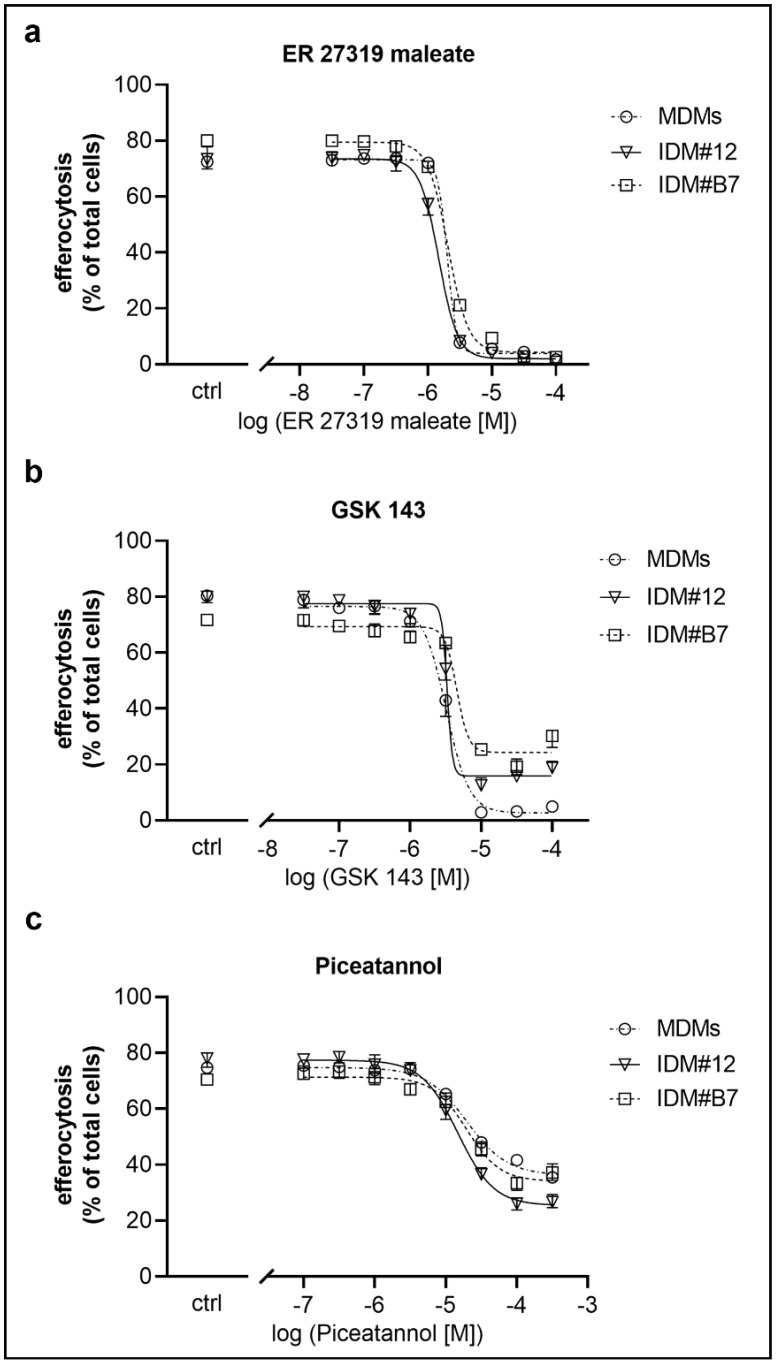

Figure 18. Spleen tyrosine kinase (Syk) inhibitors modulate efferocytosis in both iPSC- and monocyte-derived macrophages. (a-c) Concentration-dependent reduction of efferocytosis induced by Syk inhibitors in IDMs and MDMs. Macrophages were treated overnight with the Syk inhibitors ER 27319 maleate (a), GSK 143 (b) or piceatannol (c). Plates were measured 5 hours after prey cell addition in the Opera Phenix HTS System. Data points are representative (IDMs: N = 3-4; MDMs: N = 6-8) and show median ± IQR (n = 14; some error bars are not visible).

Hereby ER 27319 maleate displayed the highest potency with an IC_{50} value range between 1.5 and 2.1 µM for the three cell types. The potency of GSK 143 was slightly lower, showing an IC_{50} value range between 3.2 and 4.6 µM. Piceatannol appeared to have the lowest potency of the tested Syk inhibitors with IC_{50} values of approximately 15 µM (IDM#12) and 20 µM (IDM#B7 and MDMs). The treatment with GSK 143 in MDMs and the treatment with ER 27319 maleate in all macrophage types resulted in a virtually complete efferocytotic inhibition, being similarly effective as the treatment with cytochalasin D (Fig. 17 d). In contrast, only a partial inhibition was observed with piceatannol, which left a residual efferocytosis activity of approximately 30 % at its maximal concentration.

In summary, a robust high-content-imaging-based efferocytosis assay with an endpoint measurement after five hours was established where IDMs and MDMs displayed comparable pharmacology. As demonstrated by the analysis of Syk modulation, this miniaturized cellular assay lends itself to the pharmacological drug discovery of substances with the ability to modulate efferocytosis.

2.3 Development of miniaturized co-cultures between senescent epithelial cells and macrophages

One aim of this work was to elucidate the relationship between cellular senescence and macrophage efferocytosis activity in the context of fibrotic diseases. To establish a link in the direction of lung fibrosis, two human lung epithelial cell types were employed for senescence induction: primary small airway epithelial cells (SAECs) and A549 cells, derived from an adenocarcinomic human lung epithelial cell line. The resulting phenotype after treatment with senescence-inducing agents was characterized based on typical associated markers. Due to the lack of appropriate miniaturized assays targeting senescent markers, two bead-based AlphaLISA immunoassays were developed detecting the human CDK inhibitors p16 and p21 in cellular lysates. The efferocytotic activity of macrophages in the senescent context was analyzed using the previously established high-content-imaging-based efferocytosis assay with adaptations to the resulting triple co-culture system consisting of senescent epithelial cells, macrophages, and pHrodo-labeled prey cells.

2.3.1 Approaches to induce a senescent program in primary human small airway epithelial cells

Primary SAECs out of the 1 mm bronchiole area were used to establish a physiologically relevant model for cellular senescence in fibrotic lung disease. Two different approaches were tested in order to induce a senescent program in different lots (donors) of these cells. To simulate ageing, the primary cells were serially passaged until replicative senescence was induced. Alternatively, the CDK4 and CDK6 inhibitor palbociclib, the topoisomerase II inhibitor etoposide and recombinant human TGFβ1, which all three had previously been demonstrated to induce senescence[45–47] were administered to the SAECs. The cellular morphology, activity of SA-β-galactosidase, presence of p16 and p21, and gene expression patterns with respect to proliferation markers, senescence-associated markers and SASP-related factors were analyzed after serial passaging or treatment of the cells.

2.3.1.1 Replicative senescence induction in primary human small airway epithelial cells by serial passaging

To induce replicative senescence in the primary SAECs, the cells were serially passaged until their proliferation potential was exhausted. To track the proliferation potential of different SAEC donors during the passaging steps, the cumulative population doublings were calculated over the whole time in culture. As shown in Fig. 19 a, cells derived from donor 18TL179344 achieved the highest number of population doublings (49 doublings). Cells from the donors 672324 and 18TL180367 only reached a lower number of doublings (21 and 17 doublings, respectively). The 49 doublings of donor 18TL179344 correlated to 15 passages. At this stage, the cells were markedly positive for SA-β-galactosidase (Fig. 19 b). Further, and in comparison to earlier passage numbers, the cells accumulated lysosomes, which could be observed as intracellular white spheres in brightfield microscopy (Fig. 19 c-e). Likewise for the other three donors, the serial passaging resulted in substantially enlarged and flattened cell bodies, as well as accumulated lysosomes (Fig. S14). On the mRNA level, the donors 18TL179344 and 19TL148583 showed a similar expression pattern of analyzed markers (Fig. 19 f and h). *Marker Of Proliferation Ki-67* (*MKI67)* was shown to be downregulated, while the senescence markers *CDKN2A (p16)* and *CDKN1A (p21)* were upregulated in comparison to a younger passage, respectively. Except for *CCL2* and *CXCL1*, the expression patterns of the SASP-related genes were similar between the two donors. The two other donors 672324 and 18TL180367 also exhibited a comparable expression pattern (Fig. 19 g and i). However, the expression level of *MKI67* was either not detectable or remained unchanged. *CDKN2A* and *CDKN1A* were downregulated for donor 18TL180367 and only slightly upregulated for donor 672324 in comparison to a younger passage. The expression patterns of the SASP-related genes were similar between these two donors and showed an upregulation of *CCL2*, *CXCL1*, various interleukins and *MMP3*, *MMP7*, *MMP9* and *MMP10*.

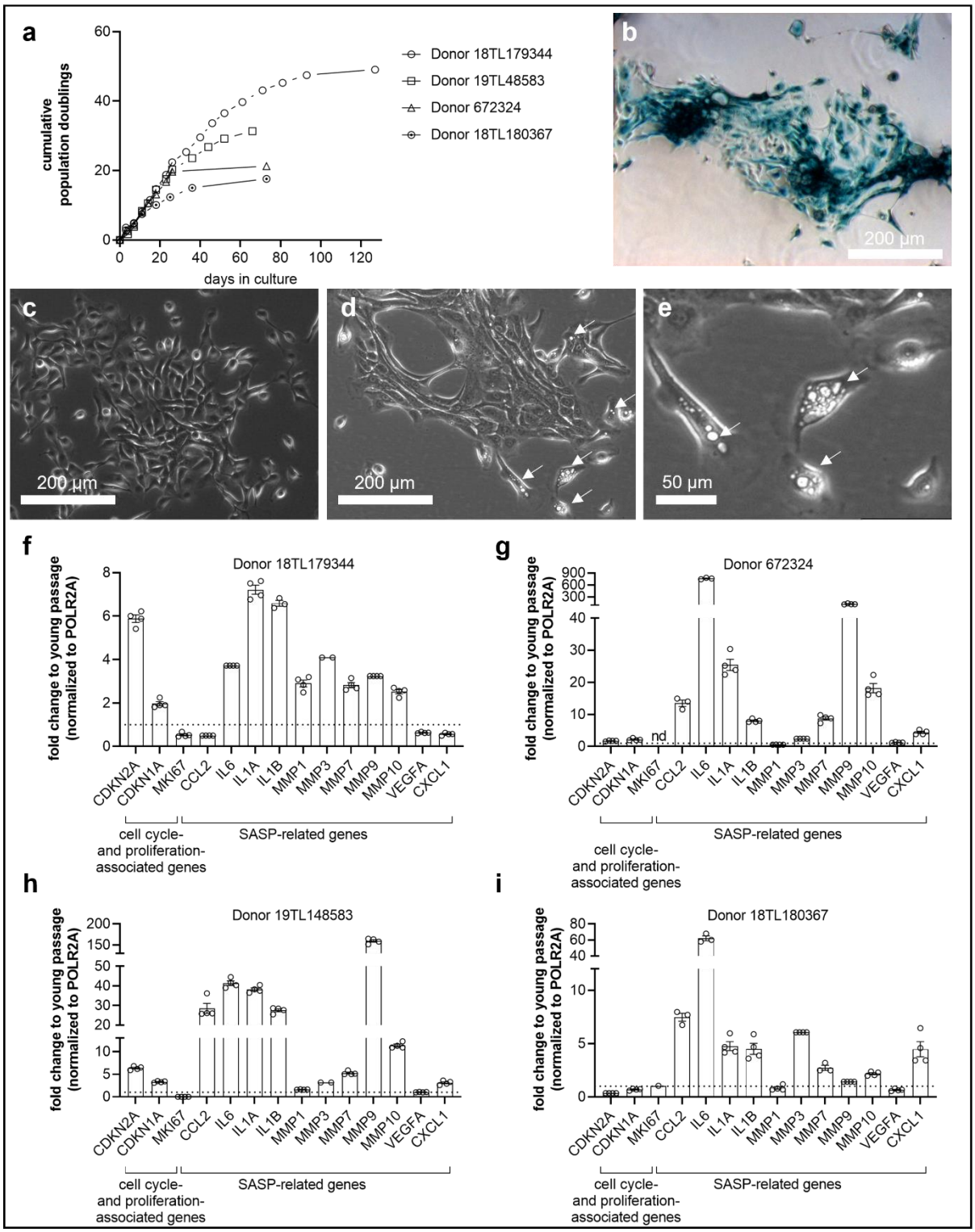

Figure 19. Serial cell passaging induces a senescent cellular phenotype in primary small airway epithelial cells. (a) Cumulative population doublings in SAECs derived from four different donors (lots). **(b)** Senescence-associated β-galactosidase staining of SAEC donor 18TL179344 (passage 15). Enzymatic activity is shown by the blue-colored areas (N = 4). **(c-e)** Representative morphological changes during serial passaging with SAEC donor 18TL179344 for passage 3 (c) and passage 15 (d, close-up in e) shown by brightfield images (N = 4). White arrows point at intracellular lysosomes. **(f-g)** Analysis of cell cycle-, proliferation- and SASP (senescence-associated secretory phenotype)-associated genes by RT-PCR for the SAEC donors 18TL179344 (f), 672324 (g), 19TL148583 (h) and 18TL180367 (i; mean ± SEM; n = 4). The fold change was determined in relation to a young passage, respectively; nd = not detected.

2.3.1.2 Senescence induction with anti-cancer drugs and TGFβ1 in primary human small airway epithelial cells

To overcome the long duration of replicative senescence induction by serial passaging (up to several months), an alternative senescence inducing approach was tested out. Due to genetic aberrations in immortalized cell lines, replicative senescence induction is restricted to primary cells only[45]. In contrast, the senescence induction with different chemicals, for instance, is also possible for cell lines which exhibit a virtually unlimited proliferation potential. To cause a senescent state, SAECs from donors 18TL179344, 18TL80367 and 672324 were treated with either one of the anti-cancer drugs (etoposide or palbociclib) or with TGFβ1. Seven days after treatment, the cells were analyzed with respect to senescence markers (data for donors 18TL180367 and 672324 are partially shown in the supplementary figures Fig. S15, S16, S18 and S19). Associated morphological changes in shape and size were assessed by brightfield images and an immunolabeling of α-tubulin. The treatment with etoposide and palbociclib resulted in substantially enlarged and flattened cell bodies, while the effect of the treatment with TGFβ1 was not that pronounced for donor 18TL179344 (Fig. 20), but for the other tested donors (Fig. S15 and S16). Additionally, the cells derived from all tested donors accumulated lysosomes after treatment with the three substances. Moreover, the cells developed irregular cellular structures, e.g., bubble-like shapes, which was a unique feature after palbociclib treatment (Fig. 20, Fig. S15 and Fig. S16).

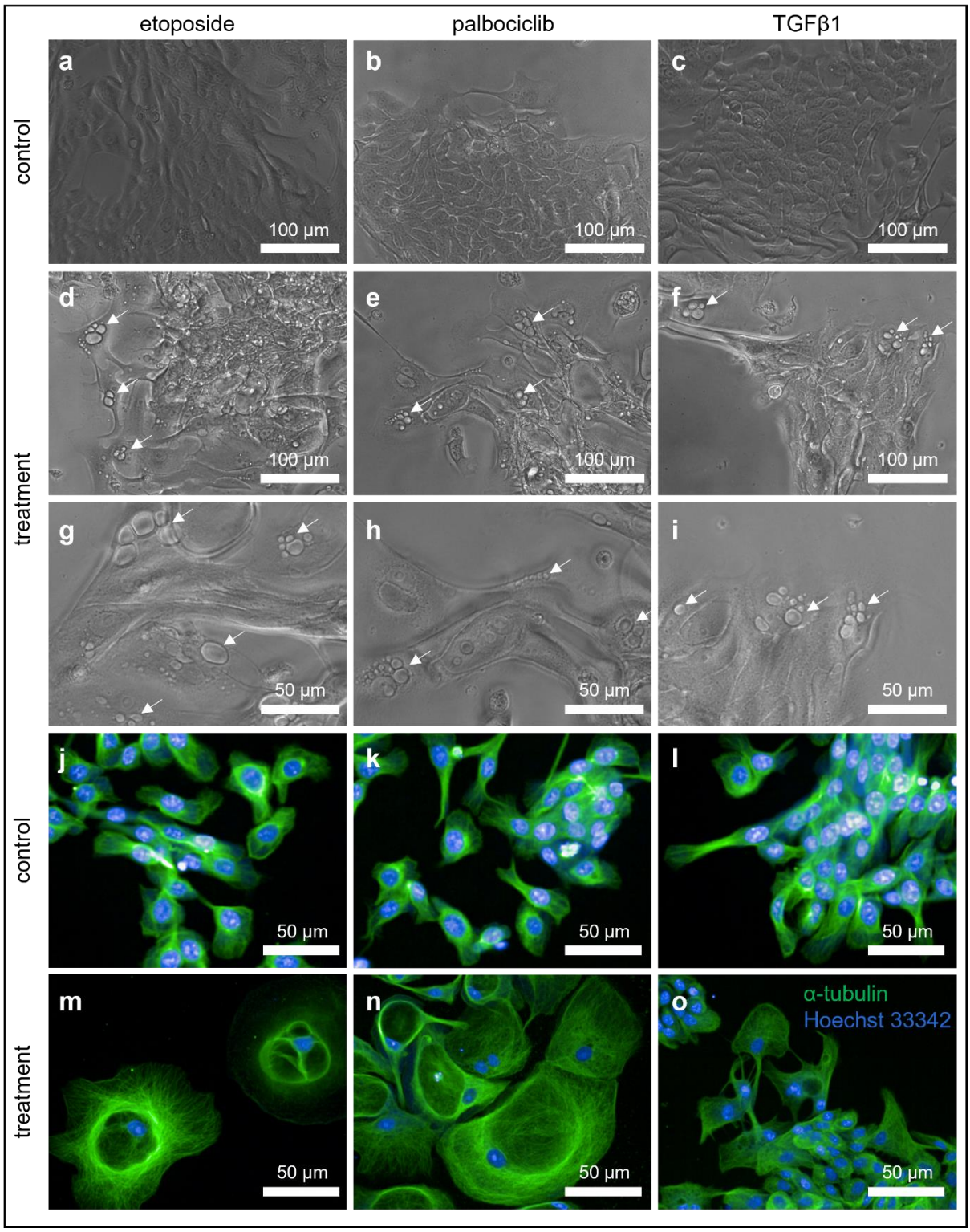

Figure 20. Treatment with anti-cancer drugs or TGFβ1 induces a senescent morphology in primary small airway epithelial cells. (a-i) Morphological changes in SAECs (lot 18TL179344) upon treatment with either etoposide (d, close-up in g), palbociclib (e, close-up in h) or TGFβ1 (f, close-up in i) in comparison to the respective control shown by brightfield images (a-c; n = 6, N = 3). White arrows point at intracellular lysosomes. **(j-o)** Change in cell size in SAECs (lot 18TL179344) upon treatment with either etoposide (j), palbociclib (k) or TGFβ1 (l) in comparison to the respective control (m-o) shown by an immunolabeling of α-tubulin. All parameters were set globally across images and therefore the relative intensity can be quantitatively compared (n = 6, N = 1).

For the treatment with etoposide and palbociclib, a non-quantitative SA-β-galactosidase staining exhibited an increased activity of the enzyme compared to vehicle-treated control cells in all three donors (Fig. 21 a and b). A quantitative SA-β-galactosidase assay revealed a significantly enhanced enzyme activity upon stimulation with either etoposide, palbociclib or TGFβ1 with an at least 2.5-fold increase in all three tested donors (Fig. 21 c-e). Hereby, the TGFβ1 treatment showed the most pronounced effect. Additionally, it was shown that cells derived from donor 18TL179344 exhibited the lowest basal β-galactosidase activity (Fig. 21 c).

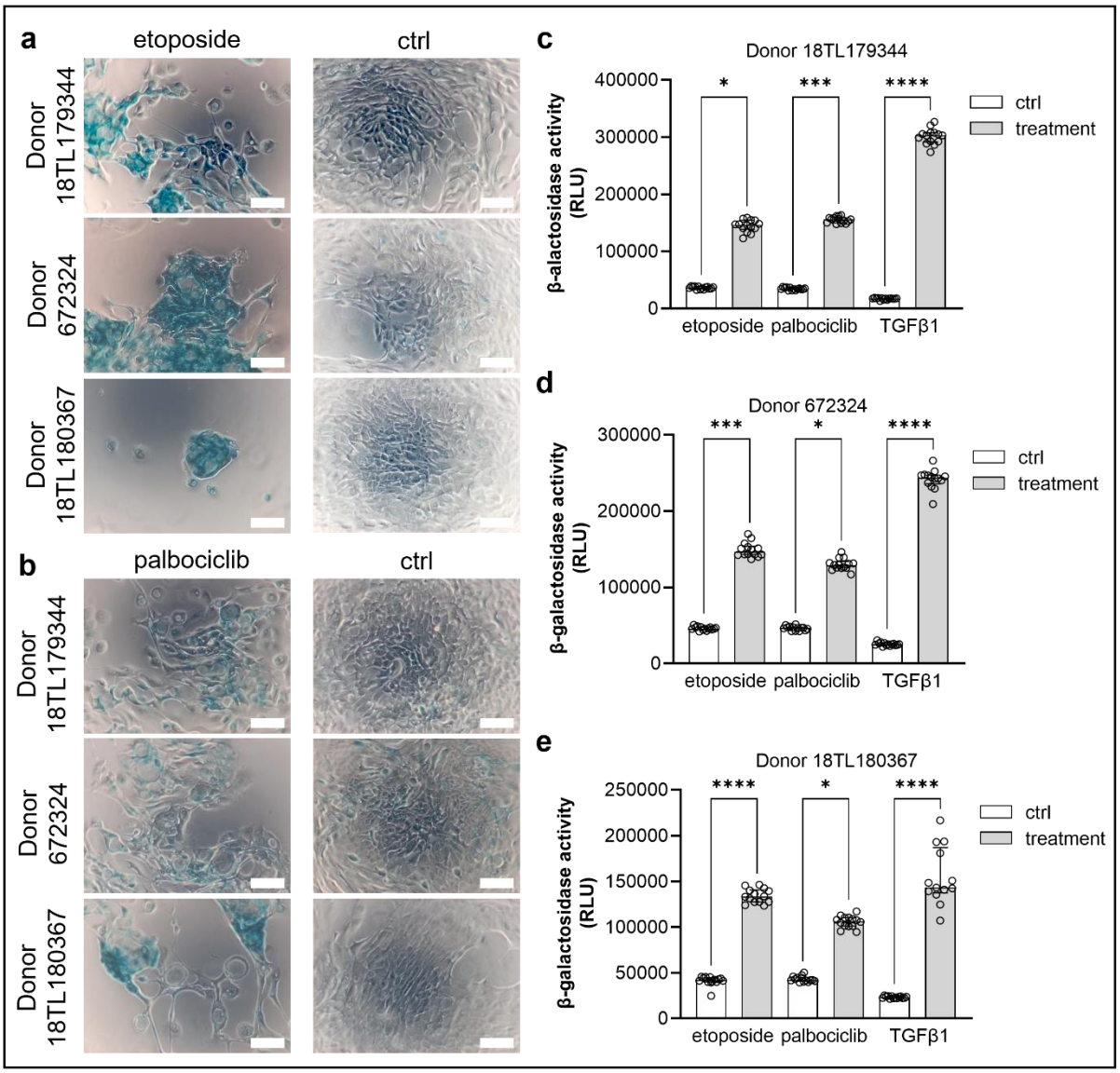

Figure 21. Treatment with anti-cancer drugs or TGFβ1 increases the enzymatic activity of the senescence-associated β-galactosidase in primary small airway epithelial cells. (a+b) Staining of senescence-associated β-galactosidase in different SAEC donors upon treatment with either etoposide (a) or palbociclib (b) in comparison to the respective control (n = 3, N = 1). Enzymatic activity is shown by the blue-colored areas. Scale bar = 50 µm. **(c-e)** Quantified activity of senescence-associated β-galactosidase upon treatment with either etoposide, palbociclib or TGFβ1 in comparison to the respective control in the SAEC donors 18TL179344 (c), 672324 (d) and 18TL180367 (e; median ± IQR; n = 14). Kruskal-Wallis-test: *p < 0.05, ***p < 0.001, ****p < 0.0001.

The mRNA analysis of cell cycle-, proliferation-, ‚don‘t eat me‘-signal- and SASP-associated genes by RT-PCR revealed different expression patterns for the tested agents and different donors (Fig. 22 a-c, Fig. S17-S19). Especially the expression levels of the SASP-related genes, e.g., *CCL2*, different interleukins and MMPs, differed between the conditions and donors. *Lamin B1* (*LMNB1)* and *MKI67* were downregulated (or not detected) for all treatment conditions and donors. *CDKN1A* was slightly upregulated, while *CDKN2A* was downregulated or remained unchanged. The genes encoding the don‘t eat me‘-signals *CD24* and *CD47* were either downregulated or were not affected by the treatment. *Glutaminyl-peptide cyclotransferase* (*QPCT),* encoding a protein that modifies CD47, was strongly upregulated for donor 18TL180367. On the protein level, the treatment with either etoposide or palbociclib resulted in significantly elevated levels of MMP7 in the supernatants of cells derived from donors 18TL179344 and 672324 (Fig. 22 d and e). For donor 18TL180367, the treatments significantly reduced the MMP7 levels.

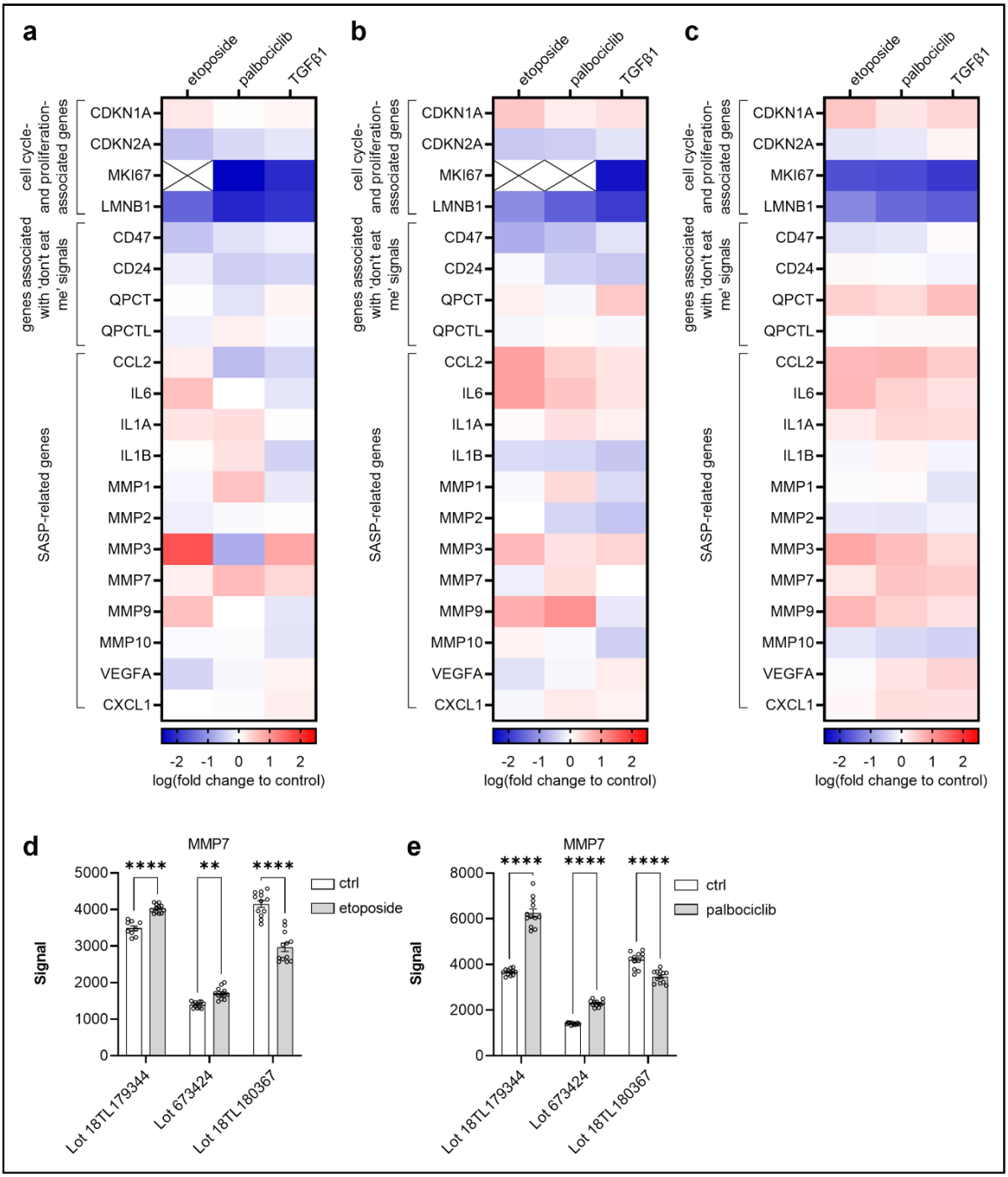

Figure 22. Treatment with anti-cancer drugs or TGFβ1 modulates the levels of senescence markers in primary small airway epithelial cells. (a-c) Analysis of cell cycle-, proliferation-, ‚don't eat me' signal- and SASP (senescence-associated secretory phenotype)-associated genes by RT-PCR for the SAEC donors 18TL179344 (a), 672324 (b) and 18TL180367 (c) upon treatment with either etoposide, palbociclib or TGFβ1. Data are presented by a heatmap (based on mean ± SEM; n = 4, N = 2 for etoposide and palbociclib, N = 1 for TGFβ1 treatment). Upregulation (red) and downregulation (blue) of genes is indicated as log of fold change relative to controls. Crossed-out areas = not detected. **(d+e)** MMP7 protein levels upon treatment with either etoposide (d) or palbociclib (e) in the supernatants of the SAEC donors 18TL179344, 672324 and 18TL180367 (mean ± SEM; n = 12, N = 1). Two-way ANOVA: **p < 0.01, ****p < 0.0001.

To verify the senescence markers p16 and p21 also on the protein level, self-developed anti-p16 and anti-p21 AlphaLISA immunoassays were applied. Only the treatment with palbociclib and TGFβ1 led to increased p16 levels, while etoposide partially even decreased the p16 levels (Fig. 23 a, c, and e). Additionally, it was shown that cells derived from donor 18TL179344 exhibited the lowest basal p16 levels shown by the vehicle treatment (Fig. 23 a). Similarly, etoposide treatment resulted in a decrease of p21 protein levels for donors 18TL179344 and 673424. Only for donor 18TL180367, the treatment led to a slight increase. Palbociclib and TGFβ1 treatment provoked an elevation of p21 levels, except for donor 672324 showing a significant decrease (Fig. 23 b, d, and f).

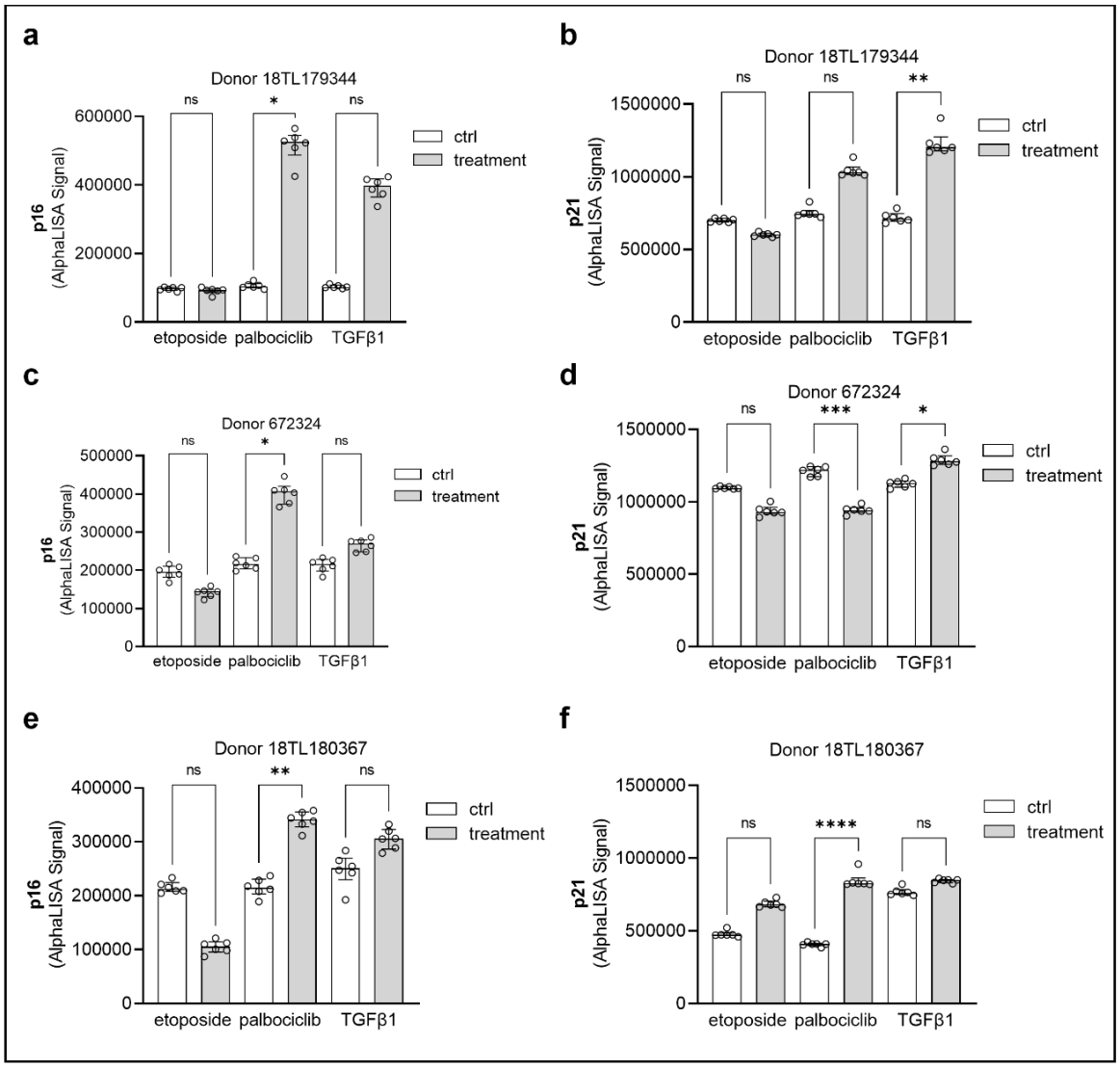

Figure 23. Treatment with anti-cancer drugs or TGFβ1 modulates the protein levels of the senescence markers p16 and p21 in primary small airway epithelial cells. (a, c, e) AlphaLISA assay detecting p16 in SAEC donors 18TL179344 (a), 672324 (c) and 18TL180367 (e) upon treatment with either etoposide, palbociclib or TGFβ1 in comparison to the respective control (mean ± SEM; n = 6, N = 1). Kruskal-Wallis-test: *p < 0.05, **p < 0.01, ns = not significant. **(b, d, f)** AlphaLISA assay detecting p21 in SAEC donors 18TL179344 (b), 672324 (d) and 18TL180367 (f) upon treatment with either etoposide, palbociclib or TGFβ1 in comparison to the respective control (median ± IQR; n = 6, N = 1). Kruskal-Wallis-test: *p < 0.05, **p < 0.01, ***p < 0.001, ****p < 0.0001, ns = not significant.

To further analyze the effect of the treatment on the ‚don't eat me'-signal CD47, an immunolabeling of the protein was performed which showed an accumulated CD47 abundance on the cellular surface for the three treatments (Fig. 24).

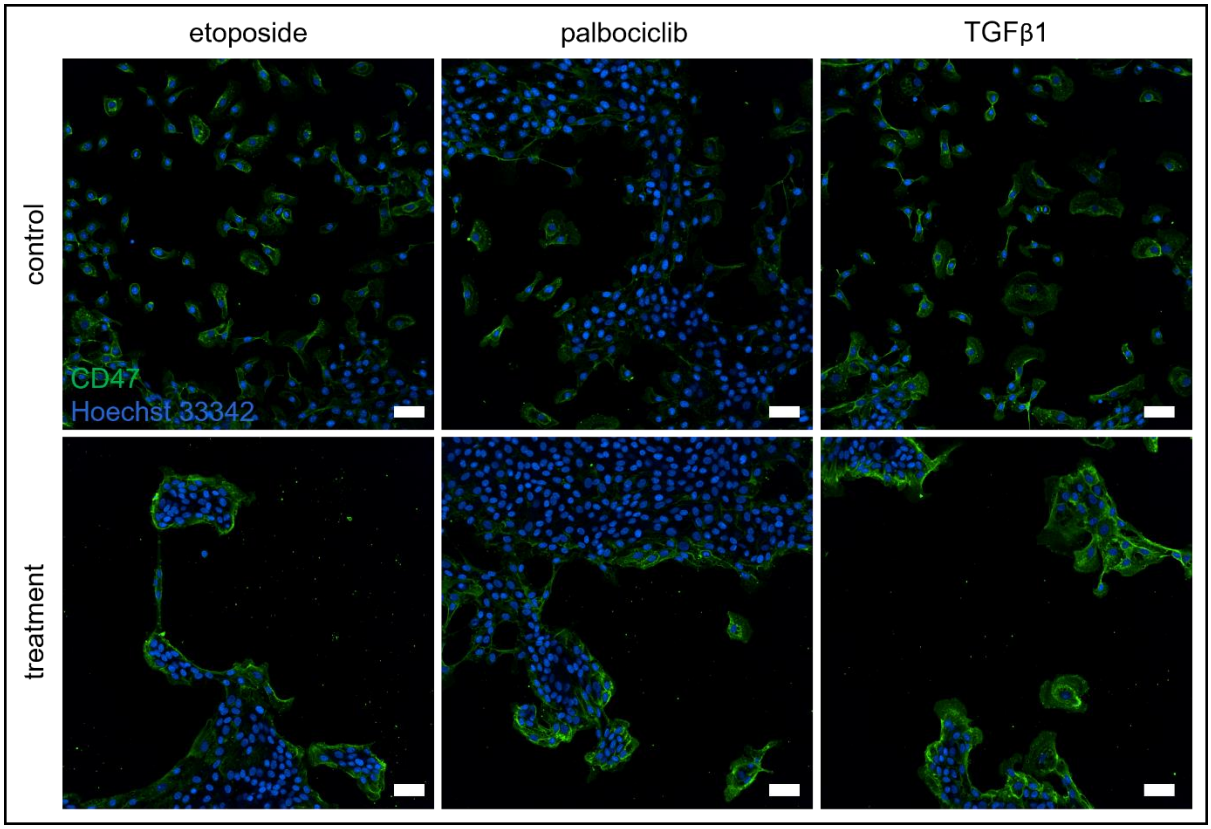

Figure 24. Treatment with anti-cancer drugs or TGFβ1 modulates the ‚don't eat me' signal CD47 in primary small airway epithelial cells. Immunolabeling of CD47 in combination with Hoechst 33342 using SAEC donor 18TL179344 upon treatment with either etoposide, palbociclib or TGFβ1 in comparison to the respective control (N = 1). All parameters were set globally across images between conditions and therefore the relative intensity can be quantitatively compared. Scale bar = 50 µm.

Combined, these results show that a stimulation with either etoposide, palbociclib or TGFβ1 resulted in the development of different features of cellular senescence, such as irregular shape and increased size, elevated SA-β-galactosidase activity, modulation of p16, p21 and CD47 as well as the emergence of specific senescence-associated gene expression patterns. On this account, it is assumed that cells treated with these senescence-inducing agents were in a senescent state and were further referred to as 'senescent cells'.

2.3.2 Miniaturization of co-cultures between senescent epithelial cells and macrophages

Aiming to elucidate the relationship between cellular senescence and macrophage efferocytosis activity, the previously established efferocytosis assay with macrophages derived from both iPSCs and monocytes was applied in presence of senescent epithelial cells. To this end, existing co-culture approaches[39] were miniaturized and adapted to the efferocytosis assay presented in this work in order to achieve a higher throughput. To increase the throughput for existing macrophage-epithelial co-culture models in the context of senescence and efferocytosis, the adaptations shown in Fig. 25 were carried out. The existing model was working with the 96-well microplate format, labeling only the irradiated prey cells (Fig. 25 a). After prey cell addition, the assay was run in a kinetic mode using the IncuCyte imaging platform. For the miniaturized model, the plate format was switched to 384-well microplates (Fig. 25 b). In order to distinguish between epithelial cells and macrophages, and to assign true efferocytosis events within macrophages, the CellTracker green labeling of macrophages was maintained, as with the previously established efferocytosis assay. After adding pHrodo-labeled irradiated prey cells, the plate was measured after a fixed incubation period before live-cell imaging using the Opera Phenix. The subsequent efferocytosis quantification was conducted as previously shown.

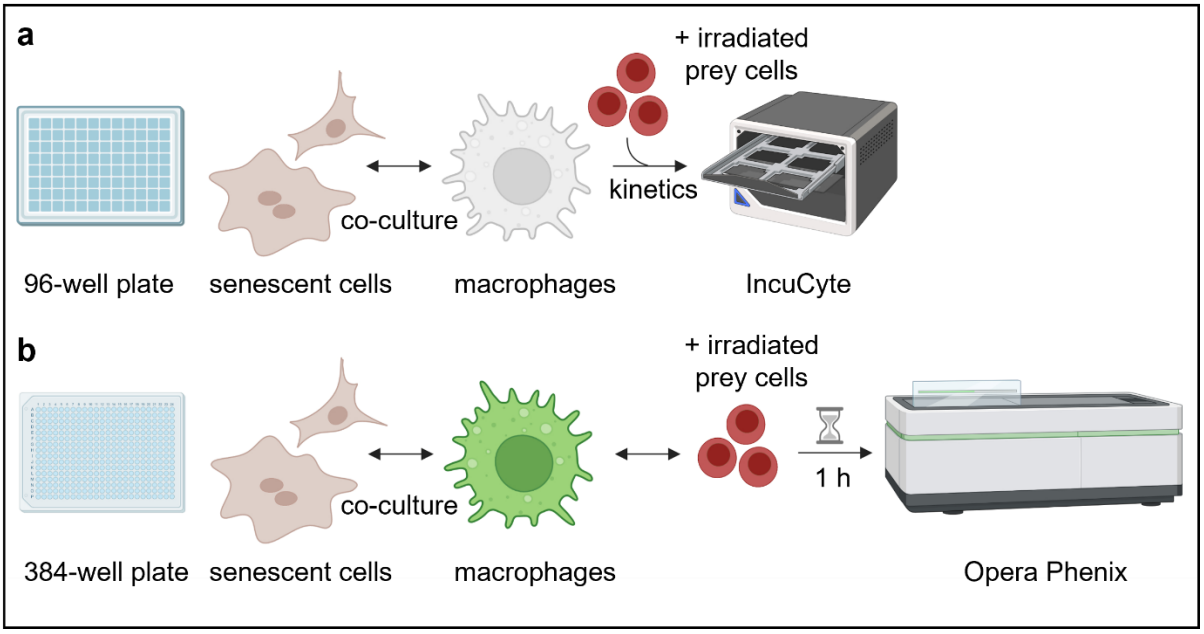

Figure 25. Schematic set-up of the miniaturized efferocytosis co-culture assay variant. (a+b) Set-up of the 96-well (a) and 384-well (b) microplate based efferocytosis co-culture assay. For both variants, macrophages were co-cultured overnight with senescent or control epithelial cells. A pre-requisite for the miniaturized assay was the CellTracker labeling of the macrophages. The next day irradiated and pHrodo-labeled Raji prey cells were added and the microplate was measured in a kinetic mode using the IncuCyte (a) or was measured after an incubation time of one hour using the Opera Phenix (b).

2.3.2.1 Impairment of macrophage efferocytosis activity by senescent cells

Using the established human triple co-culture system consisting of senescent epithelial cells, macrophages derived from iPSCs and monocytes, and pHrodo-labeled irradiated prey cells, the impact of signals from senescent epithelial cells on the macrophage's efferocytosis capacity was investigated. For this approach, senescent or control cells and macrophages were co-cultured overnight and subsequently exposed to irradiated prey cells before live cell imaging after a fixed incubation period (Fig. 26 a). To minimize the basal senescent activity in control cells, primary SAECs derived from donor 18TL179344 were selected for the co-culture model. These cells derived from the youngest donor among the tested ones showed the lowest SA-β-galactosidase activity and p16 protein levels in vehicle-treated cells, which rate among the most reliable senescence markers to date[77] (see Fig. 21 and Fig. 23). On this account, it was assumed that these cells possessed the lowest basal senescence. IDM#12 in co-culture with etoposide-treated SAECs resulted in an increase of efferocytosis positive macrophages in comparison to macrophages in the presence of control cells (Fig 26 c). For palbociclib-treated SAECs, only the co-culture with IDM#B7 showed a significant decrease of the efferocytotic activity (Fig. 26 d). Exclusively for the TGFβ1-treated SAECs the percentage of efferocytosis positive macrophages was significantly reduced (Fig. 26 e). Due to the inconclusive results, the experiment was repeated using human A549 cells. Analogous to the primary SAECs, the A549 cells were treated with either etoposide, palbociclib or TGFβ1. The treated cells exhibited several features of senescent cells, e.g., an increased size and irregular morphology (Fig. S20 a and b), an increased SA-β-galactosidase activity (Fig. S20 c and d), a modulation of several senescence-associated genes on the mRNA level (Fig. S22) and elevated p21 (Fig. S21) and CD47 protein levels (Fig. S23). The percentages of efferocytosis positive macrophages in the presence of senescent A549 cells were significantly decreased in comparison to macrophages co-cultured with control cells (Fig. 26 f-h). This effect was similar for both IDMs derived from two lines and MDMs after treatment of A549 cells with etoposide, palbociclib or TGFβ1, respectively.

Senescent cells exhibit a special secretome (SASP), through which they modify their surroundings[77]. These soluble factors potentially present an instrument through which senescent cells mediated the observed efferocytotic inhibition. In order to analyze whether the suppressed efferocytotic activity was mediated by a direct cell-to-cell contact between senescent cells and macrophages or via secreted soluble factors, macrophages were cultured overnight in conditioned medium derived from senescent or control A549 cultures, followed by the addition of irradiated pHrodo-labeled prey cells (Fig. 26 b).

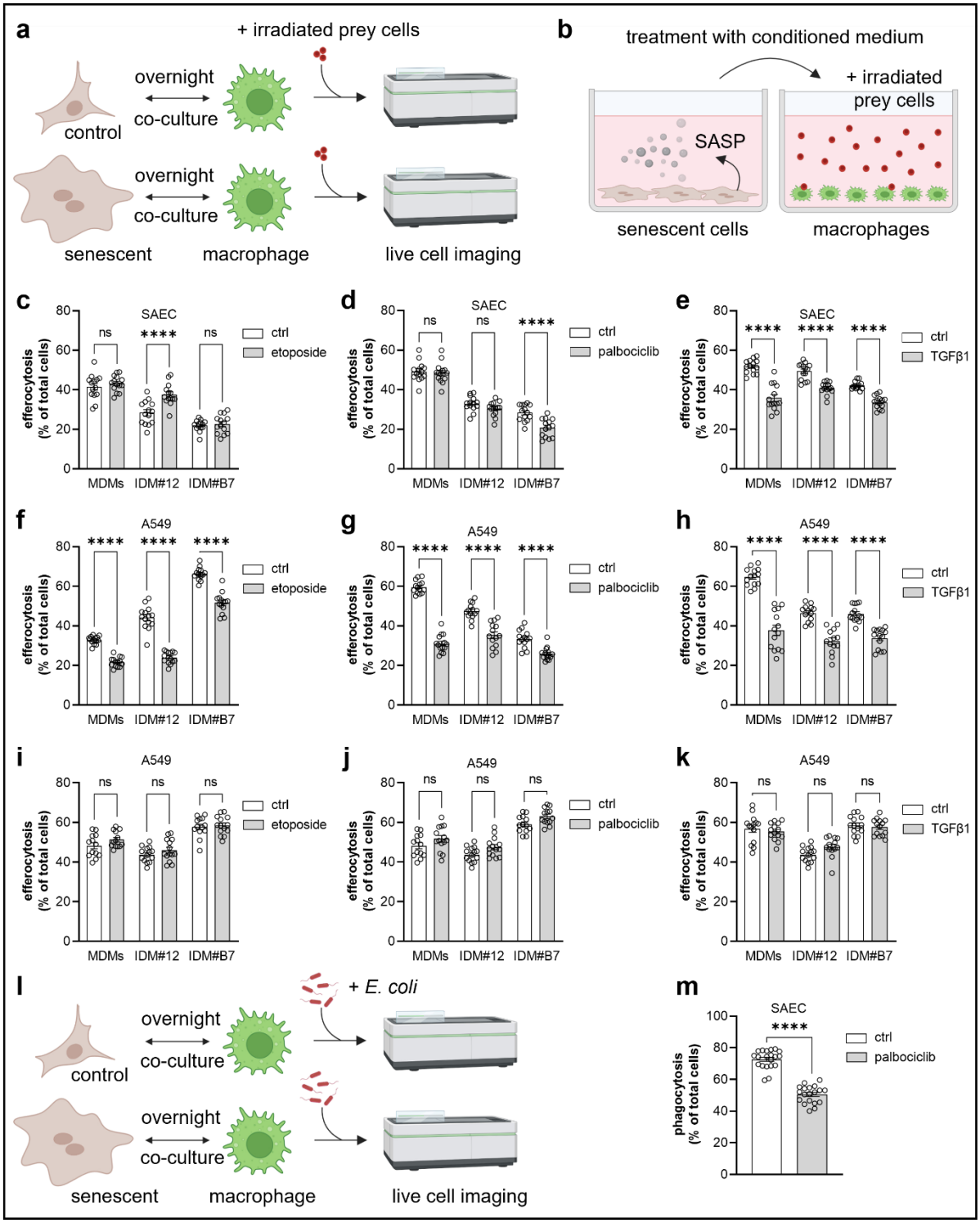

Figure 26. Senescent cells impair the macrophages' ability to remove irradiated cells or *E. coli* particles. **(a+b)** Schematic of the co-culture efferocytosis assay set-up. CellTracker-labeled macrophages were either in direct cell-cell contact with senescent or control cells (a) or were treated with conditioned medium derived from senescent or control cultures, containing SASP (senescent-associated secretory phenotype)-molecules (b). After an overnight incubation, irradiated pHrodo-labeled prey cells were added, and the measurement was conducted after one hour using the Opera Phenix. **(c-e)** Efferocytotic activity of IDMs and MDMs in combination with senescent or control SAECs (donor 18TL179344). Senescence was induced with either etoposide (c), palbociclib (d) or TGFβ1 (e; mean ± SEM; n = 14, N = 2). One-way ANOVA: ****p < 0.0001, ns = not significant. **(f-h)** Efferocytotic activity of IDMs and MDMs in combination with senescent or control A549. Senescence was induced with either etoposide (f), palbociclib (g) or TGFβ1 (h; mean ± SEM; n = 14, N = 3-7). One-way ANOVA: ****p < 0.0001.

Figure legend continues on the next page

(i-k) Efferocytotic activity of IDMs and MDMs treated with conditioned medium derived from senescent or control A549 cultures. Senescence was induced with either etoposide (i), palbociclib (j) or TGFβ1 (k; mean ± SEM; n = 14, N = 1 (etoposide, TGFβ1), N = 2 (palbociclib)). One-way ANOVA: ns = not significant. **(l)** Schematic of the co-culture phagocytosis assay set-up. The co-culture procedure was identical to the set-up in (a). **(m)** Phagocytotic activity of IDM#B7 in combination with senescent or control SAECs (donor 18TL179344). Senescence was induced with palbociclib (mean ± SEM; n = 20, N = 2). T-test: ****p < 0.0001.

In the absence of A549 cells, the percentages of efferocytosing macrophages remained unchanged, independently from the macrophage source or senescence-inducing treatment (Fig. 26 i-k). In another approach, it was analyzed if the inhibition of efferocytosis forced by senescent cells on macrophages was extendable towards an inhibition of bacterial phagocytosis (Fig. 26 l). In a set-up consisting of palbociclib-treated SAECs in combination with IDM#B7, the percentage of macrophages showing phagocytotic activity was significantly reduced when they were exposed to pHrodo-labeled *E. coli* bioparticles (Fig. 26 m). Additionally, live cell imaging revealed that macrophages interact with but do not remove senescent SAECs (Fig. S24). In this set-up, senescent cells were recognized by the bubble-like irregular cellular structure, which was detected uniquely after palbociclib treatment. It was observed that senescent cells remained motile and that senescence signals had no negative effect on the macrophage mobility. Instead, the macrophages swarmed over the senescent cell surface but did not eliminate them during the analyzed period. In another experimental approach independently from senescent epithelial cells, Raji prey cells with a knockout (KO) for the ‘don’t eat me’-signal CD47 were applied (Fig. S13 b), showing a slight but significant increase of the efferocytotic activity in MDMs and IDM#B7 in comparison to wildtype prey cells (Fig. S13 c). In summary, these data indicate that senescent cells suppress both the macrophage’s efferocytosis and phagocytosis capacity, likely by direct cell-cell contacts with CD47 being a potential candidate to mediate this process.

2.3.2.2 Restoration of macrophage efferocytosis function by senolytic treatment of senescent epithelial cells

Since previous experiments demonstrated a senescence-mediated suppression of the macrophages' efferocytotic activity, the potential restoration of the macrophage function was investigated by the application of senolytics. Senolytics are small molecule drugs for the selective elimination of cells being in a senescent state by the induction of an apoptotic program[48]. For this approach, the Bcl-2 inhibitor ABT263 (navitoclax) was tested for apoptosis induction in senescent A549 cells prior to macrophage efferocytosis quantification. A549 cells were selected as an epithelial cell model in this set-up since these cells exhibited a greater assay window of efferocytosis suppression upon treatment with different senescence-inducing agents in comparison to primary SAECs (see Fig. 26). In this experimental set-up, A549 cells being in a senescent state induced either by etoposide, palbociclib or TGFβ1 were treated for 48 hours with ABT263. To track the apoptotic state, the percentage of Caspase 3/7 positive and PS externalizing cells detected by Annexin V binding were assessed by live-cell imaging over a time course of 48 hours after the addition of senolytics (Fig. 27). Over time, ABT263-treated cells became slowly positive for Caspase 3/7 and Annexin V for each of the senescence-inducing conditions (Fig 27 a-f). After 48 hours in presence of ABT263, a significant increase of Caspase 3/7 and Annexin V positive cells was observed (Fig. 27 g and h). The strongest effect was shown by TGFβ1-induced senescence in combination with ABT263, which led to 97 % Caspase 3/7 and 75 % Annexin V positive cells. The impact on previously etoposide- and palbociclib-treated cells was weaker, with 47 % (etoposide) or 62 % (palbociclib) Caspase 3/7 positive cells and 31 % Annexin V positive cells after senolytic treatment. The amount of vehicle-treated positive cells was the highest for TGFβ1-treated cells (34 % Caspase 3/7 positive cells, 16 % Annexin V positive cells). To assess the specificity of ABT263 to push only senescent cells into apoptosis, vehicle-treated control cells were also treated for 48 hours with the senolytic drug. The treatment of control cells resulted in up to 6 % positive cells for either Caspase 3/7 or Annexin V in palbociclib- or TGFβ1-treated cells (Fig. S25). Only etoposide-treated populations reacted with a significant increase in cells being positive for the two markers with 15 % (Caspase 3/7) and 7 % (Annexin V). The apoptosis induction with senolytics was also shown by the co-treatment with Dasatinib and Quercetin for each of the senescence-inducing agents (Fig. S26). At least 84 % of the cells were positive for both markers. However, the percentages of vehicle-treated positive cells were similarly increased (up to 87 %). On this account, the more effective senolytic drug ABT263 was used for all subsequent experiments.

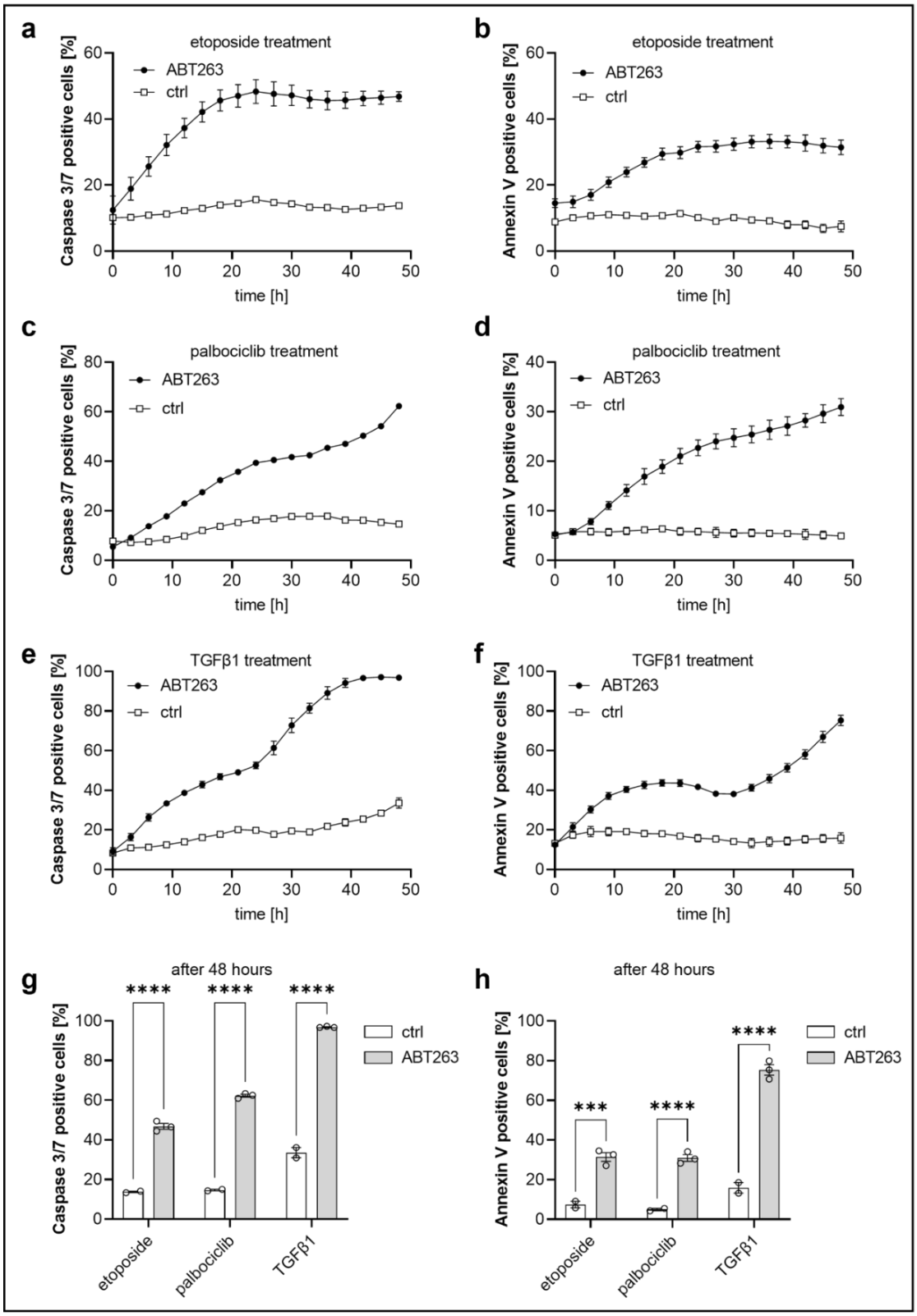

Figure 27. The senolytic drug ABT263 induces apoptosis in senescent A549 cells. A549 were treated with either etoposide, palbociclib or TGFβ1 to induce senescence. Senescent cells were treated with ABT263 for 48 h. **(a-f)** Percentage of Caspase 3/7 positive (a, c, e) and Annexin V positive (b, d, f) A549 cells after senescence induction by etoposide (a+b), palbociclib (c+d) or TGFβ1 (e+f) in presence of ABT263. Data points are representative (N = 3) and show mean ± SEM (n = 2-3). **(g+h)** Percentage of Caspase 3/7 positive (g) and Annexin V positive (h) A549 cells after senescence induction and treatment with ABT263 after 48 hours. Data points are representative (N = 3) and show mean ± SEM (n = 2-3). Two-way ANOVA: ***p < 0.001, ****p < 0.0001.

The senolytic stimulation along with an apoptosis induction possibly switches senescent cells into targets for macrophage removal. Consequently, a novel approach was used to assess the effect of senolytic treatment on the interplay of macrophages with senescent cells. In this set-up, A549 treated with either etoposide, palbociclib or TGFβ1 were incubated with ABT263 for 48 hours and subsequently labeled with pHrodo to enable an efferocytosis analysis. Macrophages were added and efferocytosis was quantified in the absence of additional Raji prey cells. The senolytic stimulation of senescent cells resulted in a significant increase of efferocytotic events, shown by extremely elevated pHrodo signals within macrophages (Fig. 28 a and b). Significantly higher numbers of efferocytosing macrophages of up to 24 % were found for each condition and macrophage source (Fig. 28 c-e). The strongest effect was shown for IDM#B7 in combination with etoposide-treated senescent A549 cells. However, ABT263 stimulation of vehicle-treated control cells also led partially to an increased efferocytotic activity, especially for the TGFβ1 vehicle treatment (Fig. S27). In summary, these data indicate that the senolytic agent ABT263 acts virtually selective in driving only senescent cells towards apoptosis. Moreover, ABT263 increased the efferocytotic capacity of macrophages in co-cultures with these cells.

In summary, the senescence induction in both primary SAECs and A549 by etoposide, palbociclib and TGFβ1 resulted in the development of distinct characteristics of cellular senescence, representing the heterogeneity of the senescent phenotype. Thus, these three induction methods can be used as a complementary model for cellular senescence in fibrotic respiratory diseases, covering different features of the senescent phenotype. Using the established miniaturized efferocytosis assay involving co-cultures of macrophages and senescent cells, it was possible to show an impaired efferocytotic and phagocytotic capacity in the senescent context. The selective apoptosis induction in senescent A549 was triggered through stimulation with the senolytic agent ABT263. Finally, the application of ABT263 treated senescent A549 in efferocytosis assays was shown to increase the macrophage's efferocytotic activity.

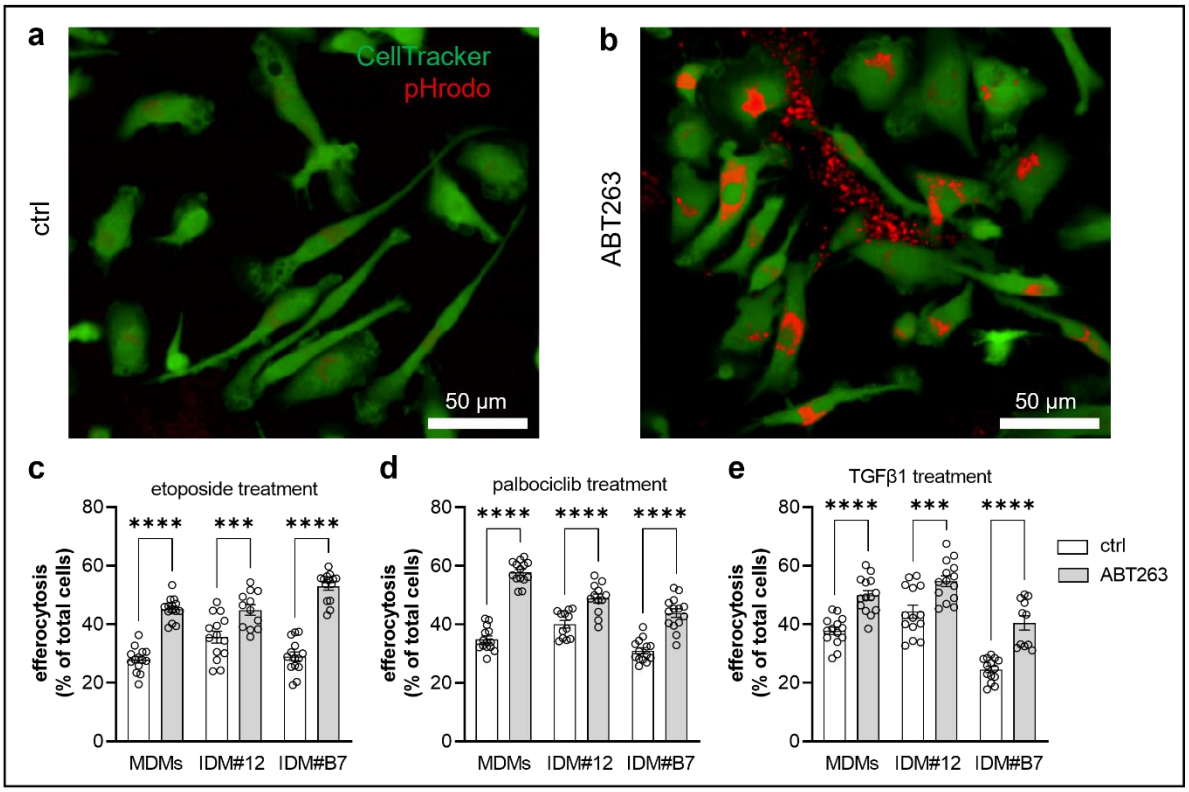

Figure 28. Senolytics restore the macrophage's efferocytotic capacity. Senescent pHrodo-labeled A549 cells were stimulated with ABT263 for 48 h. **(a+b)** Representative efferocytosing macrophages co-cultured with senescent A549 (palbociclib) treated with ABT263 (b) or ctrl (a). All parameters were set globally across images between conditions and therefore the relative intensity can be quantitatively compared (N = 2). **(c-e)** Representative senolytics-dependent increase of efferocytosis by macrophages in co-culture with senescent cells (mean ± SEM; n = 14, N = 2). Senescence was induced with etoposide (c), palbociclib (d) or TGFβ1 (e). One-way ANOVA: ***p < 0.001, ****p < 0.0001.

3. Discussion and perspectives

Macrophages are versatile players of fibrosis and exhibit a unique role with being involved in different phases of the fibrotic cascade[7]. Hence, there exists potential of modulating this cell type for therapeutic benefits. The lacking ability to access, isolate and maintain human functional macrophages as they are found *in vivo* significantly limited the efforts to analyze and understand these cells and their role in disease[78]. This thesis aimed to fill the gap of the unmet need for physiologically relevant *in vitro* drug discovery assays to target macrophage functions in fibrotic diseases. Therefore, an upscaled protocol was established to differentiate hiPSCs into macrophages to enable drug discovery applications. Using the hereby derived IDMs, a high-content-imaging-based assay in the 384-well and 1536-well microplate format was established, enabling both an efferocytosis- and phagocytosis-based assay for medium- to high-throughput applications in various disease indications (e.g., fibrosis, cancer). Applying the latter, the effect of senescent epithelial cells on pivotal macrophage functions was shown by a miniaturized co-culture set-up.

3.1 Upscaled process for the differentiation of human iPSCs towards derived macrophages

In vitro studies on macrophages traditionally have been limited by lacking numbers of suitable model cells. Available cell lines such as THP-1 cells (a human leukemia monocytic cell line) allow for high experimental robustness and cellular expansion to large quantities but are unable to recapitulate many features of how true macrophages act *in vivo*. Tissue-resident macrophages are scarce and virtually inaccessible in the human system. While the generation of primary macrophages by *in vitro* differentiation from isolated blood monocytes provides to some extent higher numbers of model cells, it still presents a low-yield and time-consuming approach[56,78]. In the murine system, it was also shown that macrophages may be derived from T or B cells by direct reprogramming[79]. However, the latter technique does not overcome the issue of using a limited number of primary source cells. In contrast, by the development of the iPSC technology, it became possible to revert somatic cells into a different cell type through transition via a pluripotent state that lends itself to large scale expansion[78]. With respect to drug discovery applications, especially for macrophages, the application of iPSCs provides a constant and scalable source and overcomes the limited availability and donor variability of other existing macrophage models derived from primary monocytes. Moreover, iPSCs are amenable to manipulation by genome editing methods, expanding possible applications of derived macrophages[78].

To obtain such a constant and scalable source of macrophages and to overcome the limitations of existing models, an improved feeder cell-free method of differentiating hiPSCs into macrophages was developed. The protocol established in this study is based on two previously published protocols[55,56] and differs from other macrophage-directed differentiation methods[57–60] in that it is based on a two-dimensional culture with multiple macrophage progenitor harvests. The two-dimensional culture of hiPSCs allowed for the efficient differentiation induction from single cell clones. In contrast, the induction of macrophage differentiation from embryonic bodies is less homogeneous, resulting in limited reproducibility[61]. Moreover, the omission of feeder cells reduces the variability of the differentiation process. During the development of this protocol, the colony growth format turned out to be a pre-requisite for successful differentiation induction. Possibly, the round colonies favored the formation of the required organoid-like structure, which evolved during the differentiation process. In consequence, a transfer step was inserted between hiPSC expansion and differentiation, switching from monolayer towards colony growth (Fig. 3 and supplementary Fig. S5). The colony growth-adapted hiPSCs were cryopreserved in large cell batches well suited for medium- to high-throughput applications. During the transfer step to colony growth, the cells maintained their pluripotent cellular state, which is a pre-requisite for an effective differentiation (Fig. 4 and 5, supplementary Fig S6 and S7). Even though lines 201B7 and ChiPSC22 showed the weakest pluripotency marker abundance, differentiation was still successful. ChiPSC line 7 was excluded from subsequent experiments, since these cells behaved differently during the differentiation, which may be due to divergent growth rates of these cells. Principally however, the differentiation towards macrophages was successfully performed from all five employed iPSC lines, highlighting the robustness of the developed protocol.

To further adapt this protocol for medium- to high-throughput applications, a cryopreservation step for macrophage precursors was established. These frozen differentiation intermediates are useful for a batch-wise supply of cell aliquots during medium- to high-throughput purposes. Evaluating the differentiation potential of cryopreserved and non-cryopreserved MPCs, flow cytometry analyses revealed a positive impact of the freezing process towards macrophage maturation, shown by elevated macrophage marker expression (Fig. 9). Cryopreservation could have a selection pressure onto the cells. Potentially, this step could affect the differentiation process by modulating surface receptors of the progenitors needed for receiving differentiation signals. The capability of the re-thawed progenitors to differentiate more efficiently into macrophages corroborates the feasibility of the implemented cryopreservation step.

The presented protocol enables several progenitor harvests per differentiation campaign. This increases the efficiency of the method compared to protocols working with single time-point harvesting[80–82]. Gutbier et. al recently published a protocol that demonstrated a high yield production of MPCs by an experimental setup with multiple harvests[58]. However, they produced a relative yield (number of generated MPCs derived from a single iPSC) of 70 to 250 compared to the yield of around 16.000 achieved in the present work (Table 2). Furthermore, their protocol did not allow for cryopreservation of intermediate cells with acceptable recovery rates. Another research group successfully implemented a freezing-thawing step of progenitors in their recently published protocol, but their single time-point harvesting only generated a yield of approximately 14[80]. Their final IDM yield (number of generated IDMs derived from a single iPSC) was around 110. With the protocol presented in this study, a final IDM yield of 50.000 was achieved.

The IDMs produced in this work exhibited similar morphological and functional profiles as their primary cell counterparts (Fig. 6, 7, 11-13, supplementary Fig. S8). Upon thawing and re-seeding with M-CSF, the MPCs switched from suspension to adherent cells and assumed a predominantly spindle-like shape over the time course of seven days, similar to matured MDMs. Both MDMs and IDMs expressed high levels of the leukocytic lineage surface marker CD45[63], the monocytic lineage marker CD14[62] and the macrophage markers CD163 and CD206[64], which is consistent with IDMs produced by other protocols[59,80,83]. The purity of the generated macrophage population was shown by a percentage portion of close to 100 % of the cells being positive for both CD45 and CD14. These $CD45^+/CD14^+$ cells were additionally positive for both CD163 and CD206 (CD163: > 66 %; CD206: > 76 %; including all applied iPSC lines). Only for the tested maintenance medium StemFit Basic04 CT, the resulting MPC and IDM populations were heterogeneous, potentially explicable by the medium composition (Fig. 7). The contained FGF-2 possibly possessed lower protein stability properties compared to the freshly added protein when using the other tested media. However, FGF-2 is needed for maintaining pluripotency of the cells and lack of functional FGF-2 could therefore have a negative impact on the subsequent differentiation capacity of iPSCs[61].

A key macrophage function is their plasticity towards different macrophage subsets through which they rapidly react and adapt to transitions in their local environment[2]. Several recent studies suggested a similar transcriptional profile of IDMs compared to MDMs, also upon polarization[56,84]. However, mRNA levels do not necessarily correlate with the actual protein abundance. Accordingly, changes in the cellular proteome responses in differentially polarized IDMs and MDMs were analyzed by a quantitative proteomics approach (Fig. 12). Using LPS to induce a pro-inflammatory polarization and an IL-4/IL-13 cocktail to drive the macrophages towards an anti-inflammatory, pro-homeostatic condition, IDMs and MDMs responded

collectively in a similar manner. However, individual proteins were differentially expressed between the MDMs and IDMs. This observation was also shown by Gutbier et. al[58] and may be due to donor-to-donor variations of the used MDMs but may also demonstrate slight differences between the two macrophage types. Accordingly, when analyzing a certain macrophage target, its existence must be verified if applying IDMs. PCA revealed a separation of IDMs and MDMs on the component 2 (source effect). As a result of transcriptomic analyses, it was proposed that IDMs resemble tissue-resident macrophages due to the recapitulation of embryonic hematopoiesis during the differentiation protocol. MDMs are derived from monocytes that develop in the bone marrow and therefore have another origin, which may explain the separation of the two macrophage types[61,78].

More importantly, the generated IDMs behaved similarly as their primary cell counterparts regarding their functional activities. The cells reacted with mediator release of TNFα after simulating fungal infection and were able to phagocytose and efferocytose, with comparable kinetics after adding either *E. coli* conjugated bioparticles or prey cells (Fig. 11, 13, 16, supplementary Fig. S8 and S10). This is in accordance with the work of other research groups, in which a comparable uptake of *E. coli* particles between MDMs and IDMs[56] or between bone marrow-derived macrophages (BMDMs), RAW264.7 cells (a murine macrophage-like cell line), THP-1 cells and IDMs[69] was demonstrated.

Applying iPSC-based differentiation protocols towards macrophages, iPSCs are cultured in conditions that guide their differentiation through a developmental trajectory mirroring embryonic hematopoiesis. According to transcriptomic studies, it was proposed that the derived macrophages constitute a more relevant model for tissue-resident macrophages compared to MDMs[61,78]. The here applied multi-step protocol is likewise recapitulating states of embryonic hematopoiesis, by driving the cells consecutively through states of mesodermal development, hemogenic endothelium, hematopoiesis, myeloid specification, and final macrophage maturation (Fig. 6 and 10). In addition, macrophage progenitors or IDMs may be converted to tissue-specific macrophages, such as Kupffer cells or alveolar macrophages. Tilman et al. described the generation of alveolar macrophages by culturing progenitors with conditioned medium from lung cells as a novel model for respiratory research, for instance[85]. The generation of tissue-specific macrophages applying this protocol could be implemented by either culturing the MPCs or matured IDMs with conditioned medium or tissue-specific cells from the respective niche.

Both the developmental pathway directed by this protocol and the assessed functionality of generated IDMs justifies their usage to study macrophages *in vitro*. Moreover, this work presents a high-yield differentiation protocol that allows for multiple harvesting of macrophage

progenitors originating from a two-dimensional iPSC culture, bypassing the need of feeder cells and embryoid bodies. Hence, the macrophages generated in this study present a physiologically relevant platform suitable for both basic research and drug discovery.

3.2 Development of a miniaturized high-content-imaging-based efferocytosis assay

Efferocytosis of apoptotic cells is a key feature of macrophages and its quantification *in vitro* has traditionally been challenging. In this work, a high-content-imaging-based efferocytosis assay with an endpoint measurement after 5 hours was established. To set up a reproducible and robust efferocytosis assay, a homogeneous and efficient induction of apoptosis is essential[86]. To avoid that an apoptosis-inducing chemical agent, such as staurosporine[87], was carried over from the prey cells to the macrophages, induction of apoptosis was carried out by UV radiation[88,89] using a UV chamber. This allowed for a higher throughput in combination with a uniform apoptosis induction. To determine the kinetics of apoptosis induction, a live-cell imaging of irradiated and non-irradiated control cells was performed, identifying apoptotic cells by the application of Caspase 3/7 and Annexin V dyes (Fig. 14 a+b). At the corresponding efferocytosis assay endpoint, the majority of the irradiated cells had undergone apoptosis. Also among non-irradiated control cells a smaller portion of the cells was apoptotic, which is most likely the consequence of spontaneous apoptosis induction due to normal cellular turnover[90].

So far, different assays to assess the efferocytotic uptake of labeled prey cells have been developed, using either microscopy or a flow cytometry-based approach[58,91–94]. However, most of these assays, especially the flow cytometry-based ones, are unable to discriminate between prey cells that were truly engulfed and those only attached to the macrophage surface. Likewise, a microscopy-based approach e.g., using the more commonly applied IncuCyte imaging platform[69] may not provide the optical resolution to clearly identify efferocytotic events. A better distinction between bona fide engulfment and surface adherence of the prey cell could be achieved by confocal microscopy. For this reason, the described efferocytosis assay in this study was established using a confocal imaging device, the Opera Phenix reader. Additional advantages of the Opera Phenix reader are that it enables higher throughput and can readily be integrated into robotic systems. Further, the good optical resolution allows this device to reveal characteristics related to macrophage morphology together with the functional effect on efferocytosis. Accordingly, the error rate reached to virtually zero when measuring with the Opera Phenix, while the IncuCyte-based approach exhibited appreciably higher error bars (supplementary Fig. S12).

The selected CellTracker dye labeling the macrophages can be used in combination with paraformaldehyde-based fixation of the cells. Therefore, it is well suited for any immunolabeling following the efferocytosis assay, e.g., to analyze the efferocytosis-dependent effects on a certain target. Confocal stack measurements on exemplary samples demonstrated that the pHrodo signal originated from an intracellular compartment within macrophages, verifying true efferocytosis events (Fig. 14 f). To achieve a higher throughput, real time kinetics cannot be used. The measurement of a 384-well plate (5 images per well) and a 1536-well plate (1 image per well) takes approximately 20 minutes, depending on various parameter settings (e.g., exposure time). The Opera Phenix can only measure one plate at a time, and alternating imaging of multiple plates for kinetic measurements is challenging. In addition, the movement of the plates in and out of the Opera Phenix live-cell chamber could have a negative impact on the functional activity of the cells due to varying temperature and CO_2 conditions. In consequence, endpoint measurements should be applied when higher throughput is required, real time kinetic measurements may be employed for the characterization of fewer drug candidates. In order to select an appropriate timepoint at which to measure the efferocytotic activity, the assay was run in a kinetic mode using the live-cell chamber of the Opera Phenix during assay development (Fig. 16, supplementary Fig. S10). Based on the live kinetics data, an incubation time of five hours after prey cell addition was set for use, since the efferocytotic rate passed into a plateau after this timepoint. This is consistent with previous findings showing that efferocytosis is a relatively fast and efficient process *in vivo*[12,95]. For instance, almost no residual extracellular apoptotic cells were detectable within less than one hour after the injection of several millions of these cells into the peritoneum of a mouse[93]. The efferocytotic uptake of Raji prey cells was similar between the IDM lines and the MDMs, emphasizing their biological comparability with respect to this cellular function. Because of spontaneous apoptosis induction due to normal cellular turnover[90] (compare Fig. 14 a+b), a basic uptake of non-irradiated control cells was observed, which was also shown by another research group[96].

To enable a quantification of the efferocytotic rate, a co-localization image analysis algorithm was developed (Fig. 15). As mentioned above, previous efferocytosis analysis approaches were often unable to discriminate between prey cells that were truly engulfed and those only adhering to the macrophage surface[69]. Even approaches that had been based upon pH-sensitive dyes suffered from background fluorescence at neutral pH and other fluorescent artefacts e.g., in the presence of auto-fluorescent test compounds[97]. False-positive efferocytosis events also emerged when utilizing the IncuCyte imaging platform, particularly for non-irradiated cells (supplementary Fig. S12). The presented analysis algorithm bypassed this issue by restricting spot detection only to the macrophage areas as defined by a distinct

fluorophore label. The respective macrophage was classified as “efferocytosis positive” if the integrated fluorescence intensity of all pHrodo-labeled spots surpassed a pre-defined threshold. Using pHrodo-conjugated *E. coli* particles instead of pHrodo-labeled irradiated prey cells, the same analysis algorithm was used for a high-content-imaging-based phagocytosis assay. This assay quantifies the uptake of *E. coli* particles during kinetic measurement or may be set up as an assay with a fixed endpoint measurement. As established previously[66,96,98], cytochalasin D was employed as a positive control for efferocytosis or phagocytosis inhibition. The comparison between vehicle- and cytochalasin D-treated cells served to define the threshold settings for image analysis. The latter adjustment was necessary to overcome issues such as donor or differentiation batch variability.

In accordance with the work of others[96,99], the treatment with cytochalasin D was reflected by a significant decrease of the number of efferocytosis positive cells, as quantified by the above-described image analysis algorithm. Furthermore, a concentration-response titration of cytochalasin D produced comparable IC_{50} values between the different macrophage types, re-emphasizing the comparability of the generated IDMs with MDMs (Fig. 17, Table 6). The robustness of the assay was shown by assessing the Z’ and RZ’ values for various IDM and MDM preparations, for the 384-well and miniaturized 1536-well format. For 384-well and 1536-well microplates, liquid handling is more challenging than for the 96-well format – the latter being frequently employed in a more academic context. Bar and Zweifach[67] demonstrated that a Z’ value of 0.4 provides reasonable power to identify active compounds in a screening campaign. All 384-well and 1536-well microplates measured in this study surpassed this threshold. An efferocytosis assay with a different set-up established by Hall-Roberts et. al. reported an RZ’ value of 0.7 when comparing vehicle and cytochalasin D treatment[100]. However, their assay was established in the 96-well format, limiting the throughput. Further miniaturized efferocytosis assays were published by Santulli-Marotto et. al.[96] and Clark et. al[99]. While the former did not elaborate on the statistical robustness of the assay, the latter reported RZ’ values between 0.5 and 0.8[99]. However, their assay was based only on 384-well microplates and the usage of MDMs. One advantage of the assay established by Clark et al.[99] presents the possibility of cell fixation before imaging, being beneficial for high-throughput applications. A robust fixation-based assay was not feasible with the here presented set-up, which could be attributed to a differently used pHrodo dye. However, combining the assay established in the presented study with the IDMs that are differentiated using frozen progenitor cell batches qualifies this set-up for drug discovery applications. To enable a larger high-throughput campaign, a scheduled workflow for on time prey cell preparation and high-content-imaging needs to be established.

Syk is a non-receptor tyrosine kinase de-regulated in IPF patients[70]. In addition, it was shown that Syk inhibition prevented bleomycin-induced fibrosis and inflammation in the skin and in the lung[71,72]. Previous studies on macrophages already demonstrated that inhibition of Syk suppressed inflammatory responses, e.g., TNF production[101,102]. Moreover, Syk inhibition was also reported to prevent phagocytosis in RAW264.7[103] and in bone marrow-derived dendritic cells (BM-DCs)[104]. Furthermore, Kitai et al. revealed that the modulation of the upstream receptor of Syk, Dectin-2, and CARD9 (Caspase recruitment domain-containing protein 9), being downstream of Syk, affected the actin polymerization process in BM-DCs[104]. Accordingly, Syk inhibitors might be speculated to have an influence on efferocytosis. To challenge this hypothesis and to validate simultaneously the applicability of the assay, the Syk inhibitors ER 27319 maleate, GSK 143 and piceatannol were applied in the efferocytosis assay. Indeed, the suppression of Syk-mediated signaling revealed a negative efferocytosis modulation with a comparable pharmacology in IDMs and MDMs (Fig. 18, Table 7). Piceatannol is an inhibitor of both the Syk and Lyn kinase function, reported to inhibit Syk and Lyn with IC_{50} values of approximately 10 µM and 100 µM, respectively, in an *in vitro* kinase assay[76]. In the efferocytosis assay, piceatannol caused a partial inhibition of prey cell uptake with IC_{50} values of 15 µM, 20 µM and 20 µM for IDM#12, IDM#B7 and MDMs, respectively. The partial character of the inhibition may be due to the non-specificity of piceatannol and its modulation of other signaling events in the macrophages. GSK 143 is a more specific inhibitor of the Syk kinase function[74] with a reported IC_{50} value of 323 nM in lymphocytes[105]. In the presented efferocytosis assay, the potency of GSK 143 was weaker (IC_{50} values ranges from 3.2 to 4.6 µM), which may be due to different signal amplifications in the respective signaling pathways. Unlike piceatannol and GSK 143, ER 27319 maleate is selectively interfering with the Syk activation process and thus, it is not a direct inhibitor of the kinase activity[73]. This compound showed the highest potency among the tested ones with an IC_{50} range between 1.5 and 2.1 µM, while previously an IC_{50} value of 10 µM had been reported for the effect of ER 27319 on various signaling pathways in rat RBL-2H3 cells[73]. Since all three Syk inhibitors showed an impact on the efferocytotic activity without any previous active stimulation of the kinase, the Syk signaling pathway was apparently in a constitutively active condition in the employed macrophages. In summary, the positive effect of preventing fibrosis by Syk inhibition shown by other research groups may be based upon diminishing the inflammatory branch of fibrosis, by a reduction of the TNF production[101,102], for instance. On the contrary, based on the collected data, efferocytosis-based tissue repair processes might be impaired. Further analyses will be required to explore this phenomenon. In addition to different Syk inhibitors, other tools or compounds were tested in this set-up that are associated with fibrosis modulation[106,107] (supplementary Fig. S13). Applying Dexamethasone treatment of macrophages, a positive efferocytosis modulation was shown, as previously reported by

others[96,99]. Recently, it was shown that pro-fibrotic macrophages could be generated *in vitro* by treatment with a cocktail made of IL-4, IL-13 and TNFα[107]. In the presented assay, this stimulation resulted in decreased efferocytosis activity (supplementary Fig. S13). However, when applying the single cocktail components, this effect could be reduced to TNFα only. This observation is in accordance with previous findings, where a pro-inflammatory polarization state induced by TNFα is described, being linked to a decreased efferocytotic function[108].

In summary, the here presented high-content-imaging-based efferocytosis assay was established utilizing IDMs and MDMs that displayed comparable pharmacology, as demonstrated by the analysis of Syk inhibitors, Dexamethasone, and a pro-fibrotic cocktail. In addition, a similar set-up utilizing the same analysis method enables the quantification of phagocytosis. These miniaturized cellular assays lend themselves to the pharmacological drug discovery of substances with the ability to modulate either efferocytosis or phagocytosis.

3.3 Development of miniaturized co-cultures between senescent epithelial cells and macrophages

Both incidence and severity of IPF increase with higher age, assuming that aging presents a key risk factor for the disease onset[42]. Senescent cells accumulate during ageing and markers of senescence were detected in both IPF patients and animal models, linking the disease with senescence[24]. Recently, the negative impact of senescent cells on the macrophage's efferocytosis function was shown[39]. Using the previously established high-content-imaging-based efferocytosis assay, the aim was to validate this observation via a miniaturized approach of senescent epithelial cells and macrophages. Moreover, senolytics were applied to restore the diminished efferocytosis activity.

In this work, senescence was induced by either serial passaging of primary SAECs (replicative senescence) or by treatment of the latter in combination with the lung epithelial cell line A549 using different agents. Depending on the age of the SAEC donor, the Hayflick limit[109] was reached and the proliferation potential was exhausted after varying passages. This approach of senescence induction presents the most physiological set-up and mimics the ageing organism. However, this *in vitro* induction is both laborious and time consuming since multiple passaging cycles are required (up to months). Furthermore, this method is restricted to primary cells only, thereby excluding immortalized cell lines such as the here employed A549[45]. The second technique to induce senescence in this work is based on treatments with either etoposide, palbociclib or TGFβ1 over a time course of seven days. In comparison to the replicative approach, this presents a fast method to artificially activate a senescence program in both primary and immortalized cell lines. Moreover, it benefits from increased reproducibility.

The chemotherapeutic agent etoposide is deployed as an anti-cancer drug by acting as a topoisomerase II inhibitor, thereby inducing DNA double-strand fraction[46]. In contrast, the drug has been shown to drive senescence at lower doses in A549 cells[39]. The CDK4/6 inhibitor palbociclib is likewise used for cancer therapy that activates senescence, but not apoptosis, being reported for lung fibroblasts and SAECs, for instance[39,49]. The third approach involves the treatment with TGFβ1, a pro-fibrotic protein and key mediator in fibrotic conditions[26]. TGFβ1 protein levels are augmented in IPF patients and animal models, and its signaling pathway is one of the most upregulated ones in aberrant epithelial cells[26,110]. Moreover, the protein was already shown to induce senescence in bronchial epithelial cells and A549[47,111]. Accordingly, the application of TGFβ1 to trigger senescence represents a physiologically relevant model in the context of IPF. However, the pathways and mechanisms being involved in TGFβ1-mediated senescence induction still remain elusive, but one possibility is telomerase activity inhibition[36,111]. One option to better recapitulate the fibrotic niche in IPF patients *in vitro* could be a model that utilizes epithelial cells originating from an old donor, which show already a replicative senescence. This approach would prevent the need for the time-consuming and laborious induction of replicative senescence by serial passaging. The treatment of these cells with TGFβ1 could then intensify the senescent phenotype and introduce pro-fibrotic signals.

The two employed approaches, the replicative and the artificial senescence induction by anti-cancer drugs or TGFβ1 treatment, resulted in the appearance of distinct established senescence characteristics in SAECs and A549 (Fig. 19-24, supplementary Fig. S14-S23). Senescent cells exhibit a dynamic and heterogeneous phenotype, and there is no existing exclusive marker to identify them[45]. Some reliable and often used markers include an increase of size and irregular cell morphology, elevated p16 and p21 levels, an accumulation of lysosomes with increased SA-β-galactosidase activity, and release of multiple SASP-associated molecules. These features were (partly) detected in the serially passaged SAECs and in cells treated with etoposide, palbociclib or TGFβ1, implying a successful senescence induction with the different stimuli. Though, the different methods resulted in the development of distinct senescence signatures, thus representing the great heterogeneity of this phenotype. Especially for the SASP-associated factors, different expression patterns were observed. Importantly, some of the identified upregulated factors are also used as IPF biomarkers or are known to be elevated in patients and animal models, such as MMP7 and CCL2[112,113]. Various cell types found in the lungs of IPF patients have been shown to be in a senescent state, such as epithelial cells and fibroblasts, with an increase of SA-β-galactosidase activity, and elevated p16 and p21 levels. Moreover, it was also shown that senescent fibroblasts act pro-fibrotically by triggering a fibrotic phenotype in healthy fibroblasts through their secretome[24]. Also in the established bleomycin mouse model, the drug leads to different senescence characteristics[24].

Post-treatment with the anti-cancer compounds or TGFβ1, an accumulated protein abundance of CD47 was detected using SAECs and A549, a known 'don't eat me' signal for macrophages[114]. CD47 was reported to be elevated in fibroblasts derived from IPF patients and anti-CD47 treatment weakened fibrosis *in vivo* and furthermore increased the phagocytotic activity of macrophages[39,115]. Accordingly, the different employed approaches in this study may be utilized as a complementary model in fibrotic lung diseases to induce a cellular senescence program, covering diverse aspects of the senescent disease phenotype.

As already mentioned, senescent cells expand during ageing and are enriched in lungs of IPF patients. Furthermore, levels of senescent biomarkers were upregulated with increased disease severity[24,42]. In addition to a senescent signature of the IPF lung, a strong conglomeration of non-ingested apoptotic corpses, accompanied with diminished efferocytotic activity of lung macrophages, was documented for IPF patients[19]. These important findings indicate that senescent cells in combination with attenuated efferocytosis activity may be potential key drivers of fibrosis. In drug discovery, the miniaturized analysis of physiologically relevant cellular models is of pivotal importance, enabling screenings for biological targets which aim to identify pharmacologically active compounds[116]. Miniaturization of assays without significantly reducing the physiological relevance is a key challenge in this field[116]. Pathobiological mechanisms contributing to IPF are regulated by an interaction between multiple different cell types and involve macrophage-mediated processes[7]. Thus, co-cultures between macrophages and epithelial cells, the key players in IPF development, are of interest to increase the physiological relevance. Consequently, there is an unmet need in drug discovery for miniaturized co-cultures involving these two important cell types to analyze their crosstalk. Based on this, the aim was to miniaturize co-cultures between macrophages and senescent epithelial cells to mimic the fibrotic setting, which was utilized to analyze the resulting efferocytosis capacity. The previously described efferocytosis assay and the set-up of Schloesser et al.[39] was exploited as a basis for the development of the miniaturized co-culture in the 384-well format (Fig. 25). Automated seeding of both cell types in combination with automated washing steps after treatment with senescence-inducing agents (BioTek Washer), high-content-imaging (Opera Phenix), and a robust image analysis workflow enables medium- to high-throughput applications.

In this study, the senescent cells were utilized as a tool to study the effect on macrophage functions. The application of senescent A549 in the co-culture significantly reduced the efferocytotic activity of macrophages for both IDMs and MDMs (Fig. 26 f-h). Importantly, it was excluded that the macrophages incorporate the senescent cells (supplementary Fig. S24). In contrast, they only swarmed over and around the senescent cells. However, when utilizing primary SAECs as the senescent epithelial component in a direct co-culture set-up, the

observed negative efferocytosis modulation was not as clear as with the used A549 cells (Fig. 26 c-e). This could be explained by a basal senescence of the SAECs due to their primary origin and an expansion step over several passages prior to their application in the set-up. However, the effect was visible for TGFβ1-induced senescence. Moreover, palbociclib-induced senescence in SAECs exhibited additionally a suppression of the phagocytotic activity of macrophages (Fig. 26 m). Therefore, the set-up should be verified with non-expanded primary SAECs and other senescent cell types, like fibroblasts. Importantly, the negative impact on efferocytosis was only observed when employing direct co-cultures with cell-cell contacts between macrophages and senescent cells. This effect was absent when treating macrophages with conditioned medium derived from senescent cultures (Fig. 26 i-k). Accordingly, these data imply that only direct cell-to-cell signaling between macrophages and senescent cells can modulate the efferocytotic activity. This is supported by different independent studies showing that the 'don't eat me' signal CD47 modulates efferocytosis. Furthermore, a blockade of the protein amplified the efferocytotic capacity[39,117]. As mentioned previously, CD47 is elevated in IPF patients and anti-CD47 treatment weakened fibrosis *in vivo*[115]. The 'don't eat me' signal was also upregulated in SAECs and A549 cells upon treatment with senescence-inducing drugs in the here presented work (Fig. 24 and supplementary Fig. S23). CD47 is located on the cell surface[50] and could mediate the efferocytosis suppression in a direct co-culture. A blockade with anti-CD47 antibodies, for instance, might also restore the efferocytosis activity in the presented co-culture set-up and needs to be verified.

Resulting limitations from the complex experimental set-up present the different seeding timepoints and densities of senescent and control cells, as well as the timepoint of plate measurement. A simultaneous seeding was not possible, since control cells would still proliferate and thus, would lead to incomparable cell densities. To bypass this problem, control cells were seeded at a later timepoint with overnight vehicle treatment prior to macrophage seeding. To achieve similar cell densities between conditions, the cell numbers were optimized using microscopy confluency masks in the brightfield channel. When keeping the original assay endpoint of five hours, the effect of senescent cells was not significant. However, kinetic measurements over 24 hours showed that this effect was only visible after the first hour post prey cell addition (data not shown). On this account, the plate measurement was performed one hour after prey cell addition in the co-culture set-up. This observation might be explained by the balance between 'eat me' and 'don't eat me' signals that the macrophages receive during the assay. Over time, the majority of irradiated prey cells becomes apoptotic and thus, increase the abundance of 'eat me signals'. Thereby, the 'eat me signals' superimpose the 'don't eat me' signals originating from the senescent cells and increase the efferocytosis

activity. In summary, the miniaturized co-culture showed the same results reported by the study of Schloesser et. al[39], the suppression of efferocytosis by senescent cells. However, the presented set-up needs to be verified with additional senescent cell types, such as fibroblasts, and with non-expanded primary SAECs. Nonetheless, the advantage of the miniaturized set-up presents the possibility of testing huge compound libraries in the assay to identify pharmacologically active substances being able to inhibit this effect.

Applying the described miniaturized co-culture set-up, senolytics were utilized to restore the diminished efferocytosis activity. These small molecules target the upregulated SCAPs, thereby eliminating senescent cells by induction of apoptosis. The potential benefits of senolytics were already shown by different studies in the context of lung fibrosis, in animal models and patients[24,43,51]. Importantly, SCAPs may be also active in non-senescent cells. Accordingly, senolytics may cause a concentration-dependent cytotoxicity in proliferating cells. The senolytics ABT263 or a cocktail of Dasatinib and Quercetin were applied for 48 hours. Only up to 14 % cells positive for Caspase 3/7 or Annexin V were detected in non-senescent controls treated with ABT263 (supplementary Fig. S25), representing physiological cell turnover[90]. The Dasatinib/Quercetin combination led to more than 80 % of apoptotic cells (supplementary Fig. S26), however, the percentages of vehicle-treated positive cells were similarly increased. In contrast, ABT263 was less effective and resulted in 47-97 % (Caspase 3/7) or 31-75 % (Annexin V) apoptotic cells, depending on the treatment with the senescence-inducing agent (Fig. 27). The increased efficiency of Dasatinib and Quercetin could be explained by the fact that the two substances modulate different SCAPs[48]. Cells triggered to activate their senescence program via TGFβ1 treatment apparently showed an increased sensitivity for apoptosis induction by ABT263. This could be traced back to strongly upregulated SCAPs. In another study, etoposide-triggered senescent A549 were treated overnight with the two-fold concentration compared to the presented set-up, leading to twice as many apoptotic cells. To increase the percentage of apoptotic cells, the used concentrations and treatment duration could be optimized without causing cytotoxicity in non-senescent control cells.

Since the senolytic treatment resulted in apoptosis of senescent A549, a different approach was used when combining the senolytic treatment, the co-culture and the efferocytosis assay. A549 cells were labeled with pHrodo after senolytic treatment and efferocytosis assays were performed in the absence of the standard Raji prey cells, to discriminate between the engulfment of apoptotic senescent A549 cells and apoptotic Raji cells. A549 cells treated with ABT263 showed significantly higher efferocytotic activity of macrophages compared to vehicle-treated control cells (Fig. 28). This is in line with the study of Lee et. al that utilized a rat model of ischemic heart disease[118]. The researchers reported that senescent cells were

eliminated by macrophages via efferocytosis upon treatment with ABT263. Moreover, the expression of pro-inflammatory factors and MMPs was reduced and macrophages showed a phenotypic switch towards pro-repair, emphasizing the beneficial effects of senolytics. However, in the here presented study, similar effects were observed for non-senescent control cells (supplementary Fig. S27). A reduction of cytotoxicity to achieve a diminished efferocytosis rate of the control cells could be addressed by further optimizing the concentration and treatment duration. Another approach could be the application of second-generation senolytics, that have been designed for highly specific targeting of senescent cells. This is achieved by strategies utilizing senescence-associated markers, such as the reliable increased β-galactosidase activity, for instance. These involve β-galactose-conjugation of prodrugs or β-galactose-coating of nanoparticles that are both processed and activated by the enzyme[119]. A second class of senotherapeutics are senomorphics, small molecules targeting senescent cell signaling by the suppression of the SASP without eliminating the cells[48]. However, this work suggests that senescence-mediated efferocytosis blockade is primarily induced by direct cell-cell contacts, being independent of SASP signaling pathways. Thus, senomorphics are not expected to show a modulatory effect on the efferocytotic activity in the co-culture with senescent cells. However, a combined approach of the two senotherapeutic classes could be beneficial.

The distinction between uptake of apoptotic senescent cells and Raji prey cells presents a limitation of the developed assay. This challenge could be addressed by a combination of an additional pHrodo dye. Combined usage of red and green fluorescent pHrodo dyes may quantify the removal of both cell types in parallel. However, the labeling of macrophages needs to be adapted accordingly, which are detected in the green channel, being crucial for the analysis algorithm. Nonetheless, total elimination of apoptotic senescent cells for the restoration of the efferocytosis capacity continues to be challenging in this set-up. Senescent cells show an increase in size[48], which may hamper their proper engulfment. Moreover, it might be more valuable to directly target the communication between macrophages and senescent cells itself. As previously mentioned, the usage of anti-CD47 antibodies, for instance, showed a positive effect on the efferocytotic activity of macrophages[39,117], preventing the need for senolytic apoptosis induction.

In summary, different approaches showed successful induction of a senescence program in epithelial cells. The fibrotic niche was recapitulated *in vitro* by the combination of senescent epithelial cells and macrophages in a miniaturized co-culture, demonstrating impaired efferocytosis in this context. Moreover, senolytic treatment of senescent epithelial cells triggered their apoptosis and resulted in increased efferocytotic activity, offering a therapeutical approach to treat fibrotic diseases.

4. Conclusion

One of the fundamental challenges in drug discovery is the need for physiologically relevant cellular *in vitro* models that are able to recapitulate the disease situation in patients. Many of the reported models lack relevant cells and cannot be applied for large-scale drug screening campaigns. Hence, there is an unmet need for miniaturized cell models and drug discovery assays that support the development of novel therapeutic concepts.

Particularly for macrophages, there is a clear potential of modulating this cell type for therapeutic approaches, since they are involved in different phases of the fibrotic cascade and thus, possess a unique role in the fibrotic context. To overcome the limitations of existing macrophage models, directed differentiation of human iPSCs was applied to establish a constant and scalable source of derived macrophages. The applied multi-step protocol recapitulates states of embryonic hematopoiesis and results in cells that resemble tissue-resident macrophages with respect to ontogeny. These IDMs were shown to exhibit similar morphological and functional profiles as their primary cell counterparts and thus, present a physiological relevant platform suitable for both basic research and drug discovery.

To analyze macrophage functions in fibrotic diseases, a high-content-imaging-based assay in the 384-well and 1536-well microplate format was established, enabling both an efferocytosis- and phagocytosis-based assay for medium- to high-throughput applications. Utilizing IDMs and MDMs, the cells showed comparable pharmacology, as demonstrated by the analysis of Syk inhibitors, Dexamethasone, and a pro-fibrotic cocktail.

By the use of differently induced senescent epithelial cells, the effect of senescence signals on pivotal macrophage functions was shown by a miniaturized co-culture set-up, demonstrating impaired efferocytosis and phagocytosis activity in this context. Moreover, senolytic treatment of senescent epithelial cells triggered their apoptosis induction and resulted in increased efferocytotic activity.

Pharmacological treatment opportunities for IPF patients are still insufficiently available. At the same time, the existing drugs are inadequate in modulating the natural course of the disease. Consequently, there is an unmet need for innovative therapeutic approaches. The insights gained from this study imply that senescent cells may be a potential cause of restricted efferocytosis activity. Based on these results, addressing senescent cells and their communication with macrophages could present a promising therapeutical concept.

Taken together, the achievements of this work built up a novel disease relevant platform being valuable for both basic research and preclinical drug discovery applications allowing to model

features of the fibrotic niche *in vitro*. Furthermore, this work emphasizes the high utility value of human iPSC-derived model cells in preclinical drug discovery to analyze sophisticated biological processes. The insights gained from this study are expected to have an impact on future research involving lung epithelial-macrophage crosstalk and ultimately, may open new routes to innovative therapeutic paths in the context of fibrosis and beyond.

5. Material and methods

5.1 Differentiation of hiPSCs towards macrophage-like cells

5.1.1 Maintenance of hiPSCs (ChiPSC lines and 201B7)

Cellartis human iPSC (ChiPSC) lines were purchased from Takara Bio Europe AB (ChiPSC7, cat. Y00275; ChiPSC12, cat. Y00285; ChiPSC18, cat. Y00305; ChiPSC22, cat. Y00325). The iPSCs were cultured according to the manufacturer's instructions in a feeder free environment as a monolayer. Briefly, cells were maintained on COAT-1 (cat. Y30012, Takara Bio Europe AB) coated cell culture flasks in a humidified atmosphere at 37 °C and 5 % CO_2 with a daily media change using freshly prepared Cellartis DEF-CS 500 complete medium consisting of Cellartis DEF-CS 500 Basal Medium (cat. Y30011, Takara Bio Europe AB), supplemented with DEF-CS GF1 (diluted 1:333; cat. Y30016, Takara Bio Europe AB) and DEF-CS GF2 (diluted 1:1000; cat. Y30016, Takara Bio Europe AB). DEF-CS GF3 (diluted 1:1000; cat. Y30016, Takara Bio Europe AB) was only added to Cellartis DEF-CS 500 complete medium when the cells were thawed, passaged, or cryopreserved and was not added to the maintenance medium. Prior to hiPSCs seeding, a T-25 flask (cat. 430168, Corning) was coated with 0.1 mL/cm^2 of COAT-1 diluted 1:20 in 1 × Dulbecco's Phosphate buffered saline (D-PBS (+/+); cat. 14040083, Thermo Fisher Scientific) for at least 20 min at 37 °C and 5 % CO_2. Cryopreserved cells were thawed and seeded at 6 × 10^6 cells in Cellartis DEF-CS 500 complete medium and were cultured for three days until passaging. After reaching 80 % confluency, cells were washed with 1 × D-PBS (−/−; cat. 14190144, Thermo Fisher Scientific) and detached using 40 µL/cm^2 of 1 × TrypLE Select Enzyme (cat. 12563-011, Life Technologies). After 5 min at 37 °C, the flask was rinsed with 10 volumes of Cellartis DEF-CS 500 complete medium. Cells were centrifuged at 200 g for 5 min and were re-seeded at a density of 4 × 10^4 cells per cm^2 (four days culture) or at 5 × 10^4 cells per cm^2 (three days culture) in Cellartis DEF-CS 500 complete medium. For cryopreservation, the cells were resuspended at 6 × 10^6 cells per mL in STEM-CELLBANKER (cat. 11890, Amsbio) for long-term storage at -150 °C.

As a reference hiPSC line growing in the colony format by default, line 201B7[120] was used in this study. The cells were maintained by seeding 2 x 10^3 cells per six-well (cat. 140675, Thermo Fisher Scientific) at 37 °C with 5 % CO_2 in StemFit Basic03 (cat. SFB-503, Ajinomoto) supplemented with 10 µM of Y-27632 (ROCK inhibitor; cat. 10-2301, FOCUS Biomolecules) for the first 48 h and 100 ng/ml fibroblast growth factor (FGF)-2 (cat. 233-FB-025, R&D

Systems) in pre-coated plates with 0.1 mL/cm^2 iMatrix-511 (cat. AMS.892012, Amsbio), diluted 1:125 in 1 × D-PBS (−/−) at 37 °C for 1 h. The medium was changed every other day for one week passaging the cells at 80 % confluency. For passaging, the hiPSCs were washed once with 1 × D-PBS (−/−) and detached with 40 µL/cm^2 of 1 × TrypLE Select Enzyme. After 4 min at 37 °C, the enzyme was neutralized with StemFit Basic03 supplemented with 100 ng/ml FGF-2 and 10 µM of Y-27632 and removed by centrifugation at 300 g for 5 min. For long-term storage at -150 °C, the cells were resuspended at 0.5 × 10^6 cells per ml in Cryostor CS10 (cat. C2874-100ml, Sigma-Aldrich). For some experiments, the maintenance medium was switched to StemFit Basic 02 (cat. SFB-500, Ajinomoto) or StemFit Basic 04 Complete Type (cat. SFB-504-CT, Ajinomoto).

5.1.2 Transfer to colony-like growth and cell banking

A pre-requisite to successfully differentiate hiPSCs to macrophage-like cells using this protocol is a colony growth of the stem cells. To switch the ChiPSC lines from monolayer growth to colony formation, the Cellartis DEF-CS 500 complete maintenance medium was replaced by StemFit Basic03 and the COAT-1 coating was replaced by laminin iMatrix-511 coated plates (Fig. 29 a). Prior to hiPSC transfer, six-well plates were coated with 0.1 mL/cm^2 of iMatrix-511 diluted 1:125 in 1 × D-PBS (−/−) for 1 h at 37 °C and 5 % CO_2. After seven days in Cellartis DEF-CS 500 complete medium on COAT-1 coated flasks after thawing, including one passaging step, cells were detached as described above and resuspended after centrifugation in StemFit Basic03, supplemented with 10 µM of Y-27632 for the first 48 h and 100 ng/ml FGF-2. Cells were seeded at 2 × 10^3 cells per six-well with medium changes every other day. After seven days, the transferred cells growing in colonies were cryopreserved. For that, hiPSCs were washed once with 1 × D-PBS (−/−) and detached with 40 µL/cm^2 of 1 × TrypLE Select Enzyme. After 4 min at 37 °C, the enzyme was neutralized with StemFit Basic03 supplemented with 100 ng/ml FGF-2 and 10 µM of Y-27632 and removed by centrifugation at 300 g for 5 min. The transferred cells were cryopreserved at 0.5 × 10^6 cells per ml in Cryostor CS10.

5.1.3 Differentiation of hiPSCs into macrophage-like cells

To differentiate into iPSC-derived macrophages, two previously published protocols[55,56] were adopted and modified in a two-dimensional cell culture system (Fig. 29 b). For that, cryopreserved transferred cells from the ChiPSC lines and 201B7 cells were thawed and seeded at 2 × 10^3 cells per iMatrix-511 pre-coated six-well in StemFit Basic03 supplemented with 100 ng/ml FGF-2 and 10 µM of Y-27632 for the first 48 h (day 0). After seven days with medium changes every other day, the cells were detached as described above and seeded

either at 100 cells per iMatrix-511 pre-coated six-well or at 1.8×10^3 cells in iMatrix-511 pre-coated T-175 flasks (cat. 10127340, Thermo Fisher Scientific) in StemFit Basic03 supplemented with 100 ng/ml FGF-2 and 10 µM of Y-27632 for the first 48 h (day 7). The medium was changed every other day until day DoD0, when the formed colonies reached a size of 400–750 µm. At this day, mesoderm differentiation was induced by switching the maintenance medium to complete Essential 8 medium (cat. A1517001, Gibco), supplemented with 80 ng/ml Vascular endothelial growth factor A (VEGF-A; cat. 293-VE-050, R&D Systems), 80 ng/ml Bone morphogenetic protein 4 (BMP-4; cat. 314-BP-050, R&D Systems) and 4 µM CHIR99021 (cat. 4423, Tocris Bioscience). At DoD2, hemogenic endothelium was induced by replacing with Essential 6 medium (cat. A1516401, Gibco), supplemented with 80 ng/ml VEGF-A, 50 ng/ml FGF-2, 50 ng/ml Stem cell factor (SCF; cat. 255-SC-050, R&D Systems) and 2 µM SB431542 (cat. 1614, Tocris Bioscience). At DoD4, the cells were treated with complete StemPro34 medium (cat. 10639011, Gibco), supplemented with 1 × Glutamax (cat. 35050061, Gibco), 40 ng/ml VEGF-A, 50 ng/ml SCF, 10 ng/ml Thrombopoietin (TPO; cat. 288-TPN-025, R&D Systems), 50 ng/ml IL-3 (cat. 203-IL-050, R&D Systems) and 50 ng/ml Fms-related tyrosine kinase 3 ligand (FLT-3L; cat. 308-FK-025, R&D Systems). At DoD7, the cells received StemSpan™ SFEM II medium (cat. 09655, Stem Cell Technologies) supplemented with 1 × StemSpan™ $CD34^+$ Expansion Supplement (cat. 02691, Stem Cell Technologies). At DoD9 and DoD11, fresh StemSpan™ SFEM II medium supplemented with 1 × StemSpan™ $CD34^+$ Expansion Supplement was added to the cells without removing the existing medium, respectively. From DoD14 on, floating progenitor cells were collected and filtered through 30-µm strainers (cat. 130-098-458, Miltenyi Biotec). The cells were cryopreserved using Cryostor CS10 at 1×10^7 cells per ml for long-term storage at -150 °C and are further referred to as freezable macrophage progenitors (MPCs). The remaining cells were maintained with fresh StemSpan™ SFEM II medium supplemented with 1 × StemSpan™ $CD34^+$ Expansion Supplement. Fresh medium was added twice per week until the next harvest (once per week for a total of four weeks).The cryopreserved MPCs were thawed in StemSpan™ SFEM II medium and seeded at 5×10^6 cells per T-75 flask (cat. 156499, Thermo Fisher Scientific) with DMEM (cat. 31966021, Gibco), supplemented with 10 % heat-inactivated fetal bovine serum (HIFBS; cat. 16140071, Gibco), 1 % non-essential amino acids (NEAA; cat. 11140035, Gibco), 1 % Penicillin-Streptomycin (Pen/Strep; cat. 15140-122, Gibco; complete macrophage medium) and 100 ng/ml Macrophage colony-stimulating factor (M-CSF; cat. 216-MC-100/CF, R&D Systems) for 7 days. After 3-4 days, the cells were treated with another 100 ng/ml M-CSF for final macrophage differentiation. Cellular imaging was conducted with EVOS XL Core and EVOS M5000 Imaging System (Thermo Fisher Scientific).

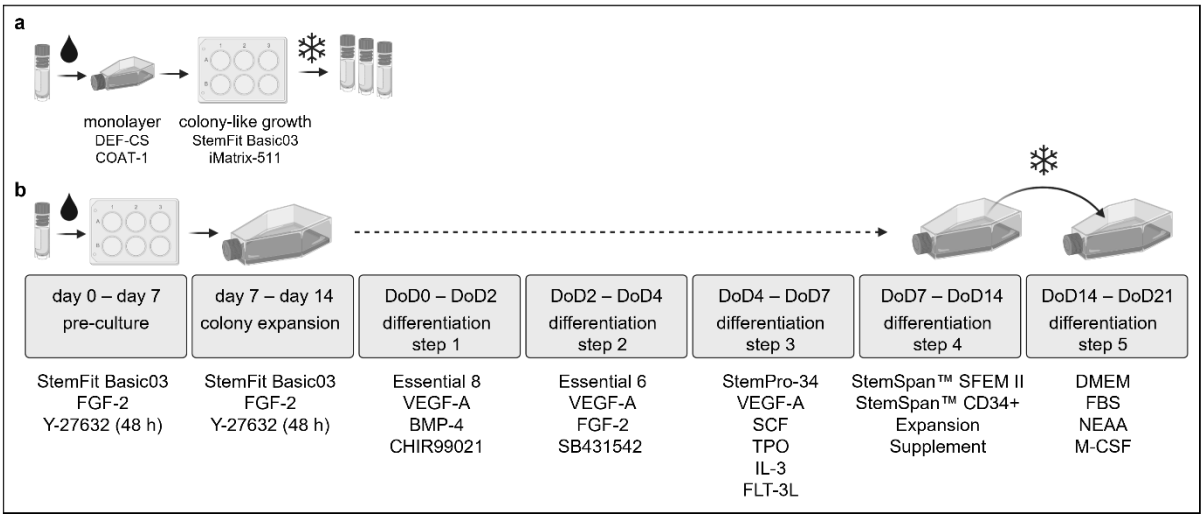

Figure 29. Optimized stepwise differentiation protocol of hiPSCs towards derived macrophages including colony transfer and cell banking steps. (a) Transfer to colony growth and cell banking of ChiPSC lines. After one week of monolayer culture, ChiPSC lines were transferred to colony growth by switching the cell culture medium and coating for one week, followed by cryopreservation. **(b)** Previously cryopreserved ChiPSC lines as shown in (a) and line 201B7 were thawed and kept for one week in a pre-culture before seeding for colony expansion and subsequent differentiation induction in T-175 flasks at day of differentiation (DoD) 0. Stepwise differentiation of progenitors was achieved during 14 days by periodic provision of different factors through media changes. Between DoD7 and DoD14, medium was not exchanged, but added freshly every other day. From DoD14 on, progenitors were harvested weekly for up to four times. Progenitors were frozen and after thawing, the cells were seeded for final macrophage maturation.

5.2 Isolation of primary human monocytes from whole blood and differentiation to macrophages

For this study, anonymized blood samples were obtained from different human healthy volunteers obtained from our internal blood donation service following ethical standards and local regulation. In order to isolate monocytes for subsequent macrophages differentiation, LeucoSep 50 ml tubes (cat. 227290, Greiner Bio-One) were filled with 15 ml Ficoll-Paque PLUS (cat. 17-1440-03, GE Healthcare) and centrifuged for 30 sec at 1000 g. The blood samples with a volume of 100 ml per donor (1 % Natrium-Heparin) were diluted with 20 ml of 1 × D-PBS (−/−) and distributed into LeucoSep tubes. Peripheral blood mononuclear cells (PBMCs) were separated by density gradient centrifugation (20 min, 800 g at room temperature, without deceleration). Cells were collected from the interphase and were washed three times with 1 × D-PBS (−/−) at 300 g for 10 min. After the penultimate washing step, all PBMC pellets from the same donor were pooled and counted. Subsequently, cells were resuspended in pre-cooled 1× D-PBS (−/−) containing 2 mM Ethylenediaminetetraacetic acid (EDTA; cat. 15575-038, Invitrogen) adjusting the cell concentration to 1 × 10^7 cells/ml. Monocytes were isolated by immunomagnetic negative selection using the Pan Monocyte Isolation Kit (cat.130-096-537, Miltenyi Biotec) and the autoMACS® Pro Separator according to the manufacturer's recommendations (Miltenyi Biotec). Isolated primary human monocytes

were cultured at a density of 8 × 10^6 cells in 40 ml of complete macrophage medium and 50 ng/ml M-CSF in T-75 flasks for 7 days at 37 °C and 5 % CO_2. After 3-4 days, another 50 ng/ml of M-CSF were added to the cell culture flask for final maturation.

5.3 Small airway epithelial cell culture

Primary human small airway epithelial cells out of the 1 mm bronchiole area were purchased from Lonza. Cryopreserved cells (passage 2) were cultured and differentiated according to manufacturer's instructions. The cells were expanded in a T-175 flask (passage 3) using Pneumacult™-Ex Plus Medium (cat. 05040, 05426, Stem Cell Technologies), supplemented with 0.5 ml hydrocortisone (96 µg/ml; cat. 07925, Stem Cell Technologies) and 1 % Pen/Strep, at 37 °C and 5 % CO_2. When 80 % confluency was reached, cells were splitted into three T-175 flasks (passage 4). Cells were cryopreserved in CryoStor® CS10 with 3 × 10^6 cells per vial. Cell passaging was performed using an Animal Component-Free Cell Dissociation Kit (cat. 05426, Stem Cell Technologies) for 10 minutes at 37 °C. The detached cells were centrifuged at 200 g for 5 minutes and re-suspended in the respective medium.

Table 8. Details about the used healthy donors of SAECs in this study.

Donor (lot)	Sex	Age (years)
18TL179344	Female	25
19TL148583	Male	29
18TL180367	Male	45
672324	Female	73

5.4 A549 cell culture

The human epithelial lung cell line A549, derived from a carcinoma, was purchased from ATCC (cat. CCL-185). The cells were expanded in a T-75 flask using F12K Nut Mix Medium (cat. 21127030, Gibco), supplemented with 10 % FBS (cat. 16000-044, Gibco) and 1 % Pen/Strep, at 37 °C and 5 % CO_2. When 80 % confluency was reached, cells were splitted into three T-75 flasks. Cells were cryopreserved as master stock in supplemented F12K Nut Mix Medium containing 10 % Dimethyl Sulfoxide (DMSO; cat. D2438, Sigma-Aldrich). The cells were further expanded in T-175 flasks and cryopreserved after several passages as working stock with 3 × 10^6 cells per vial when confluency was reached, using supplemented F12K Nut Mix Medium with 10 % DMSO. Cell passaging was performed using 1 × TrypLE Express (cat. 12605010, Gibco) solution for 5-10 min at 37 °C. The enzymatic reaction was stopped with the twofold volume of supplemented F12K Nut Mix Medium. The detached cells were centrifuged at 125 g for 5-7 min and re-suspended in the medium.

5.5 Raji and Jurkats cell culture

Raji (cat. CCL-86) and Jurkats (cat. TIB-152) suspension cells were obtained from ATCC and were cultured in T-75 flasks using RPMI1640 + Glutamax-I Medium (cat. 61870-010, Gibco) with 10 % FBS and 1 % Pen/Strep at 37 °C and 5 % CO_2. Cells were passaged twice per week at 4 × 10^5 viable cells/ml and were maintained by addition of fresh medium or replacement of medium by centrifuging at 250 g for 6 min. Cells were cryopreserved in supplemented medium containing 10 % DMSO.

5.6 Immortalized Human Alveolar Cells Type I cell culture

Immortalized Human Alveolar Cells Type I (iAlveoli) were purchased from abm (cat. T0487). The cells were cultured in T-75 cell culture flasks using Prigrow III Medium (cat. TM003, abm), supplemented with 10 % FBS and 1 % Pen/Strep at 37 °C and 5 % CO_2. Prior to cell seeding, flasks were pre-coated with 2.5 ml of Applied Cell Extracellular Matrix (cat. G422, abm) at room temperature. Coating was aspirated after one hour and flasks were placed under the laminar flow to dry off. When 80 % confluence was reached, cells were splitted into four pre-coated T-25 flasks. Cells were cryopreserved as master stock in respective supplemented medium containing 10 % DMSO. The cells were further expanded in pre-coated T75 flasks and frozen after several passages as working stocks with 3 × 10^6 cells per vial when confluency was reached, using supplemented medium containing 10 % DMSO. Cell passaging was performed using 1 × TrypLE Express solution for 5-10 min at 37 °C. The enzymatic reaction was stopped with the twofold volume of respective supplemented medium. The detached cells were centrifuged at 200 g for 3 min and re-suspended in their medium.

5.7 Senescence induction

5.7.1 Replicative senescence

Cryopreserved SAECs at passage 2 derived from different donors (see Table 8) were thawed and seeded in T-75 flasks. Cells were cultured until confluency was reached, passaged as described above and re-seeded in a flask. The cells were serially passaged until their proliferation potential was exhausted. In every passaging step, samples for gene expression profiling and β-galactosidase staining were prepared. The population doublings were calculated as follows:

$$\text{Population doublings (PD)} = \frac{\log\left(\frac{\text{harvested total cell number}}{\text{seeded live cell number}}\right)}{\log 2}$$

5.7.2 Treatment with anti-cancer drugs or TGFβ1

Cryopreserved SAECs at passage 4 derived from different donors (see Table 8) and A549 were thawed and seeded in 20 µl per 384-well (cat. 6057302, Perkin Elmer) or in 100 µl per 96-well plate (cat. 161093, Thermo Fisher Scientific; Fig. 30). The next day, cells were treated with etoposide (cat. E1383-25MG, Sigma-Aldrich; 10 µM), palbociclib (cat. PZ0383-5MG, Sigma-Aldrich; 4.5 µM), or TGFβ1 (cat. 7754-BH-005/CF, R&D Systems; 5 ng/ml). Cells treated with etoposide and TGFβ1 were washed after 24 h using a BioTek EL406 Washer Dispenser and cultured with their respective medium for another six days without media changes. Palbociclib treatment was maintained for the time course of seven days without media changes. To generate a non-senescent control, SAECs and A549 cells were additionally seeded at a later timepoint and treated with vehicle controls, to prevent confluency resulting from an excessive proliferative capacity of non-senescent cells. This resulted in a comparable cell density between control and treated cells. As vehicle controls, 0.1 % DMSO (etoposide; 1:1111), 0.1 M HCl (cat. H9892-100ML, Sigma-Aldrich; palbociclib; 1:1000), and 4 mM HCl in 0.1 % (w/v) bovine serum albumin (BSA)/D-PBS (cat. A3059-100G, Sigma-Aldrich; TGFβ1; 1:200) were used. Seven days after the respective treatment, the cells were washed three times with 1 × D-PBS (−/−) using a BioTek EL406 Washer Dispenser to remove residual compounds and epithelial cell medium. Subsequently, the cells were prepared and analyzed for gene expression profiling, for amplified luminescent proximity homogeneous (AlphaLISA) assays, β-galactosidase quantification, and immunolabeling. Supernatants were collected and stored at -20 °C to analyze with a Lanthanide chelate excite (LANCE®) assay.

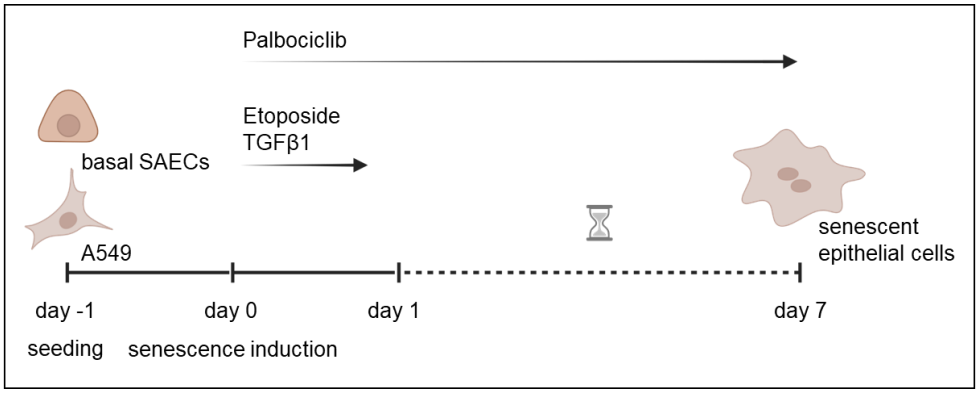

Figure 30. Experimental procedure of senescence induction. After seeding and overnight culture of basal SAECs or A549, cells were treated with either palbociclib, etoposide or TGFβ1. Etoposide and TGFβ1 treatment was performed for 24 h, followed by washing with D-PBS. Palbociclib was present for seven days.

To generate conditioned medium derived from cells treated with either etoposide, palbociclib or TGFβ1, A549 were seeded in T-175 flasks and senescence induction was performed as previously described. After the seven days of treatment, cells were washed with

1 × D-PBS (−/−) and cultured for 72 h with 15 ml of macrophage medium. Medium was collected and stored at -20 °C for future use in efferocytosis assays.

5.7.3 Treatment with senolytics

To induce senolysis in A549 treated with etoposide, palbociclib or TGFβ1, the cells were incubated for 48 h with different senolytics. For this, cells were cultured in 96-well plates and senescence was induced as described above. After seven days, the cells were washed with 1 × D-PBS (−/−), followed by the addition of senolytics in combination with apoptosis dyes. A549 were treated with 1 µM ABT263 (navitoclax; cat. 79381, Cell Signaling Technology) or with a combination consisting of 1 µM Dasatinib (cat. SML2589-50MG, Sigma-Aldrich) and 1 µM Quercetin (cat. 117395, Tocris Bioscience). The senolytics were diluted in A549 medium, supplemented with IncuCyte® dyes. Senolysis was monitored by Caspase-3/7 green dye (cat. 4440, Sartorius; diluted 1:1000) or Annexin V red dye (cat. 4641, Sartorius; diluted 1:200) by imaging every 3 h for up to 48 h. Imaging was performed using the IncuCyte® S3 Live-Cell Analysis System, IncuCyte® Cell-by-Cell Analysis Software and IncuCyte® 2021B Software (Sartorius). At each timepoint, 4 images per well were taken in the brightfield, red (acquisition time 400 ms) and green channel (acquisition time 300 ms) using a 20 × objective and the non-adherent cell by cell scan type.

5.8 Karyotyping and pluripotency assessment of hiPSC lines

5.8.1 Molecular karyotyping of hiPSC lines

Molecular karyotyping of the used ChiPSC lines was performed by LIFE & BRAIN GmbH. Cells were cultured in DEF-CS medium and COAT-1 coated flasks. The low-resolution karyotyping based on genotyping of at least 700,000 markers assessed with Illumina microarray.

5.8.2 PluriTest™ analysis

The hiPSC cell lines ChiPSC7, ChiPSC12, ChiPSC18, ChiPSC22 and 201B7 were tested for their pluripotency using the PluriTest™ service provided by Life Technologies. In this assay, the transcriptome of the samples was assessed against a > 450 cell/tissue types reference data set, including 223 human embryonic stem cell lines, 41 iPSC lines, somatic cells, and tissues to generate a pluripotency and novelty score. The pluripotency score indicates how good the samples compare to the PluriTest™ model. Positive pluripotency values refer to a strongly expressed model-based pluripotency signature. The novelty score gives evidence of how good the model fits for the tested sample. Low novelty scores suggest a good reconstruction of the tested sample with the model-based pluripotency matrix. For this assay,

RNA was isolated from hiPSCs with the PureLink™ RNA Mini Kit (cat. 12183025, Invitrogen) according to the manufacturer's protocol and was quantified using the NanoDrop™. The GeneChip® was prepared by adding 100 ng total RNA. A bioinformatical analysis of the samples validated the pluripotency potential by creating a pluripotency score (PluriCor) and a novelty score (NovelCor). Passing the PluriTest™ means a significant overlap with the pluripotency matrix, while failing gives evidence for a non-pluripotent state of the tested sample. A non-iPSC sample was included as negative control. The scatter plot gives a visualization of the pluripotency score (y-axis) and the novelty score (x-axis). Displayed in red and blue are the empirical distributions of pluripotent (red) and non-pluripotent (blue) samples included in the reference data set.

5.8.3 Scorecard™ analysis

The hiPSC cell lines ChiPSC7, ChiPSC12, ChiPSC18, ChiPSC22 and 201B7 were tested for pluripotency and trilineage differentiation potential using the hPSC Scorecard™ assay service provided by Life Technologies. In this assay, RNA was isolated using the PureLink™ RNA Mini Kit (cat. 12183018A, Invitrogen). The DNase-treated RNA was used to generate complementary DNA (cDNA) according to the High-capacity cDNA Reverse Transcription kit with RNase Inhibitor (cat. 4374966, Applied Biosystems). The cDNA samples were prepared for quantitative reverse transcription polymerase chain reaction (RT-qPCR) using the TaqMan® hPSC Scorecard™ Kit (cat. A14872, Applied Biosystems). The gene expression data were analyzed using the web-based hPSC Scorecard™ analysis software to confirm the pluripotency of the samples and predict their differentiation potential and outcome.

5.9 Gene expression profiles

For the gene expression analysis, the Cells-to-CT 1-Step TaqMan Kit (cat. A25602, Invitrogen) was used according to the manufacturer's instructions. Briefly, cells were washed once with cold 1 × D-PBS (−/−) and lysed with DNase/lysis solution (dilution 1:100). After 5 min, stop solution was added with one tenth of the DNase/lysis solution volume and incubated for 2 min. The generated lysates were stored at -20 °C. For the RT-qPCR, 1 µl of lysate was added to a final reaction volume of 10 µl containing 2.5 µl of TaqMan 1-Step RT-PCR Mix, 0.5 µl of the respective 20 × TaqMan Gene Expression Assay (cat. 4351370, FAM Dye, Thermo Fisher Scientific), as listed in Table 9, and 6 µl of nuclease-free water (cat. AM9922, Invitrogen). Gene expression levels of individual genes were normalized to the reference gene encoding glyceraldehyde-3-phosphate dehydrogenase (GAPDH) or RNA polymerase II subunit A (POLR2A). Calculated $2^{(-\Delta ct)}$ values (expression relative to GAPDH or POLR2A) were plotted in analysis graphs.

Table 9. List of TaqMan Gene Expression Assays used within this study.

Target gene	Assay ID	Vendor
GAPDH	Hs02758991_g1	Applied Biosystems
POLR2A	Hs00172187_m1	Applied Biosystems
LIN28	Hs00702808_s1	Applied Biosystems
MYC	Hs00153408_m1	Applied Biosystems
NANOG	Hs02387400_g1	Applied Biosystems
PODXL	Hs01574644_m1	Applied Biosystems
POU5F1/ OCT4	Hs00999632_g1	Applied Biosystems
SOX2	Hs01053049_s1	Applied Biosystems
LMNB1	Hs01059210_m1	Applied Biosystems
MKI67	Hs00606991_m1	Applied Biosystems
CD24	Hs04405695_m1	Applied Biosystems
CD47	Hs00179953_m1	Applied Biosystems
CDKN1A	Hs00355782_m1	Applied Biosystems
CDKN2A	Hs00923894_m1	Applied Biosystems
QPCT	Hx00202680_m1	Applied Biosystems
QPCT/L	Hs01012164_gH	Applied Biosystems
TP53	Hs01034249_m1	Applied Biosystems
CCL2	Hs00234140_m1	Applied Biosystems
CXCL1	Hs00236937_m1	Applied Biosystems
IL1A	Hs00174092_m1	Applied Biosystems
IL1B	Hs01555410_m1	Applied Biosystems
IL6	Hs00174131_m1	Applied Biosystems
MMP1	Hs00899658_m1	Applied Biosystems
MMP3	Hs00968305_m1	Applied Biosystems
MMP7	Hs01042796_m1	Applied Biosystems
MMP9	Hs00957562_m1	Applied Biosystems
MMP10	Hs00233987_m1	Applied Biosystems
VEGFA	Hs00900055_m1	Applied Biosystems

5.10 Immunofluorescence staining

Pluripotency marker proteins in undifferentiated hiPSCs, either cultured in DEF-CS and COAT-1 coated plates (monolayer, ChiPSC lines only) or cultured in StemFit Basic03 and iMatrix coated plates (colony growth, all tested iPSC lines), or senescence markers of SAECs and A549 were visualized by immunolabeling and confocal microscopy. For this purpose, the cells were washed once with 1 × D-PBS (−/−) and were subsequently fixed with 4 % (v/v) paraformaldehyde solution (PFA; cat. 252549-500ml, Sigma-Aldrich) in 1 × D-PBS (−/−) for 15 min at room temperature. For intracellular staining purposes, the cells were washed three times with 1 × D-PBS (−/−) and permeabilized with 0.3 % (v/v) Triton™ X-100 (cat. T8787-100

ml, Sigma- Aldrich) in 5 % BSA diluted in 1 × D-PBS (−/−) for 30 min at room temperature. Unspecific antibody binding was blocked by incubating the cells with 5 % (v/v) BSA in 1 × D-PBS (−/−) for one hour at room temperature. The used primary antibodies shown in Table 10 were diluted according to the manufacturer's instructions in 1 × D-PBS (−/−) containing 1 % (v/v) BSA and 2.5 µg/ml Hoechst 33342 (cat. H3570, Thermo Fisher Scientific) and were incubated together overnight at 4 °C. The next day, the cells were washed three times with 1 × D-PBS (−/−). When using non-conjugated primary antibodies, secondary antibody (Table 10) incubation was followed in 1 % (w/v) BSA/D-PBS (−/−) for two hours at room temperature in the absence of light. Cells were washed three times with D-PBS (−/−) and stored at 4 °C. Imaging of immunolabeled cells was performed using the high-content imager Opera Phenix (Perkin Elmer) and image analysis was conducted using Columbus™ software, version 2.8.2 (Perkin Elmer).

Table 10. List of primary and secondary antibodies and applied dilution factors in this study.

Antibody	Catalog number	Vendor	Dilution
Anti-Oct4a, Alexa Fluor 555 conjugated	4439	Cell Signaling	1:50
Anti-Sox2, Alexa Fluor 488 conjugated	53-9811-82	Invitrogen	1:100
Anti-Nanog, Alexa Fluor 647 conjugated	5448	Cell Signaling	1:200
Anti-α-Tubulin, Alexa Fluor 488 conjugated	53-4502-82	Invitrogen	1:100
CD47	MA5-11895	Invitrogen	1:100
p16	CF500036	OriGene	1:100
p21	MA5-14949	Invitrogen	1:100
Anti-Mouse IgG, Alexa Fluor 488 conjugated	A-11029	Invitrogen	1:1000
Anti-Rabbit IgG, Alexa Fluor 546 conjugated	A-11010	Invitrogen	1:1000

5.11 Flow cytometry analyses

Flow cytometry analyses using multicolor antibody panels were performed at different stages of iPSC differentiation towards macrophages. The panel for analysis at DoD2, DoD4 and DoD7 consisted of anti-human KDR, anti-human CD34 and anti-human CD45. The cells were harvested as described above using TrypLE Select Enzyme. At DoD14, floating progenitors were harvested as described above and analyzed with a panel including anti-human CD45, anti-human CD14 and anti-human CD34. Analysis of IDMs was performed at DoD21 and analysis of MDMs was performed 7 days post-seeding of isolated monocytes. IDMs were washed once with 1 × D-PBS (−/−), and MDMs and IDMs were harvested using a cell scraper (cat. 83.1831, Sarstedt) and then centrifuged at 300 g for 5 min. For each staining, 2×10^5 cells were transferred into a 96-well V-bottom plate (cat. 3894, Corning) and incubated with 50 µl blocking buffer, consisting of 10 % FBS, 2 mM EDTA and 1 % FcR Blocking Reagent

(cat. 130-059-901, Miltenyi Biotec) in 1 × D-PBS (−/−) for 10 min in the dark at 4°C. According to the manufacturer's instructions, the cells were stained with the respective multicolor antibody panel (Table 11), including a viability dye (cat. 565388, BD), or the respective fluorescence minus one (FMO) control in the dark for 15 min and at 4 °C. Unstained controls were incubated with blocking buffer. Cells were washed twice with 200 µl wash buffer, consisting of 10 % FBS and 2 mM EDTA in 1 × D-PBS (−/−). To each well, 200 µl of wash buffer was added before transferring the cells into a 96-well round-bottom plate (cat. 650979, Corning). The plate was measured with the LSRFortessa X-20 using the High Throughput Sampler (BD Biosciences). Samples were analyzed using the FACSDiva (BD Biosciences) and FlowJo 10.7 (FlowJo LLC) software.

Table 11. List of antibodies and used concentrations for flow cytometry experiments in this study.

Antibody	Catalog number	Isotype control	Vendor	Volume per 2 × 10^5 cells
Anti-CD45	563792	563547	BD	2 µl
Anti-CD14	BIOZBLD-367104	BIOZBLD-400114	BioLegend	2 µl
Anti-CD163	741003	563330	BD	2 µl
Anti-CD206	550889	555751	BD	8 µl
Anti-CD34	562577	562438	BD	2 µl
Anti-KDR	560494	554680	BD	4 µl

5.12 Analysis of macrophage activation

5.12.1 Analysis of mediator release by d-zymosan treatment

To verify secretory functions of the generated IDMs, they were stimulated together with MDMs with depleted zymosan (d-zymosan; cat. tlrl-zyd, InvivoGen). For that, macrophages were seeded at 2 × 10^4 cells in 100 µl per well in a 96-well plate in macrophage medium, supplemented with 10 ng/ml M-CSF. The next day, macrophages were treated with different concentrations of d-zymosan or vehicle control (sterile endotoxin-free water) over night. To analyze the macrophage response, the V-Plex Human TNFα Kit (cat. K151QWD-2, Mesoscale) was used according to manufacturer's instructions. Briefly, the plate was washed three times with 150 µl wash buffer per well before adding 25 µl of sample or standard solution per well. After an incubation time of two hours at room temperature with shaking at 500-1000 rpm, the plate was washed three times. Subsequently, 25 µl of antibody solution per well were added and incubated for two hours at room temperature with shaking at 500-1000 rpm. After three washing steps, 150 µl of read buffer were added and the plate was measured using an MSD reader.

5.12.2 Proteomics analysis after polarization

To assess the polarization capability of generated IDMs, they were stimulated together with MDMs (derived from three donors) with different protein cocktails and analyzed at the level of their proteome. For this, macrophages were seeded at 0.5 × 10^6 cells per six-well in complete macrophage medium supplemented with 50 ng/ml M-CSF. The next day, the cells were treated with different proteins and combinations (LPS, IL-4/IL-13, TNFα, IL-4/IL-13/TNFα) for 24 h in complete macrophage medium supplemented with 50 ng/ml M-CSF and 0.5 % DMSO in all conditions (Table 12).

Table 12. Stimulants and applied concentrations used to polarize macrophages derived from iPSCs and monocytes.

Treatment	Catalog number	Vendor	Concentration
LPS	L6143-1MG	Sigma-Aldrich	10 ng/ml
IL-4	204-IL-010/CF	R&D Systems	10 ng/ml
IL-13	213-ILB-025/CF	R&D Systems	10 ng/ml
TNFα	210-TA-005/CF	R&D Systems	10 ng/ml

After treatment, cells were washed twice with cold D-PBS (−/−), lysed in in 300 µl 95 °C hot sodium deoxycholate (SDC; cat. D6750, Sigma-Aldrich) lysis buffer (1 % SDC in 100 mM triethyl ammonium bicarbonate (cat. 90114, Thermo Fisher Scientific), including 10 mM tris-(2-carboxyethyl)-phosphine (cat. 77720, Thermo Fisher Scientific) and 40 mM chloroacetamide (cat. C0267, Sigma-Aldrich)) and boiled (20 min, 95 °C, 350 rpm). DNA was sheared with 0.5 µl Benzonase® Nuclease (250 U/µl; cat. 71205, Merck Millipore) and 2 mM MgCl2 (cat. M8266, Sigma-Aldrich) at 37 °C for 30 min at 500 rpm. Protein amount was quantified using the Pierce™ BCA Protein assay (cat. 23227, Thermo Fisher Scientific). 250 µl of cell lysate was digested using 2 µg Trypsin/Lys-C Mix (cat. V5073, Promega; 1:50 protease:protein ratio). After digestion, peptides were purified using the iST-NHS HT 192 x Sample Preparation Kit (cat. P.O.00083, PreOmics) according to the manufacturer's instructions. In short, the samples were mixed 1:1 with the stop solution, incubated for 5 min and subsequently loaded onto the iST-NHS cartridges. Peptides were washed with Wash 1 and Wash 2 (200 µl each), eluted two times with 100 µl Elute and dried *in vacuo* in a Concentrator plus (Eppendorf). Peptides were resuspended in LC-Load and peptide amounts were quantified with the CBQCA assay (cat. C6667, Thermo Fisher Scientific) using the peptide digest assay standard (cat. 23295, Thermo Fisher Scientific).

Peptides were separated on an UltiMate 3000 RSLCnano system and analysed on an Orbitrap Fusion Lumos Tribrid mass spectrometer (Thermo Fisher Scientific). 2 µg peptides per sample were loaded onto a 100 µm × 2 cm Acclaim PepMap C18 trap column (5 µm, 100 Å; cat.

164199, Thermo Fisher Scientific) for 6 min with 3 % acetonitrile (ACN)/0.1 % trifluoroacetic acid (TFA) and a constant flow of 10 µl/min and separated on a 75 µm × 75 cm EASY-Spray C18 column (2 µm, 100 Å; cat. ES905, Thermo Fisher Scientific) at 60 °C with a flow rate of 300 nl/min. Solvents used were 0.1 % formic acid (A) and 80 % ACN/0.1 % formic acid (B). Samples were separated from 8 % to 35 % B in 104 min and 95 % in 2 min with a total measurement time of 160 min. The spray was initiated by applying 1.7 kV to the EASY-Spray emitter. The ion transfer capillary temperature was set to 275 °C and the radio frequency of the ion funnel to 30 %. All samples were acquired in the data-independent acquisition (DIA) mode with 33 dynamic isolation windows using Xcalibur 4.3 (Thermo Fisher Scientific). The full scan was acquired in the orbitrap covering the mass range of mass-to-charge ratio (*m/z)* 300 to 1,650 with a mass resolution of 120,000, a normalized automatic gain control (AGC) target of 500 % and a maximum injection time of 60 ms. The monitored mass range for MS2 scans was *m/z* 200-2000 with a resolution of 30000, a maximum injection time of 54 ms, a normalized AGC target of 4000 % and a default charge state of 3 for each window. Precursors were fragmented by higher energy collision-induced dissociation using 30 % collision energy.

DIA raw files were searched against the UniProtKB/Swiss-Prot human database (downloaded in January 2023, containing 20,404 protein sequences) using DIA-NN 1.8.1 with default settings except the following changes. Up to two missed cleavages were allowed. Oxidation of methionine and acetylation of the protein N-terminus were selected as variable modifications allowing a maximum number of one per peptide. Peptide length ranged from 7 to 50, precursor charge from 2 to 5, precursor *m/z* from 300 to 1650 and fragment ion *m/z* from 200 to 2000. “FASTA digest for library-free search” and “match between runs” were enabled. Protein inference was set to “protein names (from FASTA)” with “--relaxed-prot-inf” as additional option. “Double-pass mode” was the used neural network classifier, “robust LC (high precision)” the quantification strategy and “RT-dependent” the cross-run normalization. Another normalization step was applied to address donor variability of MDMs. Therefore, the median of protein intensities was calculated for each donor and protein and used to calculate normalization factors. Principal component analysis and volcano plots were created with Perseus (version 1.6.7.0).

5.13 AlphaLISA® assay development

Due to the lack of appropriate miniaturized assays targeting senescent markers, two AlphaLISA® assays were developed detecting the human CDK inhibitors p16 and p21 in cellular lysates. To identify selective antibody pairs binding to different epitopes of the human p16 or p21 protein, respectively, a variety of anti-p16 and anti-p21 antibodies was pre-selected and tested in combinations (Table 13).

Table 13. Antibodies targeting p16 or p21 tested for the application in AlphaLISA® immunoassays. Each antibody was conjugated to AlphaLISA® acceptor beads and biotinylated, respectively, before application in the assay, except for cat. BAF1047, which was purchased in a biotinylated format.

Target	Catalog number	Vendor
p16	ab244050 capture	Abcam
p16	ab244050 detector	Abcam
p16	NBP2-98881	Novus Biologicals
p16	92803BF	Cell Signaling Technology
p16	80772BF	Cell Signaling Technology
p16	NBP3-06989	Novus Biologicals
p16	ab54210	Abcam
p16	ab186932	Abcam
p16	ab189034	Abcam
p16	ab219723	Abcam
p21	ab241799 capture	Abcam
p21	ab241799 detector	Abcam
p21	MAB1047	R&D Systems
p21	NBP2-43697	Novus Biologicals
p21	BAF1047 (pre-biotinylated)	R&D Systems

For this, anti-p16 and anti-p21 antibodies were manually conjugated to 1 mg of AlphaLISA® acceptor beads (cat. 6772001, Perkin Elmer) according to the manufacturer's guide. In brief, acceptor beads were washed once with D-PBS (−/−) and centrifuged at maximum speed for 15 min. The pellet was mixed with 0.1 mg of the respective antibody, 1.25 µl of 10 % Tween-20 (cat. 28320, Thermo Fisher Scientific), 10 µl of a 400 mM solution of NaBH3CN (cat. 156159, Sigma-Aldrich) in water and the appropriate volume of 100 mM (4-(2-hydroxyethyl)-1-piperazineethanesulfonic acid) (HEPES) buffer (cat. 44686S, Cell Signaling Technology) at pH 7.4 to obtain a final reaction volume of 200 µl. The mixture was incubated for 24 h at 37 °C with mild agitation using a rotary shaker (Eppendorf). Next, 10 µl of carboxymethoxylamine (cat. C13408, Sigma-Aldrich) solution in 800 mM NaOH (cat. 35254-1L, Honeywell) was added to the reaction and incubated for one hour at 37 °C using a rotary shaker. After a centrifugation step at maximum speed at 4 °C, the bead pellet was washed twice with 200 µl of 100 mM Tris-HCl (cat. 15568025, Invitrogen) at pH 8.0. Between the washing steps, the solution was sonicated. After the last centrifugation step, the beads were resuspended at 5 mg/ml in 200 µl of D-PBS (−/−) with 0.05 % Proclin-300 (cat. 48912-U, Sigma-Aldrich), vortexed and sonicated, prior to storage at 4 °C. The same antibodies listed in Table 13 were biotinylated using the EZ-Link™ Sulfo-NHS-LC-Biotinylation Kit (cat. 21435, Thermo Fisher Scientific) and served as capture antibodies in combination with the acceptor bead-conjugated

antibodies. Briefly, 10 mM of Sulfo-NHS-LC-Biotin were added to the respective antibody to achieve a 30-fold molar excess and incubated for one hour at room temperature. Using desalting columns, excess biotin was removed and the antibody was resuspended in D-PBS (−/−). The level of biotin incorporation was measured by an 4'-hydroxyazobenzene-2-carboxylic acid (HABA) assay.

The different biotinylated antibodies were cross-tested with several antibodies conjugated to AlphaLISA® acceptor beads for the ability to bind simultaneously to a recombinant human p16 (cat. ab84075, abcam) or p21 (cat. NBP2-22976, Novus Biologicals) standard protein. The combinations achieving the greatest signal-to-noise (S/N) ratios were further analyzed and were based on the following equation, whereby AlphaLISA signals derived from the negative (background, buffer) and positive control (signal, p16 or p21 standard) were used:

$$\text{S/N ratio} = \frac{\text{Mean (Signal)}}{\text{Mean (Background)}}$$

On this account, the selected biotinylated antibodies were titrated. To determine the sensitivity of the respective assay, decreasing p16 or p21 standard protein concentrations were tested. To further optimize, different assay set-ups (order of addition and numbers of steps), plate types (ProxiPlate-384 Plus, cat. 6008280, Perkin Elmer and small volume plate, cat. 784075, Greiner Bio-One) and volumes (20 µl and 50 µl) were tested. Based on these optimizations, the final assay protocol is described in the following section.

SAECs and A549 were seeded in 96-well plates in 100 µl at 8×10^3 cells per well. Treatment with senescence-inducing agents was performed as previously described. Cells were washed after seven days of treatment and were lysed with 50 µl of 1 × AlphaLISA® lysis buffer (cat. AL003C, Perkin Elmer), supplemented with 5 % protease inhibitor cocktail (cat. P2714, Sigma-Aldrich), for 10 min at room temperature with shaking at 350 rpm. Protein standards, biotinylated antibodies, acceptor bead-coupled antibodies and donor beads were diluted in 1 × AlphaLISA® immunoassay buffer (cat. AL000C, Perkin Elmer). Respectively, 2 µl of analyte (sample or protein standard in different concentrations), 4 µl of biotinylated antibody (5 nM) and 4 µl of antibody-conjugated acceptor beads (50 µg/ml) were added per well of a small volume 384-well plate. The mixture was vortexed, spun down and incubated for two hours at room temperature, before the addition of 10 µl of Streptavidin-coated donor beads (80 µg/ml). After vortexing, the mixture was incubated for 30 min at room temperature in the dark. After spinning down, the AlphaLISA® signal was measured using a PHERAstar FSX plate reader (BMG Labtech).

5.14 β-galactosidase staining and quantification of enzyme activity

β-Galactosidase staining was performed either for different passages of SAECs or seven days after treatment of SAECs or A549 with etoposide or palbociclib using the Senescence β-Galactosidase Staining Kit (cat. 9860, Cell Signaling Technology) according to the manufacturer's instructions. In brief, cells were washed once with D-PBS (−/−) and fixed for 10-15 min at room temperature. After two washing steps, β-galactosidase staining solution was added and incubated at 37 °C overnight in a dry incubator without CO_2. The next day, the staining solution was removed and the cells were covered with 70 % glycerol (cat. G7757-1L, Honeywell). Using light microscopy (AxioVert 135T, Zeiss), senescent cells were identified as blue-labeled cells. For the treatment with etoposide, palbociclib or TGFβ1, the β-galactosidase activity was additionally quantified using the Beta-Glo® Assay System (cat. E4720, Promega) according to the manufacturer's instructions. In short, cells cultured in a white 384-well plate (cat. 781074, Greiner Bio-One) were equilibrated to room temperature before adding 25 µl Beta-Glo® Reagent per well. As a positive control, different concentrations of a β-galactosidase enzyme derived from *E. coli* (cat. G5635-1KU, Sigma-Aldrich) were included and diluted with the respective cell culture medium. After mixing using a plate shaker, the plate was incubated for at least 30 min at room temperature before measurement using a PHERAstar FSX reader (BMG Labtech).

5.15 MMP7 Assay

MMP7 in cell culture supernatants of SAECs stimulated with either etoposide or palbociclib was quantified using the LANCE® Ultra Human MMP7 Detection Kit (cat. TRF1378C, Perkin Elmer). The assay was performed according to the manufacturer's instructions seven days after treatment. In short, 15 µl/well of samples or standard solution were transferred in a 384-well plate via CyBi-Well vario 384-Channel Simultaneous Pipettor (Analytik Jena). Subsequently, 5 µl/well of a 4 × mix of Eu-labeled and U-Light-labeled antibodies were added using a Certus Flex Liquid Dispenser (Fritz Gyger AG). The microplate was incubated for two hours at room temperature and was subsequently measured using a PHERAstar FSX reader.

5.16 Monitoring of apoptosis

Image scheduling, recording and analysis were conducted with the IncuCyte® S3 Live-Cell Analysis System, IncuCyte® Cell-by-Cell Analysis Software and IncuCyte® 2021B Software (Sartorius) in order to monitor the kinetics of apoptosis induction after irradiation. The assay plates (cat. 161093, Thermo Fisher Scientific) were pre-coated in advance with 50 µl Poly-L-Ornithine (cat. P4957, Sigma-Aldrich) per well when using suspension cells, so that they stick to the bottom, enabling a proper imaging. After one hour, the coating was aspirated, and the

plates were placed under the laminar flow to dry off. In the meantime, the cells were harvested, counted, and irradiated with Ultraviolet (UV)-C light in a UV chamber (cat. 860802, Opsytec) for 7 min. Directly after irradiation, the cells were added at 1 × 10^4 cells in 10 µl per well to the assay plate containing either IncuCyte® Caspase 3/7 Green Reagent (diluted 1:1000) or IncuCyte® Annexin V Red Reagent (diluted 1:200) in RPMI1640 + Glutamax-I Medium with 10 % FBS and 1 % Pen/Strep with 90 µl per well. Non-irradiated cells served as control. Images were taken every hour for a total of up to 24 h. At each timepoint, 4 images per well were taken in the brightfield, red (acquisition time 400 ms) and green channel (acquisition time 300 ms) using a 20 × objective and the non-adherent cell by cell scan type.

5.17 High-content imaging-based efferocytosis assay

5.17.1 Harvesting, labeling, seeding and pre-treatment of macrophages

IDMs at DoD21 of differentiation or MDMs 7 days post-seeding of isolated monocytes were harvested as described above. After centrifuging, cells were resuspended in serum-free complete macrophage medium and 10 ng/ml M-CSF containing 0.5 µM CellTracker™ Green CMFDA Dye (cat. C7025, Invitrogen), and were incubated for 45 min at 37 °C and 5 % CO_2. Subsequently, cells were washed with complete macrophage medium and 10 ng/ml M-CSF. Cells were seeded at a density of 5 × 10^3 cells per well into a black 384-well plate in 20 µl of macrophage medium supplemented with 10 ng/ml M-CSF using a Multidrop™ Combi Reagent Dispenser (cat. 5840300, Thermo Fisher Scientific). After overnight incubation, the attached macrophages were pre-treated with different concentrations of cytochalasin D (cat. 1233, Tocris) or vehicle control for one hour before prey cell addition. For the Syk inhibitor treatment, macrophages were pre-treated over night before prey cell addition with different concentrations of ER 27319 maleate (cat. 2471, Tocris), GSK 143 (cat. 6362, Tocris) and piceatannol (cat. P0453-5MG, Sigma-Aldrich) or vehicle control. Other applied treatments are listed in Table 14.

For the miniaturized assay variant, harvested macrophages were seeded at a density of 1 × 10^3 cells per well into a black 1536-well plate (cat. 6004460, Perkin Elmer) in 3 µl using a Multidrop™ Combi Reagent Dispenser. After seeding, the plates were centrifuged for 30 sec at 300 g. The next day, the cells were pre-treated with 25 nl cytochalasin D or vehicle control for one hour before prey cell addition. Compound dilution and transfer were carried out by acoustic dispensing using an Echo® 555 Liquid Handler within an Access Laboratory Workstation (Beckman Coulter). Directly after compound addition, another 2 µl of macrophage medium were added to the plates using a Multidrop™ Combi Reagent Dispenser in order to

achieve a thorough mixing (final well volume of 5 µl). For all treatments, the final DMSO concentration was 0.5 %.

Table 14. Applied treatments to modulate efferocytosis activity of macrophages. Dexamethasone and TNFα, IL-4 and IL-13 (or combinations of the three proteins) were used to pre-treat macrophages with the indicated concentrations and durations before prey cell addition. For the application of CD47 knockout (KO) Raji prey cells, the previously used Raji CD47 WT prey cells were used as control, with the same experimental set-up as previously described.

Treatment	Catalog number	Vendor	Concentration	Duration
Dexamethasone	D4902-25MG	Sigma-Aldrich	1 µM	24 hours
TNFα	204-IL-010/CF	R&D Systems	10 ng/ml	24 hours
IL-4	204-IL-010/CF	R&D Systems	10 ng/ml	24 hours
IL-13	213-ILB-025/CF	R&D Systems	10 ng/ml	24 hours
CD47 KO prey	CCL-86	ATCC	30.000 cells/well	-

5.17.2 Preparation of prey cells

To track the internalization of prey cells, the IncuCyte® pHrodo Red Cell Labeling Kit for Phagocytosis (cat. 4649, Sartorius) was used according to the manufacturer's instructions. Briefly, prey cells were harvested, counted, and irradiated in 10 cm dishes (cat. 263991, Thermo Fisher Scientific) using UV-C radiation within a UV chamber for 7 min. For some experiments, non-irradiated cells served as controls. Subsequently, control cells and irradiated cells were centrifuged and resuspended in IncuCyte® pHrodo Wash Buffer. After another centrifugation step, pellets were resuspended in IncuCyte® pHrodo Cell Labeling Buffer at a density of 1×10^6 cells/ml. Solubilized IncuCyte® pHrodo Red Cell Labeling Dye was added to the cell suspension with a concentration of 250 ng/ml. After one hour, the cells were centrifuged and resuspended in complete macrophage medium, supplemented with 10 ng/ml M-CSF. pHrodo-labeled prey cells were added at 3×10^4 cells per well (384-well plate) in 20 µl or at 6×10^3 cells (1536-well plate) in 5 µl to the previously seeded macrophages using a Multidrop™ Combi Reagent Dispenser. Assay plates were measured in the high-content imager Opera Phenix (Perkin Elmer), five hours after prey cell addition, by imaging five fields (384-well plate) or one field (1536-well plate) from each well using a 20 × objective. For some experiments, a 384-well plate was measured in a kinetic mode using the live-cell chamber of the Opera Phenix at 37 °C and 5 % CO_2 for up to 24 h. Confocal stack measurements were carried out by imaging 40 planes of a 384-well plate using a 63 × objective.

To analyze an assay variant involving PFA-fixed cells, the assay plate was first imaged in a live state of the cells. Subsequently, the cells were washed once with D-PBS (−/−) using a BioTek EL406 Washer Dispenser and fixed with 0.3 % PFA at room temperature for 15 min. After three washing steps, the plate was measured again with the same settings.

5.17.3 Image analysis algorithm

Image processing and analysis were performed using the Columbus software (version 2.8.2) from Perkin Elmer. The image analysis was based on sequential building blocks (Table 15). Input images were analyzed as individual planes with advanced flatfield correction. (1) In the first step, macrophages were detected based on their CellTracker green CMFDA signal (channel: Alexa 488). (2) Subsequently, a surrounding region was added around the found macrophages to ensure the detection of the entire macrophage. This was defined in all following steps as “whole cell”. (3) Next, engulfed prey cells were detected as so-called “spots” based on the acidic pH-enhanced pHrodo signal (channel: Alexa 568). The search for such spots was restricted to the pre-defined “whole cell” regions. That way, the residual pHrodo fluorescence from non-eaten prey cells was excluded, eliminating false-positive efferocytosis events. (4) Subsequently, the mean intensity properties of the spots were calculated based on the pHrodo signal. (5) In the next step, macrophages were selected based on the sum of the calculated pHrodo intensities of all detected spots within a single macrophage using a defined threshold. If a macrophage achieved a greater value than this threshold, it was defined as being positive for efferocytosis. The threshold was defined based on the cytochalasin D and vehicle control and was adjusted with respect to e.g., donor variability or macrophage type (i.e., IDMs or MDMs). (6) In the last step, the percentage of efferocytosis positive macrophages was calculated by the following equation:

$$\text{efferocytosing macrophages [\%]} = \left(\frac{\text{number of efferocytosis positive macrophages}}{\text{total number of macrophages}}\right) * 100$$

For the analysis of the confocal stack measurement, all measured planes were selected. For stack processing, “maximum projection” was selected with a basic flatfield correction. By the use of the XYZ view, one section was chosen and displayed to verify a prey cell uptake.

Table 15. Analysis details of the developed efferocytosis and phagocytosis assay algorithm.

Step	Building block	Channel	ROI / population	Parameter details	Output population
1	Find Cells	Alexa 488	ROI: -	Method: P Area: > 200 µm² Splitting Coefficient: 0.51 Common Threshold: 0.65	Cells
2	Find Surrounding Region	Alexa 488	Population: Cells Region: Cell	Method: A Individual Threshold: 0.7 Include Input Region	Whole Cell
3	Find Spots	Alexa 568	ROI population: Cells ROI region: Whole cell	Method: B Detection Sensitivity: 0.6 Splitting Coefficient: 1 Calculate Spot Properties	Spots
4	Calculate Intensity Properties	Alexa 568	Population: Cells Region: Spots	Method: Standard (Mean)	Intensity Spots Alexa 568
5	Select Population	None	Population: Cells	Method: Filter by Property Intensity Spots Alexa 568 Sum: > 1000000 (example value)	Cells Selected_Intensity Spots Alexa 568 Sum
6	Define Results	-	-	Method: Formula Output Formula: (a/b)*100 Population Type: Objects Variable A: Cells Selected_Intensity Spots Alexa 568 Sum - Number of Objects Variable B: Cells - Number of Objects	% Intensity Spots Alexa 568 Sum

5.17.4 Co-culture with senescent epithelial cells

To analyze the effect of cellular senescence on the efferocytotic activity of macrophages, senescent SAECs or A549 were co-cultured with macrophages before prey cell addition. For this approach, SAECs (donor 18TL179344; passage 4) or A549 were seeded in 384-well plates (Fig. 31). The next day, cells were treated with either etoposide, palbociclib or TGFβ1 as previously described. Non-senescent control cells were seeded five days later and treated the next day with the respective vehicle controls, to prevent confluency resulting from an excessive proliferative capacity of non-senescent cells. On this account, cell numbers were optimized for comparability between treated and control cells (Table 16).

Table 16. Applied cell numbers of SAECs and A549 in co-culture with macrophages in the established efferocytosis assay.

	Treatment			
Cells	Etoposide	Palbociclib	TGFβ1	vehicle
SAECs	600 cells/well	600 cells/well	400 cells/well	1200 cells/well
A549	300 cells/well	300 cells/well	200 cells/well	800 cells/well
A549 (+ ABT263)	300 cells/well	300 cells/well	100 cells/well	400 cells/well

After the respective treatment, cells were washed three times with D-PBS (−/−) using a BioTek EL406 Washer Dispenser to remove residual compounds and epithelial cell medium. Macrophages were harvested and labeled with CellTracker™ Green CMFDA Dye as previously described. The cells were added at a density of 5 × 10^3 cells per well into a black 384-well plate in 20 µl of macrophage medium supplemented with 10 ng/ml M-CSF using a Multidrop™ Combi Reagent Dispenser. After overnight co-culture, the Raji prey cells were prepared as described above. pHrodo-labeled Rajis were added at a density of 1.25 × 10^4 cells to the co-cultured macrophages and senescent epithelial cells. Assay plates were measured in the high-content imager Opera Phenix, five hours after prey cell addition, by imaging five fields of a 384-well plate from each well using a 20 × objective. In an indirect co-culture approach, macrophages were treated overnight with conditioned medium derived from A549 cells treated with either etoposide, palbociclib or TGFβ1. Conditioned medium derived from vehicle-treated A549 cells was used as a control. The efferocytosis assay was performed with the same set-up as described above.

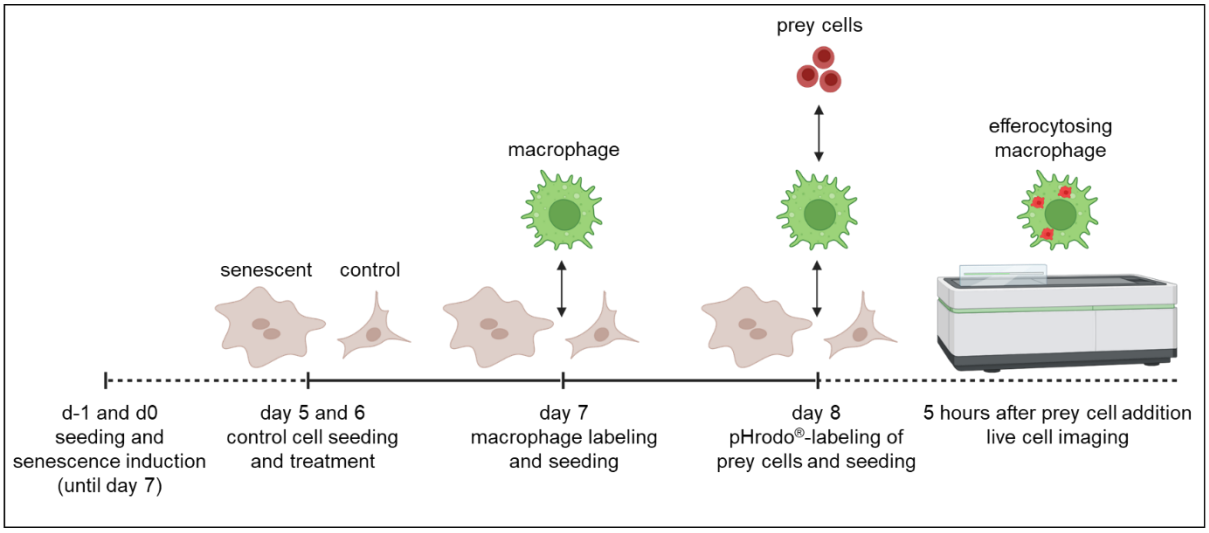

Figure 31. Experimental set-up of the efferocytosis assay involving macrophages and senescent epithelial cells in co-culture. Senescence induction of basal SAECs and A549 cells was performed after overnight culture post-seeding in 384-well plates using either etoposide, palbociclib or TGFβ as previously described. Non-senescent control cells were seeded at day 5 after senescence induction to achieve comparable cell densities between control and senescent cells. The next day, control cells were treated with the respective vehicle. CellTracker™ Green CMFDA labeled macrophages were added at day 7 to control or senescent epithelial cells, followed by seeding of pHrodo-labeled irradiated prey cells at day 8. Five hours after prey cell addition, live cell imaging was performed using the high-content imager Opera Phenix.

5.17.5 Application of senolytics in the co-culture

To test the effect of senolytics in the co-culture of macrophages with senescent A549, the senolytic agent ABT263 was applied. Senescence induction was performed following the protocol described above, while cell numbers of A549 cells were adapted to the extended timeline (see Table 16). A549 were treated seven days after senescence induction with 1 µM ABT263 or 0.1 % DMSO (vehicle control) for 48 h. Afterwards, cells were washed three times with D-PBS (−/−) to remove the residual senolytic drug. Next, A549 cells were labeled with 20 µl pHrodo per well at a concentration of 250 ng/ml. After an incubation time of one hour at 37 °C, cells were washed once with medium. Subsequently, CellTracker™ Green CMFDA Dye-labeled macrophages were added at 5 × 10^3 cells per well. Imaging was performed 24 h after the addition of macrophages using the high-content imager Opera Phenix.

5.18 Efferocytosis assay using the IncuCyte

Macrophage harvesting, labeling, seeding as well as prey cell preparation and seeding was performed as described above for the High-content imaging-based assay. After prey cell addition, the plate was measured in a kinetic mode by taking images every hour for up to 24 h using the IncuCyte® S3 Live-Cell Analysis System in a humidified incubator at 37 °C and 5 % CO_2. At each timepoint, one image per well was taken in the brightfield, red (acquisition time 400 ms) and green channel (acquisition time 300 ms) using a 20 × objective. Images were analyzed using the IncuCyte 2021B Software by calculating the total integrated intensity (RCU × $µm^2$ per image) which is corresponding to the efferocytotic activity.

5.19 High-content imaging-based phagocytosis assay

IDMs and MDMs were harvested and seeded as described above for the efferocytosis assay at 5 × 10^3 cells in 20 µl per well in 384-well plates. After overnight incubation, pHrodo™ Red *E. coli* BioParticles™ conjugates for phagocytosis (cat. P35361, Invitrogen) at a final concentration of 100 µg/ml or vehicle control were added to the microplate. The plate was measured in a kinetic mode using the live-cell chamber of the Opera Phenix at 37 °C and 5 % CO_2, imaging five fields from each well every 30 min using a 20 × objective. Image analysis was performed as described above for the efferocytosis assay (see Table 15). To analyze the phagocytotic activity resulting from a co-culture with senescent epithelial cells, macrophages were incubated overnight with SAECs treated with palbociclib according to the protocol described previously. The next day, pHrodo™ Red *E. coli* BioParticles™ conjugates were added at a final concentration of 100 µg/ml or vehicle control to the microplate. Five hours after addition of *E. coli* BioParticles™ conjugates, the plate was measured using the high-content imager Opera Phenix.

5.20 Data analysis plan

All data values are shown as mean with the standard error of the mean (SEM) or standard deviation (SD), or the median with the interquartile range (IQR; 25th to 75th percentiles), in case data sets were not normally distributed. Data from flow cytometry experiments are depicted as percentages. Biological replicates (N) were defined as individual experiments or individual donors for macrophages and were measured independently. Technical replicates (n) were generated out of the biological replicates. Experiments comparing one condition only were conducted using a T-test. Experiments comparing two conditions were analyzed using a one-way ANOVA (or Kruskal-Wallis-test for non-normally distributed data sets). Experiments comparing more than two conditions were conducted with a two-way ANOVA. Non-linear fits were based on the response vs. log (inhibitor) curves and were used for the calculation of the half maximal inhibitory concentration (IC_{50}). Robust Z' (RZ') values were calculated in Microsoft Excel using the following formula (whereby MAD = median absolute deviation, multiplied with the factor 1.483 according to Murray and Wigglesworth, 2017[68]):

$$RZ' = 1 - \frac{3*(MAD_{Max} + MAD_{Min})}{(Median_{Max} - Median_{Min})}$$

In general, the nominal alpha level was determined to be 5 % for statistical analysis in an exploratory manner and p-values of the corresponding F-statistics are shown (*p < 0.05, **p < 0.01, ***p<0.001 and ****p < 0.0001). Data input, processing, visualization, and analyses were performed using GraphPad Prism 9.3.1 (GraphPad Software).

All schemes were created with BioRender.com.

Supplementary figures

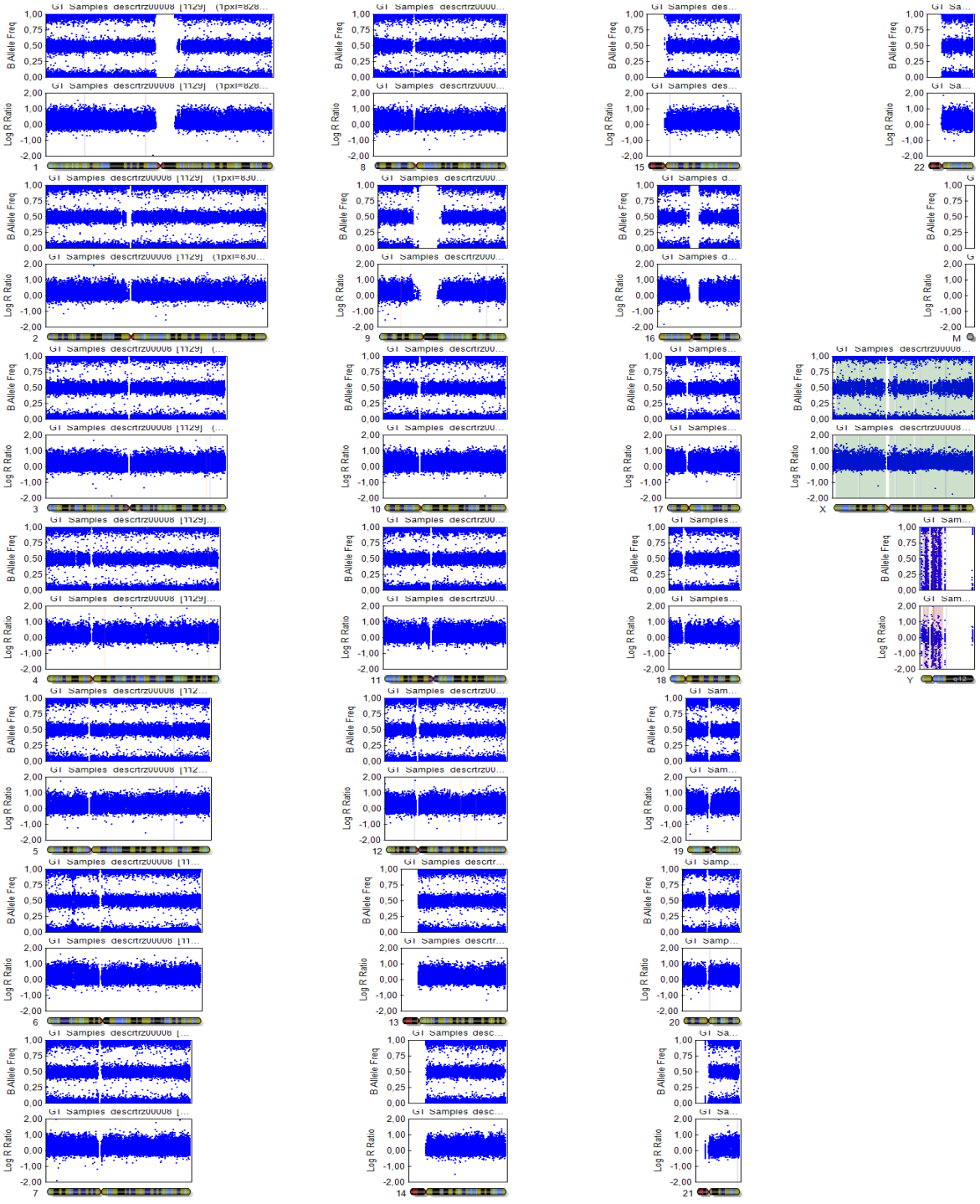

Figure S1. Karyogram of ChiPSC line 7. Karyotyping report of ChiPSC line 7 cultured in DEF-CS medium and COAT-1 coated flasks (supplier culture system) assessed with Illumina BeadArray.

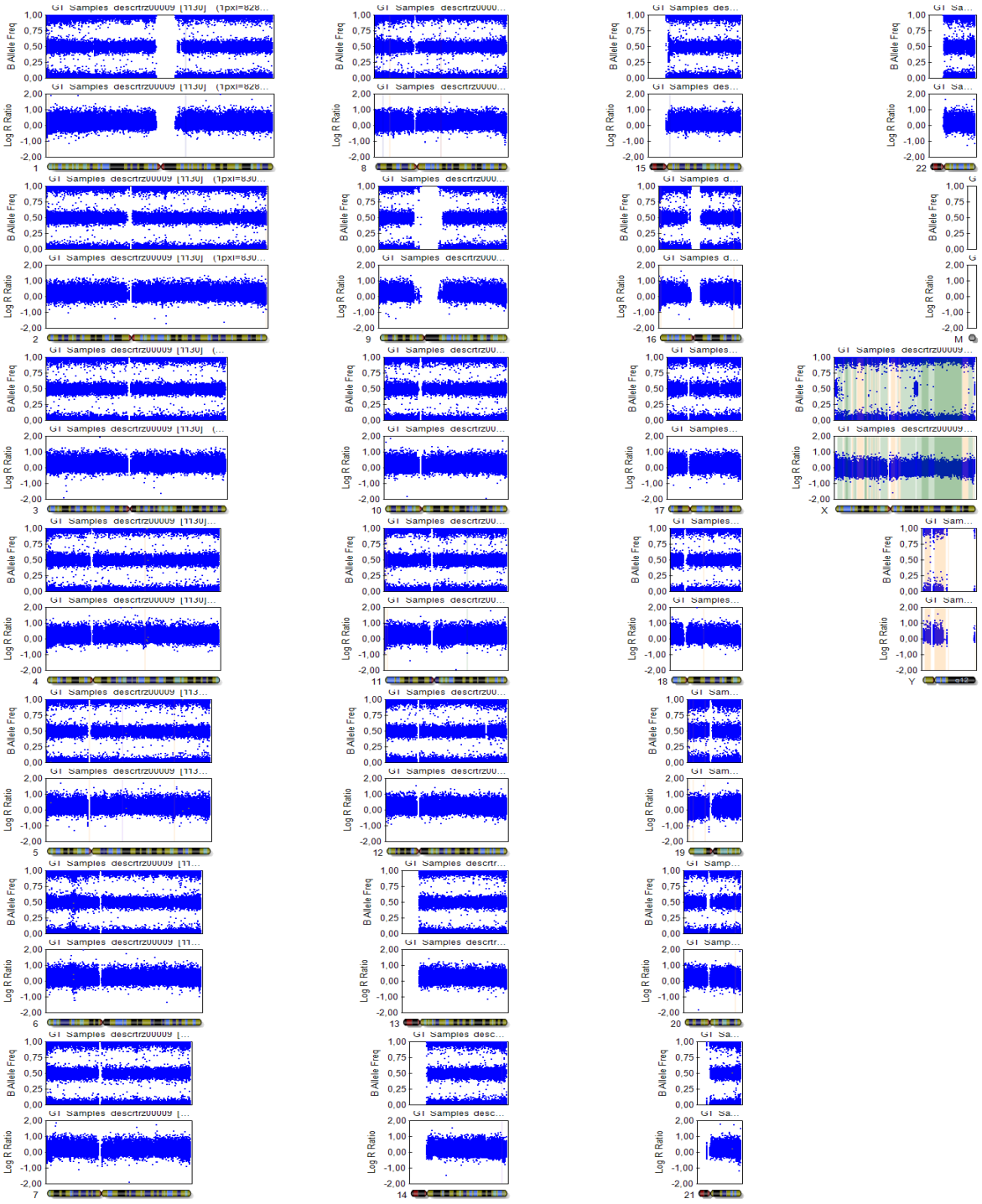

Figure S2. Karyogram of ChiPSC line 12. Karyotyping report of ChiPSC line 12 cultured in DEF-CS medium and COAT-1 coated flasks (supplier culture system) assessed with Illumina BeadArray.

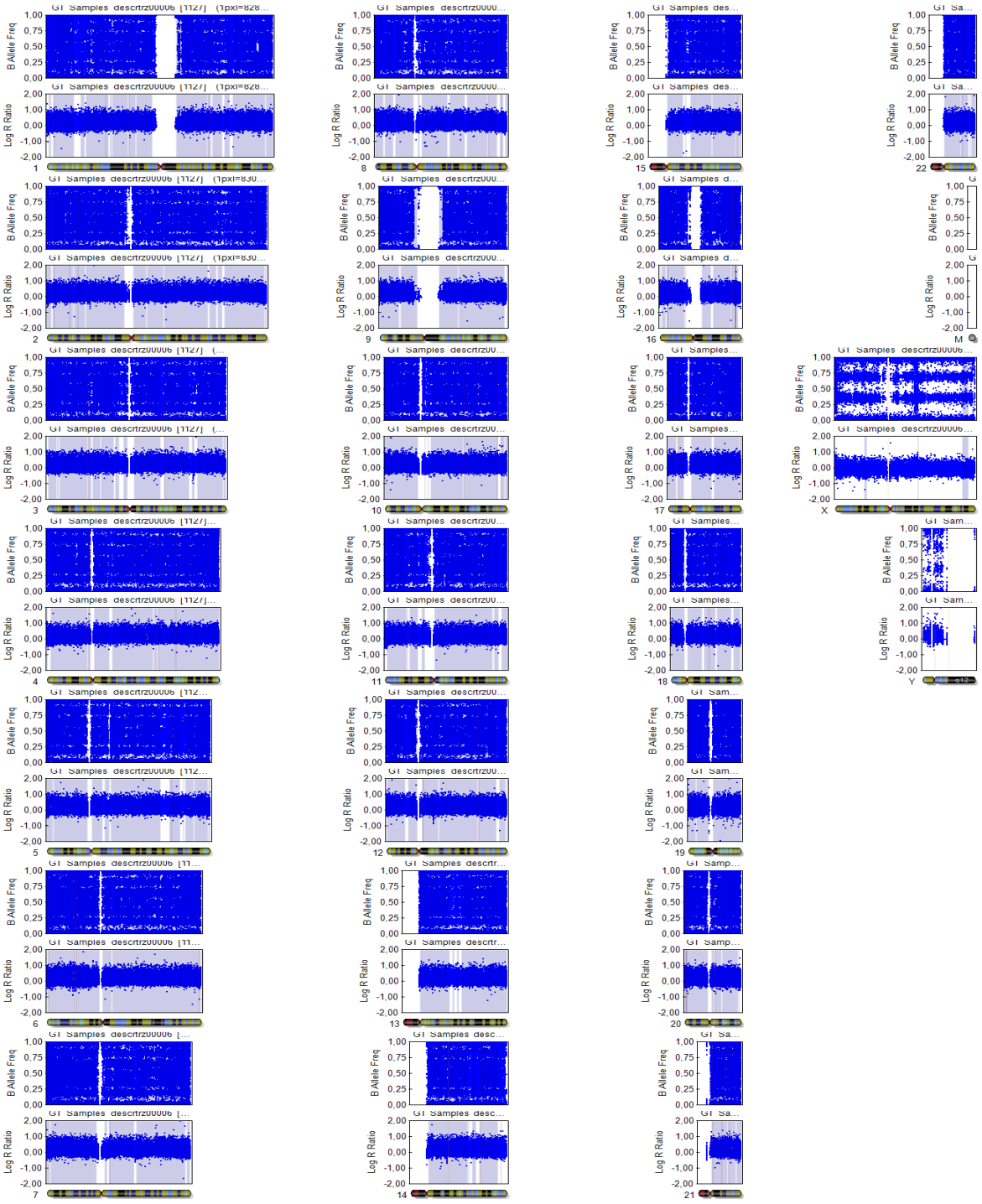

Figure S3. Karyogram of ChiPSC line 18. Karyotyping report of ChiPSC line 18 cultured in DEF-CS medium and COAT-1 coated flasks (supplier culture system) assessed with Illumina BeadArray.

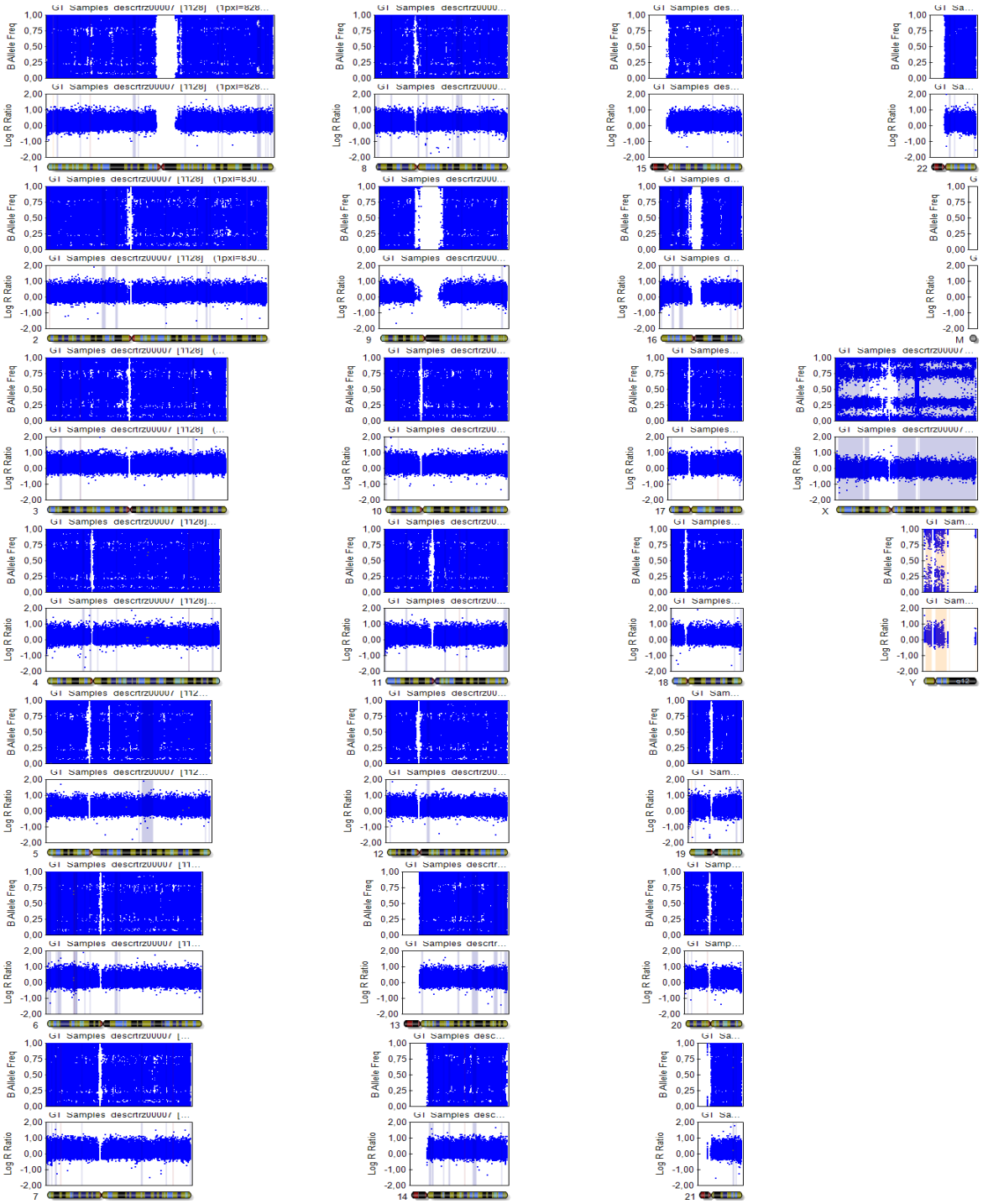

Figure S4. Karyogram of ChiPSC line 22. Karyotyping report of ChiPSC line 22 cultured in DEF-CS medium and COAT-1 coated flasks (supplier culture system) assessed with Illumina BeadArray.

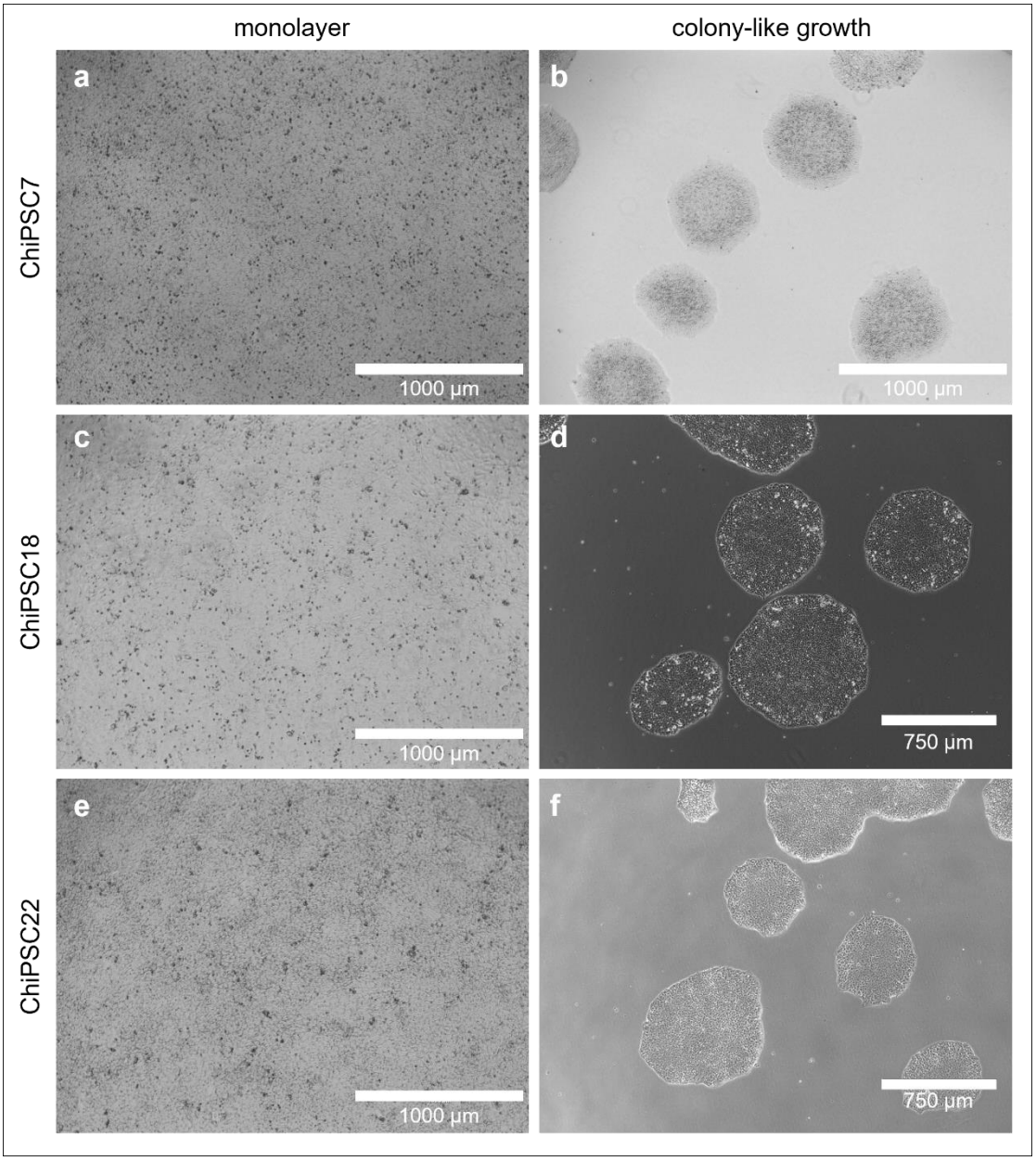

Figure S5. Culture system transfer of ChiPSC lines from monolayer to colony growth. (a, c, e) Monolayer growth of ChiPSC7 (a), ChiPSC18 (c) and ChiPSC22 (e) by culture in DEF-CS/COAT-1. **(b, d, f)** ChiPSC7 (b), ChiPSC18 (d) and ChiPSC22 (f) after transfer in a culture system with StemFit Basic03/ iMatrix-511 showing colony growth.

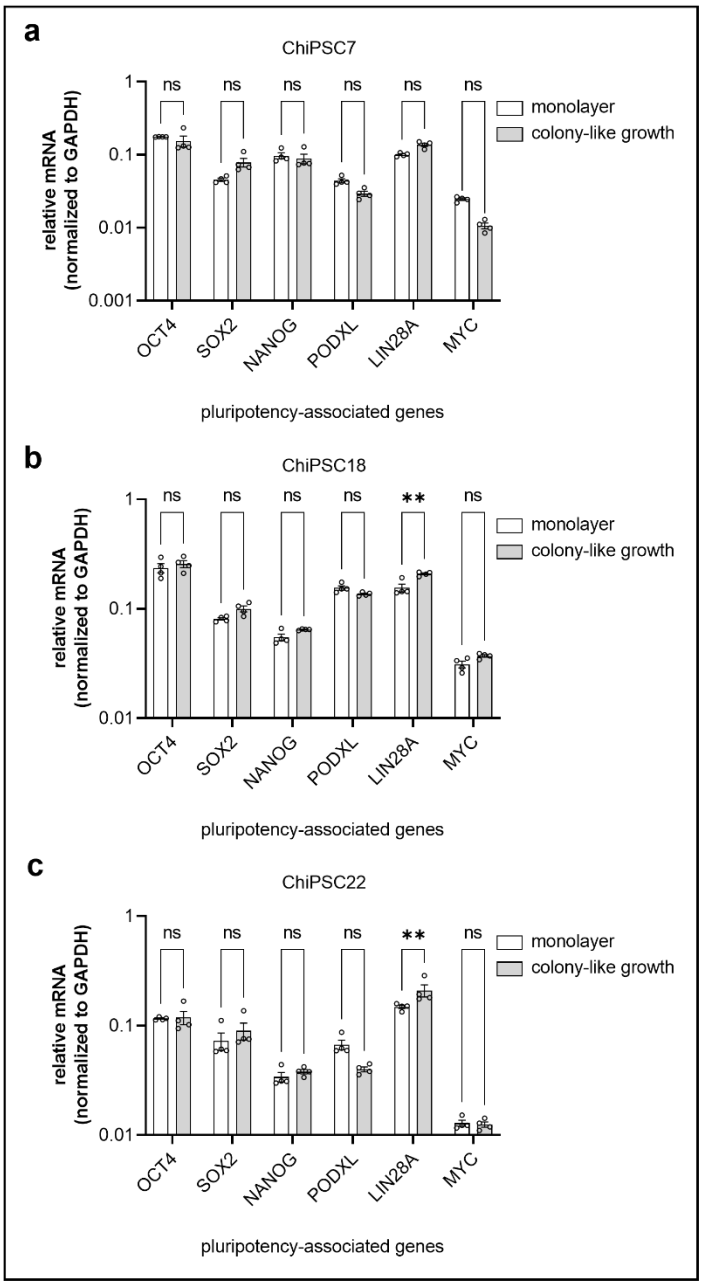

Figure S6. RT-PCR-based pluripotency analysis of ChiPSC lines. ChiPSC lines 7 (a), 18 (b) and 22 (c) were cultured either in DEF-CS and COAT-1 coated plates (monolayer growth) or were transferred and cultured in StemFit03 medium and iMatrix-511 coated plates (colony-like growth). Data show the mean ± SEM (n = 4, N = 1). Two-way ANOVA: **p<0.01, ns = not significant.

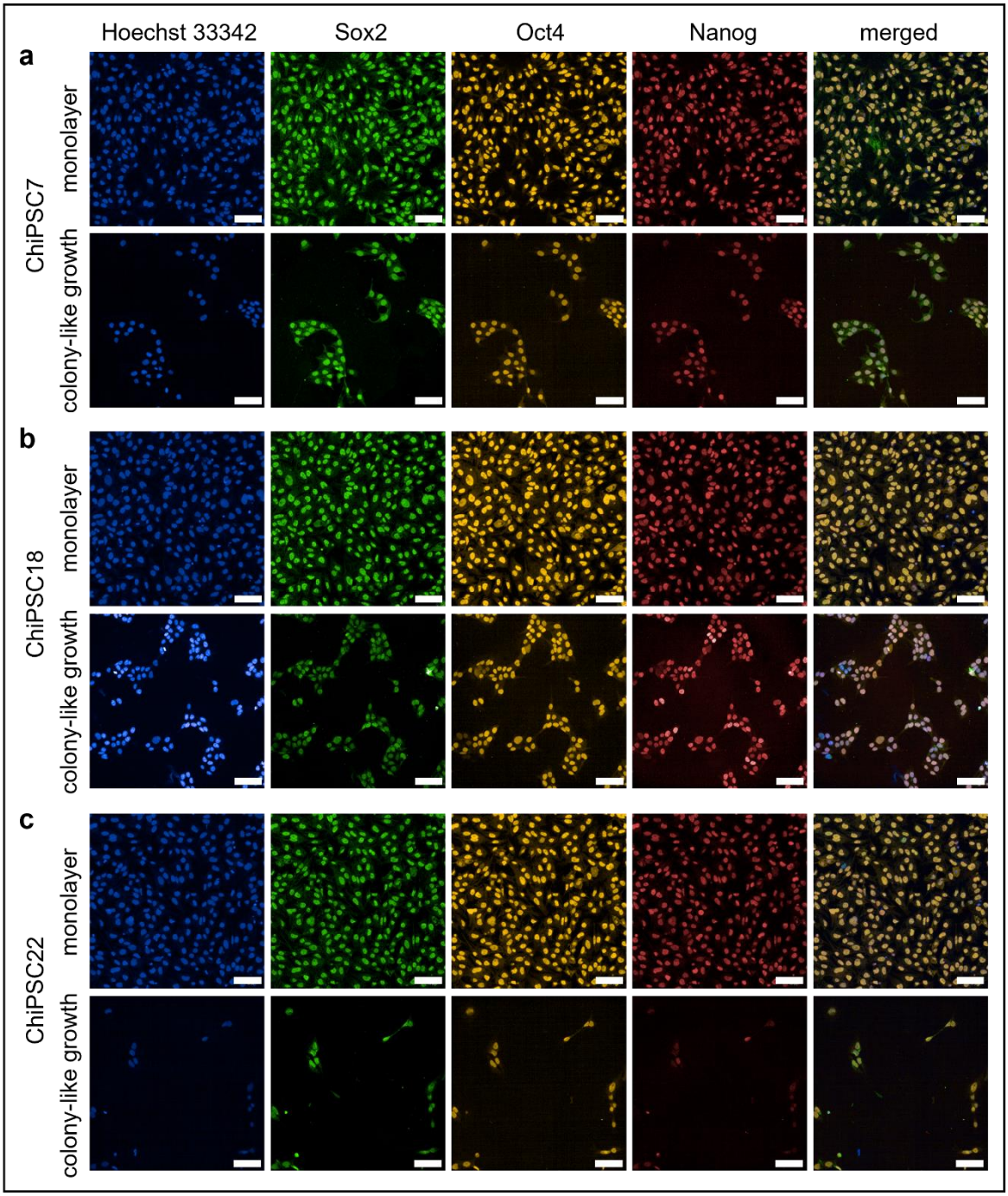

Figure S7. Immunolabeling for classical pluripotency markers in ChiPSC lines. ChiPSC lines 7 (a), 18 (b) and 22 (c) were cultured either in DEF-CS and COAT-1 coated plates (monolayer growth) or were transferred and cultured in StemFit03 medium and iMatrix-511 coated plates (colony-like growth; n = 12, N = 1). All parameters were set globally across the images and therefore relative intensity can be quantitatively compared. Scale bar = 50 µm.

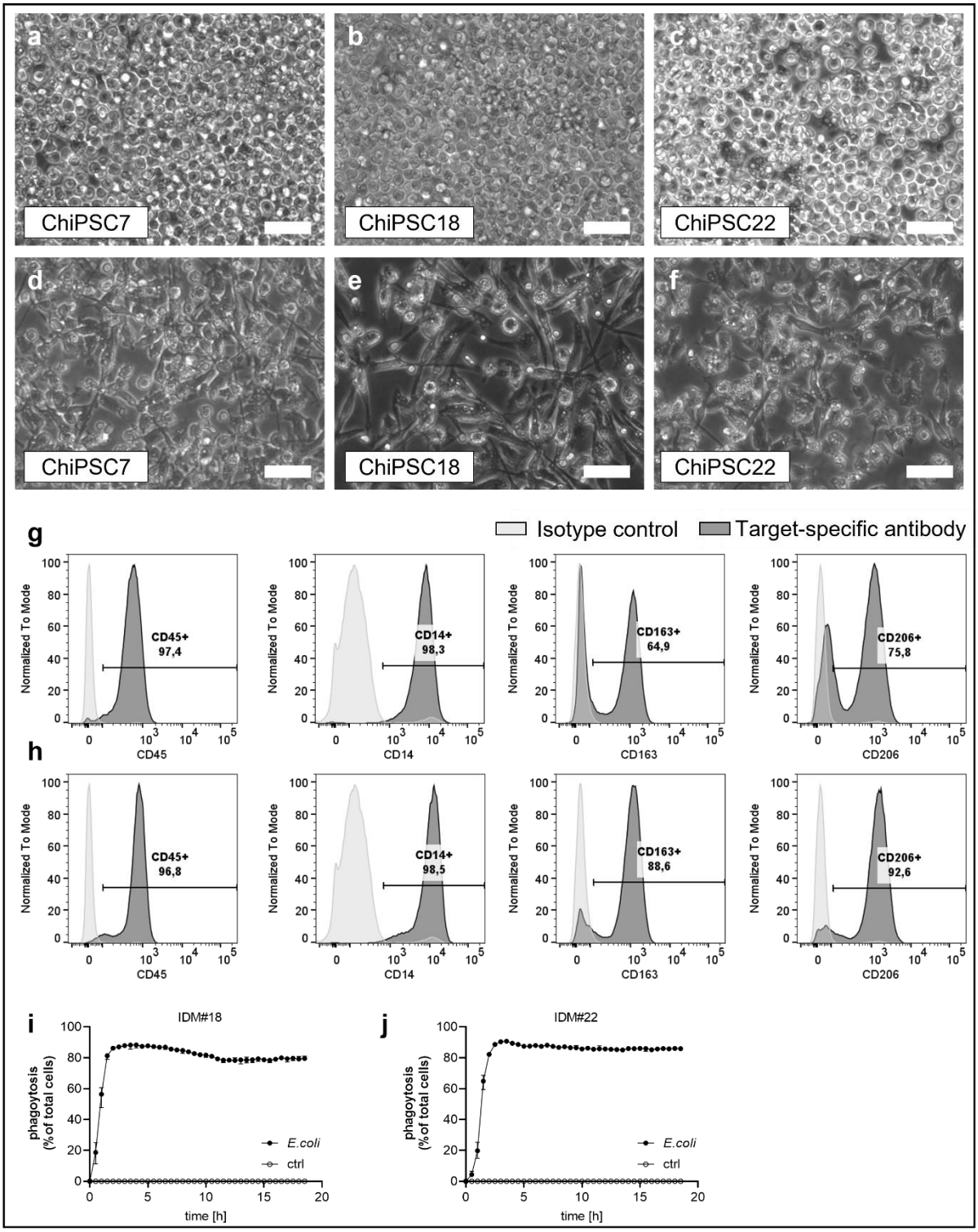

Figure S8. Differentiation of three additional ChiPSC lines to derived macrophages. (a-f) Representative morphology of macrophage progenitors (a-c) and IDMs (d-f) derived from ChiPSC line 7 (a+d), line 18 (b+e) and line 22 (c+f; N = 3). Scale bar = 50 µm. **(g+h)** Flow cytometry analysis of produced IDMs derived from ChiPSC line 18 (g) and line 22 (h) for the macrophage markers CD14, CD45, CD163 and CD206 (in %, N = 1). Gating is based on 1 % isotype control. **(i+j)** Representative phagocytotic activity of IDM#18 (i) and IDM#22 (j) treated with pHrodo-labeled *E. coli* bioparticles (median ± IQR; n = 6-12; some error bars are not visible; N = 3). Assay was measured in the Opera Phenix HTS System in a kinetic mode.

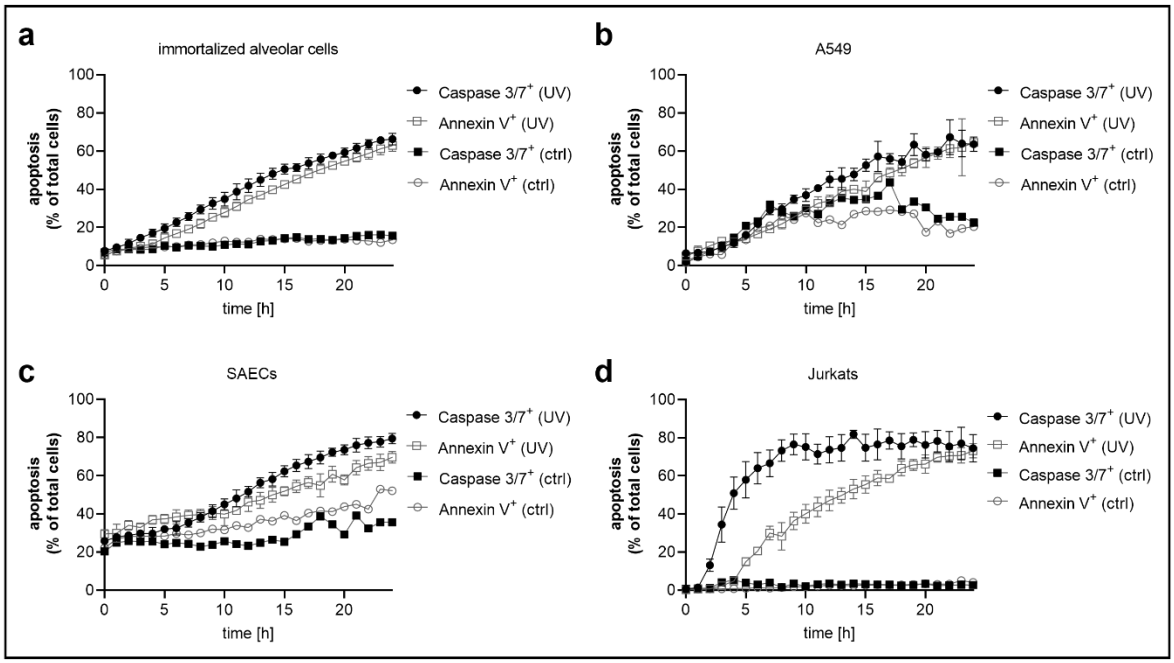

Figure S9. Apoptosis kinetics of different employed prey cells. Activity of Caspase 3/7 and exposure of Phosphatidylserine shown by Annexin V binding in irradiated (UV) and non-irradiated control prey cells over a time course of 24 h for immortalized alveolar cells (a), A549 (b), SAECs (lot 18TL179344; c) and Jurkats (d). Data points are representative (N = 6 (immortalized alveolar cells), N = 2 (A549), N = 2 (SAECs) and N = 5 (Jurkats)) and show the mean ± SD (n = 4).

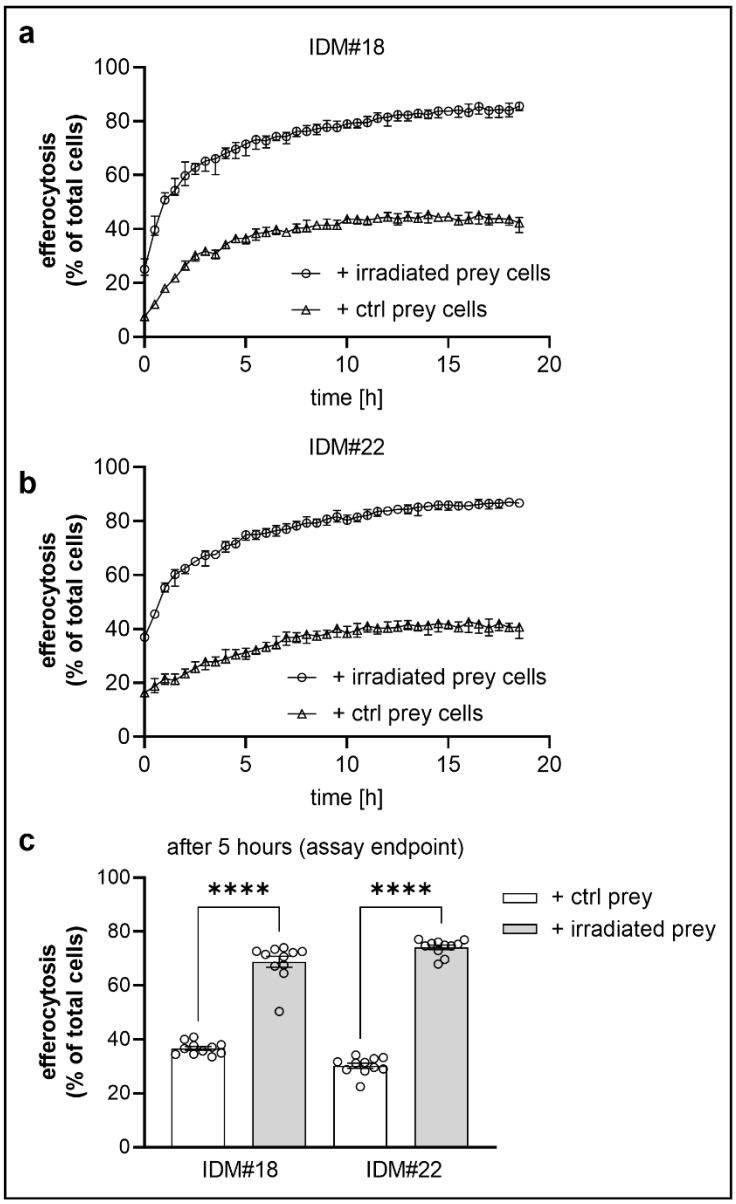

Figure S10. Irradiated Raji cells serve as prey cells macrophages derived from different ChiPSC lines. Efferocytosis data using IDMs derived from ChiPSC18 (a) and ChiPSC22 (b) incubated with irradiated or ctrl Raji cells as prey. Assay was conducted as kinetics (shown in a+b; median ± IQR; N = 1; n = 11) and extracted data for the time point 5 h after prey cell addition are shown in c (mean ± SEM; n = 11). One-way ANOVA: ****p<0.0001.

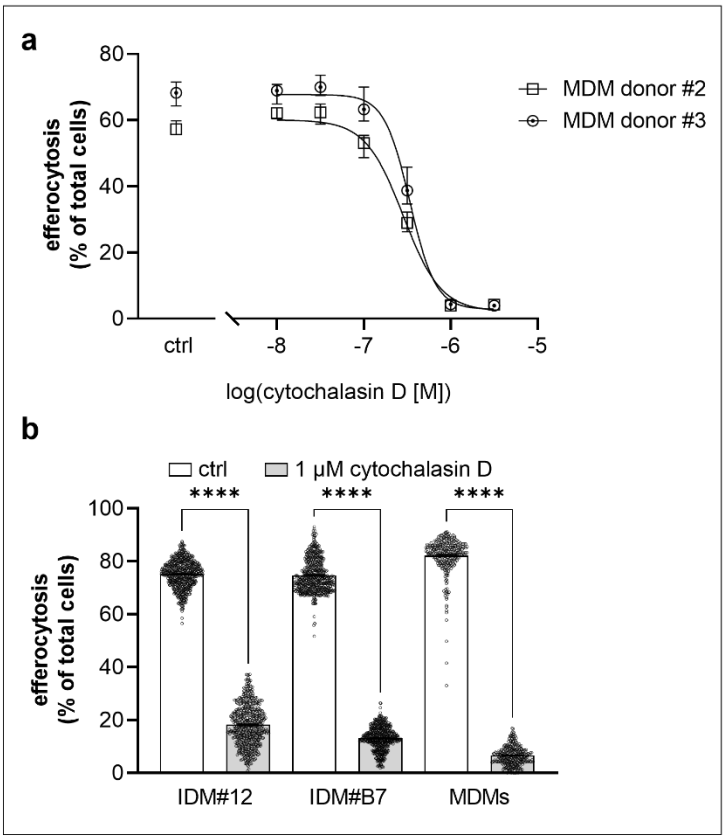

Figure S11. Pharmacological effect of cytochalasin D. (a) Concentration-dependent reduction of efferocytosis by cytochalasin D pre-treatment of MDMs from different donors. Image analysis and quantification were based on the total pHrodo intensity from detected spots within whole cells. Data points represent median ± IQR (some error bars are not visible) and show representative data for two different MDM donors (n = 14). For statistical details, please see corresponding Table S1 below. **(b)** Quantification of efferocytosis modulation in the miniaturized 1536-well microplate format. Data points are representative (N = 4 (IDM#12), N = 3 (IDM#B7) and N = 7 (MDMs)) and show mean ± SEM (n ≥ 308); one-way ANOVA: ****p<0.0001. For error bars, please see Fig. 17 e.

Table S1 Statistical details of concentration-dependent stimulation experiments with cytochalasin D in IDMs and MDMs. Data are based on non-linear fits (log(inhibitor) vs. response - Variable slope (four parameters)), see also corresponding Figure S11.

cytochalasin D Best-fit values	MDMs, donor #2	MDMs, donor #3
Bottom [%]	2	3
Top [%]	60	68
IC_{50} [nM]	280 [270; 300]	340 [320; 360]

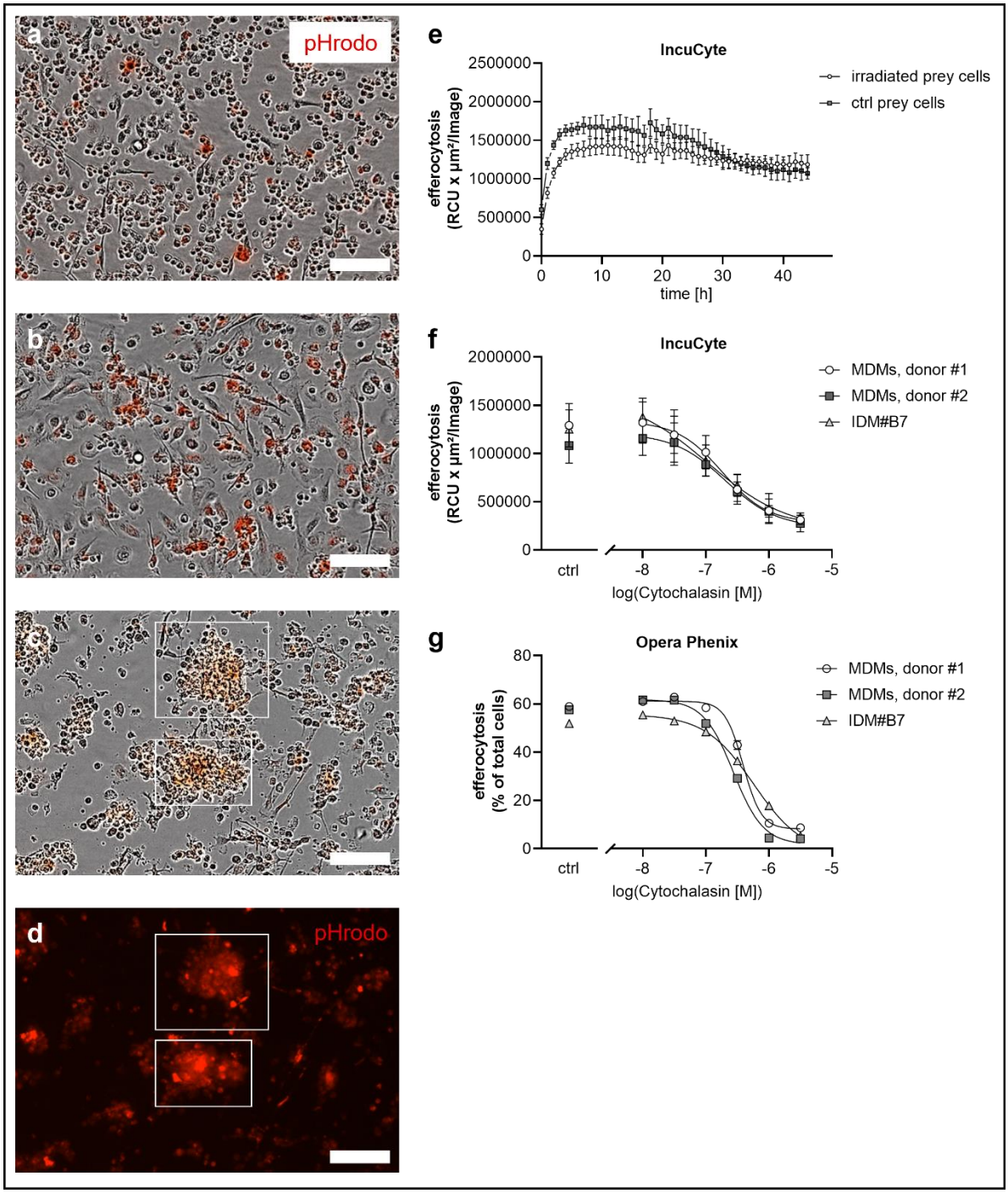

Figure S12. Efferocytosis assay comparison conducted either with the IncuCyte system or with the Opera Phenix. (a+b) Images taken with the IncuCyte system directly after prey cell addition (a) or after 24 h (b) showing efferocytosing macrophages by an increased pHrodo signal. Scale bar = 50 µm. **(c-e)** False-positive pHrodo signals in the IncuCyte system by clumping Raji prey cells shown by the taken images (c+d) and by the quantified data (e). Scale bar = 50 µm. Data show the mean ± SD (n = 14). **(f+g)** Comparison of the concentration-dependent reduction of efferocytosis by cytochalasin D pre-treatment of macrophages with the IncuCyte system (f; mean ± SD (n = 14)) and with the Opera Phenix (g; mean ± SEM (n = 14)).

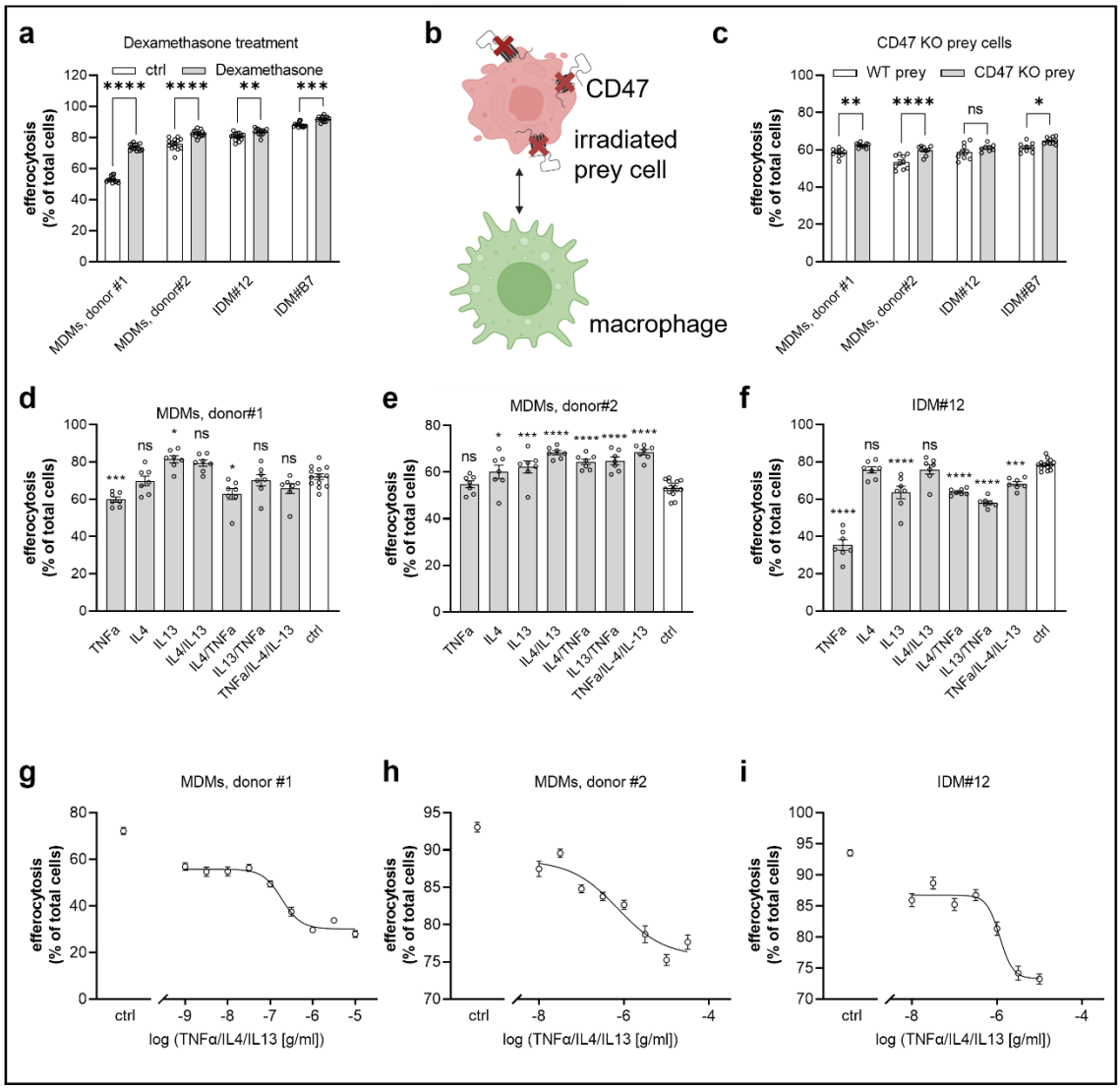

Figure S13. Modulation of the macrophage's efferocytotic activity by different treatments. (a) Modulation of efferocytosis by a dexamethasone treatment. Data are representative (N = 2 (IDMs) and N = 8 (MDMs)) and show the mean ± SEM; n = 10-12. Two-way ANOVA: **p<0.01, ***p<0.001, ****p<0.0001. **(b+c)** Modulation of efferocytosis using CD47 KO Raji prey cells in comparison to WT prey cells. Data show the mean ± SEM (n = 10-12; N = 1 (IDMs) and N = 2 (MDMs)). Two-way ANOVA: *p<0.05, **p<0.01, ****p<0.0001, ns = not significant. **(d-f)** Modulation of efferocytosis by TNFα, IL4, IL13 and different combinations in comparison to the control in MDMs (d+e) and IDM#12 (f). Data show the mean ± SEM (n = 7-14; N = 1). Two-way ANOVA: *p<0.05, ***p<0.001, ****p<0.0001, ns = not significant. **(g-i)** Concentration-dependent modulation of efferocytosis by the combination of by TNFα, IL4 and IL13 in MDMs (g+h) and IDM#12 (i). Data show the mean ± SEM (n = 14; N = 6 (MDMs), N = 1 (IDM#12)).

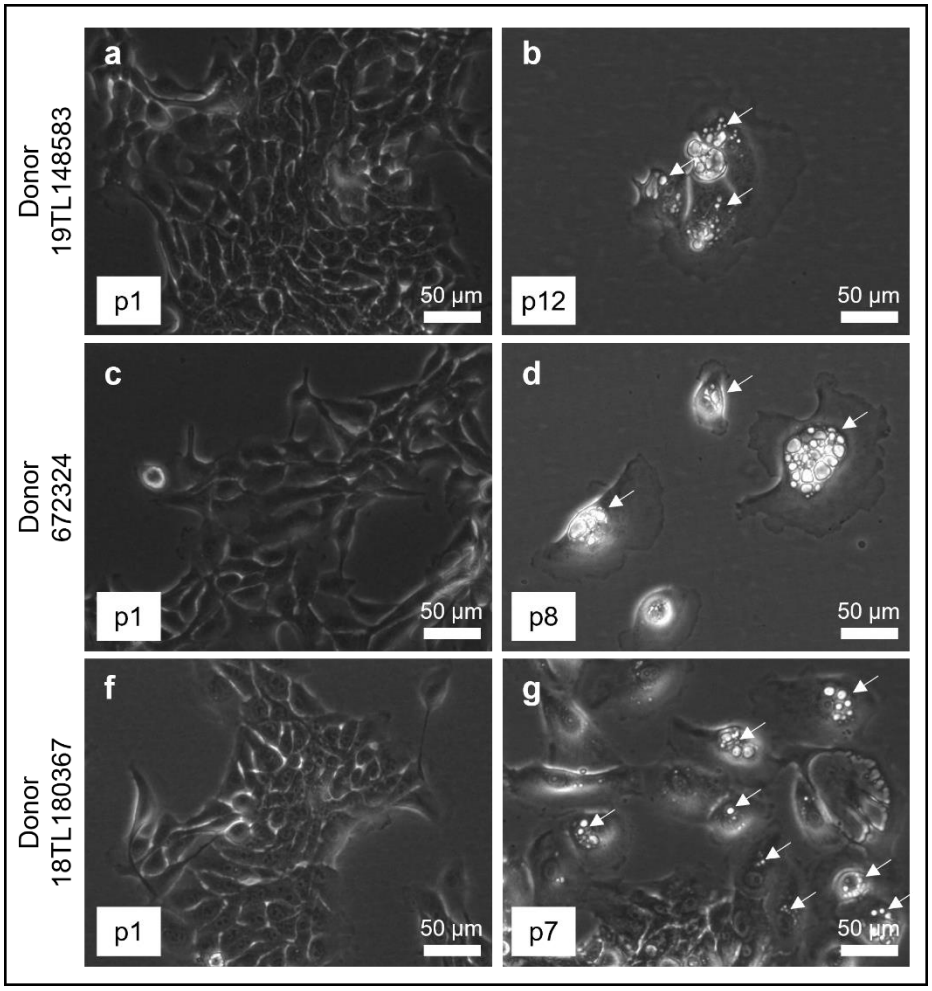

Figure S14. Serial cell passaging induces a senescent morphology in primary small airway epithelial cells. Representative morphological changes during serial passaging shown by brightfield images for SAEC donor 19TL148583 for passage 1 (a) and passage 12 (b), for SAEC donor 672324 for passage 1 (c) and passage 8 (d) and for SAEC donor 18TL180367 for passage 1 (e) and passage 7 (f). White arrows point at intracellular lysosomes.

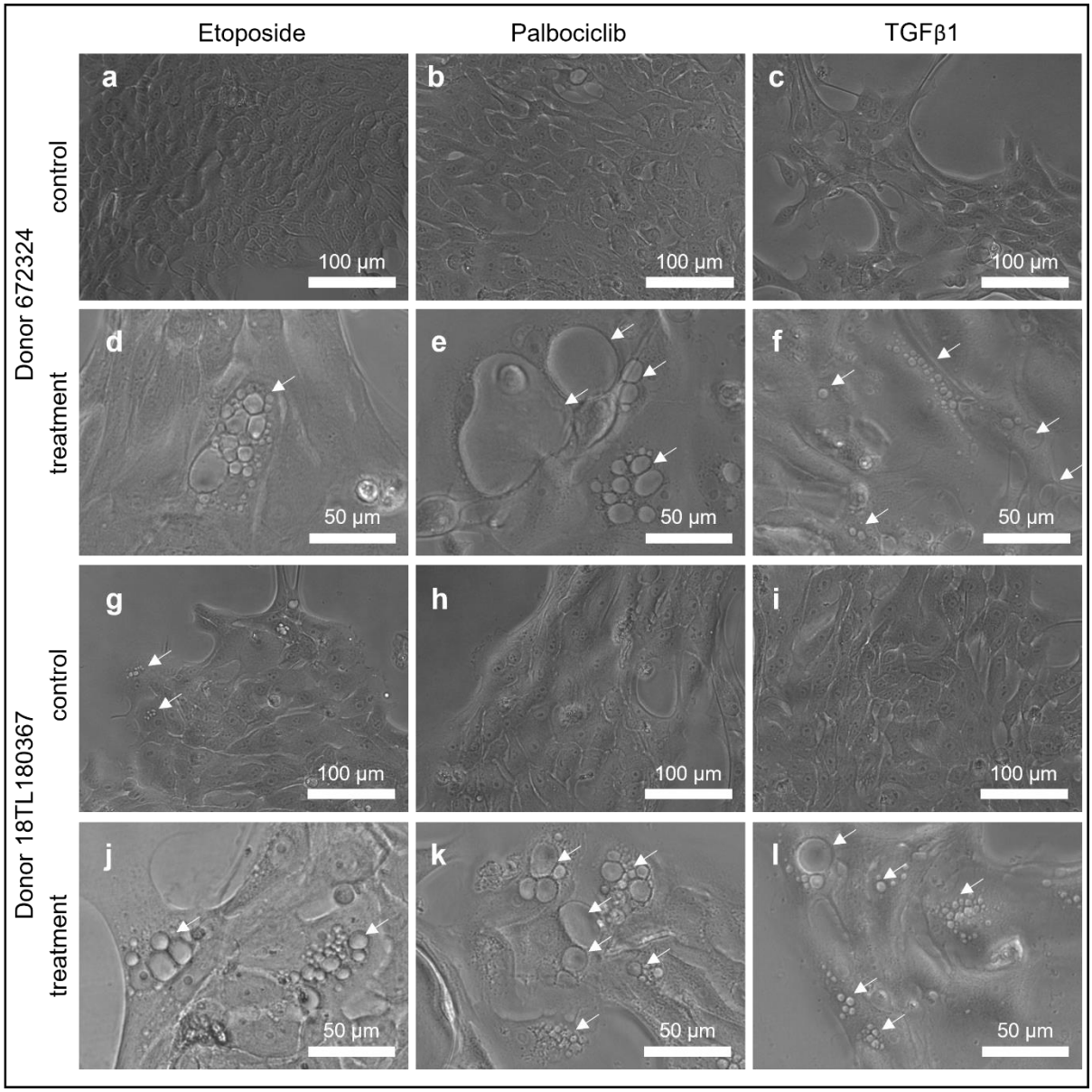

Figure S15. Treatment with anti-cancer drugs or TGFβ1 induces a senescent morphology in primary small airway epithelial cells. Representative morphological changes in SAECs donor 672324 (a-f) and 18TL180367 (g-l) upon treatment with either etoposide (d, j), palbociclib (e, k) or TGFβ1 (f, l) in comparison to the respective control shown by brightfield images (a-c, g-i; n = 6). White arrows point at intracellular lysosomes.

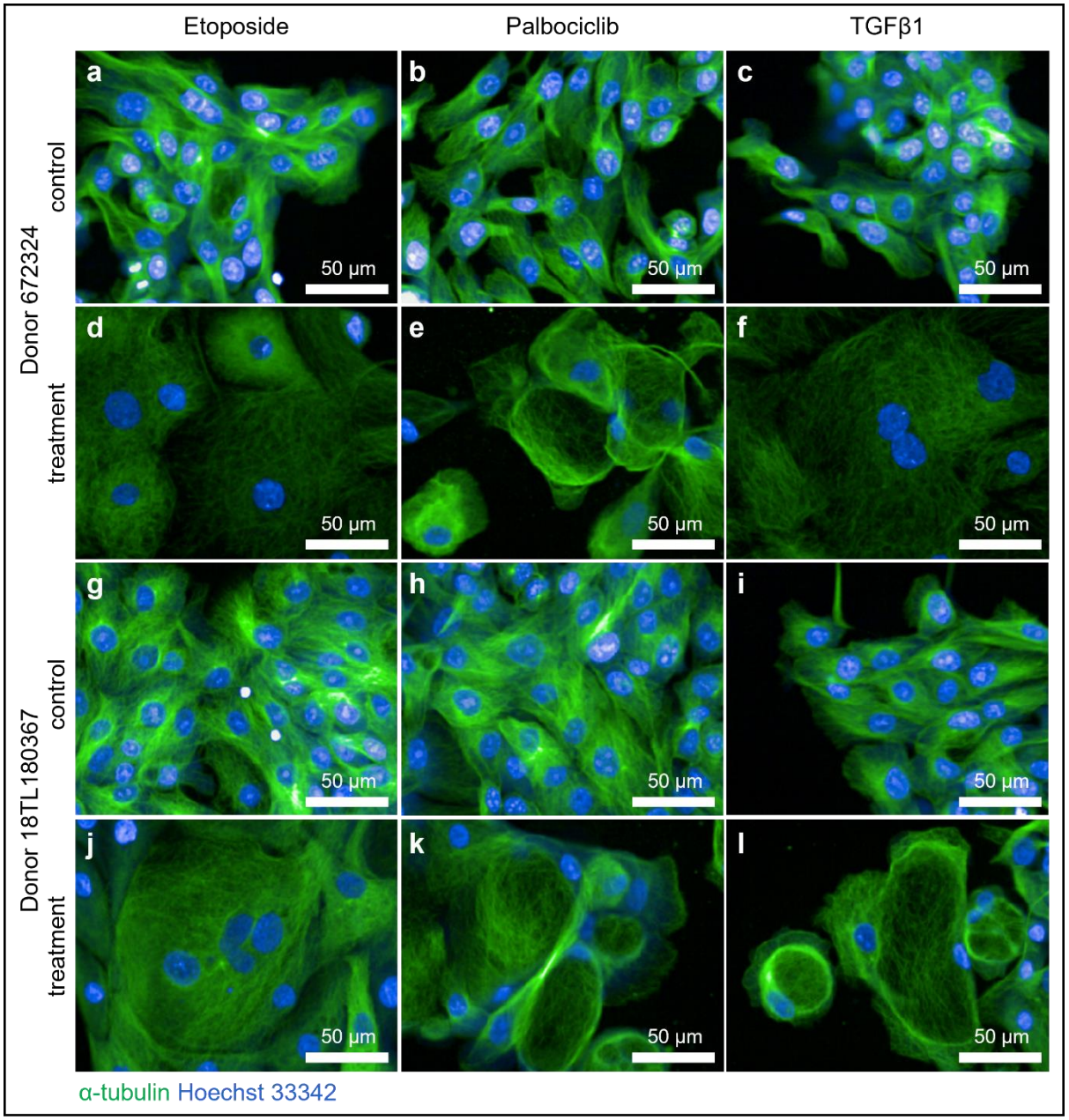

Figure S16. Treatment with anti-cancer drugs or TGFβ1 increases the cellular size of primary small airway epithelial cells. Change in cell size in SAECs (a-f: donor 672324; g-l: donor 18TL180367) upon treatment with either etoposide (d, j), palbociclib (e, k) or TGFβ1 (f, l) in comparison to the respective control shown by an immunolabeling of α-tubulin in combination with Hoechst 33342. All parameters were set globally across images and therefore the relative intensity can be quantitatively compared (n = 6, N = 1).

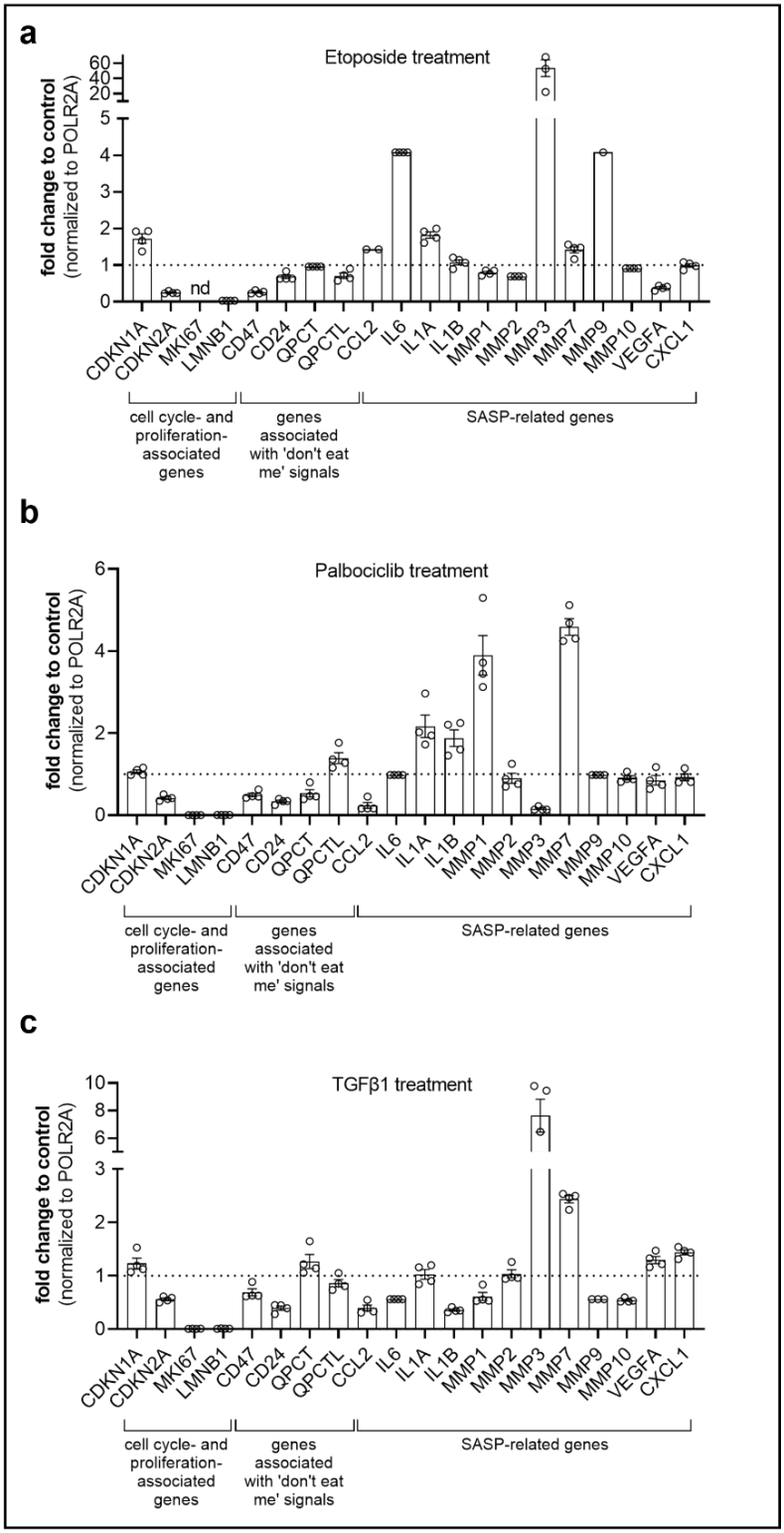

Figure S17. Treatment with anti-cancer drugs or TGFβ1 modulates the levels of senescence markers in primary small airway epithelial cells. (a-c) Analysis of cell cycle-, proliferation-, ‚don‘t eat me‘ signal- and SASP (senescence-associated secretory phenotype)-associated genes by RT-PCR for the SAEC donor 18TL179344 upon treatment with either etoposide (a), palbociclib (b) or TGFβ1 (c). Data are normalized to vehicle-treated controls. (mean ± SEM; n = 4, N = 2 for etoposide and palbociclib treatment).

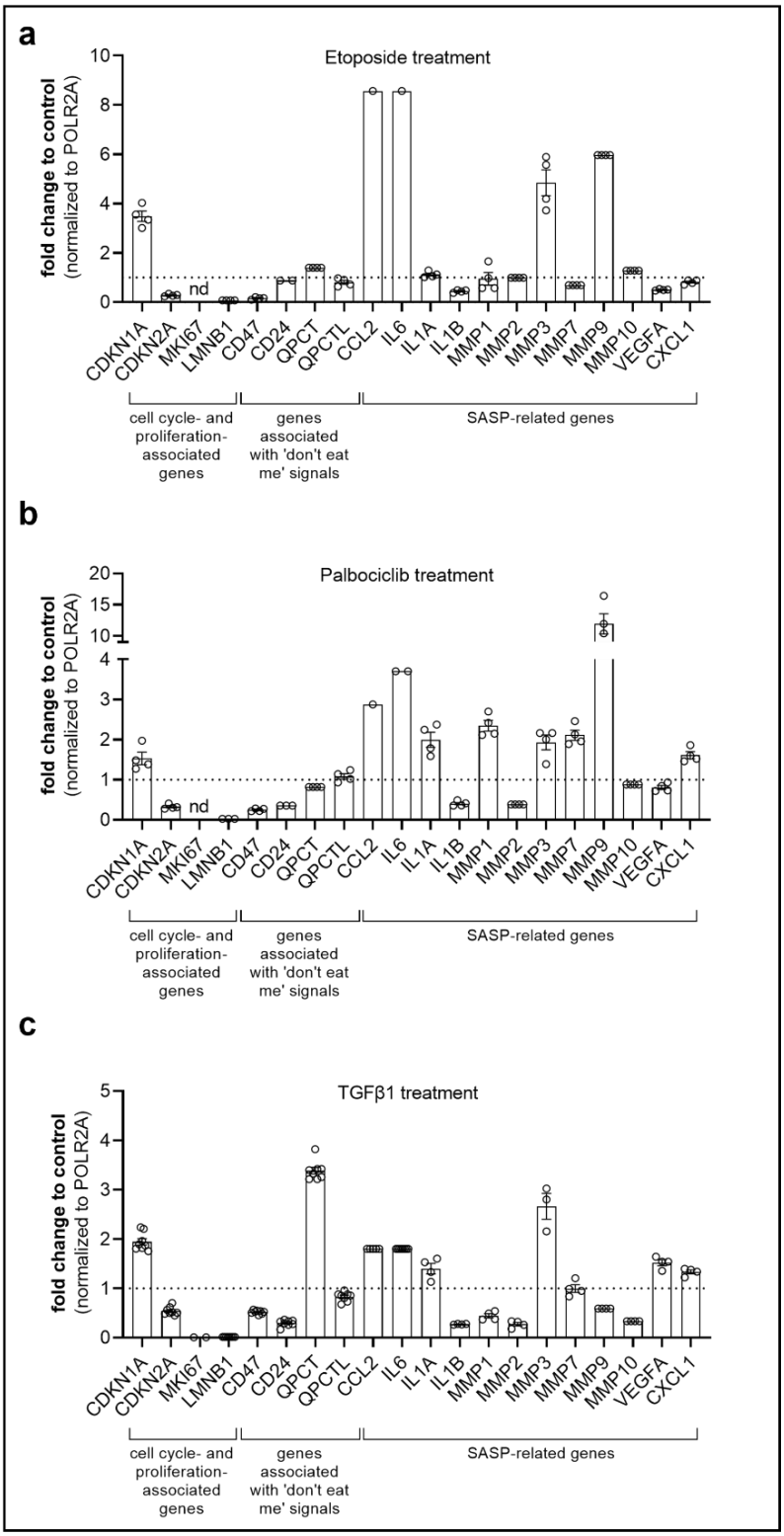

Figure S18. Treatment with anti-cancer drugs or TGFβ1 modulates the levels of senescence markers in primary small airway epithelial cells. (a-c) Analysis of cell cycle-, proliferation-, ‚don't eat me' signal- and SASP (senescence-associated secretory phenotype)-associated genes by RT-PCR for the SAEC donor 672324 upon treatment with either etoposide (a), palbociclib (b) or TGFβ1 (c). Data are normalized to vehicle-treated controls. (mean ± SEM; n = 4, N = 2 for etoposide and palbociclib treatment).

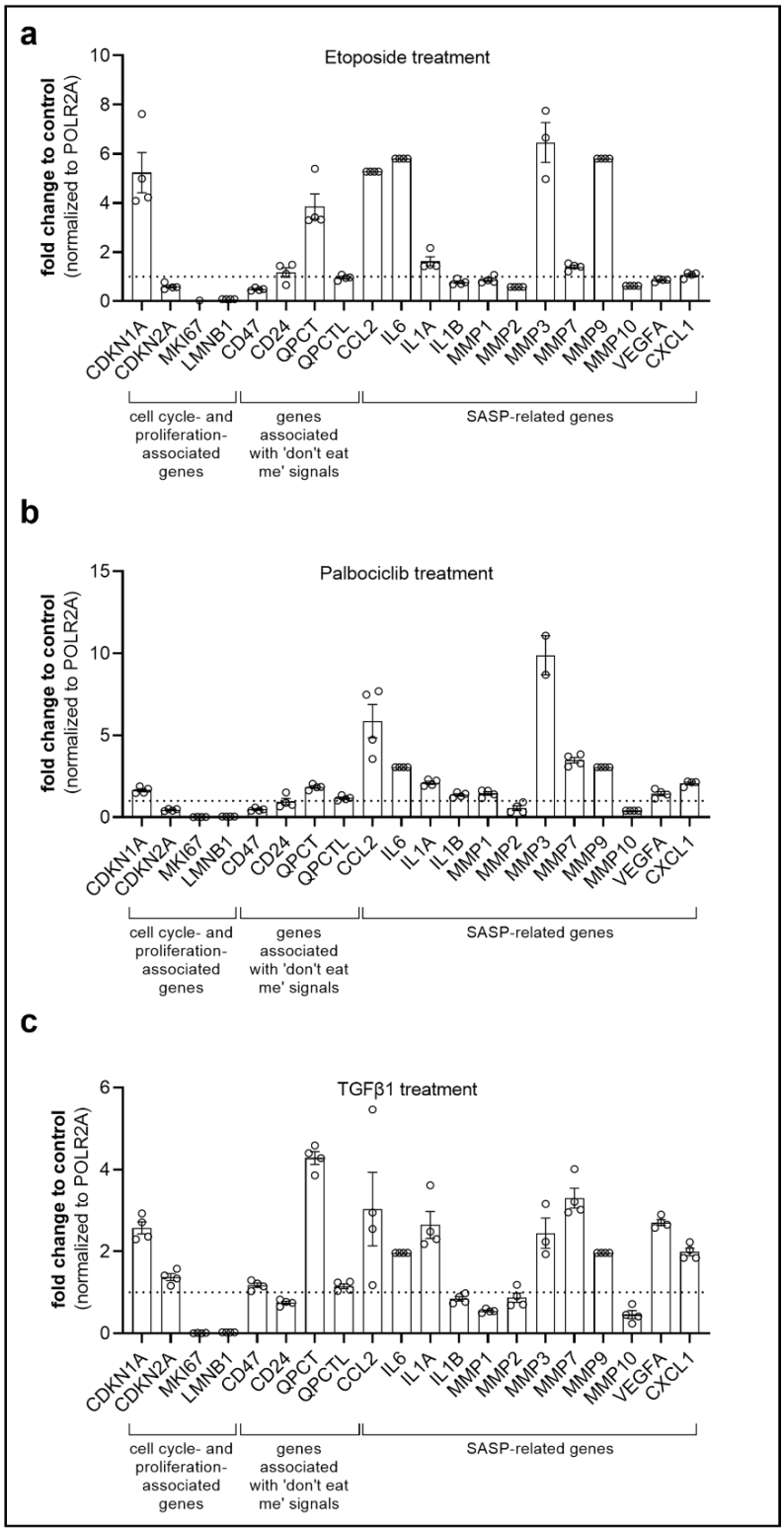

Figure S19. Treatment with anti-cancer drugs or TGFβ1 modulates the levels of senescence markers in primary small airway epithelial cells. (a-c) Analysis of cell cycle-, proliferation-, ‚don't eat me' signal- and SASP (senescence-associated secretory phenotype)-associated genes by RT-PCR for the SAEC donor 18TL180367 upon treatment with either etoposide (a), palbociclib (b) or TGFβ1 (c). Data are normalized to vehicle-treated controls. (mean ± SEM; n = 4, N = 2 for etoposide and palbociclib treatment).

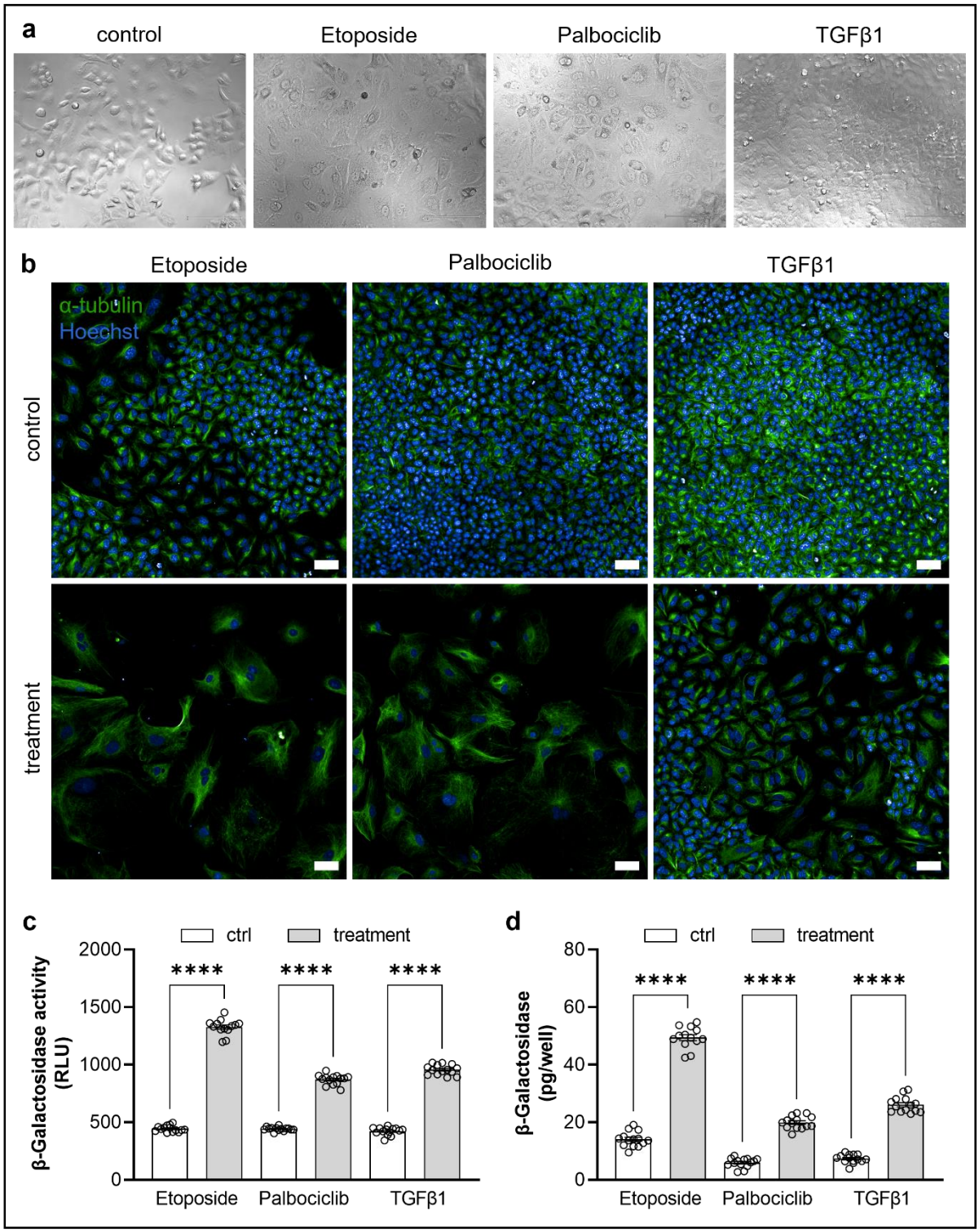

Figure S20. Treatment with anti-cancer drugs or TGFβ1 induces a senescent morphology and increased β-galactosidase levels in A549. Senescence of A549 cells was induced by treatment with either etoposide, palbociclib, or TGFβ1. **(a)** Representative brightfield images of treated A549 (N = 4). **(b)** Immunolabeling of α-tubulin (green) in combination with Hoechst 33342 (blue) of treated A549 cells. All parameters were set globally across the images and therefore relative intensity can be quantitatively compared. Scale bar = 50 µm (N = 1). **(c+d)** Representative quantification of senescence-associated β-galactosidase activity (c) and enzyme amount (d) in treated A549 (mean ± SEM; n = 14, N = 3). One-way ANOVA: ****p < 0.0001.

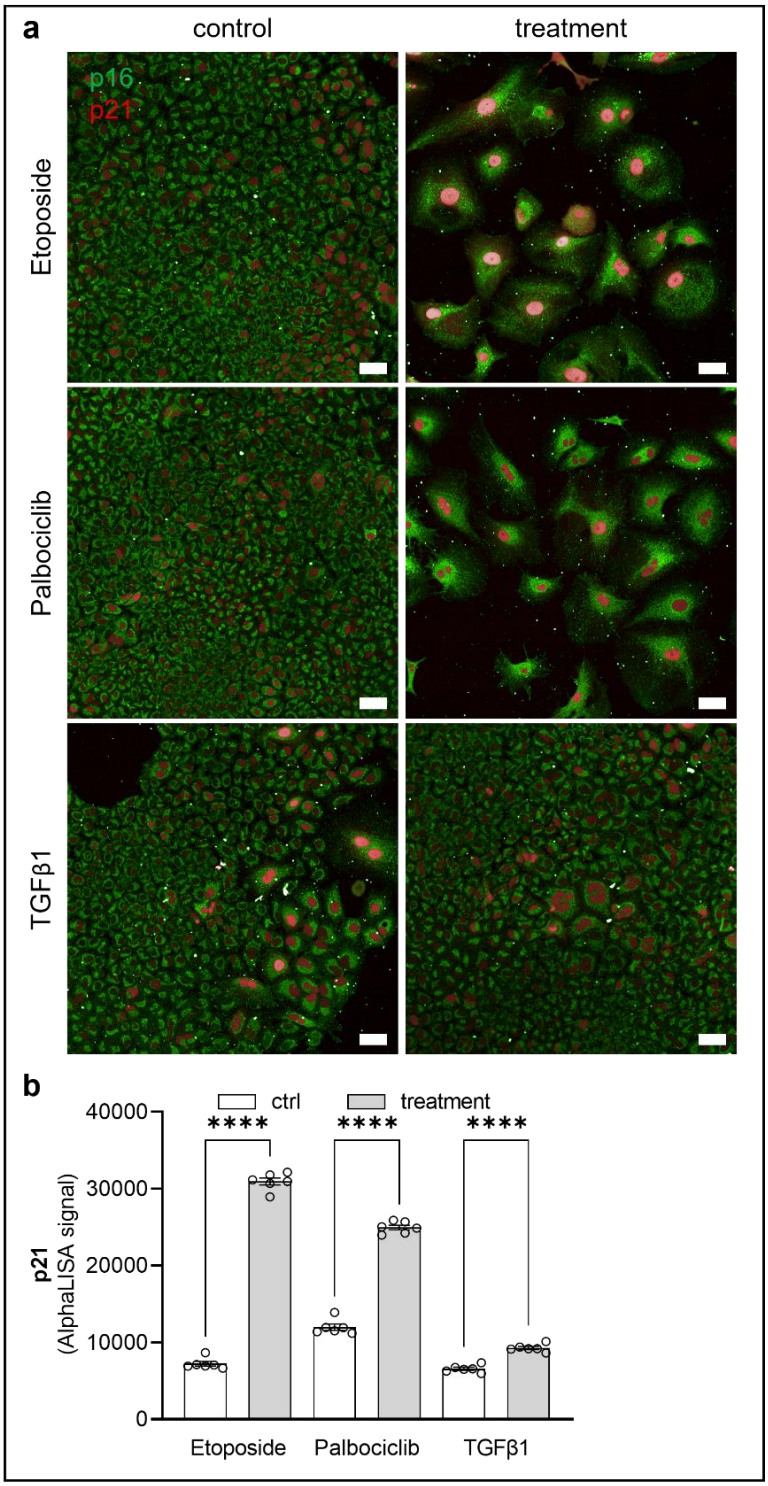

Figure S21. Treatment with anti-cancer drugs or TGFβ1 modulates p16 and p21 in A549. Senescence of A549 cells was induced by treatment with either etoposide, palbociclib, or TGFβ1. **(a)** Immunolabeling of p16 (green) and p21 (red) in treated A549 cells. All parameters were set globally across the images and therefore relative intensity can be quantitatively compared. Scale bar = 50 µm (N = 1). **(b)** Quantification of the senescence marker p21 in treated A549 (mean ± SEM; n = 6; N = 2). One-way ANOVA: ****p < 0.0001.

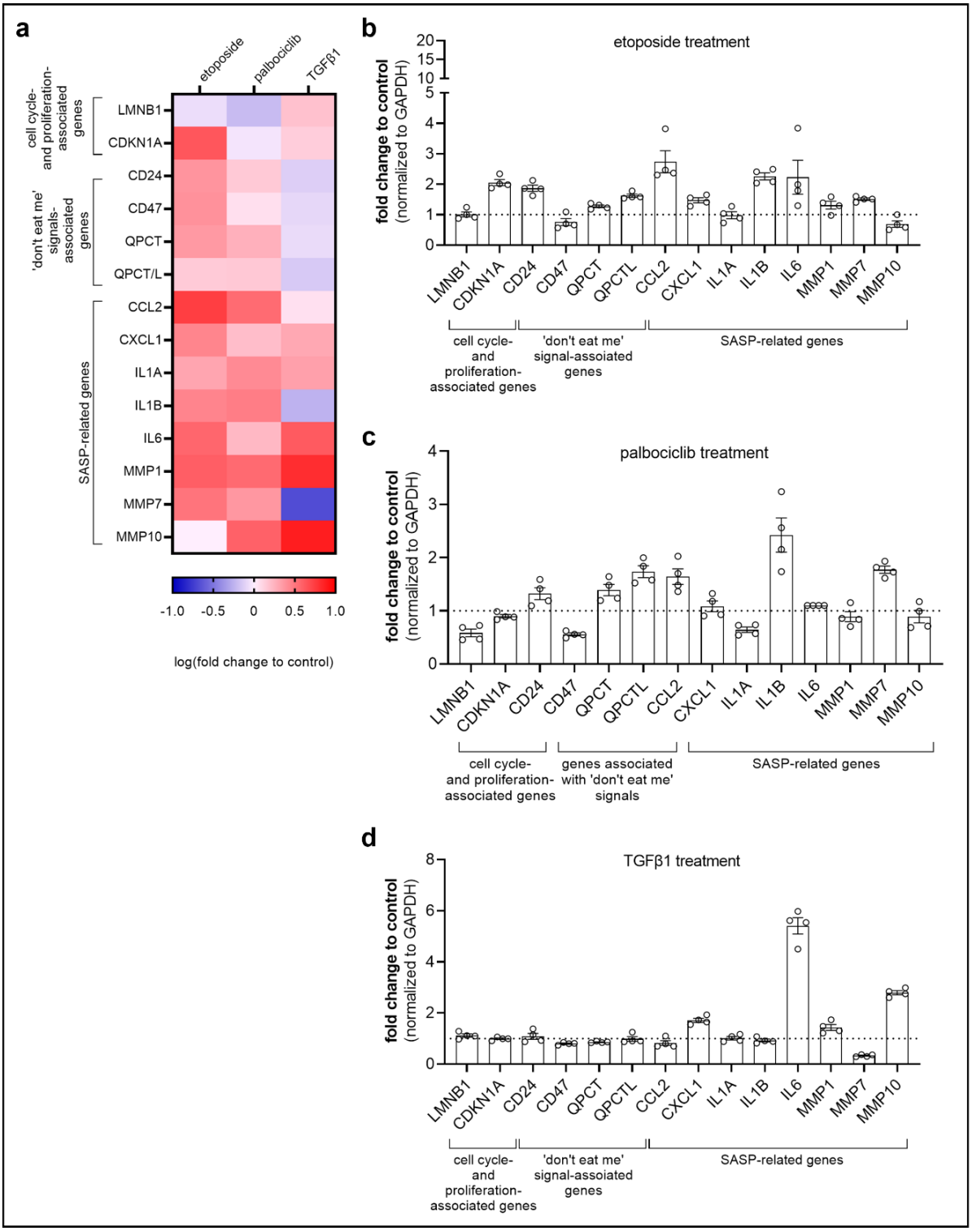

Figure S22. Treatment with anti-cancer drugs or TGFβ1 modulates the levels of senescence markers in A549. Representative analysis of cell cycle-, proliferation-, ‚don't eat me' signal- and SASP (senescence-associated secretory phenotype)-associated genes by RT-PCR in A549 upon treatment with either etoposide, palbociclib or TGFβ1 (N = 2). **(a)** Marker modulation is presented with a heatmap (based on mean ± SEM; n = 4). Upregulation (red) and downregulation (blue) of genes is indicated as log of fold change relative to controls. **(b-d)** Fold changes of genes in comparison to the respective control after etoposide (b), palbociclib (c) or TGFβ1 (d) treatment (mean ± SEM; n = 4).

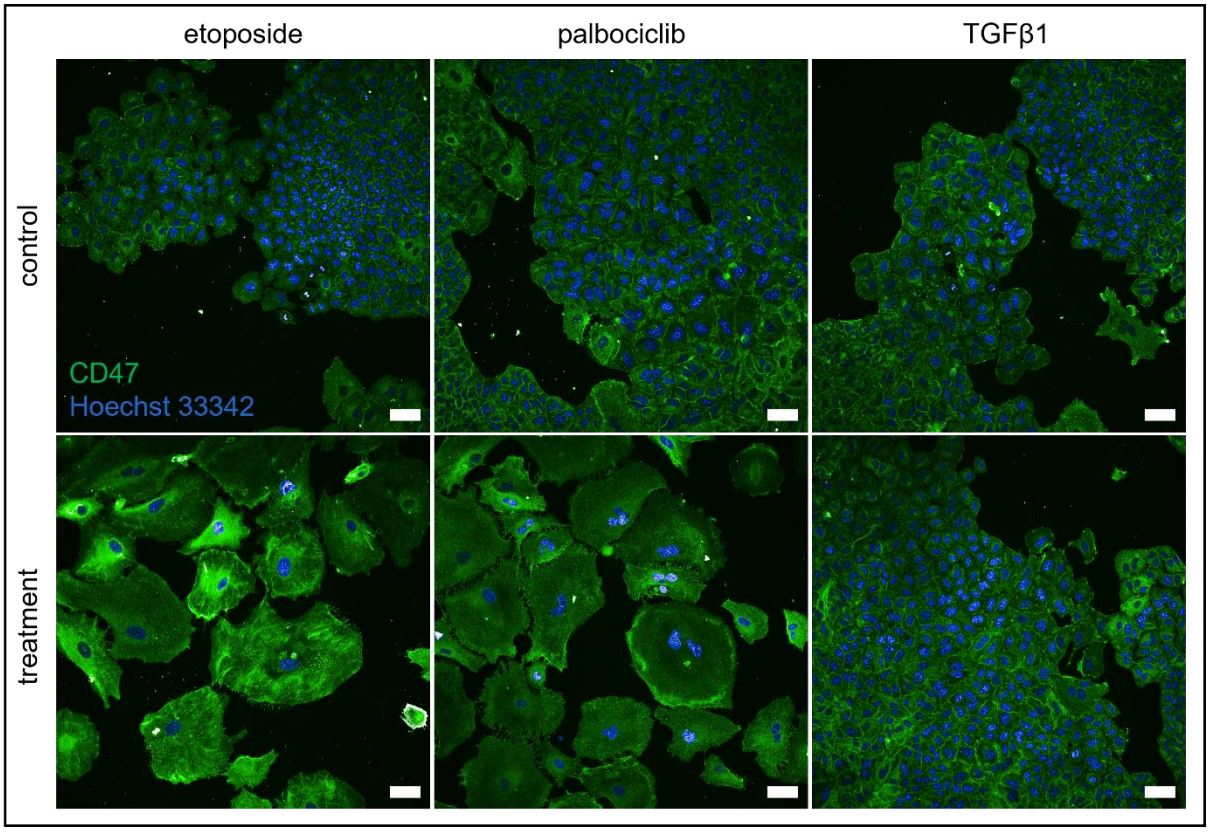

Figure S23. Treatment with anti-cancer drugs or TGFβ1 modulates the ‚don't eat me' signal CD47 in A549. Immunolabeling of CD47 (green) in combination with Hoechst 33342 (blue) in A549 cells treated with either etoposide, palbociclib or TGFβ1. All parameters were set globally across the images and therefore relative intensity can be quantitatively compared. Scale bar = 50 µm (N = 1).

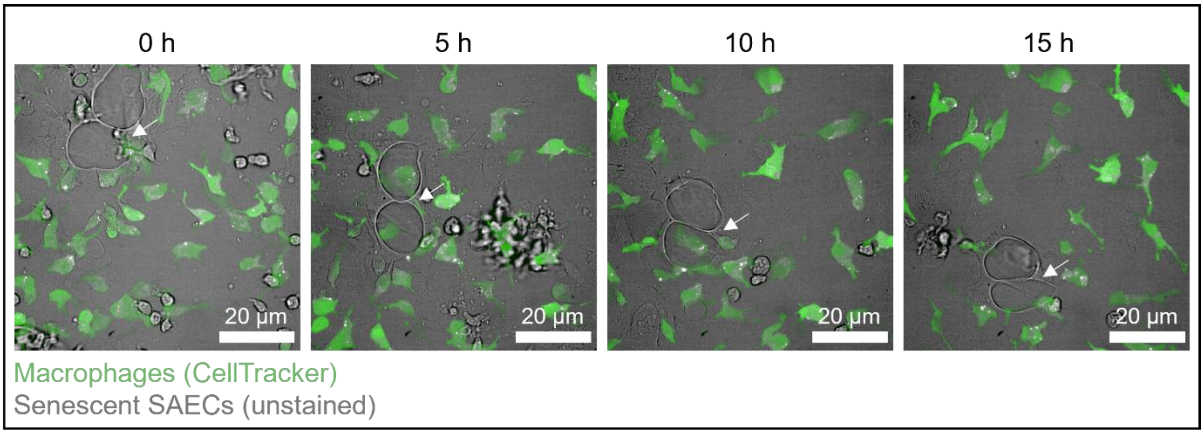

Figure S24. Macrophages interact with but do not remove senescent cells. Unstained SAECs (lot 672324, shown with white arrows) were treated with palbociclib for seven days and then co-cultured over night with CellTracker labeled macrophages (IDM#B7). Images were taken for a period of 15 h in a kinetic mode using the Opera Phenix HTS System. The same field of view is shown across time. All parameters were set globally across images and therefore the relative intensity can be quantitatively compared (n = 8; N = 3).

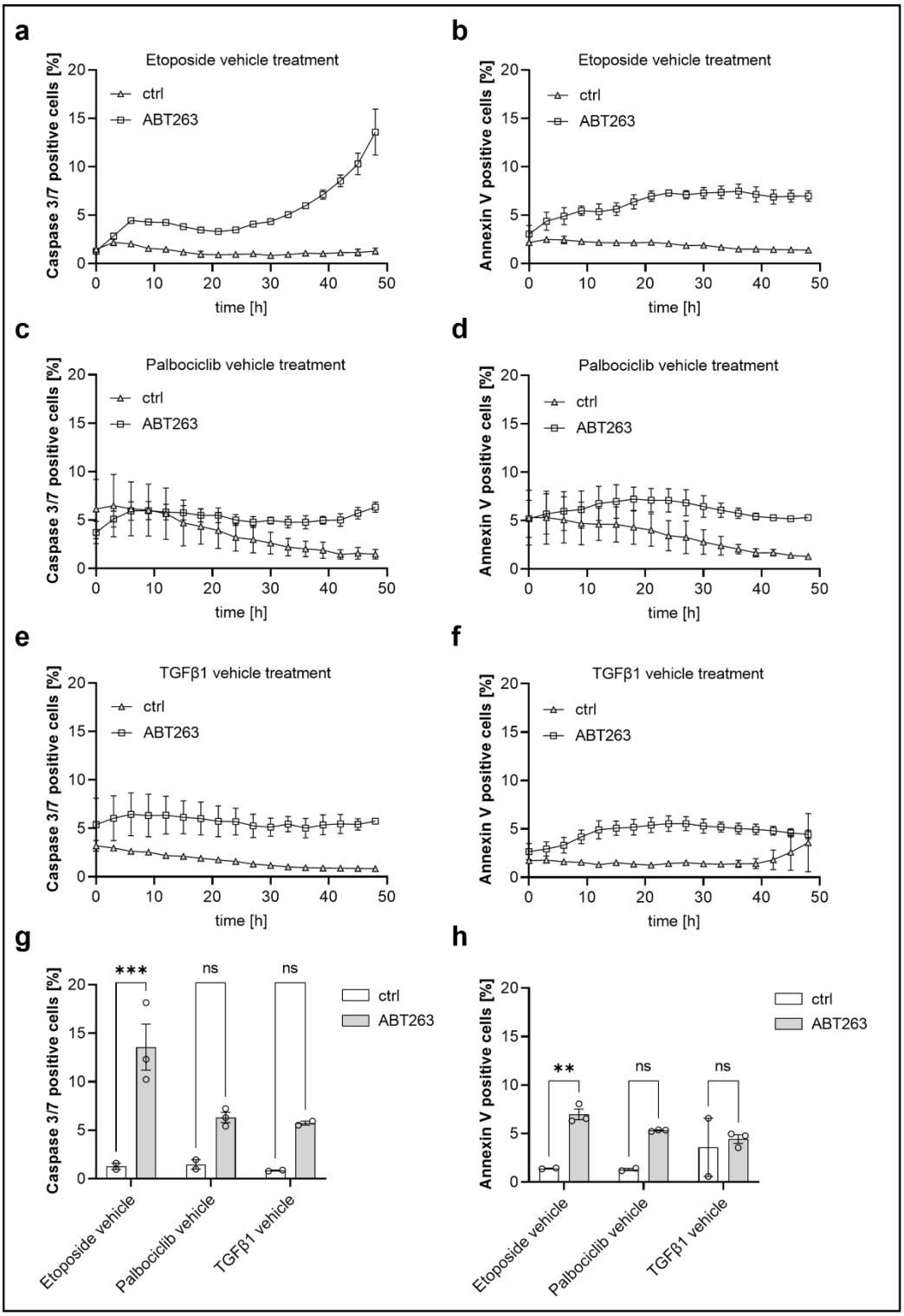

Figure S25. Specificity of the senolytic drug ABT263 in A549 cells. A549 were treated with the vehicle controls of either etoposide, palbociclib or TGFβ1 to generate control cells. Control cells were treated with ABT263 for 48 h. Activity of Caspase 3/7 and exposure of Phosphatidylserine shown by Annexin V binding over a time course of 48 hours (a-f) or after 48 hours (g+h) in A549 control cells treated with ABT263 or vehicle ctrl. **(a-f)** Percentage of Caspase 3/7 positive (a, c, e) and Annexin V positive (b, d, f) A549 cells after vehicle treatment for etoposide (a+b), palbociclib (c+d) or TGFβ1 (e+f) over 48 h in presence of ABT263. Data points are representative (N = 3) and show the mean ± SEM (n = 2-3). **(g+h)** Percentage of Caspase 3/7 positive (g) and Annexin V positive (g) A549 control cells and treatment with ABT263 after 48 hours. Data points are representative (N = 3) and show mean ± SEM (n = 2-3). Two-way ANOVA: **p < 0.01, ***p < 0.001, ns = not significant.

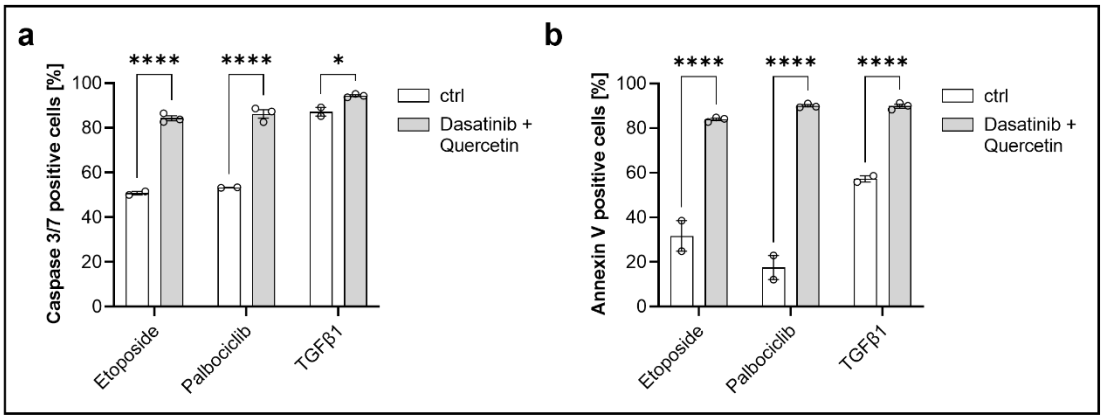

Figure S26. The combination of the senolytic drugs Dasatinib and Quercetin induces apoptosis in senescent A549 cells. A549 were treated with either etoposide, palbociclib or TGFβ1 to induce senescence. Senescent cells were treated with the combination of Dasatinib and Quercetin for 48 h. Percentages of Caspase 3/7 positive (a) and Annexin V positive (b) A549 cells after 48 h are shown. Data points show mean ± SEM (n = 3; N = 1). Two-way ANOVA: *p < 0.05, ****p < 0.0001.

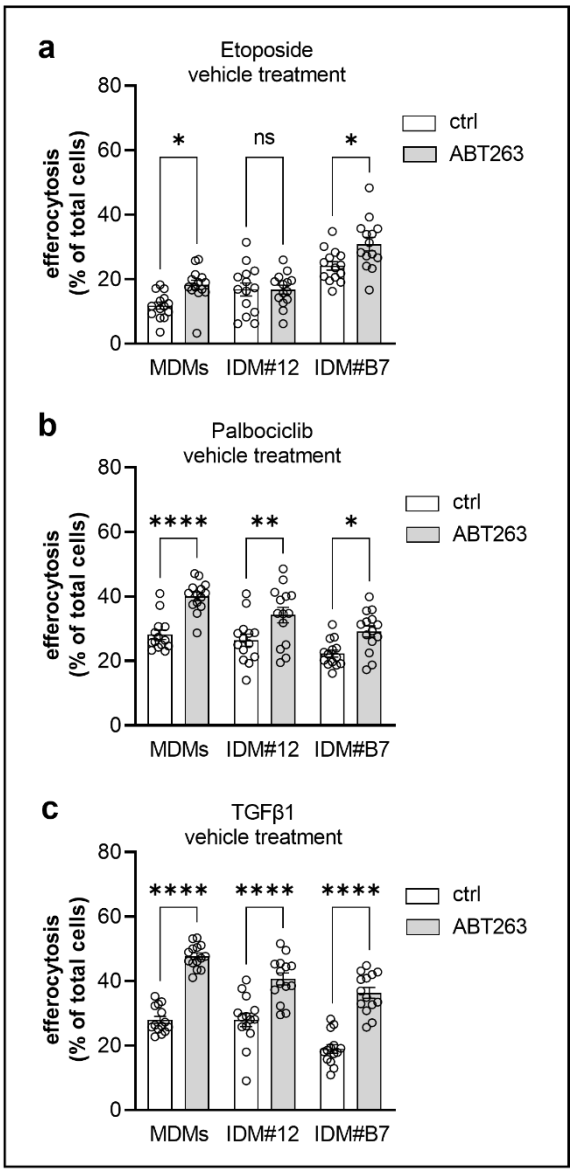

Figure S27. Specificity of the senolytic drug ABT263 in A549 cells for the application in efferocytosis assays. A549 were treated with the vehicle controls of either etoposide, palbociclib or TGFβ1 to generate control cells. Control cells were labeled with pHrodo and treated with ABT263 for 48 h. Data are representative for the senolytics-dependent modulation of efferocytosis by macrophages in co-culture with control cells, treated with the vehicle controls for etoposide (a), palbociclib (b) and TGFβ1 (c; mean ± SEM; n = 14; N = 2). One-way ANOVA: *p < 0.05, **p < 0.01, ****p < 0.0001, ns = not significant.

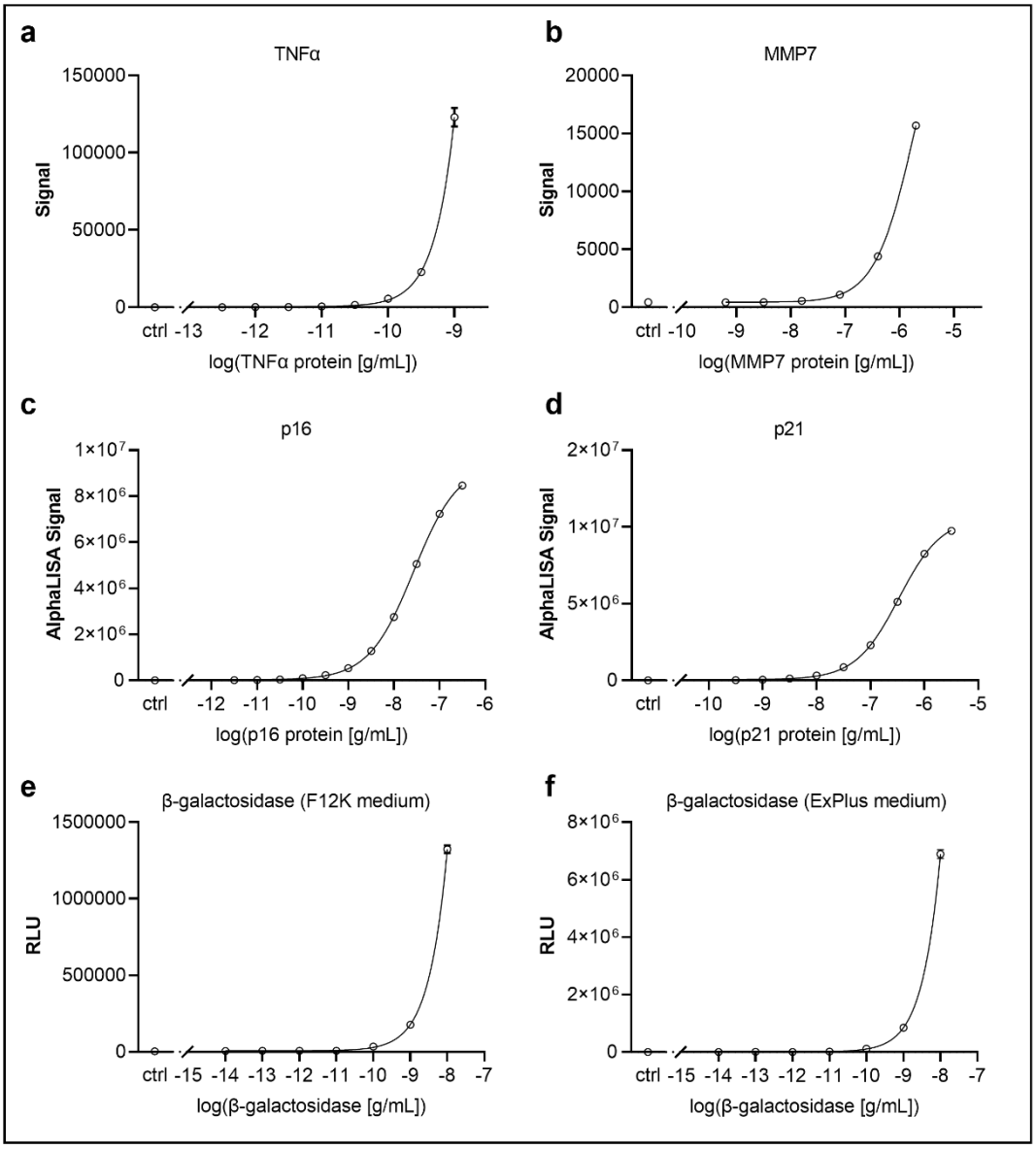

Figure S28. Standard protein curves of the applied protein-based assays. (a) TNFα MSD assay (mean ± SEM; n = 2). **(b)** MMP7 LANCE assay (mean ± SEM; n = 2). **(c+d)** AlphaLISA assays targeting p16 (c) and p21 (d; mean ± SEM; n = 5). **(e+f)** β-galactosidase assay conducted with F12K medium (e; A549) or ExPlus medium (f; SAECs; mean ± SEM; n = 5-10).

List of publications

Parts of this work are published in:

Bitzer S, Harati MD, El Kasmi KC, Schloesser D, Sauer J, Olbrich H, Schuler M, Gantner F, Heilker R. Application of human iPSC-derived macrophages in a miniaturized high-content-imaging-based efferocytosis assay. SLAS Discov. 2023 Jun;28(4):149-162. doi: 10.1016/j.slasd.2023.04.002

“Senescent Cells put Macrophages on a Diet - Cellular Senescence and Impaired Macrophage Efferocytosis in Fibrotic Diseases” Master thesis of Heiko Olbrich, University of Tübingen, October 2022

Record of contribution

Application of human iPSC-derived macrophages in a miniaturized high-content-imaging-based efferocytosis assay

Sarah Bitzer, Ralf Heilker, Karim El Kasmi and Florian Gantner conceived the project.
Sarah Bitzer, Ralf Heilker, Karim El Kasmi, Daniela Schlösser, Julia Sauer and Mozhgan Dehghan Harati designed research.
Sarah Bitzer, Mozhgan Dehghan Harati and Heiko Olbrich performed research and experiments.
Sarah Bitzer, Mozhgan Dehghan Harati and Michael Schuler analyzed data.
Sarah Bitzer visualized the data and prepared all figures.
Sarah Bitzer, Ralf Heilker and Mozhgan Dehghan Harati wrote the manuscript.
All authors reviewed the manuscript.

Senescent Cells put Macrophages on a Diet - Cellular Senescence and Impaired Macrophage Efferocytosis in Fibrotic Diseases

Sarah Bitzer, Karim El Kasmi and Daniela Schlösser conceived the project and designed research.
Heiko Olbrich performed research and experiments.
Sarah Bitzer and Heiko Olbrich analyzed data.
Heiko Olbrich visualized the data and prepared all figures.
Heiko Olbrich wrote the manuscript.
Sarah Bitzer and Ralf Heilker reviewed the manuscript.

Bibliography

1. Wynn, T. A. & Vannella, K. M. Macrophages in Tissue Repair, Regeneration, and Fibrosis. *Immunity* **44**, 450–462 (2016).

2. Park, M. D., Silvin, A., Ginhoux, F. & Merad, M. Macrophages in health and disease. *Cell* **185**, 4259–4279 (2022).

3. Ginhoux, F. & Jung, S. Monocytes and macrophages: developmental pathways and tissue homeostasis. *Nat Rev Immunol* **14**, 392–404 (2014).

4. Varol, C., Mildner, A. & Jung, S. Macrophages: Development and Tissue Specialization. *Annu Rev Immunol* **33**, 643–675 (2015).

5. Murray, P. J. Macrophage Polarization. *Annu Rev Physiol* **79**, 541–566 (2017).

6. Sica, A. & Mantovani, A. Macrophage plasticity and polarization: in vivo veritas. *J Clin Invest* **122**, 787–795 (2012).

7. Desai, O., Winkler, J., Minasyan, M. & Herzog, E. L. The Role of Immune and Inflammatory Cells in Idiopathic Pulmonary Fibrosis. *Frontiers Medicine* **5**, 43 (2018).

8. Smigiel, K. S. & Parks, W. C. Macrophages, Wound Healing, and Fibrosis: Recent Insights. *Curr Rheumatol Rep* **20**, 17 (2018).

9. Byrne, A. J., Maher, T. M. & Lloyd, C. M. Pulmonary Macrophages: A New Therapeutic Pathway in Fibrosing Lung Disease? *Trends Mol Med* **22**, 303–316 (2016).

10. Okabe, Y. & Medzhitov, R. Tissue biology perspective on macrophages. *Nat Immunol* **17**, 9–17 (2016).

11. Vandivier, R. W., Henson, P. M. & Douglas, I. S. Burying the Dead: The Impact of Failed Apoptotic Cell Removal (Efferocytosis) on Chronic Inflammatory Lung Disease. *Chest* **129**, 1673–1682 (2006).

12. Henson, P. M. Cell Removal: Efferocytosis. *Annu Rev Cell Dev Bi* **33**, 127–144 (2017).

13. Elliott, M. R. & Kodi S., R. The Dynamics of Apoptotic Cell Clearance. *Dev Cell* **38**, 147–160 (2016).

14. A., B., Amira *et al.* CD24 signalling through macrophage Siglec-10 is a target for cancer immunotherapy. *Nature* **572**, 392–396 (2019).

15. Doran, A. C., A., Jr. Y. & Tabas, I. Efferocytosis in health and disease. *Nat Rev Immunol* **20**, 254–267 (2020).

16. Hochreiter-Hufford, A. & Ravichandran, K. S. Clearing the Dead: Apoptotic Cell Sensing, Recognition, Engulfment, and Digestion. *Csh Perspect Biol* **5**, a008748 (2013).

17. Yurdagul, A., Doran, A. C., Cai, B., Fredman, G. & Tabas, I. A. Mechanisms and Consequences of Defective Efferocytosis in Atherosclerosis. *Frontiers Cardiovasc Medicine* **4**, 86 (2018).

18. Szondy, Z., Garabuczi, É., Joós, G., Tsay, G. J. & Sarang, Z. Impaired Clearance of Apoptotic Cells in Chronic Inflammatory Diseases: Therapeutic Implications. *Front Immunol* **5**, 354 (2014).

19. Morimoto, K., Janssen, W. J. & Terada, M. Defective efferocytosis by alveolar macrophages in IPF patients. *Resp Med* **106**, 1800–3 (2012).

20. Henderson, N. C., Rieder, F. & Wynn, T. A. Fibrosis: from mechanisms to medicines. *Nature* **587**, 555–566 (2020).

21. Wynn, T. A. & Ramalingam, T. R. Mechanisms of fibrosis: therapeutic translation for fibrotic disease. *Nat Med* **18**, 1028–1040 (2012).

22. Meltzer, E. B. & Noble, P. W. Idiopathic pulmonary fibrosis. *Orphanet J Rare Dis* **3**, 8 (2008).

23. Borchers, A. T., Chang, C., Keen, C. L. & Gershwin, M. E. Idiopathic Pulmonary Fibrosis—an Epidemiological and Pathological Review. *Clin Rev Allerg Immu* **40**, 117–134 (2011).

24. Schafer, M. J. *et al.* Cellular senescence mediates fibrotic pulmonary disease. *Nat Commun* **8**, 14532 (2017).

25. Glass, D. S. *et al.* Idiopathic pulmonary fibrosis: Current and future treatment. *Clin Respir J* **16**, 84–96 (2022).

26. Moss, B. J., Ryter, S. W. & Rosas, I. O. Pathogenic Mechanisms Underlying Idiopathic Pulmonary Fibrosis. *Annu Rev Pathology Mech Dis* **17**, 515–546 (2022).

27. Altorki, N. K. *et al.* The lung microenvironment: an important regulator of tumour growth and metastasis. *Nat Rev Cancer* **19**, 9–31 (2019).

28. Denney, L. & Ho, L.-P. The role of respiratory epithelium in host defence against influenza virus infection. *Biomedical Journal* **41**, 218–233 (2018).

29. Knudsen, L. & Ochs, M. The micromechanics of lung alveoli: structure and function of surfactant and tissue components. *Histochem Cell Biol* **150**, 661–676 (2018).

30. Borok, Z. Alveolar epithelium: beyond the barrier. *Am J Resp Cell Mol* **50**, 853–6 (2014).

31. Rackley, C. R. & Stripp, B. R. Building and maintaining the epithelium of the lung. *J Clin Invest* **122**, 2724–30 (2012).

32. Rock, J. R., Randell, S. H. & Hogan, B. L. M. Airway basal stem cells: a perspective on their roles in epithelial homeostasis and remodeling. *Dis Model Mech* **3**, 545 (2010).

33. Borensztajn, K., Crestani, B. & Kolb, M. Idiopathic Pulmonary Fibrosis: From Epithelial Injury to Biomarkers - Insights from the Bench Side. *Respiration* **86**, 441–452 (2013).

34. Sgalla, G. *et al.* Idiopathic pulmonary fibrosis: pathogenesis and management. *Respir Res* **19**, 32 (2018).

35. Xu, X., Dai, H. & Wang, C. Epithelium-dependent profibrotic milieu in the pathogenesis of idiopathic pulmonary fibrosis: current status and future directions. *Clin Respir J* **10**, 133–141 (2016).

36. Tominaga, K. & Suzuki, H. I. TGF-β Signaling in Cellular Senescence and Aging-Related Pathology. *Int J Mol Sci* **20**, 5002 (2019).

37. Richeldi, L., Collard, H. R. & Jones, M. G. Idiopathic pulmonary fibrosis. *The Lancet* **389**, 1941–1952 (2017).

38. Joshi, N., Walter, J. M. & Misharin, A. V. Alveolar Macrophages. *Cell Immunol* **330**, 86–90 (2018).

39. Schloesser, D. *et al.* Senescent cells suppress macrophage-mediated corpse removal via upregulation of the CD47-QPCT/L axis. *J Cell Biol* **222**, e202207097 (2022).

40. Zhang, L. *et al.* Macrophages: friend or foe in idiopathic pulmonary fibrosis? *Respir Res* **19**, 170 (2018).

41. Wynn, T. & Barron, L. Macrophages: Master Regulators of Inflammation and Fibrosis. *Semin Liver Dis* **30**, 245–257 (2010).

42. Liu, R. M. & Liu, G. Cell senescence and fibrotic lung diseases. *Exp Gerontol* **132**, 110836 (2020).

43. Nambiar, A. *et al.* Senolytics dasatinib and quercetin in idiopathic pulmonary fibrosis: results of a phase I, single-blind, single-center, randomized, placebo-controlled pilot trial on feasibility and tolerability. *Ebiomedicine* **90**, 104481 (2023).

44. Barnes, P. J., Baker, J. & Donnelly, L. E. Cellular Senescence as a Mechanism and Target in Chronic Lung Diseases. *Am J Resp Crit Care* **200**, 556–564 (2019).

45. Hernandez-Segura, A., Nehme, J. & Demaria, M. Hallmarks of Cellular Senescence. *Trends Cell Biol* **28**, 436–453 (2018).

46. Petrova, N. V., Velichko, A. K., Razin, S. V. & Kantidze, O. L. Small molecule compounds that induce cellular senescence. *Aging Cell* **15**, 999–1017 (2016).

47. Minagawa, S. *et al.* Accelerated epithelial cell senescence in IPF and the inhibitory role of SIRT6 in TGF-β-induced senescence of human bronchial epithelial cells. *Am J Physiol-lung C* **300**, L391–L401 (2011).

48. Lagoumtzi, S. M. & Chondrogianni, N. Senolytics and senomorphics: Natural and synthetic therapeutics in the treatment of aging and chronic diseases. *Free Radical Bio Med* **171**, 169–190 (2021).

49. Muñoz-Espín, D. & Serrano, M. Cellular senescence: from physiology to pathology. *Nat Rev Mol Cell Bio* **15**, 482–496 (2014).

50. Elder, S. S. & Emmerson, E. Senescent cells and macrophages: key players for regeneration? *Open Biol* **10**, 200309 (2020).

51. Justice, J. N. *et al.* Senolytics in idiopathic pulmonary fibrosis: Results from a first-in-human, open-label, pilot study. *Ebiomedicine* **40**, 554–563 (2019).

52. Bluhmki, T. *et al.* Functional human iPSC-derived alveolar-like cells cultured in a miniaturized 96-Transwell air–liquid interface model. *Sci Rep-uk* **11**, 17028 (2021).

53. Bhowmick, R. & Gappa-Fahlenkamp, H. Cells and Culture Systems Used to Model the Small Airway Epithelium. *Lung* **194**, 419–428 (2016).

54. Mao, P. *et al.* Human alveolar epithelial type II cells in primary culture. *Physiological Reports* **3**, e12288 (2015).

55. Yanagimachi, M. D. *et al.* Robust and highly-efficient differentiation of functional monocytic cells from human pluripotent stem cells under serum- and feeder cell-free conditions. *Plos One* **8**, e59243 (2013).

56. Cui, D. *et al.* High-Yield Human Induced Pluripotent Stem Cell-Derived Monocytes and Macrophages Are Functionally Comparable With Primary Cells. *Frontiers Cell Dev Biology* **9**, 656867 (2021).

57. Takata, K. *et al.* Induced-Pluripotent-Stem-Cell-Derived Primitive Macrophages Provide a Platform for Modeling Tissue-Resident Macrophage Differentiation and Function. *Immunity* **47**, 183-198.e6 (2017).

58. Gutbier, S. *et al.* Large-Scale Production of Human iPSC-Derived Macrophages for Drug Screening. *Int J Mol Sci* **21**, 4808 (2020).

59. Lopez-Yrigoyen, M. *et al.* Production and Characterization of Human Macrophages from Pluripotent Stem Cells. e61038 (2020) doi:10.3791/61038.

60. Wilgenburg, B. van, Browne, C., Vowles, J. & Cowley, S. A. Efficient, long term production of monocyte-derived macrophages from human pluripotent stem cells under partly-defined and fully-defined conditions. *PLoS One* **8**, e71098–e71098 (2013).

61. Lyadova, I., Gerasimova, T. & Nenasheva, T. Macrophages Derived From Human Induced Pluripotent Stem Cells: The Diversity of Protocols, Future Prospects, and Outstanding Questions. *Frontiers Cell Dev Biology* **9**, 640703 (2021).

62. Gustafson, M. P. *et al.* A method for identification and analysis of non-overlapping myeloid immunophenotypes in humans. *Plos One* **10**, e0121546–e0121546 (2015).

63. Nakano, A., Harada, T., Morikawa, S. & Kato, Y. Expression of Leukocyte Common Antigen (CD45) on Various Human Leukemia/Lymphoma Cell Lines. *Pathol Int* **40**, 107–115 (1990).

64. Nielsen, M. C. *et al.* Macrophage Activation Markers, CD163 and CD206, in Acute-on-Chronic Liver Failure. *Cells* **9**, 1175 (2020).

65. Huppertz, B., Frank, H.-G. & Kaufmann, P. The apoptosis cascade — morphological and immunohistochemical methods for its visualization. *Anat Embryol* **200**, 1–18 (1999).

66. Axline, S. G. & Reaven, E. P. INHIBITION OF PHAGOCYTOSIS AND PLASMA MEMBRANE MOBILITY OF THE CULTIVATED MACROPHAGE BY CYTOCHALASIN B. *J Cell Biology* **62**, 647–659 (1974).

67. Bar, H. & Zweifach, A. Z' Does Not Need to Be > 0.5. *Slas Discov* **25**, 1000–1008 (2020).

68. Murray, D. & Wigglesworth, M. High Throughput Screening Methods: Evolution and Refinement. *Chem Biology* 1–15 (2017) doi:10.1039/9781782626770-00001.

69. Kapellos, T. S. *et al.* A novel real time imaging platform to quantify macrophage phagocytosis. *Biochem Pharmacol* **116**, 107–119 (2016).

70. Higo, H. *et al.* Identification of targetable kinases in idiopathic pulmonary fibrosis. *Respir Res* **23**, 20 (2022).

71. Pamuk, O. N. *et al.* Spleen tyrosine kinase (Syk) inhibitor fostamatinib limits tissue damage and fibrosis in a bleomycin-induced scleroderma mouse model. *Clin Exp Rheumatol* **33**, S15-22 (2014).

72. Sheng, H. *et al.* Antifibrotic Mechanism of Piceatannol in Bleomycin-Induced Pulmonary Fibrosis in Mice. *Frontiers in Pharmacology* **13**, 771031 (2022).

73. Moriya, K. *et al.* ER-27319, an acridone-related compound, inhibits release of antigen-induced allergic mediators from mast cells by selective inhibition of Fcε receptor I-mediated activation of Syk. *Proc National Acad Sci* **94**, 12539–12544 (1997).

74. Liddle, J. *et al.* Discovery of GSK143, a highly potent, selective and orally efficacious spleen tyrosine kinase inhibitor. *Bioorg Med Chem Lett* **21**, 6188–6194 (2011).

75. Wang, B. & Li, J. Piceatannol Suppresses the Proliferation and Induced Apoptosis of Osteosarcoma Cells Through PI3K/AKT/mTOR Pathway. *Cancer Management Res* **12**, 2631–2640 (2020).

76. Oliver, J. M., Burg, D. L., Wilson, B. S., McLaughlin, J. L. & Geahlen, R. L. Inhibition of mast cell Fc epsilon R1-mediated signaling and effector function by the Syk-selective inhibitor, piceatannol. *J Biol Chem* **269**, 29697–29703 (1994).

77. Huang, W., Hickson, L. J., Alfonso, E., Kirkland, J. L. & Lerman, L. O. Cellular senescence: the good, the bad and the unknown. *Nat Rev Nephrol* **18**, 611–627 (2022).

78. Lee, C. Z. W., Kozaki, T. & Ginhoux, F. Studying tissue macrophages in vitro: are iPSC-derived cells the answer? *Nat Rev Immunol* **18**, 716–725 (2018).

79. Wang, H., Yang, Y., Liu, J. & Qian, L. Direct cell reprogramming: approaches, mechanisms and progress. *Nat Rev Mol Cell Bio* **22**, 410–424 (2021).

80. Cao, X., Hil, F. E. van den, Mummery, C. L. & Orlova, V. V. Generation and Functional Characterization of Monocytes and Macrophages Derived from Human Induced Pluripotent Stem Cells. *Curr Protoc Stem Cell Biology* **52**, e108 (2020).

81. Shi, J., Xue, C., Liu, W. & Zhang, H. Differentiation of Human-Induced Pluripotent Stem Cells to Macrophages for Disease Modeling and Functional Genomics. *Curr Protoc Stem Cell Biology* **48**, e74 (2019).

82. Zhang, H. *et al.* Functional Analysis and Transcriptomic Profiling of iPSC-Derived Macrophages and Their Application in Modeling Mendelian Disease. *Circ Res* **117**, 17–28 (2015).

83. Li, S. *et al.* Optimizing the Method for Differentiation of Macrophages from Human Induced Pluripotent Stem Cells. *Stem Cells Int* **2022**, 6593403 (2022).

84. Ackermann, M. *et al.* Bioreactor-based mass production of human iPSC-derived macrophages enables immunotherapies against bacterial airway infections. *Nat Commun* **9**, 5088 (2018).

85. Tilman, J., Koutsouraki, E., Humphreys, S. & Barnes, A. Late Breaking Abstract - Generating iPSC derived alveolar macrophages as a novel model for respiratory research. *European Respiratory Journal* **54**, PA2343 (2019).

86. deCathelineau, A. M. & Henson, P. M. The final step in programmed cell death: phagocytes carry apoptotic cells to the grave. *Essays Biochem* **39**, 105–117 (2003).

87. MARIANI, A. R. *et al.* Lineage-related susceptibility of human hemopoietic cell lines to apoptosis. *Anat. Rec.* **254**, 1–153 (1999).

88. Kulms, D. & Schwarz, T. Molecular mechanisms of UV-induced apoptosis. *Photodermatol Photoimmunol Photomed* **16**, 195–201 (2000).

89. Aragane, Y. *et al.* Ultraviolet Light Induces Apoptosis via Direct Activation of CD95 (Fas/APO-1) Independently of Its Ligand CD95L . *J Cell Biology* **140**, 171–182 (1998).

90. Arandjelovic, S. & Ravichandran, K. S. Phagocytosis of apoptotic cells in homeostasis. *Nat Immunol* **16**, 907–917 (2015).

91. Miksa, M., Komura, H., Wu, R., Shah, K. G. & Wang, P. A novel method to determine the engulfment of apoptotic cells by macrophages using pHrodo succinimidyl ester. *J Immunol Methods* **342**, 71–77 (2009).

92. Wang, Y. *et al.* Mitochondrial Fission Promotes the Continued Clearance of Apoptotic Cells by Macrophages. *Cell* **171**, 331-345.e22 (2017).

93. Sho, M. *et al.* Efferocytosis induces a novel SLC program to promote glucose uptake and lactate release. *Nature* **563**, 714–718 (2018).

94. Bravo, D. D. *et al.* A Real-Time Image-Based Efferocytosis Assay for the Discovery of Functionally Inhibitory Anti-MerTK Antibodies. *J Immunol* (2023) doi:10.4049/jimmunol.2200597.

95. Raymond, M. H. *et al.* Live cell tracking of macrophage efferocytosis during Drosophila embryo development in vivo. *Sci New York N Y* **375**, 1182–1187 (2022).

96. Santulli-Marotto, S. *et al.* Discovering Molecules That Regulate Efferocytosis Using Primary Human Macrophages and High Content Imaging. *Plos One* **10**, e0145078 (2015).

97. Simeonov, A. *et al.* Fluorescence Spectroscopic Profiling of Compound Libraries. *J Med Chem* **51**, 2363–2371 (2008).

98. Cvetanovic, M. & Ucker, D. S. Innate Immune Discrimination of Apoptotic Cells: Repression of Proinflammatory Macrophage Transcription Is Coupled Directly to Specific Recognition 1. *J Immunol* **172**, 880–889 (2004).

99. Clark, R., Usselmann, L., Brown, M. R., Goeppert, A. U. & Corrigan, A. A flexible high content imaging assay for profiling macrophage efferocytosis. *J Immunol Methods* **473**, 112636 (2019).

100. Hall-Roberts, H., Daniel, E. D., James, W. S., Davis, J. B. & Cowley, S. A. In vitro Quantitative Imaging Assay for Phagocytosis of Dead Neuroblastoma Cells by iPSC-Macrophages. *J Vis Exp* (2021) doi:10.3791/62217.

101. Ulanova, M. *et al.* Involvement of Syk protein tyrosine kinase in LPS-induced responses in macrophages. *J Endotoxin Res* **13**, 117–125 (2007).

102. Lin, Y.-C., Huang, D.-Y., Chu, C.-L. & Lin, W.-W. Anti-inflammatory actions of Syk inhibitors in macrophages involve non-specific inhibition of toll-like receptors-mediated JNK signaling pathway. *Mol Immunol* **47**, 1569–1578 (2010).

103. Yi, Y.-S. *et al.* Syk promotes phagocytosis by inducing reactive oxygen species generation and suppressing SOCS1 in macrophage-mediated inflammatory responses. *Int J Immunopath Ph* **36**, 03946320221133018 (2022).

104. Yuki, K. *et al.* Role of Dectin-2 in the Phagocytosis of Cryptococcus neoformans by Dendritic Cells. *Infect Immun* **89**, e00330-21 (2021).

105. Varghese, A. M. *et al.* Highly selective SYK inhibitor, GSK143, abrogates survival signals in chronic lymphocytic leukaemia. *Brit J Haematol* **182**, 927–930 (2018).

106. Sang, X. *et al.* Macrophage-Targeted Lung Delivery of Dexamethasone Improves Pulmonary Fibrosis Therapy via Regulating the Immune Microenvironment. *Front Immunol* **12**, 613907 (2021).

107. Watson, C. K. *et al.* Antifibrotic Drug Nintedanib Inhibits CSF1R to Promote IL-4–associated Tissue Repair Macrophages. *American Journal of Respiratory Cell and Molecular Biology* **68**, 366–380 (2023).

108. Korns, D., Frasch, S. C., Fernandez-Boyanapalli, R., Henson, P. M. & Bratton, D. L. Modulation of macrophage efferocytosis in inflammation. *Front Immunol* **2**, 57 (2011).

109. Hayflick, L. & Moorhead, P. S. The serial cultivation of human diploid cell strains. *Exp. Cell Res.* **25**, 585–621 (1961).

110. Ren, L.-L. *et al.* Transforming growth factor-β signaling: From tissue fibrosis to therapeutic opportunities. *Chem-biol Interact* **369**, 110289 (2023).

111. Katakura, Y. Molecular Basis for the Cellular Senescence Program and Its Application to Anticancer Therapy. *Biosci Biotechnology Biochem* **70**, 1076–1081 (2014).

112. Planté-Bordeneuve, T., Pilette, C. & Froidure, A. The Epithelial-Immune Crosstalk in Pulmonary Fibrosis. *Front Immunol* **12**, 631235 (2021).

113. Drakopanagiotakis, F., Wujak, L., Wygrecka, M. & Markart, P. Biomarkers in idiopathic pulmonary fibrosis. *Matrix Biology* **68–69**, 404–421 (2018).

114. Logtenberg, M. E. W., Scheeren, F. A. & Schumacher, T. N. The CD47-SIRPα Immune Checkpoint. *Immunity* **52**, 742–752 (2020).

115. Wernig, G. *et al.* Unifying mechanism for different fibrotic diseases. *Proc National Acad Sci* **114**, 4757–4762 (2017).

116. Mayr, L. M. & Bojanic, D. Novel trends in high-throughput screening. *Curr Opin Pharmacol* **9**, 580–8 (2009).

117. Jarr, K.-U. *et al.* The pleiotropic benefits of statins include the ability to reduce CD47 and amplify the effect of pro-efferocytic therapies in atherosclerosis. *Nat Cardiovasc Res* **1**, 253–262 (2022).

118. Lee, J.-R. *et al.* Local delivery of a senolytic drug in ischemia and reperfusion-injured heart attenuates cardiac remodeling and restores impaired cardiac function. *Acta Biomater* **135**, 520–533 (2021).

119. Chaib, S., Tchkonia, T. & Kirkland, J. L. Cellular senescence and senolytics: the path to the clinic. *Nat Med* **28**, 1556–1568 (2022).

120. Takahashi, K. *et al.* Induction of Pluripotent Stem Cells from Adult Human Fibroblasts by Defined Factors. *Cell* **131**, 861–872 (2007).